UNIVERSITÀ
DEGLI STUDI
FIRENZE

DOTTORATO DI RICERCA INTERNAZIONALE IN

CIVIL AND ENVIRONMENTAL ENGINEERING

CICLO XXIX

COORDINATORE Prof. Ing. Castelli Fabio

A METHODOLOGY FOR THE SEISMIC ASSESSMENT OF EXISTING EARTH DAMS IN ITALY

Settore Scientifico Disciplinare ICAR/07

Dottorando
Dott. Banti Erika

Banti Erika

Tutore
Prof. Lo Presti Diego

Coordinatore
Prof. Castelli Fabio

Anni 2013/2017

ABSTRACT

Many earth dams in Italy are located in seismic areas with a seismicity from moderate to high. Moreover, they were built several years ago when the seismic Italian zonation and the construction code were completely different. Their seismic stability has to be assessed in order to ensure the safety of urban areas in the downstream site near the reservoirs.

This thesis is aimed at defining a reliable and suitable methodology for the assessment of the ultimate and serviceability limit states of existing earth dams in the light of the new seismic zonation of Italy.

The core of the Thesis is a numerical study related to the investigation of the seismic response of earth dams using the finite element method.

The first step consisted in the validation of the numerical method. This was performed by comparing the experimental results obtained from two different centrifuge tests with those obtained from the numerical analyses. The main goal was to identify the most relevant influential factors and select the most appropriate constitutive models.

Secondly, a parametric study was carried out in order to quantify the influence of each relevant factor. The parametric study concerned two "ideal" existing strategic dams, which represent two typical dam sections in Italy. They are located in the south of Italy, in a site which is exposed to high seismic risk. A deterministic spectrum-compatibility method, customized to the actual Italian regulations on structures and dams (M.LL.PP., 2008 and M.LL.PP., 2014) and to the hazard of the aforementioned site, was adopted for the selection of the input time histories. Two dimensional finite models were set up to reproduce the geometric characterization of the dam structure and its foundation.

This parametric study provided a means to assess the effect of different parameters and scenarios on the seismic analysis of dams. To this aim, the results of the two dimensional analyses have been discussed focusing on the role of each factor on the response of earth dam subjected under seismic motion.

AKNOWLEDGEMENTS

I would like to express my sincere gratitude to my Italian research supervisor Professor D. Lo Presti who gave me the opportunity to study this interesting topic. I am grateful to him for guided me through this work, giving me the right suggestions.

I would also thanks my German tutor Professor J. Stahlmann for supervising my work and hosting me at the Institut für Grundbau und Bodenmechanik at Technische Universität of Braunschweig, during my stay in Germany.

I am grateful to Eng. N. Squeglia who gave me some suggestions and supports during these three years.

Moreover, I would like to express my sincere gratitude to Prof. Dong Soo Kim who gave me the possibility to stay at the Geotechnical Centrifuge Testing Center of Korea Advanced Institute of Science and Technology (KAIST) at Deajeon. During my stay, he gave me the opportunity to assist to centrifuge test on dam models. I am also grateful to the entire group of the Geotechnical Centrifuge Testing Centre and in particular, to Eng. Y. Cho who helped me during my stay.

I want to thank Mr. S. Giusti from Geotechnical Laboratory of University of Pisa, for his encouragement and help during these last three years.

Finally, I would also thanks my family and my partner Max for sharing with me this experience and for their constant support.

TABLE OF CONTENTS

LIST OF FIGURES

LIST OF TABLES

LIST OF SYMBOLS

a	Van Genuchten's fitting parameter
$a_{max,n}$	maximum acceleration related to the seismic hazard of the specific site
$a_{max,r}$	maximum acceleration of the selected input
b	crest width
B	dam width at base
[C]	damping matrix
c	coehesion
c_b	core width at base
c_c	core width at crest
c_v	coefficient of consolidation
C_U	usage coefficient (eq.4)
D	damping ratio
D_{max}	Hardin & Drnevich parameter
D_{min}	minimum damping ratio
E	Young's modulus
e_0	void ratio
E_r	intact rock Young's modulus
F	freeboard height
Fs	amplitude scale factor

$F(\omega)$	transfer function
$F(\gamma)$	backbone curve function
g	acceleration of gravity
G	shear modulus
G0 or Gmax	maximum values of shear modulus γ
H	height of the dam
i	hydraulic gradient
I	impedance ratio
I_a	Arias intensity
[K]	stiffness matrix
K	fitting parameters of eq. (5.1) and (5.2)
k_{sat}	permeability of materials
k_w	conductivity water function
m	mass
m	Van Genuchten's fitting parameter
m	fitting parameters of eq. (5.1) and (5.2)
[M]	mass matrix
M_w	moment magnitude
N	scale factor
n	porosity
n	Van Genuchten's fitting parameter
OCR	over consolidation ratio
p_{dyn}	hydrodynamic pressure
PGA	peak ground acceleration

PI	plasticity index
P_{VR}	probability of failure
RS	integral of response spectrum
S_a	spectral acceleration
T	natural period of vibration
T_R	return period
T_v	dimensionless time factor consolidation
u	displacement
$\dot{u}$	velocity
$\ddot{u}$	acceleration
v	fluid velocity
V_N	nominal life
V_R	reference period
V_s	shear wave velocity of the soil
x	horizontal direction
y	vertical direction
z	depth or elevation
w	vertical settlement
α	Yakota's fitting parameter
β	Yakota's fitting parameter
γ	shear strain
γ	unit weight
γ_{ref}	reference shear strain
γ_ω	unit weight of water
λ	Yakota's fitting parameter

λ	wavelength
Δh	mesh size
ρ	mass density
σ	normal stress
ν	Poisson's ratio
σ_m	mean confining pressure
τ	shear stress
φ	angle of shearing resistance
ψ	angle of dilatation
Ψ	suction range
ω	circular frequency of armonic load
ω_d	foundamental circular frequency of the dam
Θ_w	volumetric water content
Θ_r	residual volumetric water content
Θ_s	saturated volumetric water content

Chapter 1

INTRODUCTION

1.1. Background

Earthquakes, landslides and floods are the main natural hazards for most large storage dams. In some cases landslide-triggering and floods can be predicted from meteoric events. Moreover, landslides slowly evolving with time could be monitored. On the other hand, earthquakes can be predicted only on a probabilistic basis. Earthquake may have return periods of several hundred or thousands of years and they depend on the seismotectonic conditions of the region of interest. It is worth noticing that it is assumed a definition of the probabilistic and deterministic approaches for the assessment of the seismic hazard in agreement with Abrahamson (1992).

As an increasing number of new dams are of the embankment type, in many cases, they have reached great heights, creating reservoirs of enormous capacities. Ensuring their safety during earthquakes has been a major concern of designers and research for several decades. Advances in analytical techniques, accumulating field observations aided by recording instruments and better understanding of soil behavior under dynamic loading have led to rapid advancement in this area in recent years.

Only few cases of total failures of earth dams due to earthquake have been observed, as the cases of Sheffield Dam in 1925, the Lower San Fernando Dam in 1971 and the Fujinuma dam in 2011.

In the first two cases, total failure is mostly attributable to liquefaction, whereas in the third case, the failure is due to the significant deformations within the embankment, which determined the uncontrolled release of the entire reservoir.

The Sheffield Dam (Santa Barbara, USA) was subject to a moderate earthquake of magnitude 6.3, with a maximum ground acceleration of 0,15g. Reports indicated that sliding occurred near the base of the embankment, causing a section of about 90m in length to move bodily downstream as much as 30m. The

lower San Fernando Dam (Los Angeles, USA) was hit by an earthquake of magnitude 6.6, with its epicenter located about 14 km north-east of the dam. The maximum ground acceleration reached about 0.5 to 0.6g with a shake duration of 12 sec. During the earthquake a major slide occurred in the upstream face, taking with it the crest and the upper 9.2m of the soil on the downstream slope (Fig. 1.1).

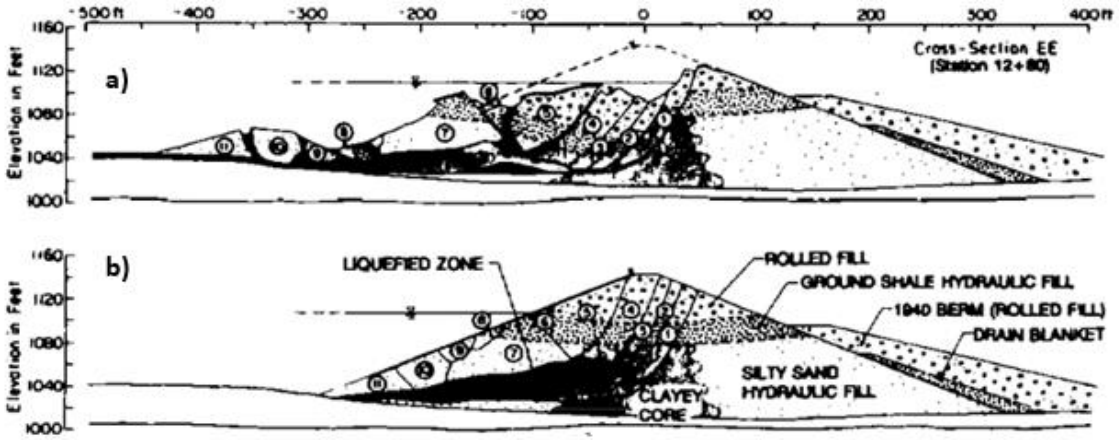

Figure 1.1 Cross-section through Lower San Fernando Dam: condition after earthquake (a) and schematic reconstruction of failed cross-section (Castro et Al. 1992)

On March 2011, a gigantic earthquake with a magnitude of 9.0 struck the Tohoku region of Japan. As a result, as many as 745 reservoirs in Fukushima prefecture were damaged. According to reports by Matsumoto (2011), almost all of these dams withstood minor to severe ground shaking and retained their reservoirs with generally minor to moderate damage. The exception to this was the Fujinuma Dam which failed shortly after the earthquake. The dam was a homogenous embankment of 18.5 m, mainly composed by an impervious material. It was located in southern Fukushima Prefecture and its construction was started in 1937 and completed in 1949. When the seismic event occurred, the reservoir was nearly full. The dam was located approximately 80 kilometers from the fault rupture and a peak ground acceleration of 0.315g was recorded near the dam location.

Figure 1.2 Fujinuma Dam Section after earthquake (GEER 2011, photo L.F. Harder)

The failure of the dam resulted in the uncontrolled release of the entire reservoir, which flowed downstream into a small village and killed 8 people (Matsumoto, 2011; Towhata et al., 2011).

Preliminary observations of the Fujinuma Dam failure (Harder et Al., 2011) verified the presence of different types or zones of fill within the embankment which were placed at different times during the intermittent construction periods of the dam. The different fills were not properly keyed together and the degree of compaction may have been relatively small. Thus, the embankment was subjected to the strength losses during the long duration of the earthquake shaking. The low resistance of the materials and the seepage within the embankment produced the sliding phenomenon on the downstream side which caused the uncontrolled release of the entire reservoir.

A large percentage of the earth dam failure in the world was due to seepage. The seepage can produce an "internal erosion". This term is generally used for describing the erosion of particles by water passing through a body of soil.

Internal erosion occurs when soils particles are detached from their parent soil and are transported through sufficiently large voids and constrictions.

Typical internal erosion mechanism can be classified into four groups, according to the different initiation mechanisms: a) concentrated leak erosion, b) backward erosion and piping, c) contact erosion and d) suffusion.

Concentrated leak erosion is produced by the enlargement of cracks due to erosion from the surface of the cracks. This phenomenon may occur due to the presence of ice lenses and to the freeze-thaw action. It may occur also in a continuous permeable zone containing coarse or poorly compacted materials, or in a crack between two zones caused by differential settlement.

Backward erosion and piping occur when detachment of the fine particles occurs and seepage exits to a free unfiltered surface. The seepage carries the fine particles downstream whereas the erosion carries on gradually upstream toward the source of water. Internal erosion by piping may be an effect of backward erosion. This phenomenon may occur if seepage continues beyond the origin of backward erosion and develops continuous pipe though the embankment.

Contact erosion occurs at the interface between two zone of different grading as at the interface between the embankment and the foundation, when the fine soil is pulled into the gabs of coarser soil.

Suffusion is the process where finer fractions move among the voids of courser fractions under the action of water flow. Suffusion implicates the soil modification and the increase of the porosity which can cause the decrease in mechanical strength of the soil.

Thus, it is of fundamental importance to limit the seepage through earth dams not only to keep the water loss within acceptable limits but also to take adequate control measures to ensure the safety of the dam.

Nonetheless most of the failures were due to seepage, the seismic analysis of these huge geotechnical constructions cannot be disregarded, especially because of the high-risk exposure and recent changes of Italian Seismic Zonation and design criteria.

In Italy, most of the existing dams was built between 50's and 90's when the seismic Italian zonation and the construction code were completely different. Among them, Zoned Earth and Rockfill dams represent one of the most common typologies of the existing dams in Italy.

Conventional design procedures for assessing seismic stability of earth dams in Italy were based traditionally on pseudo-static analyses. The revision of seismic hazard maps and design criteria has led to the necessity of assessing the seismic safety of earth dams previously built without considering those seismic induced forces. The dam exposition is generally high, related to the presence of urban areas near the reservoirs.

The new Seismic Zonation of the Italian territory and the recent seismic Italian Code NTC 08 (M.LL.PP., 2008) have led the Italian Office of the Infrastructures and Transport Ministry to issue a directive in 2014 (M.LL.PP.,2014). The new

seismic Italian classification exposes the territory to a seismic risk from moderate to high (up to PGA=0,35g).

The Ministerial directive requested that the seismic stability study of dams has to consider the understanding of the new seismic classification and incorporate up-to-date analysis techniques such as more sophisticated dynamic analyses.

Therefore, the aim of this study is the definition of a methodology for the evaluation of actual safety degree of the Italian earth Dams which could take into account of materials and local effects which can strongly affect the seismic response.

1.2. Main aim of the research

In Italy, most of earth-fill and rockfill dams were built within the twentieth-century when the seismic Italian zonation and the construction code were completely different.

The main difference is based on the selection of the seismic actions using the Probabilistic Seismic Hazard Analysis, PSHA (Cornell, 1968). This analysis aims to quantify the uncertainties (location, size, shaking intensity) about future earthquakes which may occur and produce explicit description of the distribution of future shaking at a site. Details are described in Chapter 3.

The seismic hazard associated to Italian dams is high, mostly due to the high seismicity of the territory and to the old design criteria used during construction.

The main aim of this research is to perform a methodology for the evaluation of the safety degree of existing earth dams in Italy through the evaluation of the factors which could affect their seismic response.

The research aims to investigate a series of ideal dam sections in order to establish and further improve the current knowledge of their seismic response.

Thus, in order to identify the material and geometry influential factors, a series of bi-dimensional numerical simulations was carried out.

The studied earth structures reproduce and represent two typical dam sections placed along a river bed where the effect of valley topography is not influential. In these cases, a be dimensional analysis has been performed.

First, due to lack of available data on the seismic response of real cases, two centrifuge experiments were studied to calibrate the numerical analysis (Kim M.K. et Al, 2011 and Park S.Y. et Al. 2016).

Finally, several parametric analyses were carried out to assess the effects of different factors on the predicted seismic response of earth dams. The study investigated the following factors:

- The effect of the impedance ratio I ($I = \frac{\rho_r \cdot V_{s,r}}{\rho_s \cdot V_{s,s}}$);
- Effect of earthquake input intensity;
- Effect of soil dynamic parameters;
- Effect of dam geometry;

- Combined effect of vertical and horizontal component of seismic input.

Therefore, comments were made regarding the influence of such parameters and their application on the evaluation on the seismic response of earth dams.

1.3. Layout of the thesis

The work presented in this thesis is organised in three parts. The first part consists of two chapter: Chapter 2 contains a review of the literature and the regulations related to seismic response of earth dams, Chapter 3 describes a methodology in order to define the seismic behavior of existing dams and assess their performance. The second part (Chapter 4) contains the description of the methodology used for the calibration of the adopted numerical method and the constitutive model as regards to two centrifuge experimental tests. The third part (Chapter 5) reports the parametric analysis on the sensibility of the dam seismic response respect to a series of influential factors.

Hereafter, a brief introduction on the chapters, which compose the present work.

Chapter 2 describes literature information about the characteristics of existing earth dams in Italy. Firstly, an introduction on the employed material of Italian earth-fill dams has been presented, followed by the description of the typical cross section of existing Italian earth-fill dams. Then, the principles of seismic response of soil deposits is dealt with. In the end a literature updated review on the factors affecting the dynamic dam response is given.

Chapter 3 describes the various methods used for the evaluation of the seismic analysis of earth dams. First, an overview of different methods of seismic analysis of dams has been done. Secondly, the description of a methodology adopted for the seismic behavior of existing earth dams and for assessing their performance have been carried out. Moreover, this chapter defines the evaluation of the input motions according to the actual regulations (M.LL.PP, 2008 and M.LL.PP. 2014) and the recommendation to follow for the numerical modelling of the performance of existing earth dams under seismic motions.

Chapter 4 gives information on some centrifuge tests on earth dam models that were carried out at KAIST. It also includes the numerical analyses of these tests by the finite element method (2D). The numerical analyses were calibrated on the basis of the experimental results that were obtained from two different centrifuge tests on earth dams. The numerical analyses exhibit a good agreement with the

experimental results. Several issues were addressed which provide information that need to be considered when performing the seismic analysis of earth dams when using the finite element method.

Built on the knowledge acquired from the previous chapters, ***Chapter 5*** contains several parametric studies performed to assess the effects of different parameters on the predicted seismic response of hypothetical existing earth dams. The examined factors are: (a) the effects of the impedance ratio I, (b) the effect of earthquake input intensity, (c) effects of the soil dynamic parameters, (d) effects of dam geometry and (e) the combined effect of vertical and horizontal components of seismic input.

Finally, ***Chapter 6*** summarizes the findings of this work and describes the various recommendations for further investigations.

CHAPTER 2

DYNAMIC PERFORMANCE OF DAMS

2.1. Italian Dams

In Italy, more than 9000 levees have been built and 543 of them are classified as "large dams".

Large dams are those embankments which are more than 15m high or with a reservoir volume higher than 1'000'000 mc (M.LL.PP., 2014).

These constructions may be classified as a function of their use, their shape or the materials of their structures.

According to the actual Italian Code on the Dam Design (M.LL.PP., 2014), dams may be classified as showed in Table 2.1.

The recent code classifies earth dam in function of their dimension and their utility, according to the following characteristics:

- **Small dams:** are defined as those not exceeding 15 meters in height and determining a reservoir volume not larger than 1'000'000 mc;
- **Large dams:** are defined as those embankments over 15 meters in height, creating a reservoir volume higher than 1'000'000 mc.
- **Dams of strategic importance:** whose function during an earthquake assumes a fundamental importance for the purposes of civil protection, (e.g. dams used for hydroelectric power and drinking water). Their functionality must to be efficient and guaranteed in case of an earthquake and after the seismic event;

- **Relevant dams**: for which a possible collapse after an earthquake may produce severe consequences and damages, (e.g. all the dams classified as "relevant" according to regional regulations);
- **Normal dams:** not belonging into the first and second types.

Italian Code on the Dam Design (Ministerial Decree 26/06/2014)	
Classification of Dams	
a)	**Rigid Dams**
a.1)	**Gravity Dams:** dams constructed with concrete or stone masonry. It is designed to hold back water thanks to its own weight. The structure can resist the horizontal pressure of water pushing against it.
a.1.1)	**Ordinary:** gravity dams with a triangular straight section.
a.1.2)	**Buttress dam:** gravity dams with a solid upstream side that is supported on the downstream side by a series of buttresses or supports with triangular section and buttress. They are the lightened version of the gravity dam.
a.2)	**Curved Vault Dams:** concrete dams which are curved in upstream plan.
a.2.1)	**Arch Dams:** this structure transmits the major portion of the water load to the abutments or valley sides rather than to the floor of the valley.
a.2.2)	**Arch-Gravity Dams:** this structure ensures stability by its own mass and its shape which transmits the water load to the abutments or valley sides.
a.2.3)	**Cupola's Dams:** with a complex curvature in the vertical as well as the horizontal plane. It is the most sophisticated of concrete dams, being essentially a dome or shell structure, and is extremely economical in concrete.
b)	**Embankment Dams:** large artificial dam, created by the placement and the compaction of various compositions of soil, sand, clay, or rock.
b.1)	**Homogeneous Dams:** earth dams with impervious soil: the section consists almost entirely of one type of material.
b.2)	**Zoned Earth Dams:** earth dams with impervious core and pervious shells
b.3)	**Rockfill Dams with upstream face membrane**
c)	**Weirs:** They are barriers across the horizontal width of a river which alter the flow characteristic of the water. They usually change the water level of the river.
d)	**Various Dam types:** they represent all structures which are not included in the previous types

Table 2.1 Classification of Dams, according to Ministerial Decree 26/06/2014

In Italy, most of the existing dams was built between 50's and 90's (Figure 2.1). Today the number of the existing large dams is 534, as defined by the study of the Italian Ministry of Infrastructure and Transport on February 2017 (Cisl Fp - Ministero delle Infrastrutture e Trasporti – ex Rid, 2008. About one hundred rockfill and earthfill dams have been built among them.

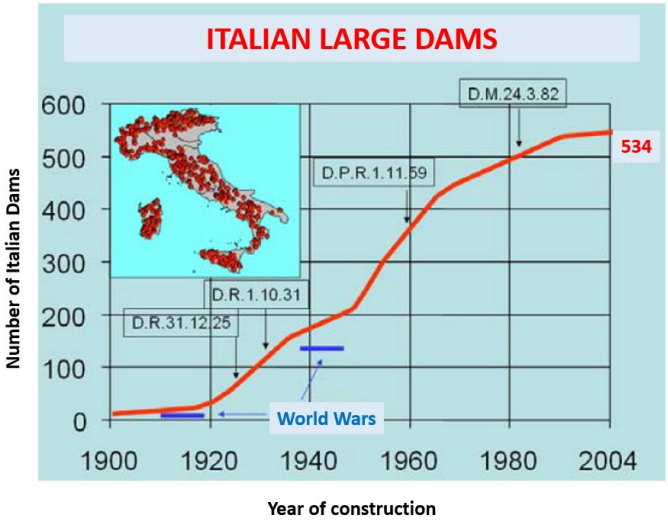

Figure 2.1: The number of Italian Dams from the 1900s (Cisl Fp - Ministero delle Infrastrutture e Trasporti – ex Rid, 2008)

Until 1950s, most of Italian earth dams were built in the North part of Italy. After the 1950s the barycentre of these works moved to the South of Italy. Thanks to the development of construction technologies it has been possible to realise these huge structures where the geological conditions were hard and it was no possible to realize concrete works. The development of construction technologies has allowed to realize huger structures with larger reservoir and higher dimensions.

Figure 2.2 shows the increase of Italian earth dam's height versus the year of construction. The figure represents the evolution of dam's height between 1920s and 1980s for three types of dams: earth-fill dams (T), rockfill dams (P) and dry-stone masonry dams (Ps). Until 1920s the dam's height was limited from about 7m and 18m. In the period between about the 1900s and the 1950s, the average height was about 20m, whereas the maximum height was 48m with the Disueri Dam in Sicily. After the 1950s, the average height has been increased up to 35m and the highest height was reached in the Lago Verde Dam and the Pedra è Othoni Dam with respectively about 74m and 77 m (Japelli and Silvestri, 2005).

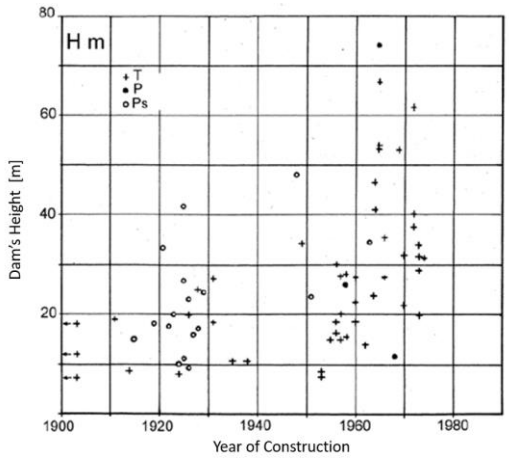

Earth-fill dams (T)
Rockfill dams (P)
Dry stone masonry dams (Ps)

Figure 2.2:The increase of earth dam height versus the year of construction in Italy (Jappelli and Silvestri, 2005).

Figure 2.3 shows the increase of dam's reservoir capacity versus the year of construction. The figure represents the evolution of Italian dam's capacity during the observed period between the 1900s and 1980s for the three types of dams: earth-fill dams (T), rockfill dams (P) and dry-stone masonry dams (Ps).

Until 1920s, in Italy, the dam maximum reservoir capacity was $3x10^6$ m^3; from 1920s to 1950s the maximum volume was $150x10^6$ m^3 and from 1951 to about 1980 the maximum volume was reached with the Monte Cotugno Dam (Japelli and Silvestri, 2005). Currently, the Monte Cotugno Dam represents the earth dam with the maximum reservoir capacity in Italy ($530x10^6$ m^3).

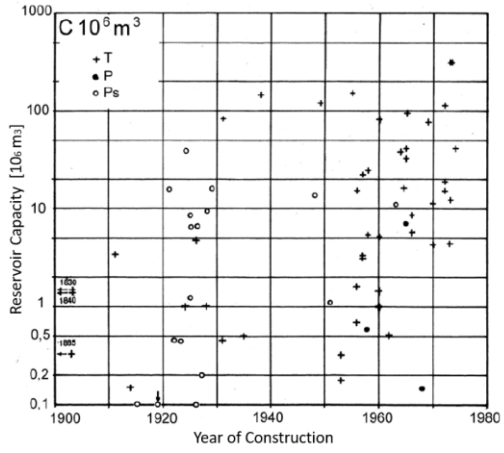

Earth-fill dams (T)
Rockfill dams (P)
Dry stone masonry dams (Ps)

Figure 2.3: The increase of earth dam reservoir capacity versus the year of construction in Italy (Jappelli and Silvestri, 2005).

According to the report of the Italian Committee of Large Dam (today named ITCOLD) the following graph (Figure 2.4) represents the state of art of the

construction typology of Italian dams: Zoned Earth and Rockfill dams represent one of the most common typologies of the existing dams in Italy.

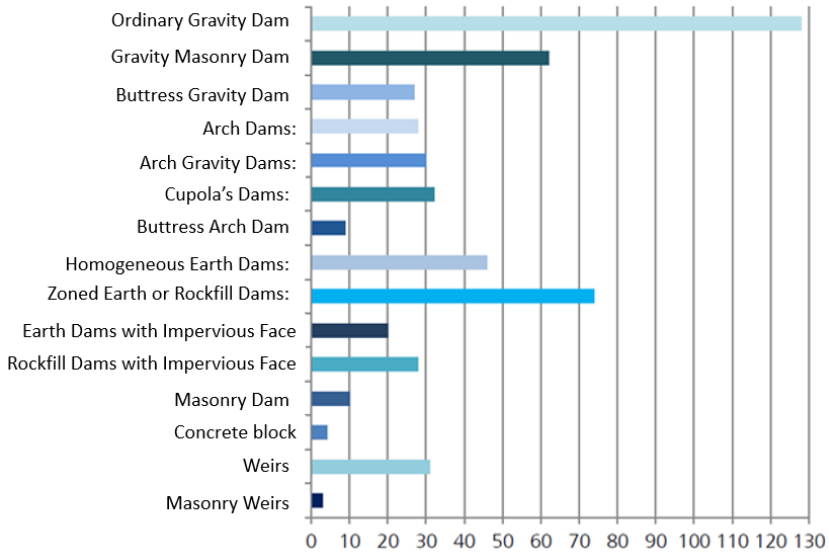

Figure 2.4: A summary of the construction typology of Italian dam (AA. VV., Riabilitazione delle dighe, ItCOLD, Maggio 2012)

In 1970s, the Italian Committee of Large Dam (ITCOLD) carried out a research on the properties of employed materials of Italian earth dams. This work was led by a research group with Prof. Eng. R. Jappelli, Prof. Eng. A. Pellegrino and Ing. T. Silvestri[1].The research was a statistical study on a group of 37 dams which were built between 1950s and 1975s.

The studied earth dams are in different zones of Italy with various geological situations and climate conditions. The group consists of:

- *29 zoned earth dams*, located in different geomorphological regions of Italy;
- *One homogeneous earth dam with fine grained soil (*Cillarese Dam);
- *3 homogeneous earth dams with coarse grained* soil with waterproof covering on the upstream face (Zoccolo and Maria al Lago Dams in the North and Monte Cotugno Dams in the South of Italy);

[1] The study was developed from the Sub-Committee of the Materials of the Italian Committee of Large Dam and its President Eng. Luigi Carati. The entire work was edited by the members of the Sub-Committee: Prof. Eng. R. Jappelli, Prof. Eng. A. Pellegrino and Ing. T. Silvestri; and with the collaboration of Eng. M. Paparo Filomarino, Eng. F. Ricciardi, Eng. A. Ambrosanio, Eng. G. Baldovin, Eng. F. Bigalli, Eng. A. Chiari, Eng. G. Cusmano, Eng. F. Dolcimasculo, Eng. F. Mercogliano, Eng. A. Motta and Eng. S. Valoroso.

- *4 waterproofing face rockfill dam* (Lago Verde Dam in the North, Contrada Sabetta in the South of Italy, the Vasca Ogliastro in Sicily and Pedra è Othoni Dam in Sardinia island).

In the next paragraphs, the report has been resumed in order to described the peculiar characteristics of existing earth dams in Italy.

2.1.1. The employed material of Italian earth-fill dams

Both natural and properly treated materials were employed for the construction of Italian earth dam structures.

Natural materials have different origins and geotechnical characteristics. Natural material grading is extremely variable and they can be classified in three groups:

- *Fine grained materials*;
- *Continuous graded materials*;
- *Coarse grained materials*.

Generally, *fine grained materials* have been employed for the construction of core zones or homogeneous embankments. According to the Jappelli's research (Japelli and Silvestri, 2005), as far as the fine-grained materials are concerned, the clay amount is always present between 5% and 40%, the plasticity is generally medium and ranges in most cases between 10% and 30% and the liquid limit ranges between 25 and 60%. Figure 2.5 shows results about the grain distribution, the plasticity index and the liquid limit for the core of some example of Italian earth dams.

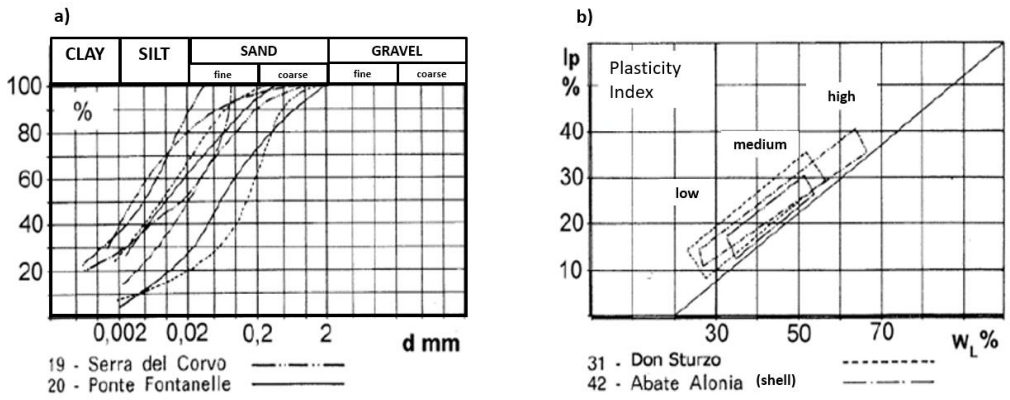

Figure 2.5: Example of grain distribution a) and plasticity areas b) for fine grain material of Italian earth dams (Japelli and Silvestri, 2005).

Continuous graded materials were used both in dam cores and shells. In the core, the clay amount usually does not exceed 40%, the silt ranges between 10-30%, the sand ranges between 20-30%, whereas the gravel is in a range between 10% and 60%. The grain distribution curves are straight, resulting in a higher permeability of the soil (Figure 2.6a). In the shells, the continuous graded materials are mostly composed by gravel with a percentage up to 80% and a minor percentage of silt and clay. In the shell, the grain distribution curves are more arcuate resulting in a reduction of the permeability of the soil (Figure 2.6b).

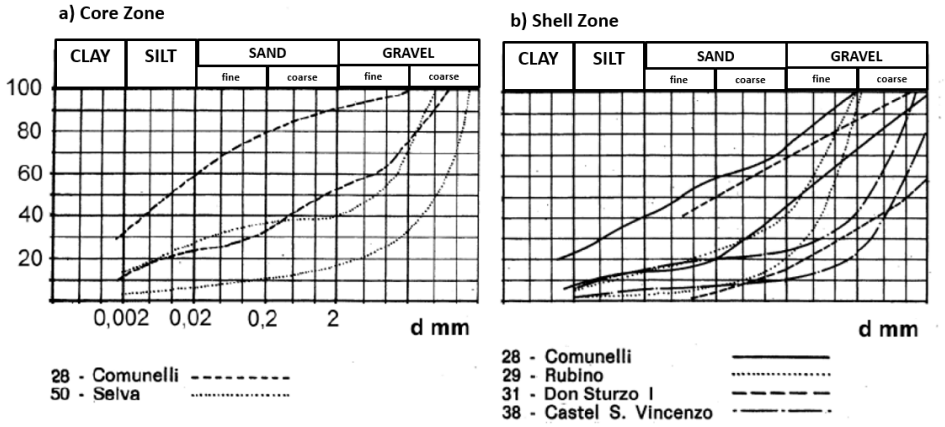

Figure 2.6: Example of grain distribution areas for continuous graded material of Italian earth dams: a) employed materials for the core zone; b) employed materials for the shell zone (Japelli and Silvestri, 2005).

Figure 2.6 shows results about the grain distribution for the core and the shell zone of some example of Italian earth dams with continuous graded material.

Coarse grained materials were used for the shells of numerous dams and for the embankment of homogeneous earth dams with impervious upstream face. These materials are characterized by a higher percentage of gravel and rock, as showed in Figure 2.7.

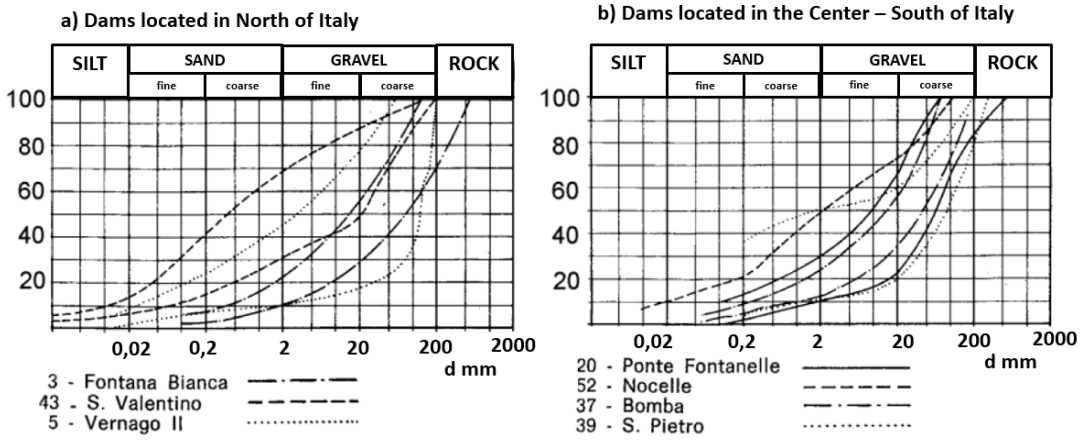

Figure 2.7: Example of grain distribution areas for coarse grained material used for existing Italian earth dams: a) dams located in the North part of Italy and b) in the center-South part (Japelli and Silvestri, 2005).

The employed ***treated materials*** can be classified in two main groups: *rockfill* and *grain mixtures*.

Rockfill has been employed for the construction of specific zone of dam embankments: drains, downstream toes, upstream surfaces, or the shells of rockfill dams. Rockfill was obtained by crushing compact and soft rocks. Their characteristic depends on the nature of the rock where they are extracted. When the material is extracted from compacted and hard rock, brownstone and basalt, the bocks can reach the maximum size of 1500 mm. When the material originates from soft limestone the grain distribution is quite variable. Figure 2.8 shows some example for the grain distribution of treated soils, used for the construction of shell zone or the embankment of existing Italian earth dams.

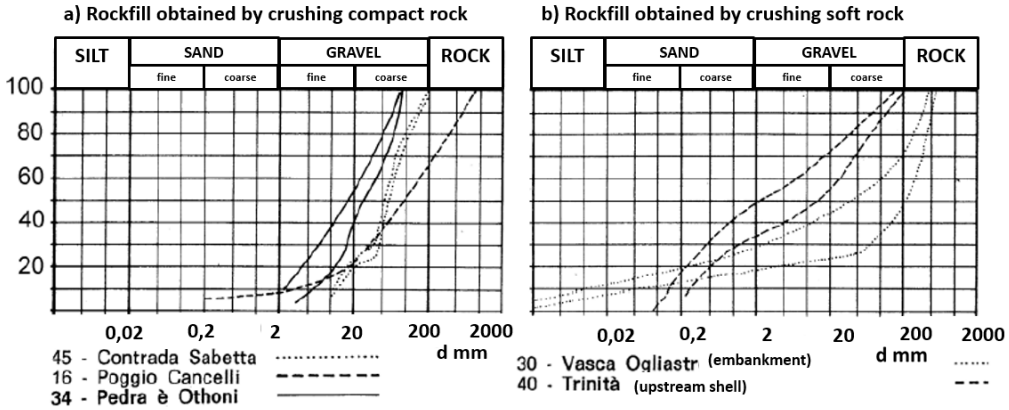

Figure 2.8: Example of grain distribution areas for rockfill material used for existing Italian earth dams: a) rockfill obtained by crushing compact rock and b) rockfill obtained by crushing soft rock (Japelli and Silvestri, 2005).

Grain mixtures were used for the contruction of the core of zoned earth dams. Observing the studied group of dams, these soils were generally employed before 1970. In the last years, there has been a reduction of the use of grain mixtures due to their excessive cost. These soils have a grain distribution very variable: 25-70% of gravel, 20-30% of sand and little amount of lime and clay (Figure 2.9).

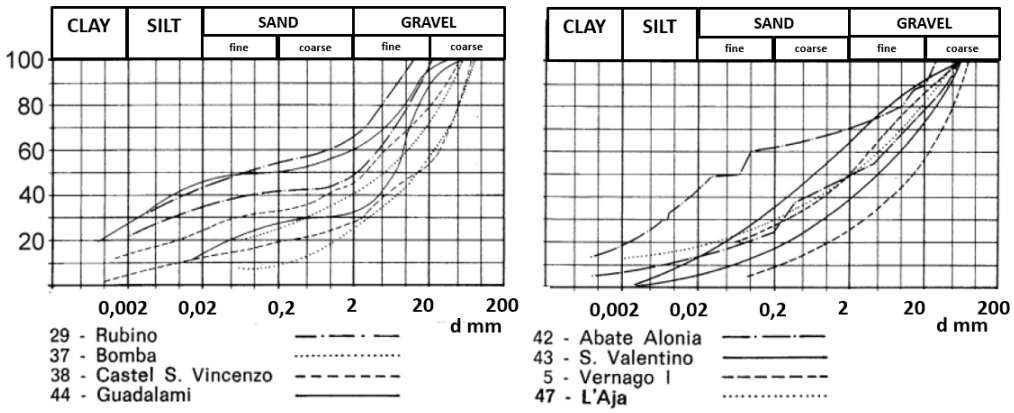

Figure 2.9: Example of grain distribution areas for mixture material used for the core zone of existing Italian earth dams

First, sieving has been used during the preparation of grain mixtures to remouve the coarser fraction from the original material (groundwater debris). Then, fine fraction (bentonite) is added with the coarser fraction and mixed in order to reduce the permeability of the soil.

Figure 2.10 shows the sieving system and the mixing plant for obtaining the core soil of Vernago Dam, in the Northern Italy.

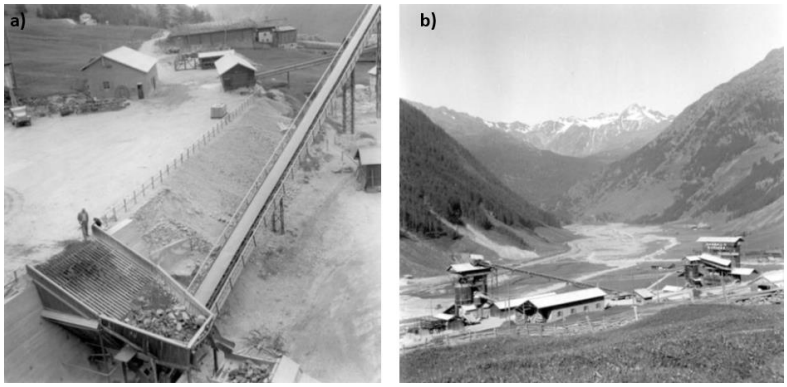

Figure 2.10: Sieving system a) and the mixing plant b) for obtaining the core soil of Vernago Dam (Japelli and Silvestri, 2005)

2.1.2. Typical cross section of existing Italian earth-fill dams

The design of embankment dams is site-specific and cannot be generalized. The design must be suited to valley shape and foundation geology, available materials and methodology of construction. Since the primary function of a dam is to create a storage reservoir behind it or to raise the water level for power generation, a narrow gorge and a wide valley on the upstream for the reservoir are the greatest asset. The design procedure requires adoption of a trial section based on available information, its check for stability and modification to meet the safety specifications and to obtain the functional requirement at minimal costs.

Although the earth dams design cannot be generalised, some executive detail must be considered.

The embankment represents the principle part of an earth-fill dam and its design must respect certain guidelines to optimize dam design. Exploring and studying the typical cross-section of existing Italian earth dam, it is possible to resume the specific characteristics of these constructions.

The typical cross section of *Italian existing zoned earth dams* is showed in Figure 2.11 and Figure 2.12.

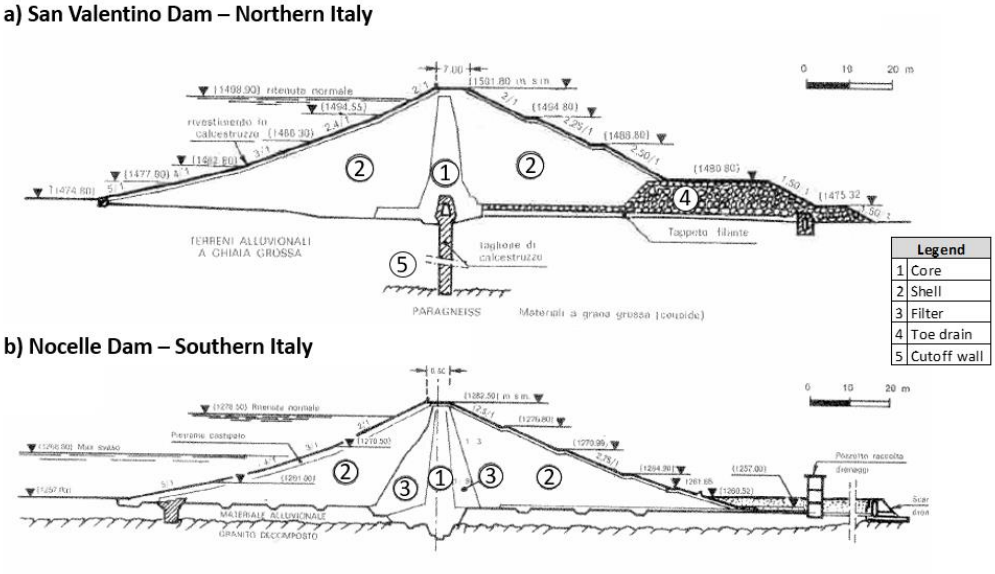

Figure 2.11: Typical cross section of existing zoned earth dam in Italy (Jappelli, Pellegrino et Al., 1981)

The observed sections (Figure 2.11 and 2.12) are characterized by an impervious zone, the "core", which is placed inside dam structure. According to Bharat and Varshney (1995), the core thickness may vary in the extreme range of 0,1H to 0,11H (Figure 2.11), but most of cases lies between 0.5 to 0.33H (Figure 2.12b).

The core can be in the central position (Figure 11 and 12b) or on the slanting slope (Figure 12a). The central core is not exactly symmetrical: it has a steeper downstream slope and a flatter slant in the upstream slope, generally of 1H:5V. Usually, the inclined core has an upstream slant of 0,5H:1V (see the example showed in Figure 2.12a). An inclined upstream core allows the downstream portion of the embankment to be placed first and the core later and reduces the possibility of hydraulic fracturing. However, a vertical core located near the center of the dam is preferred over an inclined upstream core because the former provides higher contact pressure between the core and foundation to have greater stability under earthquake loading and better access for remedial seepage control.

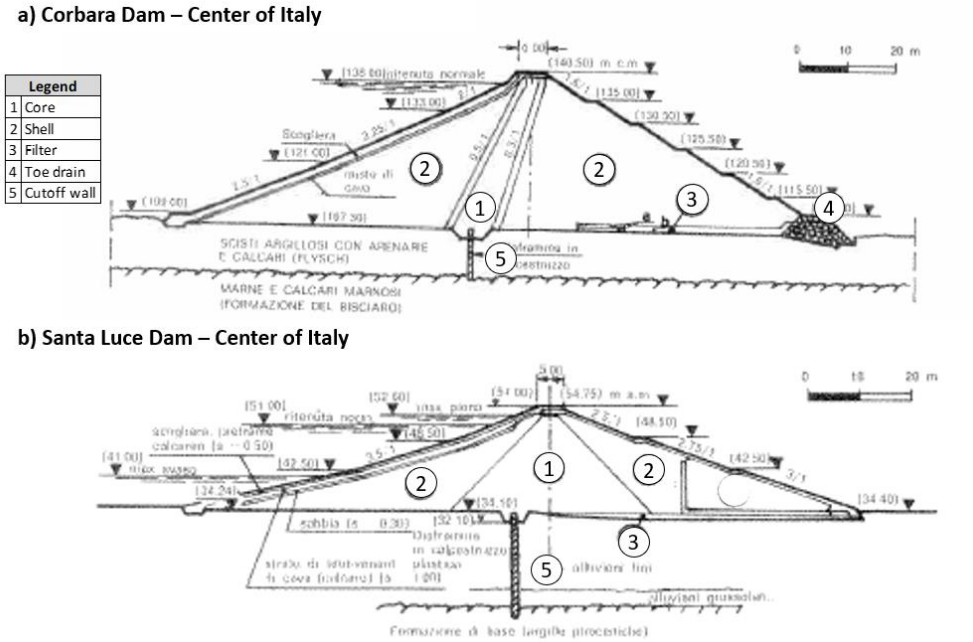

Figure 2.12: Examples of typical cross section of existing zoned earth dam in Italy (Jappelli, Pellegrino et Al., 1981)

When the grains gradation between the core and the shells is quite different, the embankment zoning should provide an adequate transition zones as the internal filtering in the Nocelle Dam (Figure 2.11b).

When the foundation is composed by loose or soft soil layers, a wall of impervious material (e.g., concrete, asphalt concrete, steel sheet, piling, etc.) must be built under the core to reduce the seep rate under the dam (Figure 2.12a and 2.11).

According to the observed group of dams (Jappelli, Pellegrino et Al., 1981), the typical upstream slope has a relatively flat slant (from 5H:1V up to 2H:1V) as insurance against possible instability being the saturated section. Downstream slopes are slightly steeper (from 3H:1V to 2H:1V).

The typical cross section of Italian existing earth-core rockfill dams is showed in Figure 2.13.

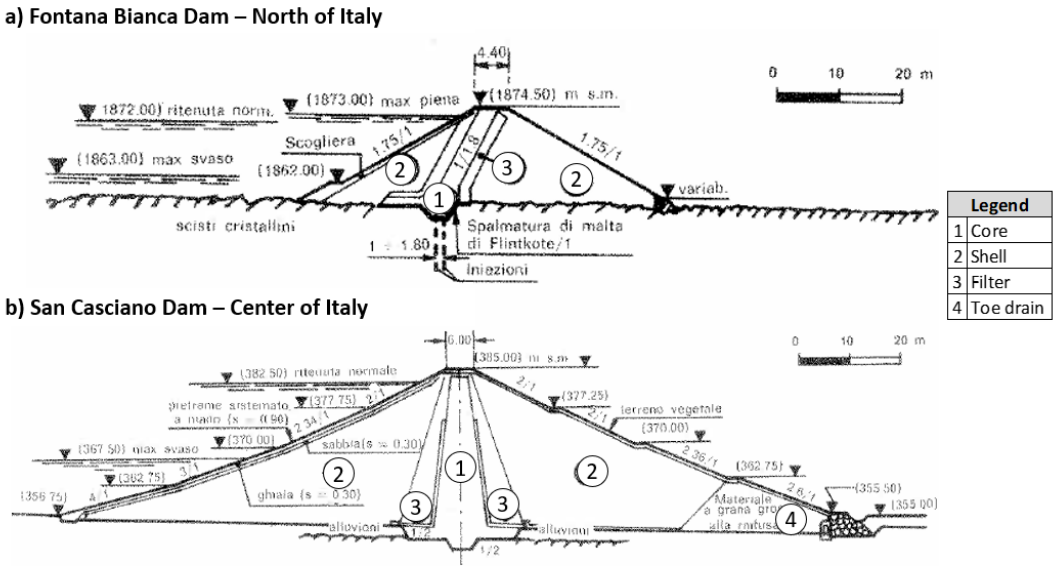

Figure 2.13: Examples of typical cross section of existing earth core rockfill dam in Italy (Jappelli, Pellegrino et Al., 1981)

The earth core rockfill dams (ECRD) are types of zoned earth dams. Rockfill dams with earth core section usually have both rockfill shell zones with an impervious core zone in the middle and transition zone and/or filters in-between (Figure 2.13 a and b). They may be further zoned using material type size gradation or different degree of compaction within each category also. The good-quality of rockfill material can provide free drainage and high shear strength. Slopes can be reduced to around 2H:1V upstream and 1.75H:1V downstream (Figure 2.13a) (or 1:2.25 upstream and 1:2 downstream for sites where only relatively poor impermeable material is available) and the material excavated in the construction

of the core can be used in the embankment, thus economizing on the use of earthworks.

Two examples of typical cross sections of Italian rockfill dams with impervious upstream face are showed in Figure 2.14.

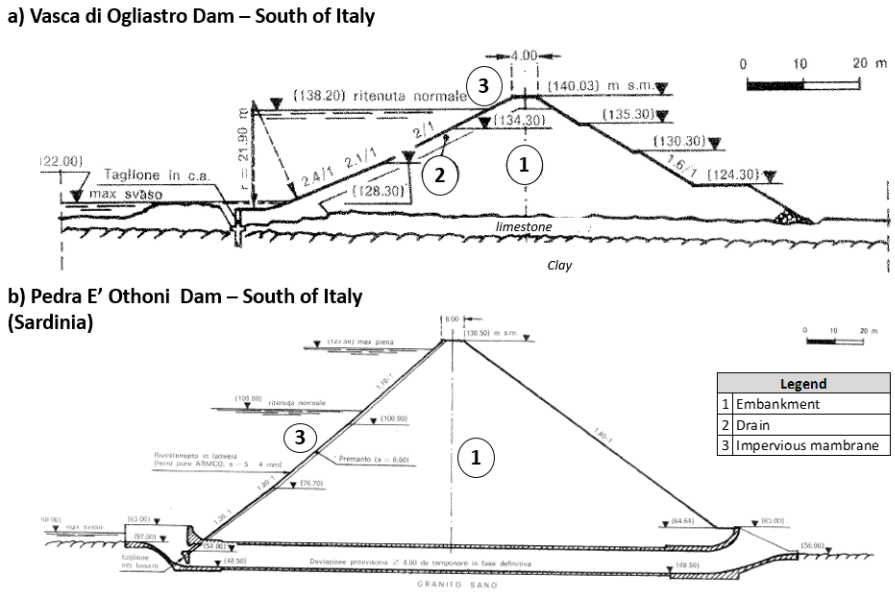

Figure 2.14: Examples of typical cross section of existing rockfill dam with impervious face in Italy (Jappelli, Pellegrino et Al., 1981)

In this type, the entire section consists of rockfill which is usually divided into different size gradations (Figure 2.14a). The impervious element is provided by an up-stream facing which is usually made with concrete or bitumen materials. This type of section should be placed on rock foundations where the suitable earth core material is not available in adequate quantity. Observing the Figure 2.14b, slopes can be reduced to around 1.1H:1V upstream and1.40H:1V downstream.

Earth dams with impervious face on the upstream slope present similar geometry. In these cases, the embankment is composed of coarse grained material and the slopes have a flatter slant.

Another example of existing Italian dam typology is represented by the Marana Capaciotti dam (Figure 2.15). This is a *homogeneous earth embankment*, of 48 m high, located in Puglia, South-East of Italy. The embankment was built between 1970 and 1975 using compacted cohesive materials (mainly sandy and clayey silts of

low plasticity) with relatively homogeneous granulometry and index properties. The embankment contains the drainage system, consisting of a sub-vertical chimney drain that discharges any seepage through the dam to a horizontal drainage gallery, and a blanket drain reaching the downstream toe of the embankment. Seepage below the embankment is prevented by a concrete diaphragm in the alluvial silt layer. Usually this type of section requires flatter slopes than zoned section due to the presence of low permeability materials.

a) Marana Capaciotti Dam – South of Italy

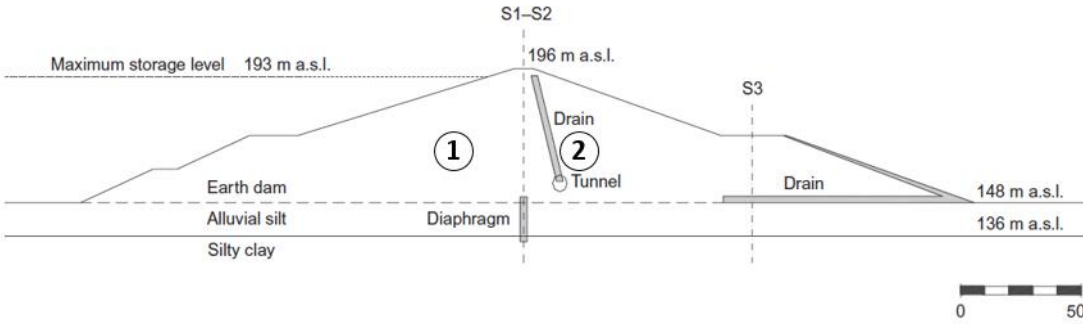

Figure 2.15: Examples of typical cross section of homogeneous earth embankment in Italy (Elia, G. et al., 2011)

In all cases, the crest width is governed by the requirement of transport during construction and traffic across the dam after construction. According to these specific guidelines, the minimum width is at least 4,0 m. Generally, the crest width is about 6 or 8 m.

The safety of embankment dams requires that they must not be overtopped (the only exception being rockfill dams of low height specifically designed to withstand overtopping). This implies that freeboard for embankment dams must be provided on a more conservative basis than for rigid dams. Freeboard is the margin provided above the high flood level to protect dam crest against wave splash, wind set-up, earthquake oscillations, etc. Observing all cases of existing Italian earth dams, the freeboard is about 0,1H. The maximum observed value is for the Cillarese zoned earth dam with a freeboard of 0,3H, located in the South of Italy.

2.2. Seismic behavior of earth crust

The study of the geotechnical earthquake engineering requires an understanding of various processes by which earthquakes occur and their effects on ground motion.

Although earthquakes are complex phenomena, advances in seismology have produced a good understanding of the mechanism and the rates of occurrence of earthquakes in most seismically active areas of the word.

The deformations occur predominantly at the boundaries between plates. As expected earthquake locations would be concentrated near plate boundaries. The map of earthquakes (Figure 2.4) confirms this expectation, supporting the theory of plane tectonics (Kramer, 1996).

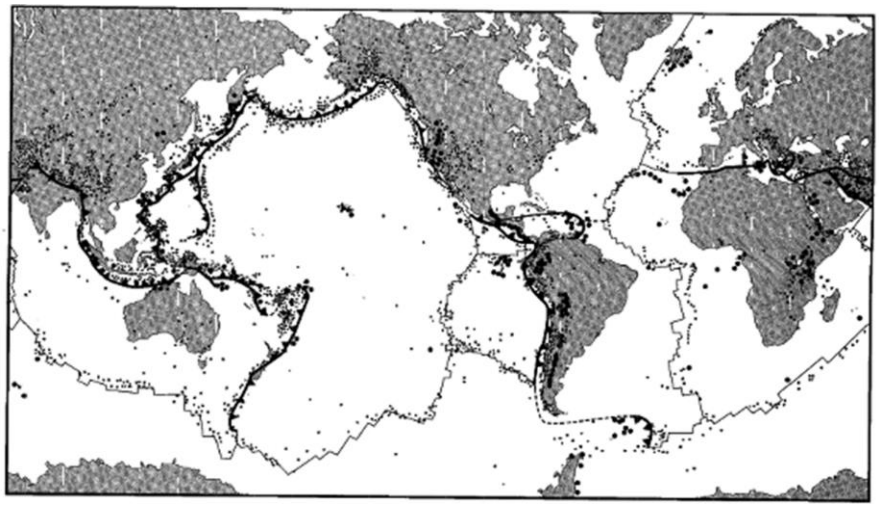

Figure 2.16 The map of earthquake epicenters (Kramer, 1996)

The most widely accepted explanetion of the source of plate movement relies on the requirement of thermomechanical eaquilibrium of earth materials.

The upper portion of the mantle is in contact with the relatively cool crust while the lower portion is in contact with the hot outer core. Obviusly, a temperature gradient must exist within the mantle. The variation of mantle density with temperature produce unstable situation of denser (cooler) material resting on the top of less dense (warmer) material. Denser material begins to sink under the action of gravity and the warmer, less dense material, begins to rise. The sinking

material gradually warms and becomes less dense; eventually it will move laterally and begin to rise again as subsequently cooled material begins to sink. This process is known as the *convection process*.

Earthquakes are generated when the accumulated strain energy is released after a gradual deformation of the lithosphere due to tectonic movements and to fault activity.

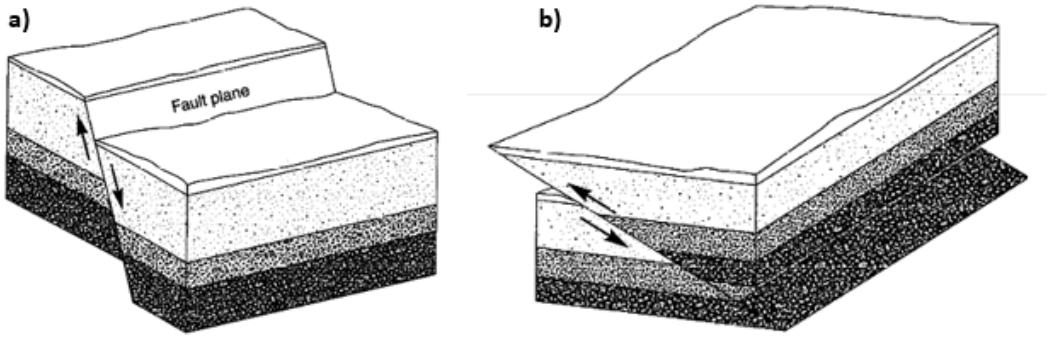

Figure 2.17 Normal faulting (a) and reverse faulting (b) (Kramer, 1996)

Different types of movement occur on a fault which depend on the predominant movement direction. The orientation of the fault plane is described by its strike and dip.

The normal fault (Figure 2.5 a) occurs when the horizontal component of dip slip movements is extensional and when the material above the inclined fault moves downward relative to the material below the fault. When the horizontal component of dip slip movement is compressional and the material above the fault moves upward relative to the material below the fault, reverse faulting is said to have occurred (Figure 2.5 b). A special type of reverse fault is a thrust fault, which occurs when fault plane has a small dip angle. Very large movements can be produced by thrust faulting: the European Alps have been created by thrust movements.

These earth movements produce two type of wave which propagate thought compression and shear mechanism. In general, when an earthquake occurs different types of seismic waves are produces: *body waves* (Figure 2.6) and *surface waves* (Figure 2.7).

The *body waves* can travel through the interior of the earth (compressional, P-waves and shear, S-waves, Fig.2.6) whereas the *surface ones* are produces by the interaction between body waves and boundaries and they are Rayleigh and Love waves (Fig. 2.7), (Kramer, 1996).

Seismic waves move from the source of the earthquake to the site of interest and they tend to attenuate with distance for the material damping and radiation phenomena. The first is related to dynamic material behavior and the second is related to the geometrical spreading of waves within the earth's space.

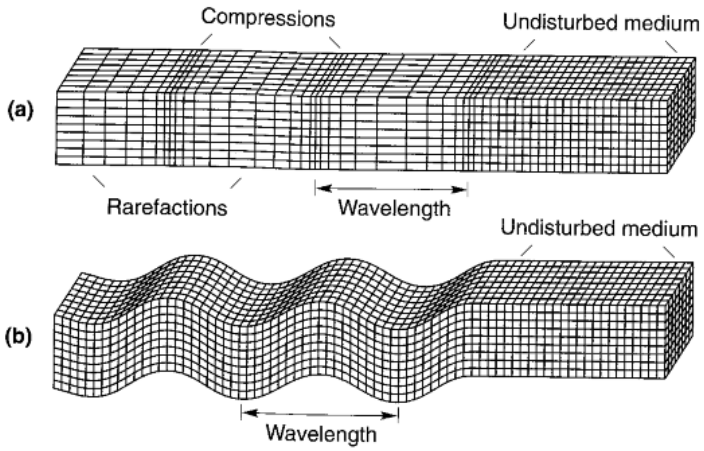

Figure2.18 Seismic body waves: P-waves (a) and S-waves (b). (Bolt, 1993)

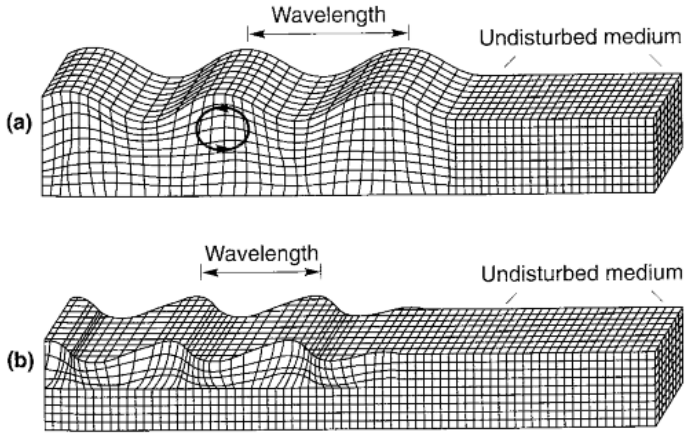

Figure 2.19 Seismic surface waves: Rayleigh waves (a) and Love waves (b). (Bolt, 1993)

The motion of these waves within the earth produces the densification of the soil and the change of soil properties. Moreover, the deformation of the structure involves in phenomena of cracking, landslides, liquefaction. When the water is

present, the soil strength can reduce significantly due to excess of pore water pressure and hence liquefaction may be observed. Liquefaction is an important issue that need to be appropriately addressed with seismic soil behavior and refers to loss of shear strength due to generation of excess pore water pressures under undrained loading.

2.2.1 Ground seismic response in a visco-elastic medium

The engineering significance of the ground response is that the soil layer may amplify or de-amplify the motion from the bedrock and even change its frequency content. Moreover, the surface topography can affect the dynamic response.

The ground response analyses are used to predict ground surface motions for the development of design response spectra, to evaluate the dynamic stresses and strains for evaluation of liquefaction hazard and to determine the earthquake-induced forces that can lead to instability of earth and earth-structures such as dams. Under ideal conditions, a complete ground response analysis would model the rupture mechanism at the source of an earthquake, the propagation of the stress waves through the earth at the top of the bedrock beneath a site and would then determine how the ground surface motion is influenced by the soil that rests above the bedrock.

The actual mechanism of fault rupture is effectively complicated.

Both analytical and numerical methodologies have been developed during the time. Analytical analysis is based on simplifying assumptions and provide valuable information about the dynamic response of soil layers (damped or undamped) on top of the bedrock (rigid or not).

In this section, the simplified analytical evaluation of the waves propagation within the soil structure has been presented. Although this simple method can rarely be applicable for the evaluation of the seismic response in complex structures, it illustrates some of the important effects of soil deposits on ground motion characteristics without undue mathematical complexity.

The analytical solution is based on the assumption that a harmonic horizontal motion at the bedrock produces vertically propagating shear waves in the

overlying visco-elastic soil with a free surface (t(z=0) =0), (Kramer, 1996), shown in Figure 2.8.

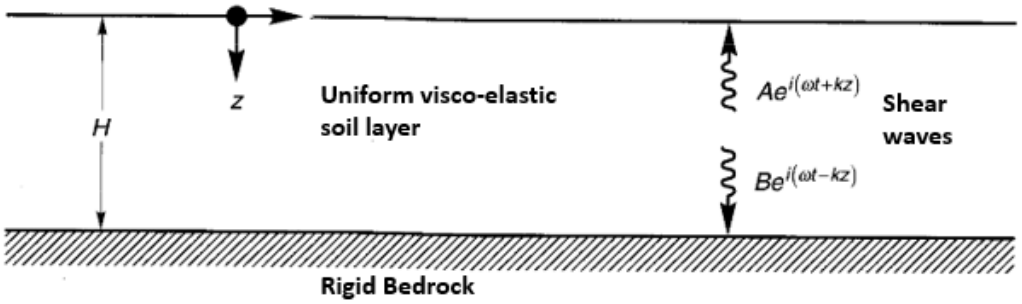

Figure 2.20 Visco-elastic soil deposit of thickness H on rigid bedrock (Kramer, 1996)

The amplification factors can be obtained as the absolute value of the Transfer Function, described as the ratio between the displacement amplitudes at any two points of the soil layer (Eq. 2.1).

$$F_{(\omega)} = \frac{u_{\max(z,t)}}{u_{\max(H,t)}} \quad (2.1)$$

Where ω is the circular frequency of ground shaking, u_{max} is the maximum amplification of the horizontal displacement, z is the depth from the surface, H is the height of the soil layer and t is the time.

The amplification ratio for a uniform visco-elastic soil layer on rigid rock is given by Eq. 2.2.

$$\left|F_{(\omega)}\right| = \frac{1}{\sqrt{cos^2(\omega H/V_s)+[D(\omega H/V\_s)]^2}} \quad (2.2)$$

Where V_s is the shear wave velocity of the soil, H is the height of the soil deposit, ω is the circular frequency and D is the damping ratio.

The variation of the amplification ratio with the frequency is shown for different level of damping in Figure 2.9.

It can be seen that the peak values of the function occur at different values of circular frequency, which correspond to the natural mode of vibration of the soil layer, ω_n (Eq. 2.3).

The n^{th} natural frequency of soil layer is given by

$$\omega_n = \frac{2n-1}{1}\frac{\pi V_s}{2H} \quad n=0,1,2,\ldots\infty \quad (2.3)$$

The greatest amplification factor will occur approximately at the lowest natural frequency ω_1, known as the fundamental frequency of the soil deposit (Eq. 2.4 and Eq. 2.5).

$$\left|F_{(\omega 1)}\right| = \frac{1}{\sqrt{cos^2(\pi/2)+[D(\pi/2)]^2}} = \frac{2}{\pi D} = \frac{0.637}{D} \quad (2.4)$$

$$\omega_1 = \frac{\pi V_s}{2H} \quad (2.5)$$

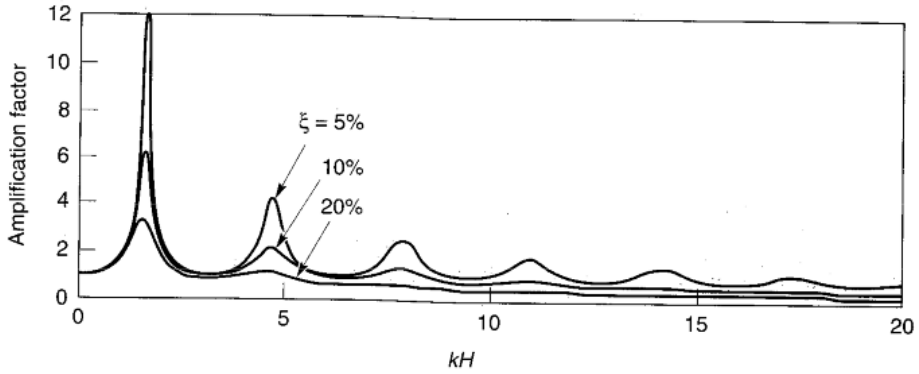

Figure 2.21 Amplification Factor for a visco-elastic soil layer in rigid rock (Kramer, 1996)

The period of vibration corresponding to the fundamental frequency is called characteristic site period, Eq. 2.6.

$$T_s = \frac{2\pi}{w_1} = \frac{4H}{Vs} \quad (2.6)$$

2.2.2 Stress-strain behavior of cyclically loaded soil

Under seismic loading, soil response can be highly nonlinear. In general, seismic waves produces the motion of the soil particles and the change of soil material properties.

The wave propagation produces a vibration into the ground which induces shear strains γ which affect the stiffness of the soil (represented by the shear modulus $G=\rho V_s^2$).

The typical shear stress-strain curve for a cyclic loading can be represented by the initial loading path (the backbone curve) and the hysteretic loop (which is related

to the stiffness of the soil and the energy dissipation developed during the motion).

The energy dissipation can be described by the Damping Ratio D, which represents the ratio between the energy dissipated (D_W) and the maximum strain energy (W), Eq. 2.7 (see Figure 2.22).

$$D = \frac{1}{4\pi}\frac{\Delta W}{W} \quad (2.7)$$

The inclination of the loop depends on the stiffness of the soil which can be described at each point by the tangential shear modulus, G_{tan}, whereas its average value over the entire loop can be approximated by the secant shear modulus, G_{sec}.

The Figure 2.22 shows that the dynamic soil properties, stiffness G and damping ratio D, change with the shear strain level, γ.

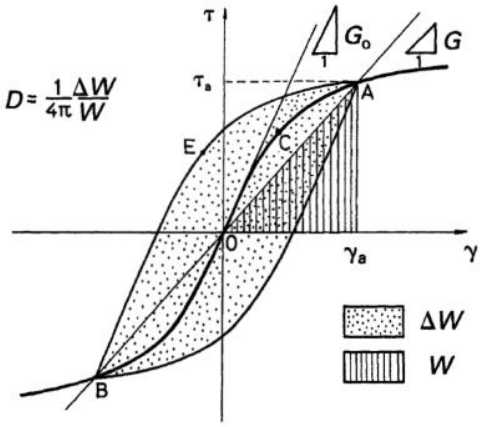

Figure 2.22 Shear stress-strain relationship – backbone curve and hysteresis loop (Ishihara, 1995)

The stiffness tends to decrease with increasing of shear strain, whereas the damping increases as the increasing of the deformation. Laboratory tests have showed that soil stiffness and damping ratio are also influenced by void ratio e_0, mean confining pressures σ'_m, plasticity index PI, over-consolidation ratio OCR, and number of loading cycles, N (Kramer, 1996).

The mechanical soil behavior under cyclic load can be represented for different level of accuracy. The accuracy depends on factors which detail the constitutive model.

2.3. Review on factors affecting the dynamic response of dams

In order to make a realistic prediction of the response of an earth dam undergone to a particular earthquake shaking, an updated review on factors which affect the dynamic response of dams has been defined.

Careful consideration must be given to the potential effects of the following major phenomena/factors:

- ✓ Seismic input;
- ✓ In-homogeneity: dependence of soil stiffness on confining pressure;
- ✓ Nonlinear-inelastic soil behavior (especially during strong earthquake shaking);
- ✓ Effects of narrow canyon geometry;
- ✓ Interaction between the dam and the supporting soil-rock system;
- ✓ Influence of Frequency-Dependent Soil Behavior on Site Response Analysis;
- ✓ Influence of soil compaction;
- ✓ Liquefaction of dam's soil
- ✓ Ground-motion asynchronism effects
- ✓ Hydrodynamic effects and dam-reservoir interaction
- ✓ Other factors.

All the aforementioned factors play a different role in the dynamic behavior of rockfill dams. Their influence depends on the type of dam and on the magnitude of the seismic event.

2.3.1. Seismic Input Motion

One of the most important factors governing the nonlinear dynamic analysis of earth dams is the definition of the input motion at the bedrock.

In order to follow this aim, the selection of specific ground motion-time histories are required.

Earthquake ground motion can be characterized by many different parameters, each of which reflects some feature of the shaking such as the peak amplitudes, the frequency content, or the energy carried in the signal. A complete characterization of the ground motion must include a measure of its duration, or more specifically the duration of that part of the signal that is strong (Bommer & Al., 2009).

For a specific ground motion, the most commonly used amplitude parameter is represented by the peak ground acceleration (PGA) (Kramer, 1996). In general PGA is related to the peak horizontal acceleration (PHA) due its natural relationship to inertial forces, indeed vertical accelerations have received less attention in earthquake engineering than horizontal accelerations. Ground motion with high peak accelerations are usually more destructive than motions with lower peak acceleration but this is not always true. In fact, earth structures subjected under earthquake with a very high peak acceleration (more than 0,5g) but for a very short time have shown really little damage.

Since earth structures are not rigid construction, their dynamic responses are very sensitive to the frequency at which they are loaded. Since earthquake motion contains a wide range of frequencies, the parameter which can meaningfully describe how the motion amplitude is distributed among different frequencies is the frequency content, typically expressed in terms of Fourier Spectra or Response Spectra. If the frequency content of a seismic motion is close to the dam's dominant oscillation frequency, resonance effect may arise and it could be very deleterious for the overall stability of embankments.

Together with the frequency content and the amplitude, the duration of a ground motion can have a strong influence on earthquake damage. Many physical processes, such as the stiffness and strength degradation of soils, the power

pressure buildup into loose and saturated sands, are sensitive to the number of load and stress reversals, which occur during an earthquake.

In fact, a motion of short duration may not produce enough load reversals and damages may not occur even for very high amplitude motion. On the other hand, a motion with a moderate amplitude but for long duration can produce enough load reversals and cause substantial damage in earth structures.

Due to the complex phenomenon of ground motion produced by an earthquake, especially into an embankment dams, it is worth to evaluate a specific methodology for the selection of a representative acceleration time history to be assigned as input motion.

As suggested by the recent seismic Italian Code NTC08, (M.LL.PP., 2008; see Chapter. 3), the selected ground motion-time histories must be compatible with the deterministic or probabilistic target response spectrum defined for the considered earthquake scenario.

The procedure consists in selecting an appropriate suite of compatible spectrum records, resumed into these three different steps:

- Definition of the reference acceleration response spectrum at bedrock for the scenario earthquake representative of the seismic hazard for the site where the dam is located, which is based on the new seismic classification of the Italian territory (OPCM n.3519 – 28/04/2006);
- Identification of the magnitude-distance (M-D) pair linked to the previous scenario;
- Selection of the spectrum-compatible acceleration time-histories.

Especially for the numerical analysis of embankment dams (Yule et Al. 2004), this procedure of selecting an appropriate suite of compatible spectrum record is still a challenging issue. Indeed, results of dynamic analysis have shown that source earthquake magnitude, distance and site class are not sufficient criteria to properly select the input motion for the dynamic analysis of earth dams in term of residual displacements.

A new multi stage procedure for the selection of specifics record seems to be more appropriate (Lanzo et Al. 2015).

Other estimators must be taken into account in order to select records and obtain a more adequate representation of dam response under seismic conditions. These estimators are:

- The significant duration Ds, proposed by Bommer et Al. (2009);
- Arias Intensity *Ia*, proposed by Travasarou et Al. (2003), which reflects three important ground motion characteristics: amplitude, frequency content and duration (Kramer, 1996).

Permanent settlements of dam crest increase with the increase of the Arias Intensity of the input motion (Brigante, 2012). According to the study of Lanzo et Al. (2015), it is interesting to note the example in Figure 2.23, where the Cerro Pedro and Gilroy#6 inputs, not selected by the specification of the actual NTC08 (M.LL.PP., 2008), present very large residual displacements on Montedoglio dam crest (Lanzo et Al. 2015).

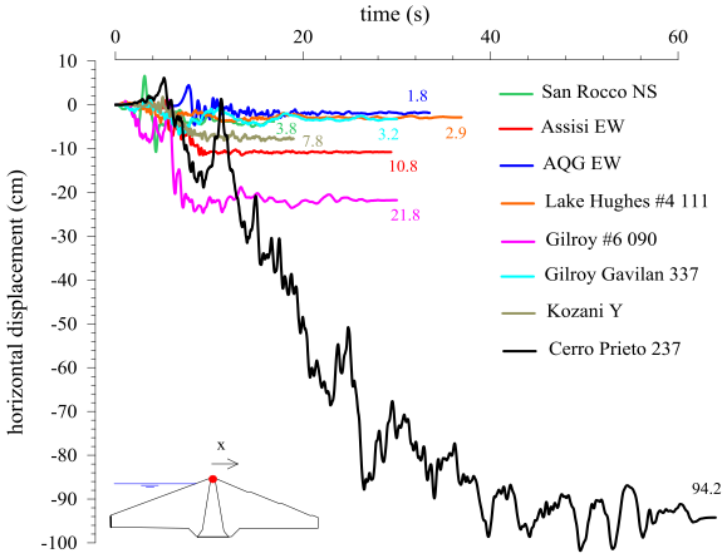

Figure 2.23 Horizontal displacement time-histories computed at crest for the 7 accelerograms selected and the Cerro Prieto 237 recording (Lanzo et Al., 2015).

2.3.2. Inhomogeneous dam materials

Earth dams are usually constructed in layers which are then compacted to increase their density and strength.

This construction process results in non-homogeneous dam material, especially concerning the shear stiffness, G_{max}, due to its spatial variation.

Laboratory investigations on soil stiffness have established the dependence of soil shear modulus G_{max} on the confining pressure. Into an earth dams, stiffness varies from point to point and increases with distance from crest and from the two inclined surfaces. Indeed, the average shear modulus G across the dam increases with depth z from the origin.

After the evaluation of parametric analysis, Gazetas (1987) showed the effect of the degree of inhomogeneity on seismic response. He used the inhomogeneous "shear beam" approach (see Par. 3.1.3) on a 2D ideal dam on a rigid base.

Gazetas (1987) expressed the average-across-the-dam modulus G in the following form, $G=G_b(z/H)^m$: where Gb is the average shear modulus at the base, H is the dam's height and the coefficient *m* mainly depends on the dam's inhomogeneity (material and geometry).

It has been noticed that higher "m" values (higher inhomogeneity) leads to:

- a sharper attenuation of mode of displacements with depth (Figure 2.24a) and almost identical fundamental frequency;
- closer-spaced higher natural frequencies (Figure 2.24b), higher displacement and acceleration amplification values at all resonances together with the greater relative importance of the higher modes (Figure2.24d)
- maximum values of shear-strain modal shapes closer to the crest (Figure 2.24c).

Together with the approach on a 2D ideal dam on a rigid base, the linear seismic response of the 120m tall and flexible uniform dam, subjected to the Taft 1952 NE earthquake and modelled as a shear beam, has been studied.

The same analysis shows how the peak acceleration and peak displacements, at the top quarter of the dam, increase with "m" increasing, and the shear stresses are hardly influenced by "*m*". As a result, shear strains, which are inversely proportional to G(z), are strongly influenced by inhomogeneity (Figure 2.25).

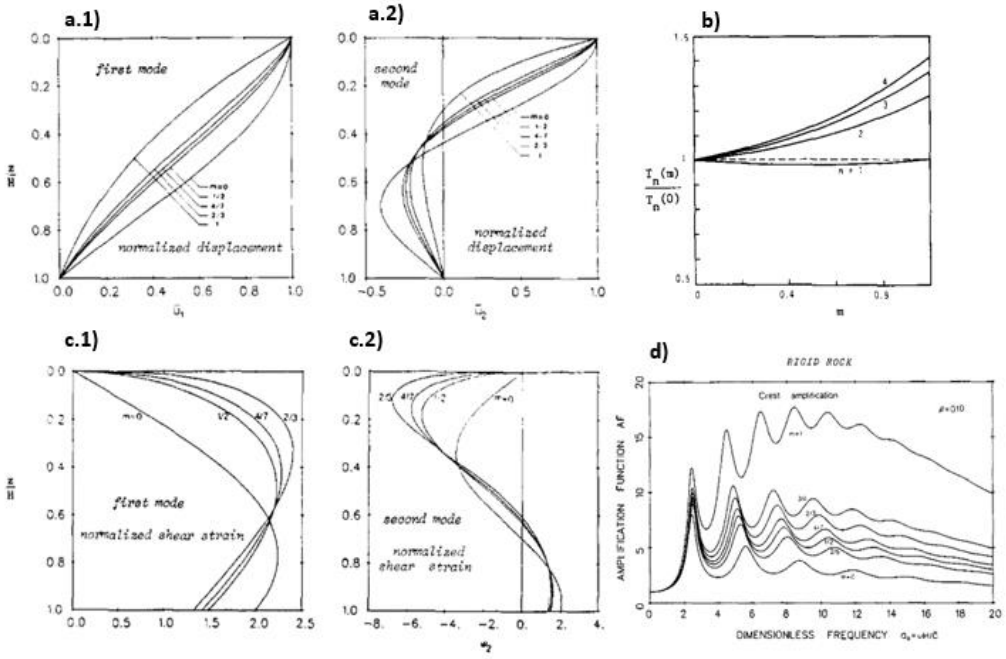

Figure 2.24 Effect of modulus inhomogeneity parameter m on modal displacements, natural periods, modal strain participation factors and amplification function for rigid rock case (Gazetas, 1987)

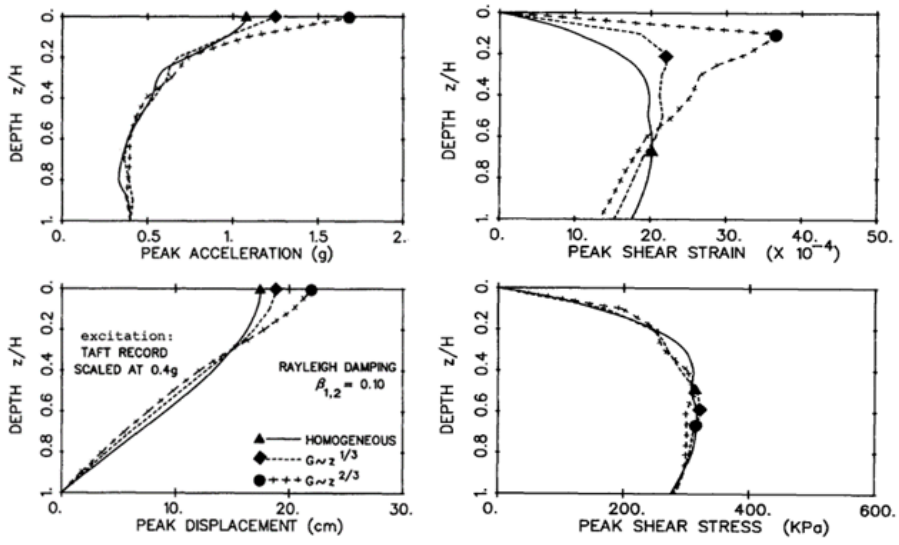

Figure 2.25Effect of inhomogeneity degree on distribution with depth of peak seismic response variable (Gazetas,1987)

2.3.3. Nonlinear inelastic soil behavior during strong earthquake shaking

In order to analyze the nonlinear inelastic soil behavior, the aforementioned case study was investigated under strong ground shaking. The 'Layered Inelastic Shear Beam' approach was used to obtain the nonlinear-inelastic response of the 120m tall dam. In this case, the average stress-average strain backbone relationship for each layer is assumed to be hyperbolic (Figure 2.26 and Eq. 2.8):

$$\tau = \tau(z,\gamma) = G(z)\frac{\gamma}{1+\frac{\gamma}{\gamma_r}} \qquad (2.8)$$

with G(z)=the low-strain elastic modulus=Gb $(z/H)^m$, and γr= the reference strain= $\tau_{max}(z)/G(z)$. These latter values can be considered, for simplicity, equal to 0,003 (moderately nonlinear) and 0,0013 (strongly nonlinear).

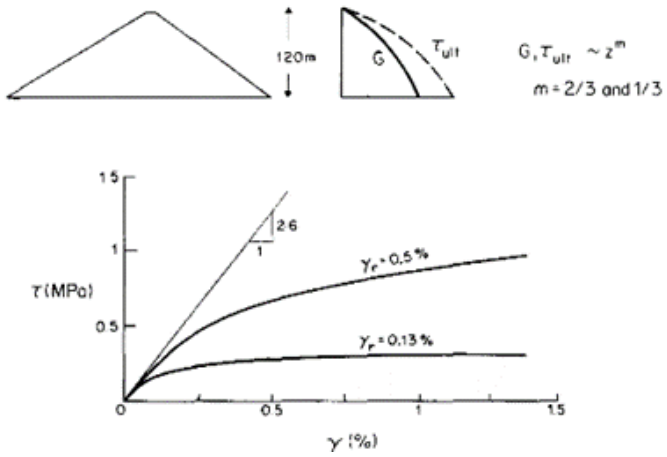

Figure 2.26 Average hyperbolic layer shear stress-strain relations used for inhomogeneity versus nonlinearity study (Gazetas, 1987)

For all types of inhomogeneity (m = 0, 1/3, 2/3) strong nonlinear action leads to substantially reduce the amplification of acceleration and shear strain (Figure 2.27). In this case, it can be observed how non-linearity can be more influential than inhomogeneity related to dam's seismic response. The peak shear strain vs depth shows similar shape comparing the linear elastic analysis with the nonlinear inelastic analysis. Then, the peak acceleration vs depth shows a consistent and strong reduction. In general, the nonlinearity tens to produce a higher damping, elongating the fundamental dam period. Thus, the resonant

effects can be avoided thanks to the extension of dam period, which is well outside the significant period range of seismic motion.

It is worth to underline how nonlinearity plays a negligible rule in case of stiff modern dams subjected to shaking having peak ground accelerations (PGA) of the order of 0.2g or less.

On the other hand, when designing against very strong potential shaking, during which the dam is expected to respond in a highly nonlinear fashion, the other listed phenomena may lose some of their importance.

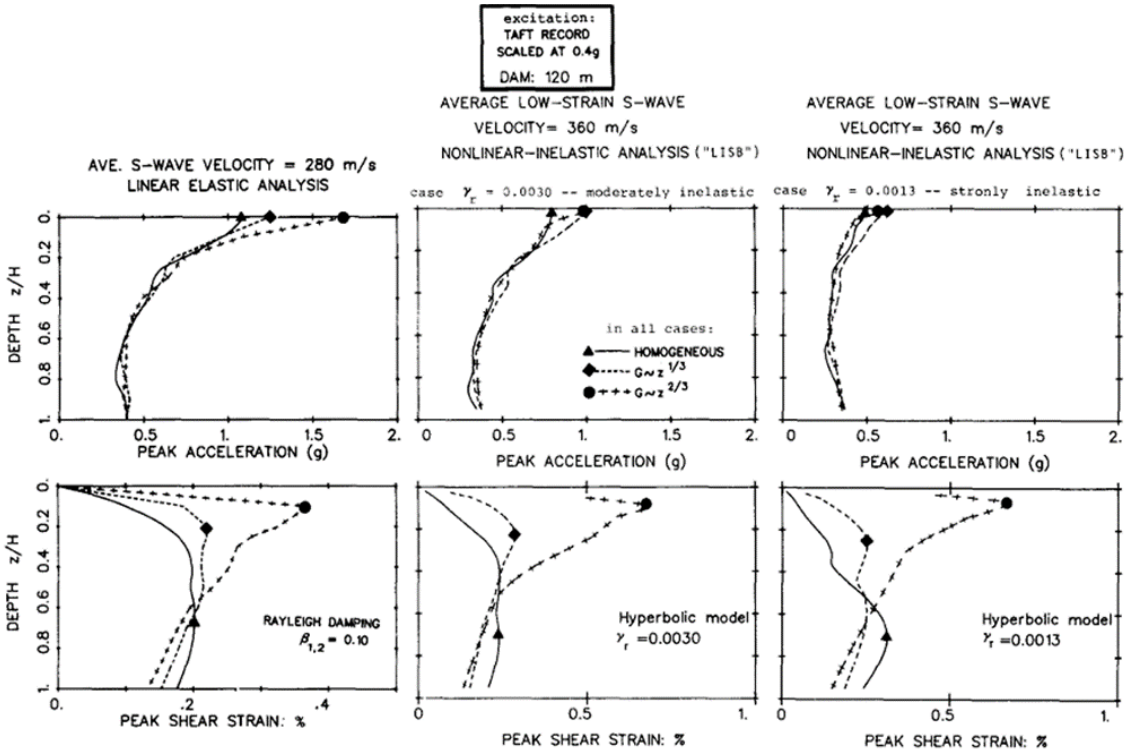

Figure 2.27 For a given excitation, with increasing nonlinear inelastic action: (a) the near-crest peak accelerations decrease and the effects of inhomogeneity tend to diminish; but (b) the peak shear strain distributions remain nearly unchanged, both in magnitude and shape (Gazetas, 1987)

2.3.4. Canyon geometry effects

The plane-strain conditions are valid only for infinitely long dams subjected to synchronous lateral base motion. In case of dams built in narrow valleys, as in mountainous regions, the presence of relatively rigid abutments creates a 3D effects which produce the natural frequencies increase and sharper displacements as the canyon becomes narrower. The 3D effects exist in the stability of an earth-rockfill dam, which is one of the main types of artificial slope and the most popular type of water-retaining structure.

The 3-D effects (the shape and dimensions of the supporting canyon) were first qualitatively studied from Hatanaka (1955) and Ambraseys (1960) who studied the seismic response of a two-dimensional a triangular shaped dam, accounting for a rigid rectangular canyon.

Subsequent works, (Mejia, Seed, & Lysmer, 1982) and (Mejia & Seed, 1983), showed that the presence of the rigid triangular boundary increased the fundamental frequencies, and seemed to substantially increase the seismic acceleration, for cross-sectional geometries.

On Figure 2.28 is shown the narrow canyon stiffening effect on the fundamental natural period, T1=T1 (L/H), of a dam for five different canyon shapes (Figure 2.28 a); $T1,\infty$ represents the natural period of an infinitely long dam under plane deformation, and L/H is the aspect ratio. Both shear-beam and finite-element based results, only for homogeneous dams, are shown in the Figure 2.28.

As it can be seen, for a given aspect ratio and canyon shape, the ratio $T1/T1,\infty$ is hardly influenced by inhomogeneity and hence Figure 2.28b may be used for estimating the canyon effects with any type of dam.

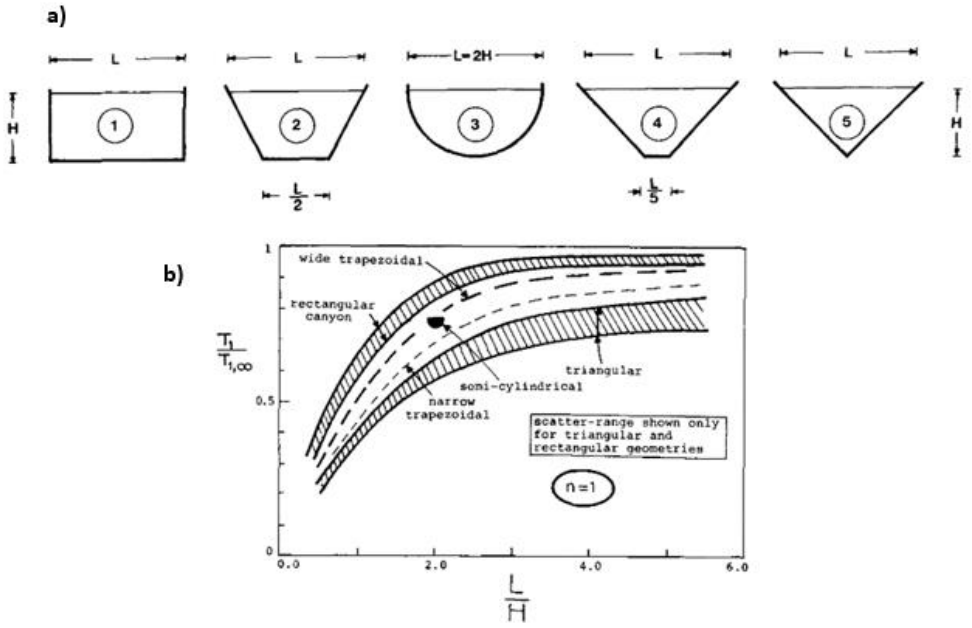

Figure 2.28 Canyon geometries (a) and their effect on the fundamental period (b), (Gazetas (1987)

On Figure 2.29, the effect of a narrow-canyon geometry on the steady-state response of a dam under harmonic rigid base excitation has portrayed. The mid-crest *Amplification Function* (AF) for semi-cylindrical dam from three-dimensional analysis and from plane shear-beam analysis have been compared.

In this figure, it is evident how the plane shear model under-predicts both the amplification at first resonance and the relative importance of higher resonances.

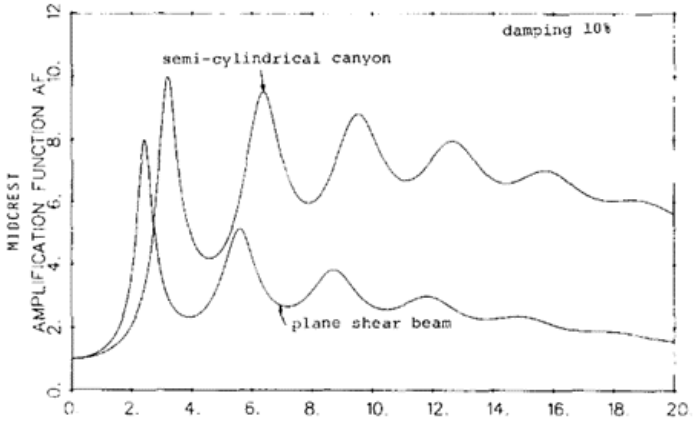

Figure 2.29 Steady-state response to harmonic base excitation: mid-crest amplification function for semi-cylindrical dam determined from 3-dimensional and from plane shear-beam analysis (Gazetas, 1987)

Comparing results on AF at mid-crest for different canyon shapes, for dams with same aspect ratio L/H=2, reveals that the value of AF at first resonance is practically independent of the exact canyon shape.

Earthquake ground excitation differs from a harmonic motion in that it contains a broad spectrum of frequencies, and it is of a random and transient nature.

Thus, the response of an idealized 120 m high dam in a U-shaped canyon has been studied, subjected to the Kern County earthquake, recorded at Taft (USA) during the 1952 and scaled to a peak acceleration value of 0.20g.

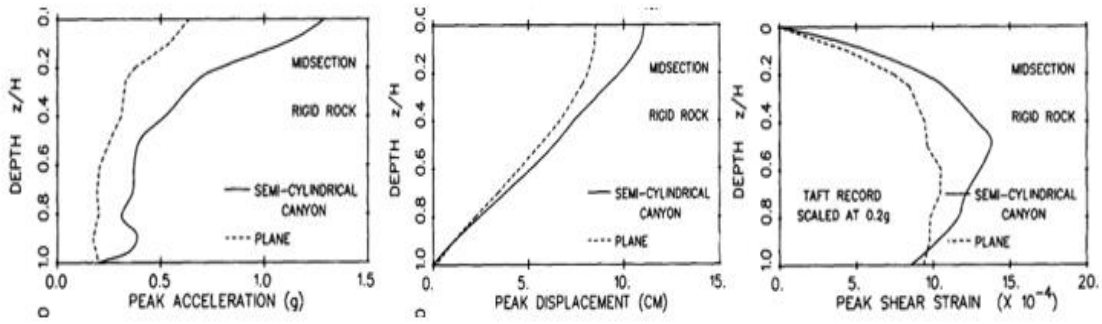

Figure 2.30 Plane versus 3D analyses: distribution with depth of peak response variables (dam:H=120m, Vs=280m/s, Damping=0.10%, PGA=0,20g - Kern County earthquake) (Gazetas, 1987)

Three sets of peak values (acceleration, displacements and strains) on dam midsection are in Figure 2.30, comparing the semi-cylindrical shear-beam canyon and plane shear beam results.

The 2D peak accelerations at the upper third of the dam are only about one-half of the 3D values whereas, displacements and strains from the two models are about equal. These trends seem to be qualitatively valid for different input motions (Dakoulas & Gazetas, 1986).

It is worth to underline that for all the above examples the stress-strain soil behavior was linear elastic. Elastic canyon effect and only later component of motion have been evaluated. In general, soil nonlinearity tends to reduce peak accelerations due to the increase of hysteretic dissipation from wave energy, and the potential removal of any potential resonances. Prevost et al. (1985) observes how nonlinearity may considerably reduce the adverse effects of narrow canyon

geometries on mid-crest accelerations. Both safety and economic factors should be considered in the design of an earth–rockfill dam.

Recent studies have also demonstrated how the 3D effect on the stability of earth–rockfill dam is necessary to obtain a reasonable balance between safety and cost. The 3D effect is sometimes regarded as the safety reserve; nevertheless, if 3D effect is ignored, construction costs may increase (Yuzhen et Al. 2005).

2.3.5. Presence of flexible dam foundation

Due to waves spreading into the supporting valley, part of input seismic energy is dissipated.

In order to take into account of this important aspect, the free-field rock outcrop input motion, rather than at dam basement, has to be considered.

Dakoulas & Hashmi (1991) derived a mathematical solution for the steady-state response of embankment dams in a simple rectangular canyon, subjected to obliquely incident SH waves. The dam is idealized as a bi-dimensional homogeneous triangular shear wedge, consisting of a linearly hysteretic material.

The method has been used in a parametric study to investigate the effects of the S-wave velocity ratio V_{canyon}/V_{dam} on the amplification function (AF) of displacement or acceleration.

Canyon rock flexibility (abutments and base) has a dramatic effect on the response of the dam, indeed it affects the amount of reflected energy that is radiated back into the half-space (canyon). The presence of a flexible canyon-rock tends to reduce the amplification peaks at resonance, especially with weak seismic excitation. Figure 2.31 depicts the amplification for a dam having L/H = 3, and for three different S-wave velocity ratios V_{canyon}/V_{dam}= 3, 10, and ∞.

The mid-crest amplification is about:

- 4 for V_{canyon}/V_{dam} = 3;
- About 6.2 for V_{canyon}/V_{dam} = 10;
- About 10 for V_{canyon}/V_{dam} =∞.

Where the S-wave velocity contrast between dam and canyon is small, mid-crest accelerations may decrease by a factor of about 2, due to the significant amounts of wave energy radiate back into the canyon half-space. Thus, this clearly demonstrates that the simple assumption of a rigid base may be conservative in rectangular canyons.

All this, however, is for dams assumed to be homogeneous. When material inhomogeneity was realistically considered, the 'whip-lash' effect would become stronger and amplification at crest should tend to increase.

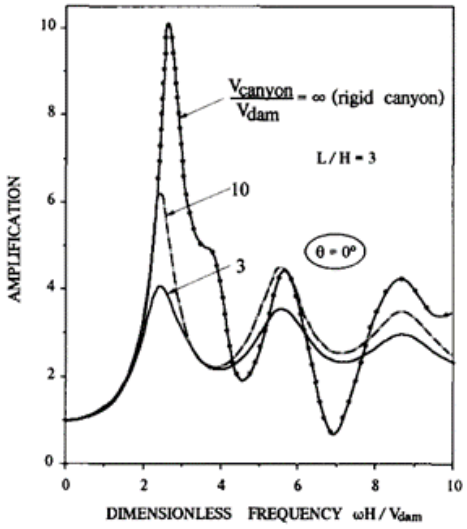

Figure 2.31 Mid-crest amplification versus dimensionless frequency for three dams with S-wave velocity ratios Vcanyon/Vdam= 3, I 0 and ∞ (rigid canyon) in rectangular canyons subjected to vertically propagating SH waves.

2.3.6. Liquefaction of dam's soil

Liquefaction is one of the most important, interesting and complex topic in geotechnical earthquake engineering. The generation of excess pore pressure under undrained loading condition is a hallmark of all liquefaction phenomena.

Liquefaction phenomena can be divided into two main groups: flow liquefaction and cyclic mobility.

The most common type of liquefaction observed in earth dam is flow liquefaction which can be extremely dangerous for the stability of the dam, as it causes large scale failures.

Flow liquefaction occurs when the shear stress for static equilibrium of a soil mass is greater than the shear strength of a soil in its liquefied state (Kramer, 1996). The flow slide failure of Sheffield Dam (Seed, Lee & Idriss, 1969) and Lower San Fernando Dam (Seed, Pyke & Martin, 1975) are examples of flow liquefaction.

Cyclic mobility occurs when the static shear stress is less than the shear strength of the liquefied soil. In this case, the deformations produce by cyclic mobility are driven by both cyclic and shear stresses.

On the embankment earth dams, the absence of the waterproofing face on the upstream slope doesn't guarantee the entire embankment is dry and thus earthquake shaking can cause pore water pressure buildup and strength degradation.

Embankments with loose or saturated sand or placed on fluvial deposit are very likely susceptible to liquefaction.

An analysis technique which considers the pore pressures generated during the cyclic loading and their effects on the stability of the earth structure should be required.

A series of methods have been developed during the years by different authors (Martin et Al., 1975), (Seed, Martin, & Lysmer, 1976), (Ishihara, Tatsuoka, & Yasuda, 1975), (Finn, Lee, Maartman, & Lo, 1978) in order to include considerations of pore pressure redistribution during and following the earthquake shaking.

2.3.7. Ground-motion a-synchronism effects

Under seismic motion, the deformability of an earth dam may induce several effects, including ground motion amplification and asynchronism between different points of dam embankment. During seismic shaking, induced earthquake waves strike dam surface and body at various angle and create reflection and diffraction phenomena. The resulting oscillations may differ in phase, amplitude and frequency content, from different point of dam body.

In an earth dam, the development of asynchronous (i.e. out of phase) motions can be related to the characteristics of the input motion (frequency content, amplitude

and duration) but also to the features of dam embankment (geometry, soil stiffness and damping).

In general, asynchronism tends to increase when higher vibration dam modes are excited. This is the case of very high dams or embankments made with a very deformable material.

Some studies in the literature show how the asynchronous effects can partially compensate the effects of local amplification into dam body. As far as the severity of the earthquake increase, dissipative effects (i.e. hysteretic damping) increase, thus reducing amplification: contextually stiffness decrease, thus enhancing asynchronism (Bilotta et Al. 2010, Bilotta & Siervo, 2012, Brigante & Sica, 2010).

From a practical viewpoint, it is important to analyze asynchronous effects when strong earthquake occur: in this case, the evaluation of dam safety with respect to global instability becomes meaningful.

2.3.8. Hydrodynamic effects and dam-reservoir interaction

The interaction between dam body and the reservoir describes the reciprocal influence exerted by the reservoir and the dam during an earthquake. The reservoir water act as a load on the upstream face, inducing stiffening effects due to increasing confining pressure of dam's soil.

Water compressibility (and associated radiation damping when the reservoir is quasi-infinite extent in the upstream direction) and energy dissipation at the reservoir bottom and sides are considered in a rigorous formulation.

A simplification consists on assuming water as incompressible. The value of the resulting entrained mass of water depends primarily on the slope of the upstream face. It reaches its maximum for a vertical face and is null for a horizontal one. Because of the inclination of the upstream face of an embankment dam, the entrained mass is limited and the simplest formulation is usually adequate (Darbre, 2000).

In general, hydrodynamic effects can be safely ignored in the estimation of the seismic response of earth dams (Bureau, Volpe, Roth & Udaka, 1985). For more details, see Paragraph 3.2.3.6..

Chapter 3

SEISMIC RESPONSE ANALYSIS OF DAMS

3.1. Dynamic Analysis Methods

A number of technique for the analysis of inertial instability has been proposed during the development of geotechnical earthquake engineering.

These techniques differ primarily in the different accuracy used for representing the earthquake motion and the dynamic response of slopes.

The various methods fall into several categories according to the main objective of the analysis:

- assessment of the stability of the dam structure (such as the pseudostatic analysis);
- calculation of the permanent displacements of the dam body (such as the sliding block method);
- evaluation of the dynamic response of the whole dam (such as the shear beam and the finite element methods).

This chapter describes the various methods used in seismic analysis of earth dams and the most important methodologies developed over the years. Finally, a discussion regarding the methodology employed in this thesis will be defined.

3.1.1. Pseudo Static method

The pseudo-static (PS) analysis represents the simplest and the oldest method for the evaluation of the seismic stability of an earth structure. The first application of this approach to seismic slope stability problems was attributed to Terzaghi (1950).

This approach assumes that dams are considered as rigid block fixed on their foundation. The effect of an earthquake is represented by inertial force, which is in some way proportional to the ground acceleration. Normally, only the horizontal component of earthquake shaking is modeled because the effects of vertical forces tends to be neglected.

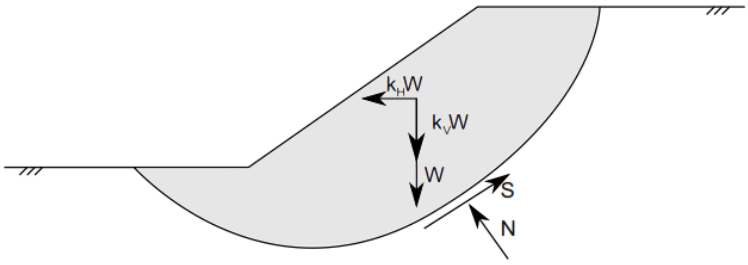

Figure 3.1 Illustration of the pseudo-static method of analysis in which additional inertial forces k_H W and k_VW are included to account for seismic loading.

The basic idea of this method is that equilibrium calculations are carried out in a similar fashion to static slope stability problems, but with the addition of the earthquake inertial loads.

Figure 3.1 illustrates the PS method: additional horizontal k_HW, and vertical k_VW, forces are included to represent the inertial seismic loads. The inertial forces are usually expressed as the weight of the soil multiplied by a seismic coefficient k (Equation 3.1 and 3.2). The seismic coefficient is defined as the ratio of the seismic acceleration to the gravitational acceleration (a_H/g).

$$F_H = \frac{a_H W}{g} = k_H W \quad (3.1)$$

$$F_V = \frac{a_V W}{g} = k_V W \quad (3.2)$$

The value of the seismic coefficient k for which the slope fails is called critical seismic coefficient and is denoted as k_c.

Terzaghi (1950) originally suggested the use of k_H=0,1 for severe earthquakes (Rossi-Forel IX), k_H =0,2 for violent and destructive earthquakes (Rossi-Forel X), and k_H =0,5 for catastrophic earthquakes. The Rossi-Forel (RF) scale was the oldest

scale for measuring earthquake intensity, developed in 1880s and used for many year with values ranging from I to X grades.

(Seed (1979) listed pseudostatic design criteria for 14 dams in 10 seismically active countries and 12 required minimum factors of safety of 1.0 to 1.5 with pseudostatic coefficients of 0.10 to 0.12. Marcuson (1981) suggested that appropriate pseudostatic coefficients for dams should correspond to one-third to one-half of the maximum horizontal peak ground acceleration, including amplification or deamplification effects, to which the dam is subjected.

As it can be seen from above discussions, there are no hard and fast rules for selection of a pseudostatic coefficient for design. The results of pseudostatic analyses are critically dependent on the value of the seismic coefficient. Selection of an appropriate pseudostatic coefficient is the most important, and the most difficult, aspect of a pseudostatic analysis.

The PS method suffers from a number of unrealistic assumptions (Seed, 1973). It does not take into account the change of material properties during earthquake loading but instead it considers the soil as a perfectly plastic material. Moreover, seismic stability is considered as a static problem, simply with the inclusion of an additional unidirectional inertial force. Therefore, it ignores the dynamic response of the dam and any associated resonance with the excitation.

Moreover, detailed analyses of historical and recent earthquake-induced landslides have illustrated significant shortcomings of the pseudostatic approach. Results of pseudostatic analyses of some earth dams (e.g., Upper San Fernando dam, Lower San Fernando dam, Sheffield dam, and Tailing dam) show that pseudostatic analyses produced factor of safety well above 1.0 for a number of dams that later failed during earthquakes.

3.1.2. Sliding Block Method

In 1965, Newmark proposed an improvement over the traditional pseudo-static method which considered the seismic slope failure only at limiting conditions (i.e. when the Factor of Safety, FS, became equal to 1) and providing information about the collapse state but no information about the induced deformations.

The Newmark's sliding block analysis method (Newmark's analysis or Sliding block method of slope stability analysis) is an engineering method used to calculate the permanent displacements for embankments and dams during seismic loading.

The fundamental principle consists on considering the failing mass from the slope as a block of sliding mass (and therefore sliding block) on an inclined surface only when the inertial force (acceleration x mass, induced by an earthquake motion) acting on it, reaches values which are equal or higher than the force required to cause sliding (Figure 3.2). The first displacement occurs when the induced acceleration exceeds a "threshold value", considered as a "critical acceleration" (a_y), which can cause the collapse and it can be readily calculated as the inertial force which produces a safety factor against block sliding lower than 1.0.

The relative acceleration is given by Equation (3.3):

$$u_{rel} = a_t - a_y \ldots..(3.3)$$

Where a_t is the ground acceleration at time t.

Sliding is initiated in the downstream direction when the upstream ground acceleration a_t exceeds the yield acceleration a_y. Several failure surface should be analyzed in order to choose that one which produces the lowest static factor of safety.

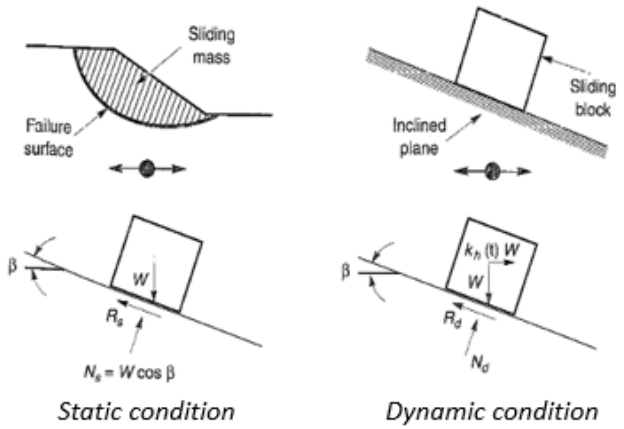

Figure 3.2 Forces acting on a block on an inclined plane: static condition and dynamic condition (Kramer, 1996)

By integrating the relative acceleration twice and assuming linear variation of acceleration, the relative velocity (Eq. 3.4) and displacement (Eq. 3.5) at each time increment can be obtained as showed by the following equations.

$$\dot{u} = \int_0^t (a - a_t)\,(t)dt \quad \forall\, a - a_y > 0 \ldots..(3.4)$$

$$u = \int_0^t \int_0^t (a - a_t)\,(t)dt \quad \forall\, a - a_y > 0 \ldots..(3.5)$$

The sum of partial displacement provides the total final displacement of the sliding block (Figure 3.3).

The Newmark's method limitation is represented by the rigid mass assumption where the earthquake induced acceleration is the same in every points of dam body.

Dam's body is a flexible structure and the seismic motion induces different inertial force in all its points. The induced seismic motion depends on the seismic input duration, its amplitude and its frequency content and on the properties which characterize dam's material.

Thus, the simplified assumption of the rigid bock can lead to an overestimation of the permanent displacements induced by seismic input.

In order to take into account of spatial variability of the seismic acceleration into dam's structure, several simplified approaches have been proposed.

Makdisi and Seed (1978) developed a simplified procedure for the prediction of permanent displacements. They accounted for the variation of the accelerations over the whole length of the slip surface and presented graphs with the variation of the maximum accelerations with respect to the height of the dam.

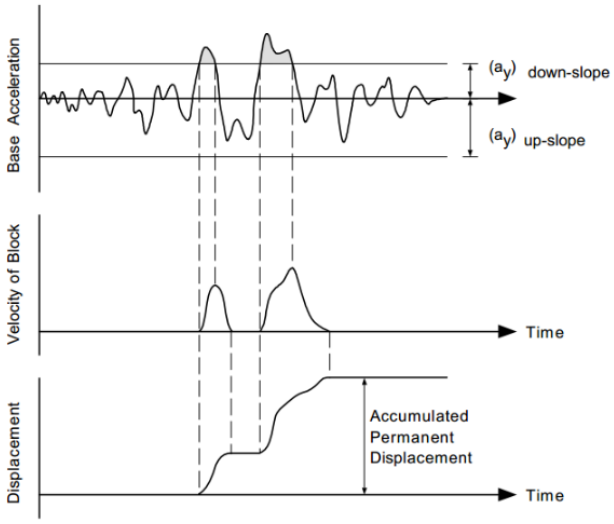

Figure 3.3 Illustration of Newmark's Method (Kramer, 1996)

A more recent and thorough study of the sliding block method was carried out by Bray and Travasarou (2007) who proposed a new method to estimate the earthquake-induced displacements. In their model, the spectral acceleration of the input motion, at a degraded period of the potential sliding mass Sa, (1.5Ts), was identified as the most efficient single ground motion intensity measure. The authors proposed a relationship to derive the seismic displacements, D. These latter were expressed as a function of the yield coefficient of the dam slope, k_y, the magnitude of the earthquake, M_w, and the spectral acceleration of the input motion at a degraded period of the dam structure, Sa (1:5 T_s). Finally, they reported that their method was validated through a number of case histories of earth dams and solid-waste landfills.

Although the improvements of the authors, these methods assume that displacements occur only when the acceleration exceed that required for slope instability ($a_H > a_y$). In fact, this method is not able to provide information about loss of freeboard which can cause the loss of dam functions, their performance and facilities.

3.1.3. Shear Beam Method

The shear beam analysis (Mononobe, 1936) was one of the first approach for the evaluation of the dynamic analysis of a two-dimensional earth structure (Fig. 3.4) and it has served as the basis for many of the newly developed models.

The initial shear-beam method was based on the following major simplifying assumption:

a) Only horizontal lateral displacements and simple shearing deformations take place;
b) Displacements and shear stresses and strains are uniformly distributed along horizontal planes across the dam;
c) The dam consists of a homogeneous material which behaves as a linear visco-elastic solid and is described by a constant shear modulus, damping ratio, and mass density;
d) The dam is either infinitely long or built in a rectangular canyon and is subjected to a synchronous (in-phase) rigid-base lateral motion.

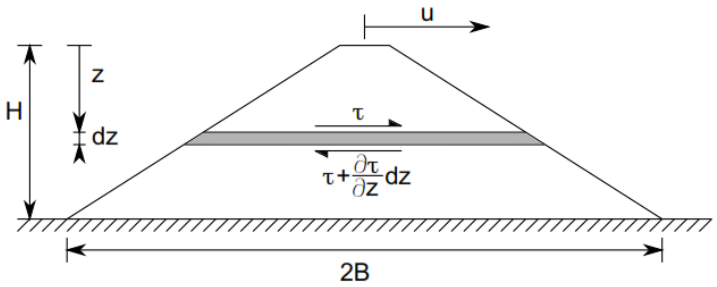

Figure 3.4 Shear beam approach for two-dimensional seismic analysis of dams. After Gazetas (1987).

With regard to assumption (a) it is noted that, in reality, every element in a dam subjected to horizontal base shaking will experience not only horizontal displacements and shearing stresses/strains, but also vertical displacements and normal stresses/strains as a result of wave reflections on the inclined surfaces of the dam. Assumptions (b) appear at first to be rather sweeping: a uniform shear-stress distribution would violate the physical requirement for vanishing stresses at the traction-free inclined surfaces of a dam. Assumptions (c) and (d) are not

crucial for the shear model; they were evaluated only in earlier stages of development of the shear beam as well as of the 2-D plane-strain model.

This approach has then been verified and extended to cover a variety of conditions in order to account for the inhomogeneity of dam's soil and the 3D effects for dams built in narrow canyon. Different closed form relations have been defined in order to calculate fundamental periods, modal displacements and amplification functions (Gazetas, 1987). This method, still simplified, does not take into account the complex nonlinear behavior of the material and the assumption (a) and (b) may be too restrictive in some case.

3.1.4. Finite Element Method

More advanced numerical methods have been developed in the latter years. These methods are able to handle more complicated boundary value problems. Those methods are the Finite Element (FE), Finite Difference (FD) and Boundary Element (BE) approaches, which are able to overcome the previous restrictions.

The FE is the most widely used method nowadays.

The popularity of these new methods is basically due to two factors:

- their capability for handling any number of zones with different materials, whereas the shear beam model (SB) assumed that the elastic properties of the dam could be represented by an average value;
- their capability of rationally reproducing the 2D and 3D dynamic stress and displacement field during earthquake shaking, whereas the simplifying assumption of uniform horizontal shear stresses in shear-beam analyses seems to violate physical requirement of vanishing stresses on the two faces of the dam.

The FE method treats a continuum as an assemblage of discrete elements defined by nodal points at their boundaries. The dynamic finite element method (FEM) solves the equation of motion (Equation 3.6) for dynamic equilibrium with time.

$$[M]\{\ddot{u}\} + [C]\{\dot{u}\} + [K]\{u\} = \{P(t)\} \quad (3.6)$$

Where [M], [C] and [K] are the mass, damping and stiffness matrices respectively, with entries referring to the nodal points. The elements $\{\ddot{u}\}$, $\{\dot{u}\}$, $\{u\}$ and $\{P(t)\}$ are the acceleration, velocity, displacement and external loading vectors respectively. The stiffness matrix, [K], and the damping [C] contain information about the constitutive behavior of the materials.

The solutions of the primary unknown (such as displacements and pore pressures) are provided at these nodes and their values at any other point in the whole domain can be obtained by using interpolation functions (see Potts and Zdravkovic, 1999).

Dynamic finite element analysis involves both spatial discretization of the problem into small regions (the finite elements) and temporal discretization according to the problem's loading history. Then, appropriate boundary conditions (both deformation and hydraulic) are applied and advanced constitutive models may be assigned to different regions and for different time periods. The acceleration time history is applied at a part of the FE mesh, normally at the soil-bedrock interface.

The development of new numerical capabilities gave the start for the growth of new dynamic approaches which considered soil non linearity whose details will be discussed at Paragraph 3.2.3.5.

3.2. The methodology for the seismic assessment of existing earth dams

During the last years, the evolution of the structural design criteria and the change of design objectives have been developed. Safety against collapse remains the most important objective, but performance in terms of functionality and economy have assumed a central role in the design criteria. In the past, dam safety was mainly related to structural safety, but today dam safety means structural safety, dam safety monitoring, operational safety and emergency planning.

Compared with previously existing regulations, European Code (EN, 1998) and, more recently, Italian Codes (M.LL.PP., 2008) have introduced *PBSD* (Performance Based Seismic Design) concepts for the design of structures.

PBSD can be understood as a design criterion whose goal is the achievement of specified performance targets when the structure is subjected to a defined seismic hazard. The specified performance target could be a level of displacements, level of stresses, maximum acceleration, mobilized strength, or a limit state. In this respect, the limit state design can be seen as a particular case of the PBSD, where the performance target is represented by the resisting force.

The formal use of performance-based design is less widespread in geotechnical engineering than in structural engineering. The reason is the heterogeneity of such geotechnical structures. Earth dams are complex structure which include several and different components (foundation, embankment, drainage systems, seepage, pipeline and operating machines) and significant uncertainties in the definition of performance targets. Significant uncertainties exist mainly for existing embankment construction. In order to predict their performance under a variety of events and, eventually, plan countermeasures aimed to optimize their management and maintenance, PBSD conventional methods for existing earth dams should be designed.

Today it is important to recognize that the earthquake load case has evolved as the critical load case for most large dams even in regions of low to moderate seismicity. Due to changes in the seismic design criteria and design concepts, it

may be necessary to perform several seismic safety checks during the long economical life of a large dam. In some cases, the national regulation did not consider dam sites as seismic ones. Some existing earth structures were designed without taking seismic loads into account and need to be seismically verified, after almost half a century of operation, due to a substantial update of the seismic classification of the dam site. This is the case of the Camastra zoned earth dam, located in the city of Potenza, in Southern Italy (Sica an Pagano, 2009).

The knowledge on the behavior of large dams during strong ground shaking is still very limited, and each destructive earthquake affecting dams may reveal some new features, which up to now may have been ignored.

Nowadays, a specific PBSD procedure for the assessment of seismic safety of existing earth dams has not been defined, yet; thus, a performance based seismic design of earth dams should be considered.

This chapter illustrate the theoretical methodology for the assessment of the seismic response of existing zoned earth dams, considering the performance-based criteria. The methodology is based on the definition of the performance of the dam which should be consistent with the structure importance. The procedure objectives are essentially aimed at verifying that dam's performance is respected and thus the relative safety level.

In order to apply the performance based seismic design (PBSD) approach for the assessment of existing earth zoned dams in Italy, the following steps have to be considered (Figure 3.5):

1) Evaluation of dam's performance criteria;
2) Definition of the input motion;
3) Definition of the dam model:
   a) Definition of its geometry;
   b) Selection and calibration of its representative constitutive model and the characterization of material properties;
4) Evaluation of dam's response;
5) Assessment of its safety level.

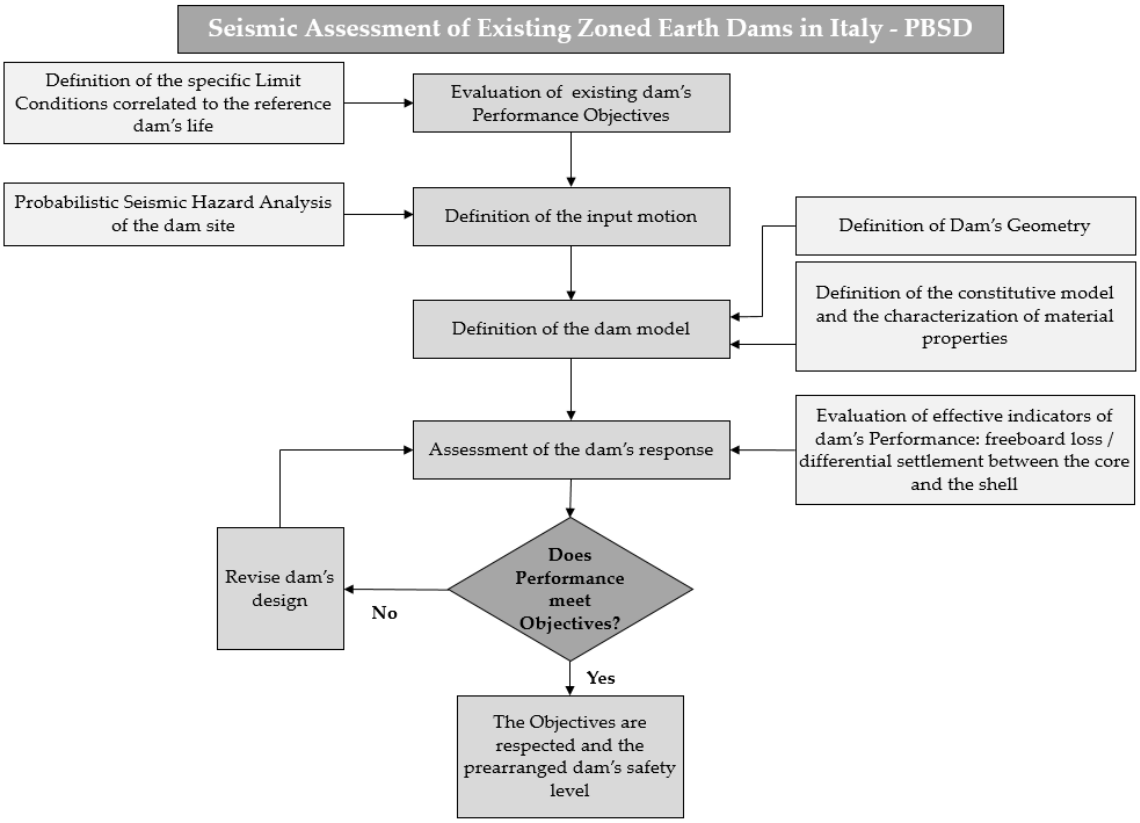

Figure 3.5:The Performance Based Seismic Design Procedure for the seismic assessment of existing earth dams

3.2.1. Evaluation of seismic performance criteria of existing earth dams in Italy

As proposed by the Italian Building Code (NTC08), the performance of a structure is based on the definition of two combined objectives: economy and safety.

In order to take into account of these two aspects, the safety of a construction must be evaluated with regards to specific limit conditions and actions which can happen into a specified period where the structure is observed (*return period TR*).

The procedures for analyzing the seismic safety level of the structure should be consistent with the functional and economical importance of the construction.

In case of an existing earth dams, the seismic analysis objectives are essentially aimed at verifying the seismic actions which could affect the main task of these structures: ensuring water tightness.

Combining the functional importance of the existing structure with the relative damage objectives that need to be verified, the limit state of performance must be predicted for existing earth dams.

The new seismic classification of the Italian territory and the recent seismic Italian code NTC08 (M.LL.PP., 2008) have led the Italian State Office for the Control of Large Dams (Ministero Infrastrutture, Direzione Generale Dighe) to issue a directive in 2014 (M.LL.PP. 26/06/2014) which has defined the limit states for the seismic performance of Italian dams.

The specific limit conditions and actions are correlated to a characteristic period T_R (*return period*), Equation (3.7), where the structure is observed and which is related to a tolerant probability of failure P_{VR}.

$$T_R = \frac{V_R}{(1-lnP_{VR})} \quad (3.7)$$

The return period T_R is also correlated to the dam's importance with the *reference period* V_R. The *reference period*, Eq. (3.8), is defined by the Italian Building Code as the product between the expected life of the dam V_N (number of the years in which the structure, subjected to the ordinary maintenance, is supposed to be

used) and its coefficient of importance C_U (depending on the importance of the construction and on the possible damages produced by collapse).

$$V_R = V_N \cdot C_U \quad (3.8)$$

According to the Ministerial Decree (D.M.), issued on 26/06/2014, (M.LL.PP. 26/06/2014), the expected life V_N of an existing dam and its usage coefficient C_U are defined in the following table. Table 3.1 depicts such values for different type of existing dams. Strategic dams are constructions which have tactical function for the civil protection and they must maintain all their services during and after an earthquake (See Chapter 2).

Dam Type	**V_N (years)**	**C_U**	**V_R (years)**
Strategic	≥ 50	2.0	100
Relevant		1.5	75
Normal		1	50

Table 3.1 Expected life of existing dam V_N and its usage coefficient C_U, (M.LL.PP., 2014)

The P_{VR} values are defined by D.M. 26/06/2014 (M.LL.PP., 2014), according to the Italian Building Code (M.LL.PP., 2008), as illustrated in Table 3.2.

The Operational Limit State (OLS) and the Damage Limit State (DLS) represent the functional limit conditions where the dams must to keep all services. The Life Safety Limit State and the Collapse Limit State are the ultimate limit states where the dam can suffer some damages but must not collapse and must retain the water reservoir.

All the mentioned limit states must not to be exceed in order to be satisfied.

In Chapter 3.2.4, the seismic response of existing earth dam will be discussed and the effective indicators of the dam performance will be defined.

<table>
<tr><td rowspan="3">Dam Type</td><td colspan="6">Limit States</td></tr>
<tr><td>Operational Limit State (OLS)</td><td colspan="2">Damage limit state (DLS)</td><td colspan="2">Life safety limit state (LLS)</td><td colspan="2">Collapse limit state (CLS)</td></tr>
<tr><td>Facilities suffer limited damages but the reservoir level can be controlled</td><td colspan="2">Slopes suffer local instabilities but the stability of the embankment is ensured. Facilities are damaged without uncontrolled release of water</td><td colspan="2">Cracks or excessive deformations of embankment and/or foundation cause uncontrolled seepage and/or overtopping. Damage of facilities affects the capability to control the reservoir level</td><td colspan="2">Global instability or liquefaction of embankment and foundation, uncontrolled release of water; high risk of human losses</td></tr>
<tr><td></td><td>P_{VR} (%) = 81</td><td colspan="2">P_{VR} (%) = 63</td><td colspan="2">P_{VR} (%) = 10</td><td colspan="2">P_{VR} (%) = 5</td></tr>
<tr><td>Strategic</td><td colspan="2">T_R= 120 years</td><td colspan="2">T_R= 200 years</td><td colspan="2">T_R= 1900 years</td><td colspan="2">T_R= 2475 years</td></tr>
<tr><td>Relevant</td><td>T_R= 45 (1) years</td><td>T_R= 90(2) years</td><td>T_R=75(1) years</td><td>T_R=150 (2) years</td><td>T_R=710(1) years</td><td>T_R=1425 (2) years</td><td>T_R=1460(1) years</td><td>T_R=2475(2) years</td></tr>
<tr><td>Normal</td><td colspan="2">T_R= 30 years</td><td colspan="2">T_R= 50 years</td><td colspan="2">T_R= 475 years</td><td colspan="2">T_R= 975 years</td></tr>
</table>

Table 3.2 Return period for different type of dams and for limit states – (1) small dams; (2) large dams, (D.M. 26/06/2014)

3.2.2. The definition of the input motion at the dam site

In the framework of performance-based seismic design and assessment, a relevant issue is the selection of a suitable set of ground motion records to represent the design seismic excitation for the dynamic analysis.

The definition of the input motion represents a crucial step in the evaluation of the seismic performance of earth dams.

First, a seismic hazard analysis has required to select the correct seismic input motion at the site where the structure is located.

There are two main methods for the quantification of an earthquake-induced hazard: the deterministic approach and the probabilistic seismic method.

The determination of the seismic hazard can be evaluated using a deterministic approach, assuming particular seismic earthquake scenarios, or a probabilistic analysis, considering uncertainties in earthquake intensity, location and observing time of a such event (return time). In the past, the deterministic seismic hazard analysis (DSHA) was prevalent, but only the probabilistic approach has been recommended by the recent building code NTC08 (M.LL.PP., 2008).

The probabilistic seismic hazard analysis PSHA (Cornell, 1968) provides the instruments for determining a more realistic seismic scenario for a specific site and with a rational manner.

The probabilistic seismic hazard analysis PSHA introduces a method for evaluating the likelihood of exceedance (or occurrence) of any level of earthquake ground shaking at a site during a given period (return period). This is achieved by combining the effects of all the possible magnitudes and earthquake locations that could affect the hazard at the investigated site.

3.2.2.1. The evolution of the seismic classification of the Italian territory

Italy is one of the countries in the Mediterranean place with the highest seismic risk, due to its particular geographic position at the convergence of the African and Eurasian plates. The highest seismicity is concentrated in the central-southern part of the peninsula, along the Apennine ridge in Calabria and Sicily

and in some northern areas, like Friuli, part of Veneto and western Liguria. Only Sardinia is not particularly affected by seismic events.

In order to reduce the effects of earthquake events on constructions and human lives, the Italian State has concentrated its action on territorial classification, based on past earthquakes intensity and frequency, and on the application of special regulations of buildings in areas classified as seismic.

Before 2003, the national territory was classified in three seismic categories (Figure 3.6) with different seismic hazard level. Between 1981 and 1984, Ministerial Decrees issued by the Ministry of Public Works had classified 45% of the national territory (2'965 Italian municipalities), in which only the 40% of the whole Italian population lives.

Figure 3.6 Seismic Classification of Italian territory related to 1984, before OPCM 3274 (2003), (http://zonesismiche.mi.ingv.it/)

In 2003, with the Order of the President of the Council of Ministers (OPCM) no. 3274, new criteria for seismic classification were published. These criteria have been based on the recent studies and processing regarding seismic dangerousness of the territory (the probabilistic seismic hazard analysis, PSHA), as mentioned before.

According to the OPCM 3274 (2003), Regions, appointed by the State, filled out a list of municipalities with the zone each of them belongs to (Table 3.3), and the entire national territory has been classified according to it (Figure 3.7).

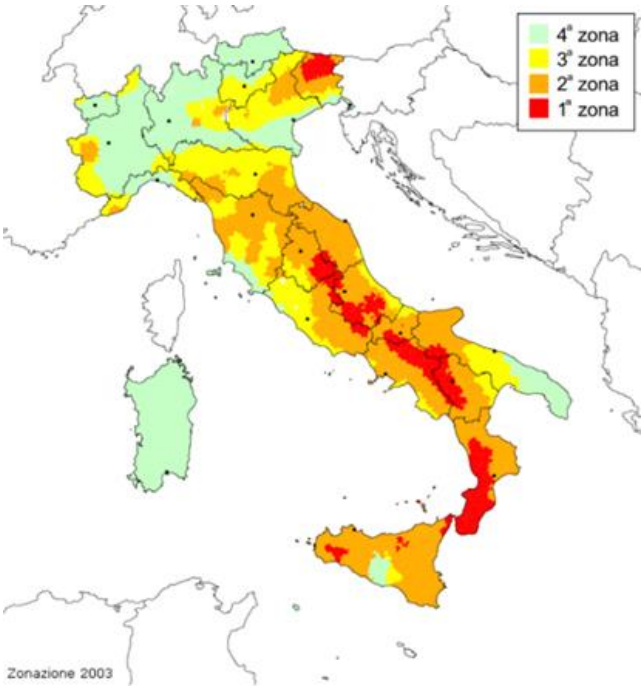

Figure 3.7 Seismic classification of Italian territory by OPCM 3274 (2003), (http://zonesismiche.mi.ingv.it/)

Moreover, each zone corresponds to a specific maximum value of the seismic action expressed in terms of maximum acceleration in rock (*zone 1*=0,35 g; *zone 2*=0,25g; *zone 3*=0,15 g; *zone 4*=0,05 g).

Zone	**Dangerous Level**	**Max PGA**
Zone 1	It the most dangerous area, where major earthquakes may occur	0,35g
Zone 2	Municipalities in this area may be affected by quite strong earthquakes	0,25g
Zone 3	Municipalities in this area may be subjected to modest shocks	0,15g
Zone 4	It is the least dangerous. Municipalities of this area have a low probability of seismic damages	0,05g

Table 3.3 Seismic classification of Italian territory by OPCM 3274 (2003)

The innovation introduced by the ordinance have been refined further on, thanks also to the studies and the collaboration carried out by the competence of national centers. These tasks are carried out with the support of scientific and operational institution, which are the excellence for the seismic risk:

- *INGV*: National Institute of Geophysics and Volcanology, for seismological aspects;
- *ReLUIS:* Network of University Laboratories of Seismic Engineering;
- *Eucentre*: European Centre for Training and Research in Earthquake Engineering for the engineering aspects.

An update of previous study (provided for by the OPCM 3274/03) has been developed by the Ordinance of President of the Council of Ministers no. 3519 of 28 April 2006.

The aforementioned recent study supplied the Regions with an updated tool for a new territorial classification. An intervals of acceleration *(a_g)*, with a probability of exceeding the threshold equal to PVR=10% in 50 years, has been introduced and assigned to the four seismic areas (Table 3.4). Details and meanings of zonation according to each Region are contained in the regulatory regional dispositions.

Zone	**Dangerous Level**	**Max PGA** **T_R=475years – P_{VR}=10% in 50%**
Zone 1	It the most dangerous area, where major earthquakes may occur	PGA> 0,25g
Zone 2	Municipalities in this area may be affected by quite strong earthquakes	0,15g<PGA< 0,25g
Zone 3	Municipalities in this area may be subjected to modest shocks	0,05g<PGA< 0,15g
Zone 4	It is the least dangerous. Municipalities of this area have a low probability of seismic damages	PGA< 0,05g

Table 3.4 Seismic classification of Italian territory by OPCM 3519 (2006) - Acceleration with probability of exceeding equal to 10% in 50 years (a_g)

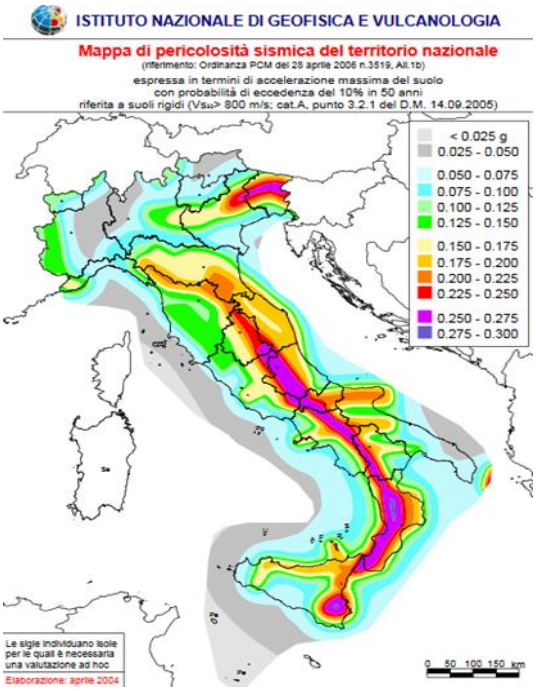

Figure 3.8 Seismic classification of Italian territory by OPCM 3519(2006) and supported by NTC08 (http://esse1-gis.mi.ingv.it/)

Actually, the Current Technical Regulations for Buildings (M.LL.PP., 2008) has modified the role that seismic classification had for planning purposes: for each area and site – and thus municipal territory – a value of peak acceleration, and consequently a spectrum of elastic response, was previously supplied to calculate seismic actions.

Since the NTC 2008 (M.LL.PP., 2008) has come into force, each construction has its own acceleration and its own acceleration response spectrum at bedrock for the scenario earthquake representative of its relative seismic hazard.

According to geographical coordinates of the project site and to the nominal design life of the construction, the hazard level can be defined for each point of the national territory, within an area of 5 m^2, regardless of local administrative borders (Figure 3.8 and 3.9).

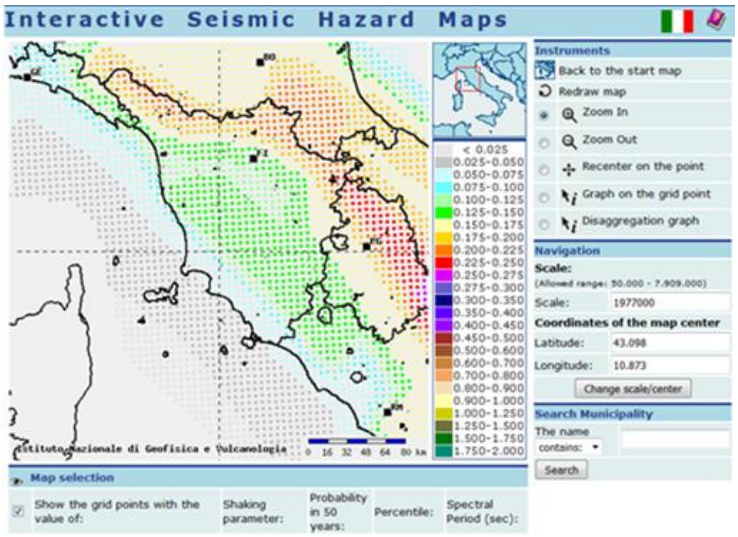

Figure 3.9 Seismic hazard Italian network, carried out by INGV (http://esse1-gis.mi.ingv.it)

Nowadays, the seismic classification (which seismic zone a municipality belongs to) is thus useful only for planning management and territorial control by relevant boards (Region, Genio, etc.).

The actual seismic hazard map of Italy has been created with the ESSE1 project (Meletti C., 2007), which is based on the probabilistic seismic hazard analysis PSHA (see Par. 3.1). The entire Italian territory has been discretized with a regular grid spaced by 0.05°.

The seismic hazard maps display two shaking parameters, PGA (horizontal peak ground acceleration) and S_a (spectral acceleration). The unit of measure is *g*, i.e. the gravity acceleration, corresponding to 9.8 m/sec^2. Only for PGA values, the associated disaggregation analysis is available.

Maps in PGA were evaluated for different probabilities of exceedance in 50 years (9 probabilities, from 2% to 81%). For each evaluation it is available the distribution of the 50th percentile (median map, which is the reference map for every probability of exceedance) and the distribution of the 16th and 84th percentiles, which give the variability of each estimate. The details about the computation of these hazard estimates are available at the page describing deliverable D2 of this project (*http://esse1.mi.ingv.it/d2.html*).

Maps in *Sa* were also calculated for the same probabilities of exceedance in 50 years (9 probabilities, from 2% to 81%) and for different periods (10 periods, from 0.1 to 2 seconds). The details about the computation of these hazard estimates are available at the page describing deliverable D3 of this project (*http://esse1.mi.ingv.it/d3.html*).

3.2.2.2. The procedure for the selection of the seismic input by the recent Building Code at the dam site

In order to properly select the seismic input motion at the dam site, procedures have been recently developed and suggested by the present building code.

The methodology used for the selection of representative acceleration time-histories is structured into three different steps:

- *Definition of the reference acceleration response spectrum at the bedrock* for the expected seismic scenario and the seismic hazard (peak ground acceleration on flat rock outcropping, PGA) at the site where the dam is located;
- *Evaluating the pair of magnitude-distance (disaggregation)* that mostly contributes to the seismic hazard of the chosen scenario;
- *Selecting a series of accelerograms* from disaggregation and carrying out the spectrum compatibility criterion.

Definition of reference elastic spectra

In order to define the reference acceleration response spectrum at bedrock for the seismic hazard of the dam site, it is required to evaluate the time of observing such as the return time T_R of such scenario, as proposed into the Table 3.2. For example, assuming the reference existing dam life V_R of 75 years, and the tolerable probability of occurrence of 5% (for the Collapse Limit State, CLS), a return periods of 1460 years must be considered.

The value of the peak ground acceleration (PGA) on horizontal rock outcropping was defined by the new seismic classification of the Italian territory (see Par. 3.2.2.1 and Figure 3.8) and enclosed into the recent seismic Italian code NTC08 (M.LL.PP., 2008).

According to the Seismic Italian Code NTC08, the seismic action in terms of elastic 5% damped acceleration response spectrum has defined for the specific PGA value at the dam site and for the selected return time T_R.

Definition of magnitude-distance pairs

The relevance of seismic hazard disaggregation is an inseparable part of a PSHA analysis. Seismic hazard disaggregation (e.g., McGuire, 1995; Bazzurro and Cornell, 1999) provides insights into the earthquake scenarios driving the hazard at a given ground motion level.

For a given point of the Italian seismic hazard map, the disaggregation analysis of the relative PGA values shows the percentage contribution to the seismic hazard estimate provided by each couple of magnitude-distance values (M-R).

The more common form of disaggregation analysis is the bi-dimensional one.

It allows to select the M-R couple which dominates the seismic scenario. This couple M-R can define the earthquake of Magnitude M at distance R from the site of interest that mostly contribute to the seismic hazard of the aforementioned site.

The results from the disaggregation analysis are provided on the web site of the National Institute of Geophysics and Volcanology, INGV, (*http://esse1-gis.mi.ingv.it/*), for each point of the Italian seismic hazard map (Fig. 3.10).

The disaggregation analysis is an important guide for simulating or selecting appropriate ground-motion time histories for nonlinear dynamic analyses of complex structure as earth dams. Indeed, it is appropriate for selecting the accelerograms which correspond to the events that are more likely to cause the exceedance of the target ground shaking level at the site of the studied dam.

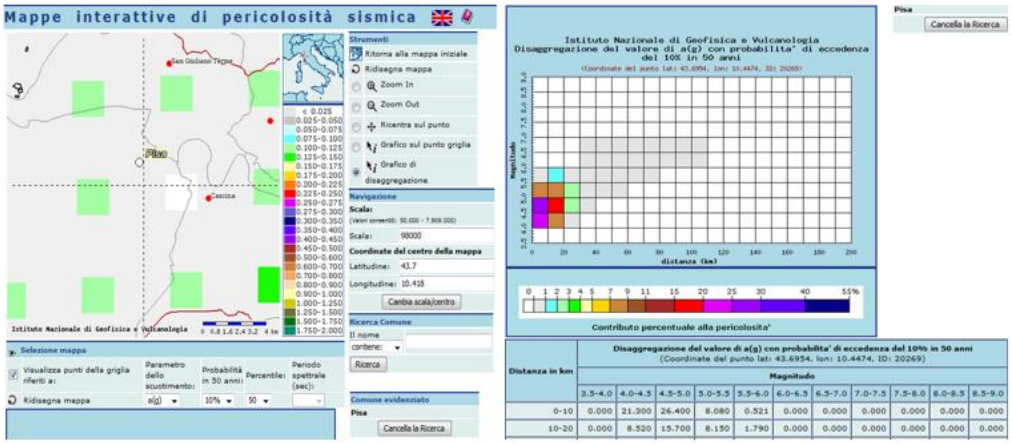

Figure 3.10 M-R distribution for disaggregation analysis for the site of Pisa, Toscany, for the probability of exceedance of 10% in 50 years, (http://esse1-gis.mi.ingv.it/)

According to the bi-dimensional disaggregation expressed in term of M-R couple, it is possible to define the three-dimensional disaggregation M-R-e (Fig. 3.11). In this case, the number ε is the standard deviations by which the (logarithmic) ground motion deviates from the median value predicted by an attenuation equation for a given M and R pair (Spallarossa & Barani, 2007).

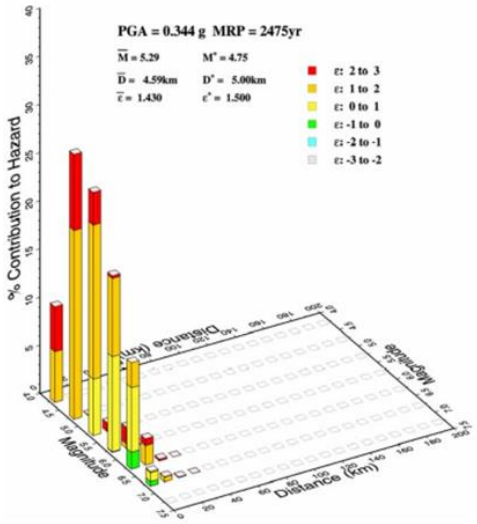

Figure 3.11 M-R-ε distributions from the disaggregation of seismic hazard calculated for a site in the northern Tuscany for a return period of 72 years (probability of exceedance of 50% in 50 years), (Spallarossa & Barani, 2007).

Selection of acceleration time-histories

In case of earth dams, the seismic actions are represented using the acceleration time Histories. Ones the magnitude M and distance intervals R are selected, a first record selection is done.

Real records are available on free-access internet databases. An example of free-access internet databases is shown into the Table 3.5.

Database	Web site
European Strong Motion Database	*http://www.isesd.cv.ic.ac.uk*
PEER	*http://peer.berkeley.edu/smcat*
PEER - NGA	*http://peer.berkley.edu/nga*
k-net	*http://www.k-net.bosai.go.jp*
Kik-net	*http://www.kik.bosai.go.jp*
COSMOS	*http://cosmos-eq.org*
Itaca	*http://itaca.mi.ingv.it*

Table 3.5 Example of free-access internet databases

The description of the seismic motion for earth structures can be accomplished using real accelerograms.

The natural accelerograms appear to be the better representation of ground motion in term of amplitude, frequency content, energy, duration and phase distribution (Bommer & Acevedo, 2004) and they are stored on on-line catalogs, which provide a free-access internet databased, as said before.

In order to find the accelerograms which are representative of the seismic hazard of the site of analysis, a specific spectrum compatibility criterion must be followed (Bommer & Acevedo, 2004).

According to the Italian Building Code 2008 (M.LL.PP.,2008), a set of accelerograms which are spectrum compatible must be selected.

The specification of NTC08 is that no value of the mean spectrum calculated for all the selected records is less than 90% of the corresponding value of the 5% target response spectrum in the period range of interest.

Due to the difficulty in finding compatible records especially for very strong motions, the candidate real accelerometer has to be first scaled to the target PGA applying a constant scaling factor Fs, Eq. (3.9).

$$F_S = \frac{a_{max,n}}{a_{max,r}} \quad (3.9)$$

Where: $a_{max,n}$ is the PGA related to the seismic hazard of the specific site, $a_{max,r}$ is the peak acceleration value of the selected time history.

According to the D.M. 2008 (M.LL.PP, 2008), the Fs value has to be higher than 0.7 but lower than 1.4.

In order to improve the aforementioned approach for the selection of appropriate set of natural records, other researches have been developed which suggest the use of other parameters such as record duration or Arias Intensity I_a (Lanzo et Al., 2015) (see Chapter. 2).

3.2.3. The definition of the dam model

The approach to predict the seismic response of a zoned earth dam is based on the definition of various issues that need to be taken into consideration to carry out appropriate and useful dynamic numerical analyses. Topics that need to be considered are the numerical model geometry, the boundary conditions and location, elements size, material constitutive models and the evaluation of dam's response.

3.2.3.1. Numerical model geometry

The model geometry is a fundamental factor which must be assessed in order to make a good prediction of the dynamic behavior of the selected problem. In case of earth dams, it is important to understand if a two dimensional analysis is sufficient to represent the real behavior. A 2D analysis is allowed for a very long dam where a plane strain behavior is expected. A 3D numerical model is desirable when dams are built in narrow canyons, when the ratio between canyon length and the height (L/H) is less than 4 (see relevant discussion in section 2.3.4 and Dakoulas & Gazetas, 1987). Dams built in narrow canyon exhibit a stiffer response than dams built in a very wide canyon. When the canyon effects are important, the 2D analysis would be inappropriate, as the real problem is stiffer than the corresponding plane strain model.

If the objective of the study is to verify the overall seismic behavior of the embankment, facilities (drainage tunnels) could be neglected in the model.

3.2.3.2. Boundary condition

In order to make a good prediction of the dynamic behavior of the selected problem, the definition of the boundary condition must be run. Boundary conditions (BCs) need to be specified in a FE analysis because theoretically the equations describing the problem cannot be solved (integrated) without specified BCs.

For dynamic analysis where wave propagation is modelled, special BCs exist that overcome the problem of wave reflections at the boundaries. These are called absorbing boundary conditions.

The most commonly used boundaries can be divided into three groups (Kramer, 1996) showed in Fig. 3.12:

- *Elementary boundaries*: boundaries with the conditions of zero displacements or zero stresses;
- *Standard Viscous boundaries* or *Local Boundaries*: boundaries with the use of viscous dashpots;
- *Consistent boundaries*: boundaries that can absorb all types of body waves and surface waves at all angles of incidence and all frequencies.

Elementary boundaries can be used to model the ground surface accurately as free (zero stress) boundary. In dynamic problems, however, such boundary conditions cause the reflection of outward propagating waves back into the model and do not allow the necessary energy radiation. The use of a larger model can minimize the problem, since material damping will absorb most of the energy in the waves reflected from distant boundaries. However, this solution leads to a large computational burden.

The use of viscous dashpots represents a common type of *Standard Viscous boundaries*. It can be shown (Wolf, 1985) that the value of the dashpot coefficient necessary for perfect energy absorption depends on the angle of incidence of the impinging wave. The Standard Viscous BC is able to perfectly absorb waves that propagate normal to the boundary due to the application of a traction condition to a free artificial boundary so that any rejected stresses are zero. This BC can be physically represented by a series of normal and tangential dashpots on the FE boundary. The effects of reflections from local boundaries can be reduced by increasing the distance between the boundary and the region of interest.

Boundaries that can absorb all types of body waves and surface waves at all angles of incidence and all frequencies are called *Consistent Boundaries.* They can be considered as an extension of the Standard Viscous BC and can be physically represented by a series of normal and tangential sets of dashpots and springs in the FE mesh boundary.

A greatly simplified example of such an assemblage is shown in Fig. 3.12.

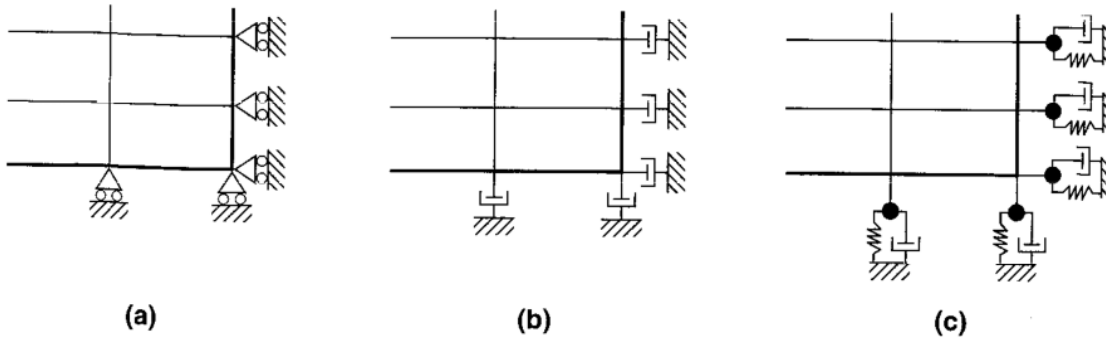

Figure 3.12 Three types of mesh boundaries: (a) elementary boundary in which zero displacements are specified; (b) local boundary consisting of viscous dashpots; (c) lumped parameter consistent boundaries (Kramer, 1996).

3.2.3.3. Boundaries location

In order to minimize the influence of the boundaries and obtaining a solution which is not affected of them, it is worth to decide where the bottom and lateral boundaries should be placed. The location of the bottom boundaries is influenced by the location of the bedrock. Generally, if the bedrock is much stiffer then the overlying soil (where the impedance ratio is high), the bedrock can be assumed to be rigid and the location of the bottom boundaries may be placed at the interface from soil and bedrock.

Lateral boundaries should be placed as far as the response close to that boundaries is similar to the free-field response. In order to determine the distance at which lateral boundaries should be placed, several analyses should be repeated for different boundary distances. The boundary must be sufficiently far away from the area of interest so that lateral boundaries do not significantly affect the dynamic response.

3.2.3.4. Element size

Discretization or meshing is one of the fundamental aspects of finite element modeling. The response of both equivalent linear and nonlinear finite-element/finite-difference models can be influenced by the model discretization. In particular, the use of coarse finite element/finite difference meshes results in the filtering of high-frequency components whose short wavelengths cannot be modeled by widely spaced nodal points. The maximum dimension of any element Δh should be limited to 1/10 (Kuhleimeyer & Lysmer, 1973) to 1/8

(Lysmer et Al., 1975) of the shortest wavelength considered in the analysis, λ_{min}, for 4-noded elements (with linear shape functions).

For 8-noded iso-parametric elements (with quadratic shape functions), Δh should be limited to 1/5 (Kuhleimeyer & Lysmer, 1973) to ¼ of the smallest shear wave velocity, V_s, of the material over the highest frequency of the input wave to be modeled, f_{max} (Eq. 3.10).

$$\Delta h = \frac{1}{(5 \div 8)} \frac{V_s}{f_{max}} \quad (3.10)$$

Where V_s is the shear wave velocity of the soil and f_{max} is the threshold frequency value to be modeled in the analysis.

3.2.3.5. Material constitutive models

The behavior of soil under cyclic loading was briefly discussed in Section 2.2.2.

As discussed in the previous section (Par. 3.1.4), advanced numerical techniques, such as the finite element method, are able to satisfy all the analysis objectives: stability, displacements and dynamic response.

The development of new sophisticated numerical methods have given the start for the growth of new dynamic approaches, which considered soil non-linearity.

The description of different possible methods which account of non-linear behavior of soil are summarized below.

The actual nonlinear hysteretic stress-strain behavior of cyclically loaded soil (Section 2.2.2) can be approximated by the ***equivalent linear soil properties***.

The *equivalent-linear approach* (Schnabel et al.,1970; Idriss et al., 1973; Idriss and Sun, 1992) essentially uses a constant value of the shear modulus, *G*, and damping, *D*, compatible with the induced shear strains, according to assumed relations describing strain dependent stiffness degradation and damping variation (e.g. Vucetic and Dobry (1991)).

A set of moduli and damping ratios is initially assumed and a series of linear analyses is conducted. Each calculation uses soil moduli and damping ratios compatible with the levels of shear strain calculated in the previous step (Figure

3.13). To select modulus and damping ratio for each iteration, an "equivalent" effective strain amplitude is estimated as a fraction (usually 2/3) of the peak shear strain.

Clearly, the arbitrary assumption of that factor is the major drawback of the method, also, the method is empirical and its convergence to the correct answer cannot be proved theoretically. For moderately strong levels of shaking the peak response values seem reasonable, while the response to very strong excitation may be overestimated or even underestimated. Since the method is essentially linear during each iteration, there's a tendency for spurious resonances to develop and thereby to exaggerate the response.

Finally, the method cannot provide information on permanent displacements and deformations, since it is basically an elastic method. Hence, there is the need to develop separate procedures for assessing residual and sliding displacement, by using the aforementioned Newmark concept or a redistribution analysis.

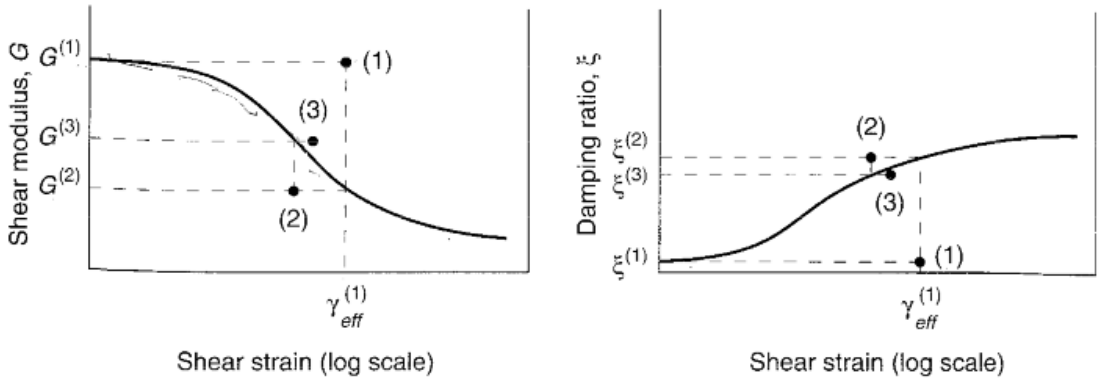

Figure 3.13 Iteration toward strain-compatible shear modulus and damping ratio in an equivalent linear analysis

The Equivalent-linear approach was used for the analysis of the failure of Sheffield dam (Seed et Al., 1969), under the 1925 Santa Barbara earthquake and of Vrymoed (1981) in the analysis of Oroville dam.

This method is widely used for evaluating the local site seismic response and has been implemented in numerous 1D and 2D codes like Shake91 (Schnabel, Lysmer, & Seed, 1972), QUAD4M (Hudson, Beikae, & Idriss, 1994) and Quake/W FEM software package (Selkuk &Terzi, 2015).

Two dimensional ***nonlinear approach*** have the enormously beneficial capability of computing pore pressures (hence effective stresses) and permanent deformations. The accuracy with which they can be computed depends however on the accuracy of the constitutive models on which they are based

Different possible approach can be performed, considering soil nonlinearity at different degree of complexity.

Such analyses can be divided into two main groups according to the manner in which the soil behavior is represented. Once group uses the *cyclic nonlinear strass-strain model*, whereas the other uses *advanced constitutive model*.

The *approximate 2D non linear effective method* (Finn, 1988) extends the 1D hyperbolic Masing model of cyclic behavior in simple shear to account for inelastic soil behavior in a bi-dimensional analysis. This method is able to represent the shear strength of the soil, and, with an appropriate pore pressure generation model, changes in effective stress during undrained cyclic loading. The model for residual pore water pressures (which arise due to plastic deformation) is an extension of the 1D Martin-Finn-Seed model (Martin, Finn & Seed, 1975) which has been widely used for site-amplification and liquefaction studies. The cyclic nonlinear model is characterized by a backbone curve and a series of "rules" that govern unloading-reloading behavior, stiffness degradation and other effects. The simplest of these models have relatively simple backbone curves and only a few basic rules. More complex models may incorporate many additional rules that allow the model to better represent the effects of irregular loading, densification and pore water pressure generation.

Figure 3.14 shows schematically the hyperbolic backbone curve (Eq. 3.11).

$$F(\gamma) = \frac{G_{max}\gamma}{1+\left(\frac{G_{max}}{\tau_{max}}\right)|\gamma|} \quad (3.11)$$

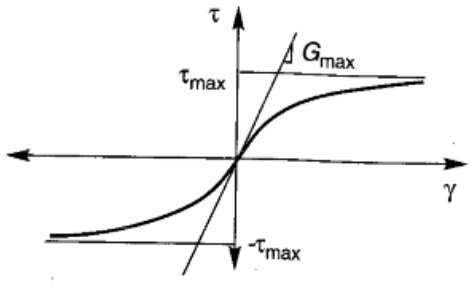

Figure 3.14 Hyperbolic backbone curve, asymptotic to $\tau=G_{max}\gamma$ and $\tau=\tau_{max}$ (and $\tau=-\tau_{max}$).

The value of the backbone slope is represented by maximum shear strain G_{max}, whereas the asymptote is represented by the strength of the soil.

The *advanced constitutive models* are based on most accurate and general methods that use basic principles of mechanics to describe observed soil behavior for general initial stress conditions, a wide variety of stress path, rotating principal stress axes, cyclic monotonic loading, high or low strain rate and drained or undrained conditions.

Generally, advanced constitutive approach requires a yield surface that describes the limit stress condition, a hardening law in order to describe changes in size and shape of the yield surface as plastic deformation occurs, and a flow rule that relates increments of plasticity strains to increments of stresses.

With the progress of computational capability, this last non-linear method has been the most used method to assess the performance of new and existing dams.

Recently, Sica et Al. (2008) investigated the seismic response of El Infiernillo dam in Mexico, using their in house software GEFDYN (Aubry et al. 1985), adopting the elasto-plastic model (Heujeux, 1935), characterized by both isotropic and kinematic hardening. The numerical model was calibrated with the measured response and a good agreement was achieved between the computed and measured acceleration and response spectra of the dam. The calibration was followed by a parametric analysis in order to investigate the influence of past loading histories on the seismic response of earth dams. It was found that if the same seismic event was repeated after the first, the computed earthquake induced crest settlements were smaller in the second motion. It was commented that the

past seismic history (a series of consecutive earthquakes) produces an effect of soil hardening on the computed loss of freeboard. Thus, the authors highlighted the advantages of using appropriate constitutive model which is able to capture soil hardening. However, as suggested by Pelecanos (2013), it should be noted that the aforementioned study did not directly compare results from different numerical analyses that consider and ignore strain hardening. Thus, this study has not been able to predict if that difference in the predicted crest settlements was entirely due to the modelled strain hardening.

Elia et al. (2011) represented fully coupled dynamic analysis of Marana Capaciotti Dam in Italy by finite element effective stress approach. It was pointed out that significant plastic strain accumulation at the toes of the dam and a large development of excess pore pressures induced because of shaking. It was commented that the work evaluated the significance of using coupled formulation along with the adoption of advanced elasto-plastic models in the analysis of earth dams to appropriately model any excess pore pressures. However, it should be noted that the numerical responses from that study were not compared with any field data (Pelecanos, 2016). Thus, the reliability of these results is uncertain due to the fact that the comparison with field data is inexistent. Therefore, further investigations are required, using available measured field data, in order to confirm or question the results of Elia et Al. (2011).

Although advanced constitutive models allow considerable flexibility and generality in modeling the response of soils to cyclic loading, their description usually requires many more parameters than the equivalent linear model or cyclic nonlinear model. The disadvantage of using the advanced constitutive model to describe the soil skeleton response is the definition of several soil parameters which require a detailed geotechnical characterization of the construction soils and the evaluation of these parameters can be difficult. Although the advanced constitutive models are more accurate and their use will undoubtedly increase, they present practical problem due to the complexity in finding all the parameters. Thus, in geotechnical earthquake engineering practice their use is limited. For this latter reason, the methodology adopted in the present study

performed the numerical response using an equivalent linear method and cyclic nonlinear analysis.

3.2.3.6. Hydrodynamic effects

In static conditions, the effect of the reservoir mainly involves the application of the hydrostatic external pressure and the saturation of the upstream part of the earth dam.

The saturation of the upstream makes a reduction of the effective stresses and hence the safety factor F_s. Therefore, if the reduction of the F_s is not significant, the safety of the dam is not involved.

In case of dynamic event, the presence of the reservoir has additional effects on the dynamic response of the dam: the developments of hydrodynamic pressures due to the vibration of the reservoir and the dam-reservoir phenomena.

The evaluation of the reservoir hydrodynamic pressure acting on the upstream face of a dam was firstly studied by Westergaard (1933), who derived an expression for the pressure on a concrete (infinitely stiff with vertical upstream face) dam. This work was based on the theory of the dilatation of elastic solids and considered the motion of the water in the reservoir under the action of harmonic horizontal excitation.

In 1952, Zangar (Zangar, 1952; Zangar and Haefeli, 1952; Zangar, 1953) studied the hydrodynamic pressures on dams with inclined upstream face. This work considered the water as incompressible and dealt with equations of fluid mechanics. Zangar (1952) understood the relation of resulting equations with the equations describing electricity. He performed experiments using electric analog and presented results obtained from both experimental and analytical expression.

The electric analog method consisted of constructing a tray geometrically similar to the dam and reservoir area. The tray experiments were conducted by first constructing a tank of sheet plastic whose boundary at one end was shaped to represent the upstream face of the dam, while at the opposite end the plastic boundary was installed in a plane (see Figure 3.15).

Since the theory assumed that the dam moves as a rigid body into or away from the reservoir water, the quantity of water displaced for any elemental height of dam was equal to the quantity displaced at any other element of height. This boundary condition can be met in the analogy by establishing a linearly varying potential along the plastic boundary representing the upstream face of the dam.

Thus, a nichrome wire was wound around this boundary to bring about the linear drop in potential. On the contrary, a constant electric potential was placed along the boundary representing the bottom of the reservoir.

The tray was then filled with an electrolyte and the streamlines were connected to a power supply and surveyed by means of a modified Wheatstone bridge which was set to read a constant potential. The distribution and magnitude of pressures on the face of the dam are obtained from the equipotential lines that are constructed from the streamlines.

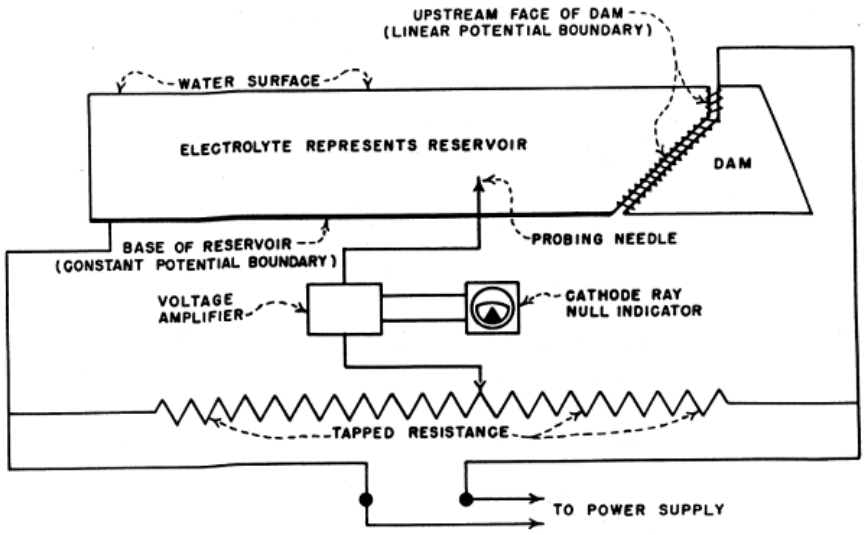

Figure 3.15 Diagrammatic layout of electric analogy tray (Zangar, 1972)

In order to make this study of general values to designers, pressures due to earthquake were determined for several shapes of dams. The studied dams were those with constant upstream slope of 0, 15, 30, 45, 60 and 75 degreed. The pressure at the base of the dam and the maximum pressure on the slope are shown in Figure 3.16.

The following equation (3.12) expresses the hydrodynamic pressures *p(y)* on a dam face:

$$p(y) = C(y)a_c\gamma_w h \quad (3.12)$$

Where a_c is the peak ground acceleration of the input motion, divided by the acceleration of gravity, g, γ_w is the unit weight of water, h is the water depth and C is the pressure coefficient obtained from Figure 3.17 (Zangar, 1952).

In the Figure 3.16, the solid lines show the experimental results (from the electric analog) and the dashed lines show the approximate solution proposed by Zangar (1952) and given by the Equations 3.13.

$$C(y) = \frac{1}{2}C_m\left[\frac{y}{h}\left(2-\frac{y}{h}\right)+\sqrt{\frac{y}{h}\left(2-\frac{y}{h}\right)}\right] \quad (3.13)$$

$$C(y=0) = 0.743\left(1-\frac{\theta^\circ}{90^\circ}\right) \quad (3.14)$$

Where, y is the vertical distance from the free surface, h is the height of the reservoir and C_m, is the maximum value of C. The variation of C and C_m with the value of the slope angle t, are shown in Figure 3.17.

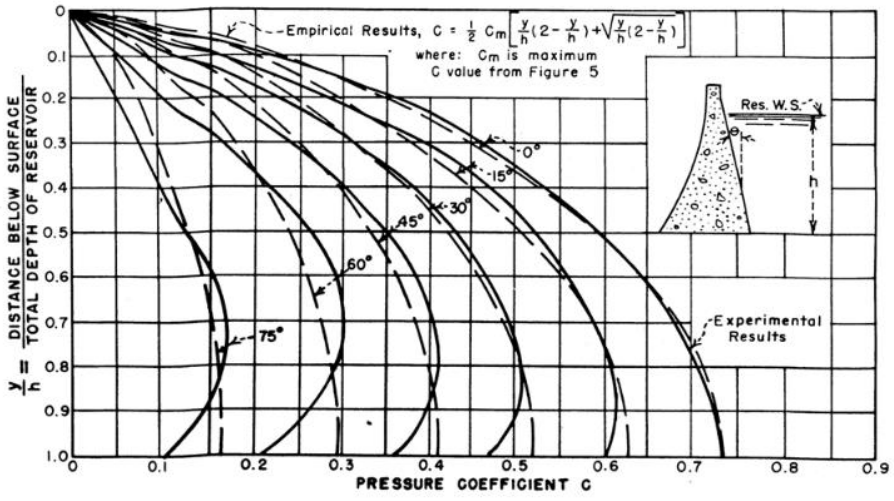

Figure 3.16 Hydrodynamic pressures on a dam face - values of the pressure coefficient C. The solid line represents experimental results, whereas the dashed line represents the empirical equation fitted by Zangar (1952)

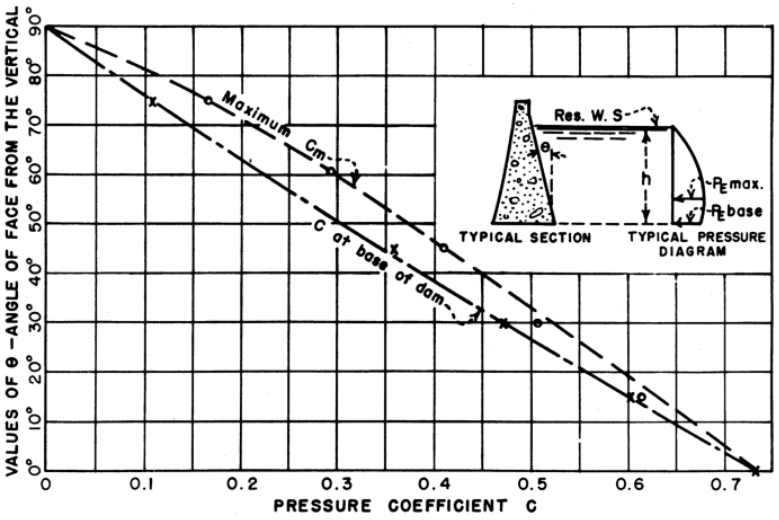

Figure 3.17 Maximum and base coefficient of hydrodynamic pressures on an inclined dam face C & Cm (Zangar, 1952)

The work of Zangar (1952) was followed by Chwang and Housner (1978) and Chwang (1978) in order to calculate the hydrodynamic pressures on rigid dam with inclined upstream face, subjected to horizontal forces.

All the previous studies concluded that in the simplest case of a rigid dam with incompressible reservoir the hydrodynamic pressures on an inclined upstream face are generally smaller than those on the case of vertical upstream face.

The hypothesis of a stiff and un-deformable dam does not consider the interaction of the structure with the reservoir during the dynamic loading. The motion of the reservoir effects the motion of the dam and vice-versa.

Hall and Chopra (1980) studied the effects of dam-reservoir interaction on the dynamic response of a dam with the finite element method, assuming elastic dam response and considering the compressibility of water (Hall and Chopra, 1982,c)

It was shown that the presence of the reservoir increases the fundamental period, T, of the reservoir-dam system (i.e. it becomes more flexible) and changes the magnitude of the dynamic response of the dam, but in case of earth dams those effects are less pronounced than in concrete dams (Hall and Chopra, 1982a,b,c).

According to the previous studies, hydrodynamic effects of the reservoir water upon the concrete facing were disregarded by Seed et al. (Seed, Seed, Lai, &

Khamenehpo-Ur, 1985) considering that this effect is no important for rockfill dams where slopes are with 1:3 (Vertical: Horizontal). These effects have deserved more attention by Boureau et al. (1985) for concrete faced rockfill dams, located in high seismic zones, where slopes were with 1:3 (Vertical: Horizontal) and water pressures are applied directly to the concrete facing. The important conclusion of the Bureau et Al. study was that the hydrodynamic effects can be safety ignored in estimating the seismic response of concrete faced rockfill dams, whereas the static water pressure on the upstream contributes to increase the lateral deformations in downstream direction, when plastic strain occurs.

Similar results were observed by more recent studies (Pelecanos, 2013; Pelecanos et Al., 2016).

Pelecanos (2013) investigated whether the presence of the reservoir alters the response of a dam and the cases in which the dynamic reservoir-dam interaction (RDI) may have detrimental effects. Both rectangular cantilever and trapezoidal homogeneous earth dams were investigated under harmonic and seismic loading (El Centro Earthquake, Imperial Valley, 1940).

The analysis demonstrated that the effects of RDI (both softening and amplification) were found to be insignificant for earth dams due to the sloped upstream face of the earth dam and to its large volume (mass). In fact, the inertial effects from the additional mass from the reservoir are small compared to the inertia of a large earth dam. Moreover, the amplification in an earth dam with a full reservoir seems to be slightly smaller than the corresponding amplification for a dam with an empty reservoir (Fig. 3.18). This could suggest that the presence of the reservoir may damp the dynamic response of earth dams (through the interactive oscillation of two bodies with different vibrational characteristics, such as fundamental period).

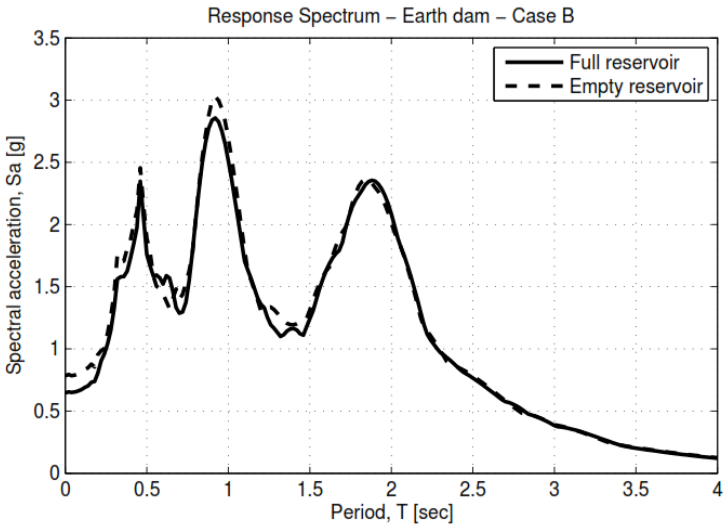

Figure 3.18 Response spectrum (for damping D= 5%) of the accelerations at the crest of the earth dam – (Case B: H=90, Vs=150m/sec) (Pelecanos, 2013).

In all the performed analyses, both the dam and the reservoir rested on a stiff ground and not deformable. The effects of reservoir-dam-foundation interaction were not considered.

Additional analysis were investigated by Pelecanos (2016) on the reservoir-dam interaction (RDI) effects.

The study further investigated the nonlinear elasto-plastic La Villita dam which was founded on a compliant soil foundation. The prototype is an earth-fill dam located in the Guerrero area in Mexico on the Balsas river. During its life, the dam has been subjected under 6 major earthquakes.

Numerical analysis of La Villita dam was carried out in order to explore its performance during earthquake. Two-dimensional (2D), static and dynamic, coupled (mechanical and hydraulic) finite element analyses with the Imperial College Finite Element Program (ICFEP) (Potts and Zdravković, 1999) were performed in an attempt to investigate the seismic behavior of dam.

La Villita Dam model was studied under two of the six earthquake events: the event of 1975 (Ms=5.9; PGA=0.04g and PGA at crest of 0,21g) and the earthquake of 1985 (Ms=8.1; PGA=0.12g and PGA at crest of 0,76g).

Figures from 3.19 to 3.21 show that differences between the analysis with a hydrostatic boundary stress and those with reservoir hydrodynamic pressures are very small. For both the seismic events the numerical analysis demonstrated that the presence of the reservoir "damped" the dynamic response of a dam (smaller acceleration and horizontal displacements, Fig. 3.19, 3.20, 3.21) even if the hydrodynamic pressures were larger (Fig. 3.22) than those obtained using relations from the literature (Zangar, 1952).

Thus, the Spectral Acceleration at the dam crest is slightly smaller for the analysis with reservoir hydrodynamic pressures for both the events (Figure 3.19). Moreover, smaller values were calculated for the horizontal accelerations and displacements in the dam core for the analysis considering the reservoir (Figure 3.20 and 3.21)

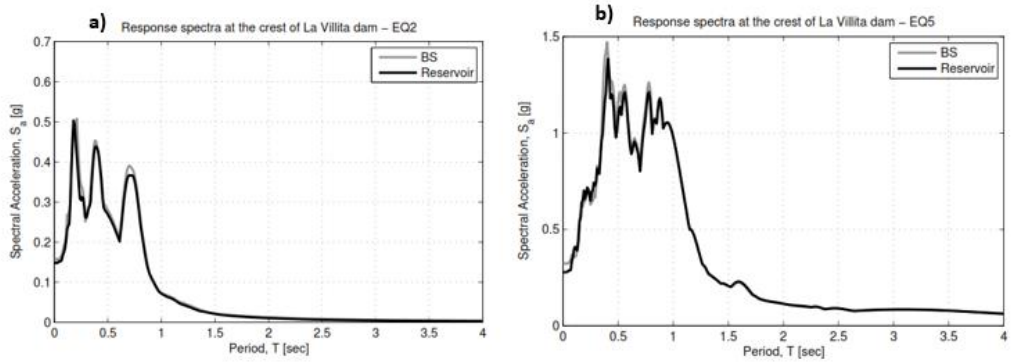

Figure 3.19 Response spectra (damping, D= 5%) at the crest of La Villita dam during the seismic events of 1975 (a) and 1985 (b), defined as EQ2 and EQ5 respectively (Pelecanos, 2013).

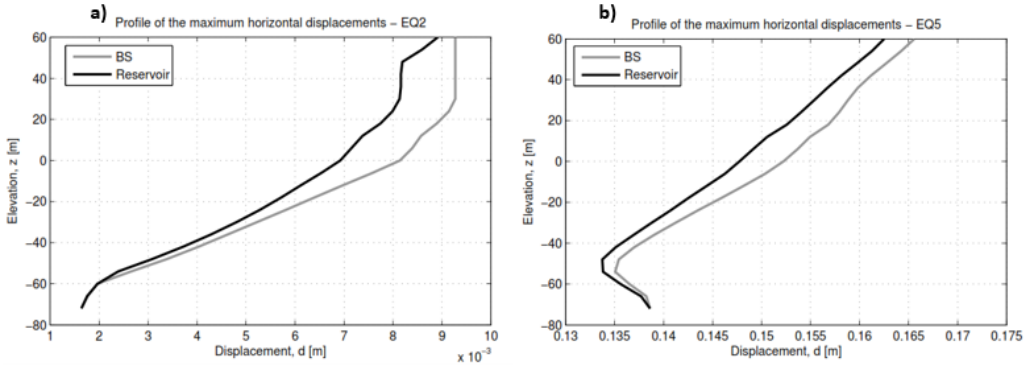

Figure 3.20 Vertical profile of the maximum values of horizontal displacement in the core of La Villita dam during the seismic events of 1975 (a) and 1985 (b), defined as EQ2 and EQ5 respectively (Pelecanos, 2013)

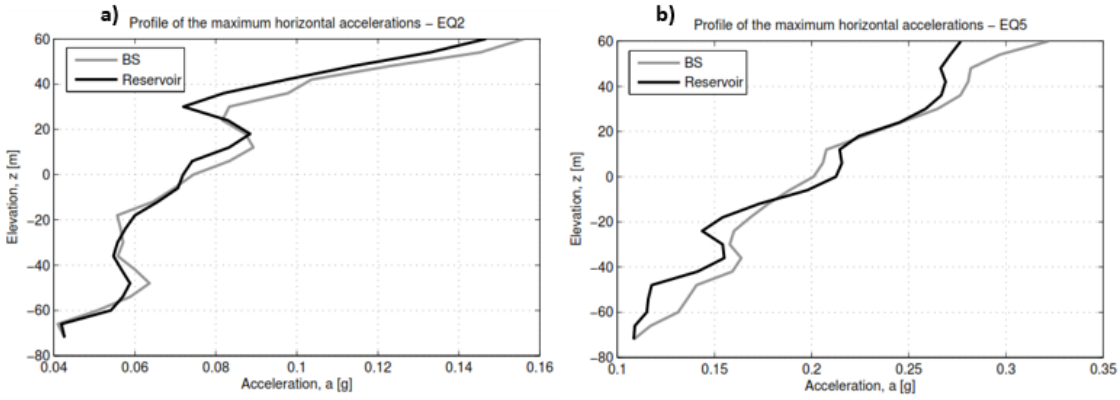

Figure 3.21 Vertical profile of the maximum values of horizontal acceleration in the core of La Villita dam during the seismic events of 1975 (a) and 1985 (b), defined as EQ2 and EQ5 respectively (Pelecanos, 2013)

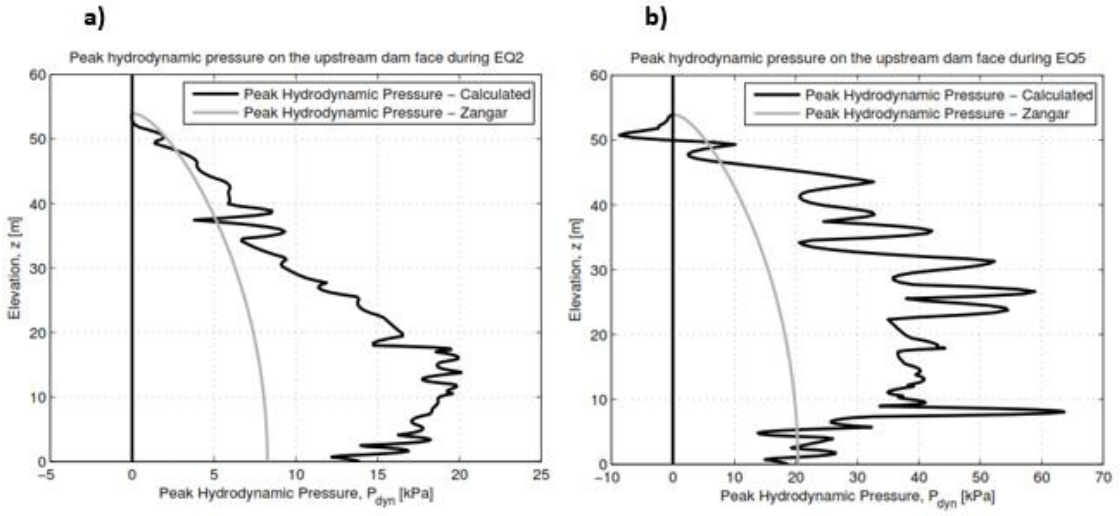

Figure 3.22 Distribution of the peak hydrodynamic pressure on the upstream face of the dam during the seismic events of 1975 (a) and 1985 (b), defined as EQ2 and EQ5 respectively (Pelecanos, 2013)

Finally, it should be noted that the effects of the reservoir-dam interaction were more pronounced for the higher intensity earthquake (defined as EQ5, see Figure 3.19b, 3.20b, 3.21b), with respect to the weaker event (EQ2, see Figure 3.19a, 3.20a, 3.21a). The results of this study is in agreement with the previous ones, showing that the reservoir-dam interaction effects are insignificant in earth dams.

According to the aforementioned studies, an important conclusion can be stated. In order to assess and evaluate the seismic response of an earth-fill dam, the hydrodynamic effects on the upstream slope due to the seismic motion can be safely ignored.

3.2.3.7. Constitutive model

An accurate prediction of the seismic performance of earth dams should investigate simultaneous aspects for describing important features observed at the soil element level. In the recent decades, advanced constitutive models were developed in order to accurately predict pore pressure built-up.

In turn, advanced constitutive models require a more accurate and difficult assessment of soil parameters.

The disadvantage of using an advanced constitutive model to describe soil skeleton response is the definition of several soil parameters and the need for detailed geotechnical characterization of the construction soils.

Two-dimensional (2D), static and dynamic, coupled (mechanical and hydraulic) finite element analyses of the La Villita dam in Mexico were performed by Pelecanos (2013) to investigate the seismic behavior of the dam. The study used the Imperial College Finite Element Program (ICFEP) (Potts and Zdravković, 1999) which implemented a nonlinear elasto-plastic model for simulating the soil material behavior. The model was able to take into account the plastic yielding (Mohr-Coulomb failure criterion) and pre-yielding degradation of stiffness and increase of damping with strain (Logarithmic cyclic nonlinear model). La Villita is a 60m high zoned earthfill dam with a central clay core and outer rockfill shells. The available records of the dam response under the two seismic events affecting the structure were employed to investigate the behavior of the structure during earthquakes and to validate the applied numerical modeling approach.

The computed response was performed in term of acceleration at the dam crest, the associated response spectra and displacements which were compared with the available field data.

It was observed that the calculated acceleration and the relative response spectra were significantly smaller than the recorded ones. The reason of those results was attributed to the two-dimensional softer system which simulated an infinitely wide canyon. The stiffening effect of the canyon geometry was considered by increasing the material stiffness of the dam, according to the study of Dakoulas and Gazetas (1987).

The dynamic analysis of la Villita Dam was then repeated with the updated value of the maximum shear stiffness and the acceleration time history and the associated response spectra at crest showed a better agreement. Different outcomes were observed for the accumulated displacements. The magnitude of computed crest settlements was found to be very small compared to the recorded values for both the seismic events. The magnitude of these deformations was not comparable to the recorded vertical settlements of the crest.

Moreover, the researcher examined the effects of using a coupled formulation for performing dynamic analysis of zoned earth dams. The study performed a parametric analysis of La Villita dam comparing the results obtained by the coupled and uncoupled formulation. It was observed that the dynamic response of the dam with coupled or uncoupled analysis was almost identical. It was evidenced by the calculated acceleration at the dam crest, the associated response spectra and displacements. It should be noted that the study did not show the influence of using a coupled formulation for performing the dynamic response of a zoned earth dam.

The work by Sica and Pagano (2009) illustrated the theoretical and the experimental procedure adopted to characterize the seismic response of the Camastra Dam, a zoned earth dam with vertical clay core, placed in a highly seismic zone of Southern Italy. The approach performed a coupled dynamic analysis implementing the GEFDYN code (Aubry and Modaressi, 1996), adopting an elasto-plastic model (Aubry et al., 1982; Aubry and Modaressi, 1996), characterized by kinematic and isotropic hardening.

The selected numerical tool allowed to compute the permanent settlements that occurred at the crest and the dynamic pore water pressures generated during the seismic event in the clayey core where the coupled approach was adopted.

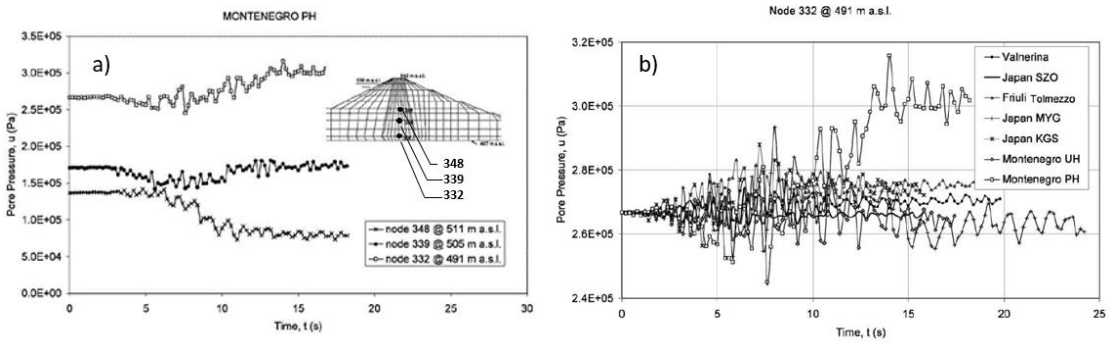

Figure 3.23: Computed pore water pressures time histories: a) at the three nodes of the core axis under the strongest earthquake (Montenegro PH) and b) at the node 332 of the core axis under the reference earthquakes (Sica and Pagano, 2009)

The analysis showed the evolution of the pore water pressures generated in the core by the earthquakes. In the case of the zoned Camastra Dam, the node close to the dam base tended to dilate and did not show a large development of excess pore water pressure, even in the case of the strongest shaking (see Fig. 3.23). According to the moderate development of excess pore water pressures, the analysis showed that the computed crest settlements were found to be lower than 0.5% of the maximum height of the dam, even for the stronger earthquakes with a return period higher than 5000 years (according to the local seismic hazard analysis). The results were well below the threshold value of 1% assumed as tolerable for the earth dam. The author highlighted the importance of using such advanced constitutive model for the seismic verification of real case of earth dams but at the same time it should be noted that the numerical predictions of the study were not compared to any field data which could confirm or not the computed results.

With regard to the computed excess pore water pressures and the permanent settlements observed at the dam crest for the stronger earthquakes, it should be noted that such complex constitutive model doesn't seem to be relevant for the prediction of the dynamic behavior of an existing zoned earth dam.

The use of such a complex constitutive model to describe soil skeleton response of earth dams involves the definition of several soil parameters. Big efforts must be devoted for characterizing the dam soils: the estimation of those parameters

requires detailed geotechnical characterization of the materials which are not often available for existing earth dams in Italy.

The aim of this work is the definition of a methodology for the seismic performance of existing zoned earth dam which should be friendly used by the potential stakeholders. For such reason, the methodology considers a simpler procedure which requires a minor number of parameters. The procedure doesn't account the effect produced by the pore water pressures at the end of the dynamic analysis but a calibration of the model shows a good agreement with the experimental and the computed results (see Chapter 4).

3.2.4. Evaluation of the dynamic response of a zoned earth dam

The seismic analysis of existing earth dams should be aimed at controlling the safety level of these structures. The objective is essentially represented by their ensuring water tightness.

At the end of the dynamic analysis, the dam behavior should be synthesized as a parameter in order to understand its performance in light of the limit states described at Par. 3.2.1 and the modern performance-based design philosophy.

Water tightness damages may be induced by strong earthquakes affecting the structure during its life.

Global sliding mechanism, freeboard loss due to permanent settlements, fractures of the water tightness element followed by erosion phenomena and the liquefaction of the embankment or the foundation soils are feared phenomena which may affect the safety level of a dam and its water tightness (Sica and Pagano, 2009).

Generally, the seismic response is defined through the evaluation of the amplification of the input motion, the stress and the strain level developed in the embankment or foundation. The seismic safety level of a dam may be controlled by the permanent settlements affecting the structures which represent the amount of deformation and damage induced by an earthquake.

In this case, a displacement based approach should be evaluated to quantify the seismic safety of the embankment.

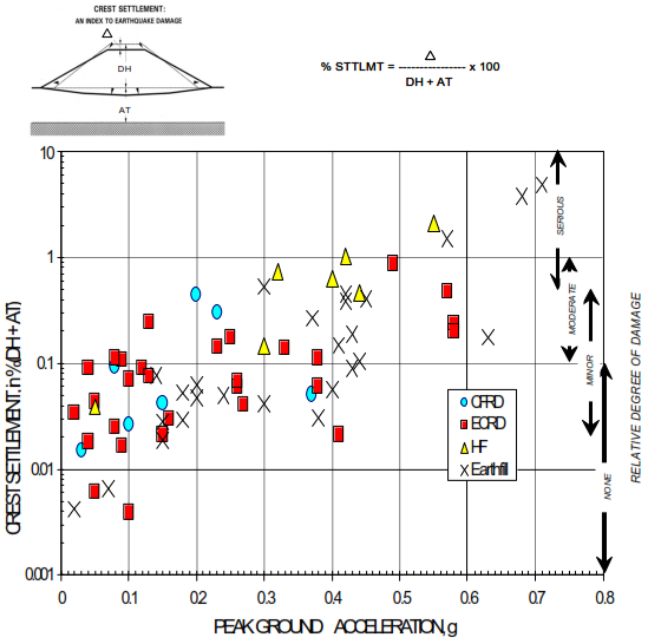

Figure 3.24 Dam crest settlements ratio (S/H) vs. PGA (Swaisgood, 2003)

The vertical settlement (in its meaning of medium vertical strain) can represent a demonstrative indicator of global instability phenomena.

According to Sica et Al. (2008), permanent settlement at the dam crest is also a suitable indicator of structure performance to characterize dam mechanical response under different seismic scenarios.

Swaisgood (2003) collected data about the settlements observed on dam's crest after past earthquakes (Figure 3.24). The crest settlement was selected as the parameter to represent the earthquake induced deformation. It was the most often mentioned quantified measurement of damage presented in the case histories. It also appears to be directly related to the severity of deformation, cracking, i.e., as the percent of crest settlement increases, the extent of deformation and cracking that occurred also increase. The diagram (Figure 3.24) plots the dams crest settlement with the Peak Ground Acceleration (PGA) on site. The figure shows also different degrees of damages related to the observed crest settlement ratio.

According to the previous research, Ishihara (2010) and Sêco & Pinto (2010) studied the effects of earthquakes on several zoned and rockfill dams. In both cases, the ratio between the measured crest settlement (S) and the dam height (H) (settlement ratio) has been related to the peak horizontal acceleration recorded at dam's base. The conclusion of both studies is that the value of 1% of settlement ratio does not compromise the stability and the serviceability of the embankment and the reservoir. Observing the seismic performance of earth dams during past earthquakes, Sica and Pagano (2009) state that earth dams did not suffer damage (with respect to water tightness) when the permanent settlement at the dam crest was lower than 1% of the maximum embankment height H.

The recent studies confirm the Swaisgood's research (2003) where the threshold value of 1% represents the transition between moderate to serious damage and it can be adopted as a plausible limit threshold to assess dam performance.

When the settlement ratio is less than 1% some local instabilities can occur but the global stability of the embankment should be ensured. This criterion has been also employed for the evaluation of the performance analysis of the Camastra dam (Sica and Pagano, 2009) and the Conza dam (Brigante and Sica, 2012).

In this case, facilities can be damaged but without uncontrolled release of water. This threshold value can be assessed as the limit where the stability of dam and its serviceability are not compromised. According to the literature, the performance criteria for the DLS in current Italian Code can be respected when the settlement ratio S/H is less than 1%.

With respect to other damage mechanisms that are very difficult to simulate; e.g. vertical fractures of the embankment due to differential settlement among different cross-sections, fractures at the contact between the embankment and structural elements, the relative displacements between the core and the rockfill dam body may represent another important performance parameter. Differential settlement can be compared with the relative settlement ratio in order to quantify the level of damage.

In the current Italian Code, the CLS occurs when global instability or liquefaction of embankment and foundation occurs.

For the evaluation of the dam performance regarding the CLS, the global sliding must be avoided in order to prevent the uncontrolled release of the reservoir water that represents a high risk of human losses.

For the CLS, Albano (2013) evaluated the limit condition of an existing bituminous faced rockfill dam. This study accounted for a methodology followed to evaluate the seismic performance of the real case and suggested that when the residual vertical settlement is lower than the freeboard, no collapse mechanism is established. The prediction of the permanent settlement at the dam crest is adopted for checking freeboard loss. The control of the vertical settlement with respect to the freeboard can be adopted as a parameter for the performance criteria of earth zoned dam for the CLS limit state in current Italian Code.

According to the indicator of dam performance proposed by Albano (2013), the performance criteria for the CLS can be respected when the vertical settlement is smaller than the freeboard F of the dam.

Chapter 4

CALIBRATION OF THE MODEL WITH CENTRIFUGE TEST

The chapter describes numerical analyses of the seismic response of two earth dam models. The finite element method was employed using a FEM (Finite Element Method) analysis and to perform the static and dynamic non-linear elasto and elasto-perfectly plastic analysis of two simulations.

The simulation of the dynamic behavior of earth dams was studied with the testing equipment of Korea Construction Engineering Development (KOCED) at the Geotechnical Centrifuge Testing Center of Korea Advanced Institute of Science and Technology (KAIST) (Kim at Al., 2013). The objective of the current work is to reproduce the observed behavior of the tests and compare the numerical prediction with the recorded response. This work was preparatory to the calibration of the numerical method and the constitutive model which will be adopted for studying the seismic behavior of existing earth dam models for a defined seismic scenario in Italy. The description of the adopted numerical method will be discussed with more details in Chapter 5.

4.1. Centrifuge Test

Centrifuge modeling can reproduce, in a small scale, the in situ stress-conditions of very high/deep geotechnical structures. Therefore, the centrifuge modeling is a very useful tool to experimentally investigate the behavior of geotechnical systems (piles, dams, etc.). Many centrifuge model tests have been conducted to investigate the behavior of dams under seismic conditions (Ng et al., 2004; Sharp and Adalier, 2006; Peiris et al., 2008).

Due to the lack of available records on the seismic behavior of real dam cases, two centrifuge experiments (Kim M.K. et Al, 2011 and Park S.Y. et Al. 2016). were used in order to calibrate the numerical analysis. These centrifuge tests have been mentioned here respectively as TEST 1 and TEST 2.

The aforementioned centrifuge tests were performed with the testing equipment of Korea Construction Engineering Development (KOCED) at the Geotechnical Centrifuge Testing Center of Korea Advanced Institute of Science and Technology (KAIST) (Kim at Al., 2013).

4.1.1. The scaling factors of the centrifuge test

Physical modeling technology using a centrifuge is currently applied in various geotechnical engineering fields: foundation system, earth structures, offshore systems, earthquake related problems, geo-environmental studies, etc. (Kimura, 1998).

The basic idea of physical modeling of geotechnical system using a centrifuge is to accelerate a reduced scale geotechnical structure to the appropriate high g-level to simulate the prototype scale stress field in the model structure.

When the model is made on a reduced scale of 1:N, it is accelerated at N times the earth gravity. In this case, the stress level at any point of the model is similar to the corresponding point of the prototype, as shown in Figure 4.1.

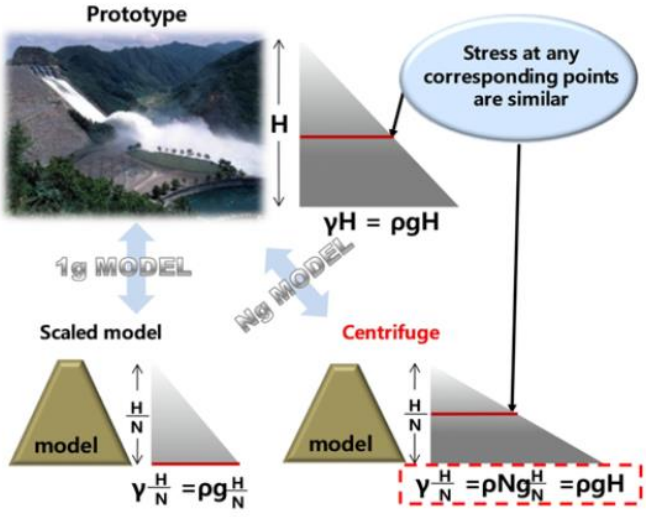

Figure 4.1 Concept of Physical Modeling using a Geotechnical Centrifuge (Kim D.S. et Al., 2013)

The centrifuge models are built at a reduced scale reproducing the same shape of the prototype structure. In this way, users can observe the structural behavior of

the model, easily. Large-scale centrifuge equipment has become available in geotechnical engineering and the centrifuge test has been applied to various geotechnical problems. In geotechnical centrifuge testing, the basic scaling law is deduced from the need to ensure the same stress between the model and corresponding prototype.

When an acceleration of N times earth gravity (g) is applied to a material of density ρ, the vertical stress σ_v at depth h_m in the model is given by the following relation (Equation 4.1):

$$\sigma_{vm} = \rho N g h_m \quad (4.1)$$

In the full scale prototype, indicated by subscript p, the vertical stress is equal to (Eq. 4.2):

$$\sigma_{vp} = \rho g h_p \quad (4.2)$$

From the fundamental concepts underlying centrifuge modeling, the vertical stresses at the model and the prototype are identical (Eq. 4.3):

$$\sigma_{vm} = \sigma_{vp} \text{ and } N h_m = h_p \quad (4.3)$$

Where the scale factor for linear dimensions is 1:N.

Basic scaling factors for physical quantities in centrifuge testing are based on a dimensional analysis using this linear dimension scale. In Table 4.1, the principal scale factors used for different variables in centrifuge modeling are synthetized. Most of the scaling factors for the modeling can be derived from those factors.

Variable	**Scaling Factor (Model vs Prototype)**
Length	N^{-1}
Acceleration	N
Density	1
Stresses	1
Strain	1
Deformations	1
Displacements	N^{-1}
Permeability	1
Hydraulic gradient	N
Loading frequency	N
Time (inertial effects)	N^{-1}
Time (seepage, consolidation, spread)	N^{-2}

Table 4.1 Scaling Factors for different variables in Centrifuge Modeling (Bilotta and Taylor, 2005)

A controversy has interested the evaluation of scaling factor for seepage phenomena. The controversy was based on the interpretation of the hydraulic gradient and the Darcy permeability (Bilotta and Taylor, 2005). According to the Darcy's Law, the flow of a fluid through a porous medium is controlled by the following equation (4.3a):

$$v = ki \quad (4.3a)$$

Where v is the fluid velocity through a porous medium, k is the soil permeability and i is the hydraulic gradient.

In fluid mechanics soil conductivity is expressed as function of intrinsic conductivity $K = k\frac{\mu}{\rho g}$. In the hypothesis of using the same fluid in the model as in the prototype, the soil permeability can be apparently governed by the gravity. The following equation describes the permeability relation between the model and the prototype (4.3b):

$$k_m = Nk_p \quad (4.3b)$$

The hydraulic gradient can be defined as the ratio between the elevation head Δs and the relative distance ΔL where the hydraulic head dissipates. The hydraulic gradient is dimensionless so it is not scaled with the acceleration ($i_m = i_p$) (Croce et Al 1984, Butterfield, 2000).

According to this first hypothesis, the fluid velocity of the model is N time the relative value of the prototype.

$$v_m = i_m k_m = i_p N k_p = N v_p \quad (4.3c)$$

Although this concept seems logical, it determines an incongruence: a soil is impervious when the gravity is null. In zero-gravity situation, the hydraulic gradient should be null and all porous soils were impervious.

Another hypothesis (Schofield,1980) is based on considering the hydraulic gradient as the ratio between pressure head and distance. In this case the gradient can be evaluated, as follow (4.3d):

$$i_m = i_p N \quad (4.3d)$$

The Darcy's conductivity can be considered as an intrinsic parameter of the soil and fluid and it can be expressed as $k_m = k_p$, so the fluid velocity is:

$$v_m = i_m k_m = N i_p k_p = N v_p \quad (4.3e)$$

According to the $k_m = k_p$ assumption, it should be noted that the intrinsic permeability is the same in the gravity field. Tan & Scott (1985) observed that this assumption is not commonly used in Soil Mechanics, but it is suitable with centrifuge modeling of seepage events.

Anyway, both hypothesis lead to same result where the fluid velocity has a scaling factor of 1:N (Eq. 4.3c and 4.3e).

The Time for seepage problem can be calculated as:

$$t_m = \frac{L_m}{v_m} = \left(\frac{L_p}{N}\right)\left(\frac{1}{N v_p}\right) = \frac{1}{N^2} t_p \quad (4.3f)$$

The scaling factor is $1:N^2$. When the prototype and the model have different conductivity values, the time function is represented by Eq. (4.3g):

$$t_m = \frac{1}{N^2}\frac{k_p}{k_m} t_p \quad (4.3g)$$

The seepage scaling factor is the same for consolidation problem where time is expressed as function of dimensionless time $T_v = \frac{c_v t}{H^2}$.

$$\frac{c_{vm} t_m}{H_m^2} = \frac{c_{vp} t_p}{H_p^2} \quad (4.3h)$$

Since $H_p = N H_m$, the following equation (Eq. 4.3h) expresses the consolidation time:

$$t_m = \frac{1}{N^2}\frac{c_{vp}}{c_{vm}} t_p \quad (4.3h)$$

4.1.2. The centrifuge testing equipment at KAIST

The centrifuge testing of KOCED at KAIST is one of the 10 biggest centrifuges in the world, in terms of maximum capacity. The centrifuge has an asymmetric design and is balanced by massive counterweight at the opposite side of the testing model. General specifications of this 5 m radius, 240 g-tons beam centrifuge, are listed in Table 4.2.

Item	Specification
Platform radius	5,0m
Max Capacity	240g-tons
Max acceleration	130g with 1300 kg payload
Max model payload	2400 kg up to 100g
Platform dimensions	1,2m(L) x 1,2m(W) x 1,2m(H)
Power consumption	220kW for full capacity operation
Fluid rotary joint	4lines – water & pneumatic (700kPa) 6lines – hydraulic oil (20Mpa)
Electrical slip ring	8lines for electrical power supply 30lines for signal transmission 4channels for video transmission
Fiber optic rotary joint	1GHz, 2 passages

Table 4.2 Specification of KOCED Geotechnical Centrifuge (Kim D.S. et Al., 2009)

Figure 4.2 illustrates configuration of the Geotechnical Centrifuge System of the KOCED at KAIST.

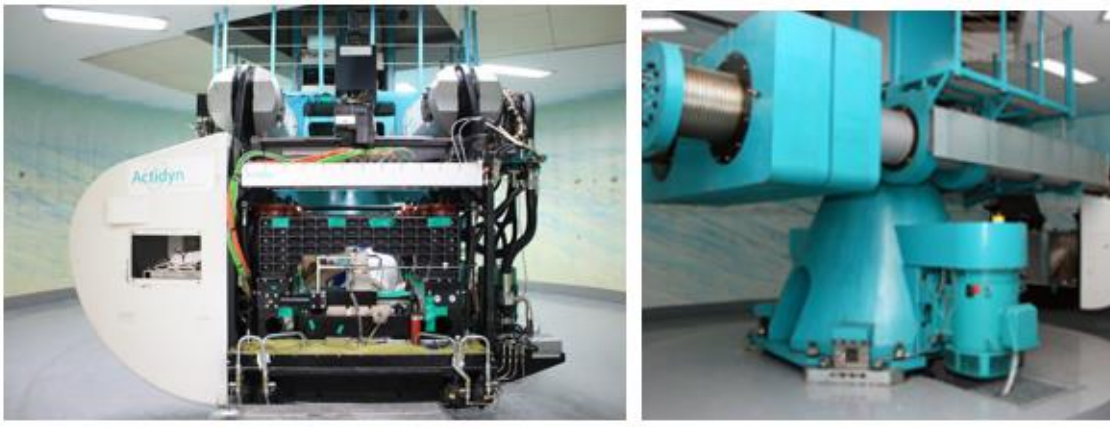

Figure 4.2 KOCED Geotechnical Centrifuge Systems

4.2. Centrifuge TEST 1

Centrifuge test 1 (TEST 1) aimed to simulate the seismic behavior of two typical cross sections of earth dams: Earth Core Rockfill Dam (ECRD) and Concrete Faced Rockfill Dam (CFRD).

This work wants to examine the seismic behavior of earth dams in Italy with a similar configuration of the studied ECRD. Thus, only the centrifuge test of the ECRD was analyzed.

Kim et al. (2011) tried to reproduce the experimental results of TEST 1 by means of numerical analyses. They used an explicit Finite Difference approach with a linear equivalent constitutive model. In practice, they used the commercial code FLAC 2D. This study has tried to reproduce the experimental results of TEST 1 by means of FEM approach. The commercial code Quake/W was used to this end. Both the linear equivalent and a true non-linear model were used with Quake/W. In the following, the experimental and the numerical results will be compared.

4.2.1. TEST 1 conditions

Based on a database of existing dams in Korea, typical cross-sections of the model was designed, as shown in Figure 4.3.

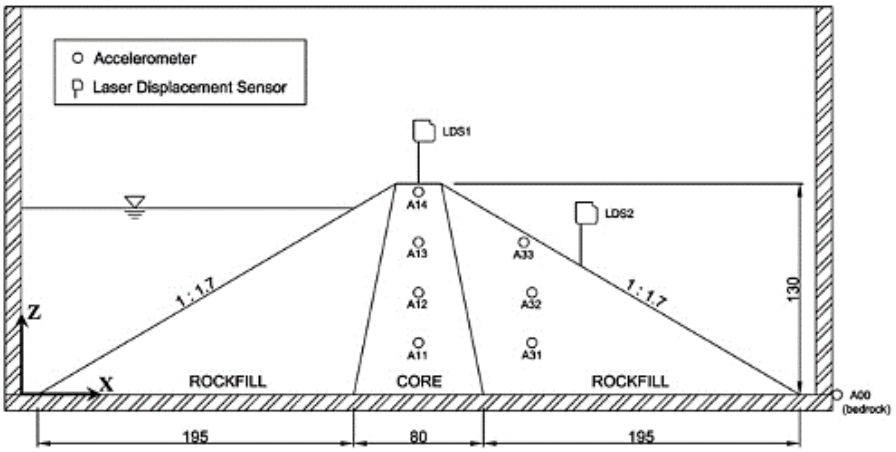

Figure 4.3 Layouts of model ECRD dam and its instrumentation (Kim M.K. et Al., 2011)

The slope of the ECRD model was 1:1.7 and the upstream and downstream directions were designed with the same selected slopes.

A scaling ratio (N) of 40 (referring to the centrifuge acceleration of 40g) was selected. The ECRD model was 130 mm high, simulating 5.2 m high in a prototype scale.

Because ECRD is mostly constructed on top of bedrock in Korea, the dam model was constructed directly on the baseplate of a soil container. In order to simulate the friction between the bedrock and the dam body, sand paper was glued onto the baseplate and the model dams were constructed on it. The side walls of the container were covered with grease to minimize side friction, resulting in a plane strain condition. The dam model was constructed with four layers to keep the densities uniform. Each layer was compacted to 95% relative compaction by a hand compactor at an approximate compaction energy of 750 kN m/m.

A thin membrane was placed on the upstream slopes of the ECRD. The membrane was also glued onto the bottom and sides of rigid container in order to prevent water from penetrating into the dam body and allowing water to be contained in the upstream side.

Therefore, the filled water imposed a water load on the upstream slope during the earthquake simulation. The upstream reservoir was filled up to 90% of the dam height.

Accelerometers were embedded in the model embankment as arrays at the center and downstream of the dam to investigate the amplification of the earthquake acceleration. Laser sensors and a high-speed camera were also mounted to measure the vertical settlement and horizontal displacement, respectively.

A series of staged tests were performed on the dam models with real earthquake history (Ofunato Earthquake, see Figure 4.4) whose horizontal acceleration magnitude was scaled from about 0.065 to 0.35g (Table 4.3).

Test numbers	**ECRD**
	Bedrock acceleration (g)
001(*)	**0.065**
002	0.082
003	0.087
004	0.098
005(*)	**0.116**
006	0.145
007(*)	**0.221**
008(*)	**0.348**

Table 4.3 Centrifuge tests with the acceleration magnitude scaled from about 0,065g to 0,35g. The starred bold writings are the selected input motions used in the numerical analysis.

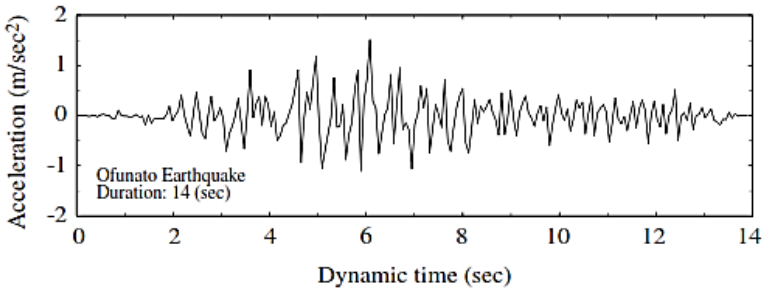

Figure 4.4 Ofunato Earthquake history (in prototype scale) (Kim M.K. et Al., 2011)

Based on the test results, the amplification of the acceleration, horizontal and vertical deformations of the dam body were analyzed.

4.2.2. Materials

The material properties of the core and the rock-fill were controlled to represent the average material properties of existing dams in Korea; they were evaluated in a triaxial compression test and in a resonant column test.

The rock-fill zones were constructed with rock-fill material collected from a dam construction site. Because the particle size of actual rock-fill material was too large, it was reduced to be suitable for small scale model. The model rock-fill materials were constituted by sieving the in-situ rock-fill materials by 20 mm sieve.

The material was reduced by a similar particle distribution method. The particle size distribution curves of the model were parallel to those of the prototype materials (see Figure 4.5), mainly attempting to simulate their original properties properly (Kim M.K. et Al., 2011) and respecting the centrifuge scaling laws.

The core material was constituted by mixing clean sand and silica silt to meet the Korean standard specification for a core zone which should contain more than 20% of fine material finer than 0.1 mm (MOCT, 2005).

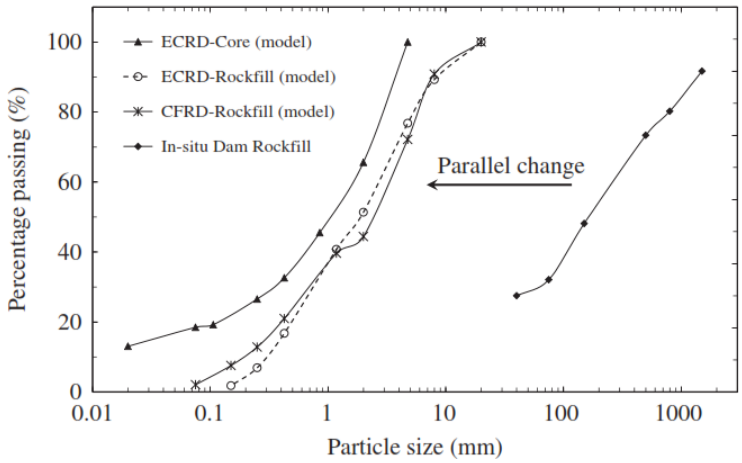

Figure 4.5 Particle size distribution curves of the prototype and model materials (Kim M.K. et Al., 2011)

To ensure that the model materials represented the prototype materials, the material properties of the models were evaluated by laboratory tests which were performed under the confining pressures expected in the in-flight centrifugal acceleration condition. The shear wave velocity of the model materials is shown on Figure 4.6 for the specified confining pressure. Those values are compared with the in-situ shear wave velocity database for existing dams in Korea.

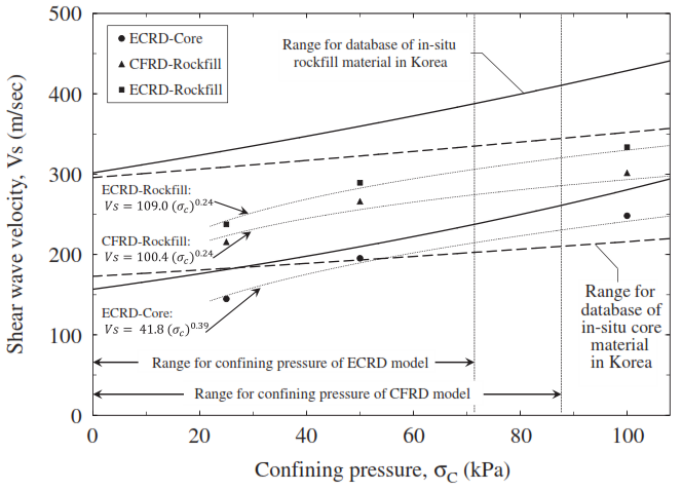

Figure 4.6 Shear wave velocity of the model materials obtained by resonant column tests (Kim M.K. et Al., 2011).

In addition, strength parameters were measured by performing triaxial shear tests with 50 mm diameter specimen constructed at the same construction condition of the centrifuge models. The construction conditions and strength parameters of the model materials are listed in Table 4.4.

Property	ECRD - rockfill	ECRD - core
γ_d (g/cm^3)	2.02	1.92
w (%)	4	9.0
γ_t (g/cm^3)	2.10	2.10
c (kPa)	2	64
φ (deg.)	40	33

Table 4.4 Material property and construction conditions of centrifuge model materials (Kim M.K. et Al., 2011).

4.2.3. Centrifuge TEST 1 Results

Results were expressed in term of horizontal acceleration time-histories and frequency contents, measured along the center line of the core and in the downstream shell.

During the stage tests, settlements were continuously measured by laser displacement sensors. The residual settlement amounts were obtained after each test. The cumulative settlements at the crest are shown in Figure 4.7.

In the following, tables and pictures show the outputs from the ECRD centrifuge *test 1*.

Test Numbers	ECRD		
	Bedrock acceleration (g)	Amplification ratio	Crest Settlement (mm)
001(*)	**0.065**	**2.00**	**-0.22**
002	0.082	2.16	-0.25
003	0.087	1.77	-0.02
004	0.098	2.00	0.42
005(*)	**0.116**	**1.29**	**0.33**
006	0.145	1.57	0.56
007(*)	**0.221**	**1.75**	**1.88**
008(*)	**0.348**	**1.84**	**9.72**

Table 4.5 Summary of the centrifuge results in the prototype scale. All tests were performed at centrifugal acceleration of 40g by using Ofunato earthquake record for input seismic load (Kim M.K. et Al., 2011)..

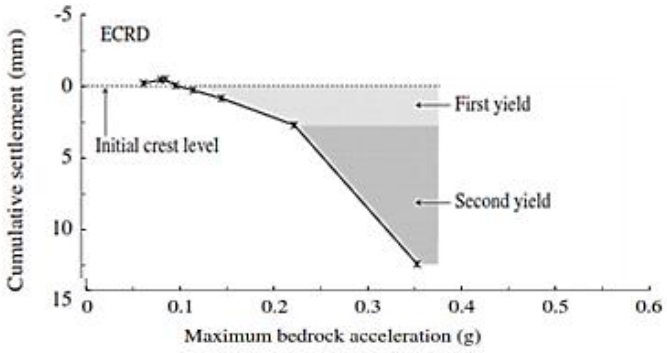

Figure 4.7 Cumulative settlement histories with increasing maximum bedrock accelerations (Kim M.K. et Al., 2011).

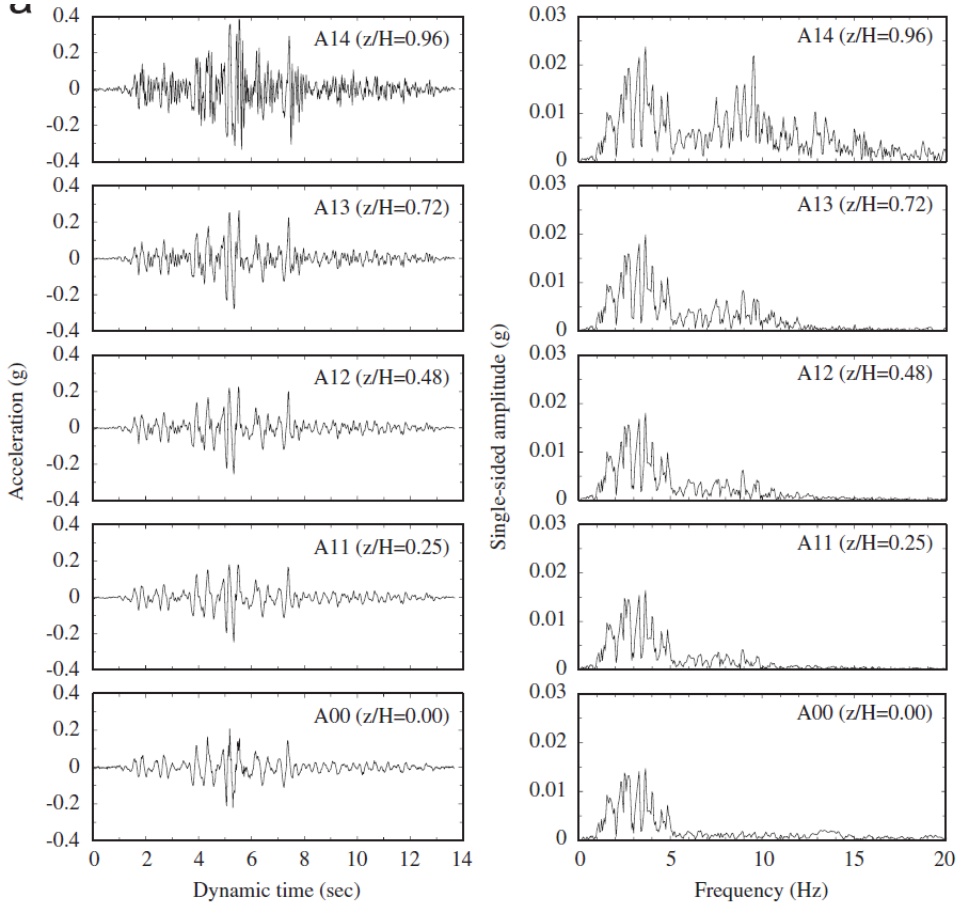

Figure 4.8 Acceleration records and Fourier spectrums at different depths of the ECRD model (maximum bedrock acceleration=0.221g) Accelerometers A00, A11, A12, A13, A14 at the center of dam (Kim M.K. et Al., 2011).

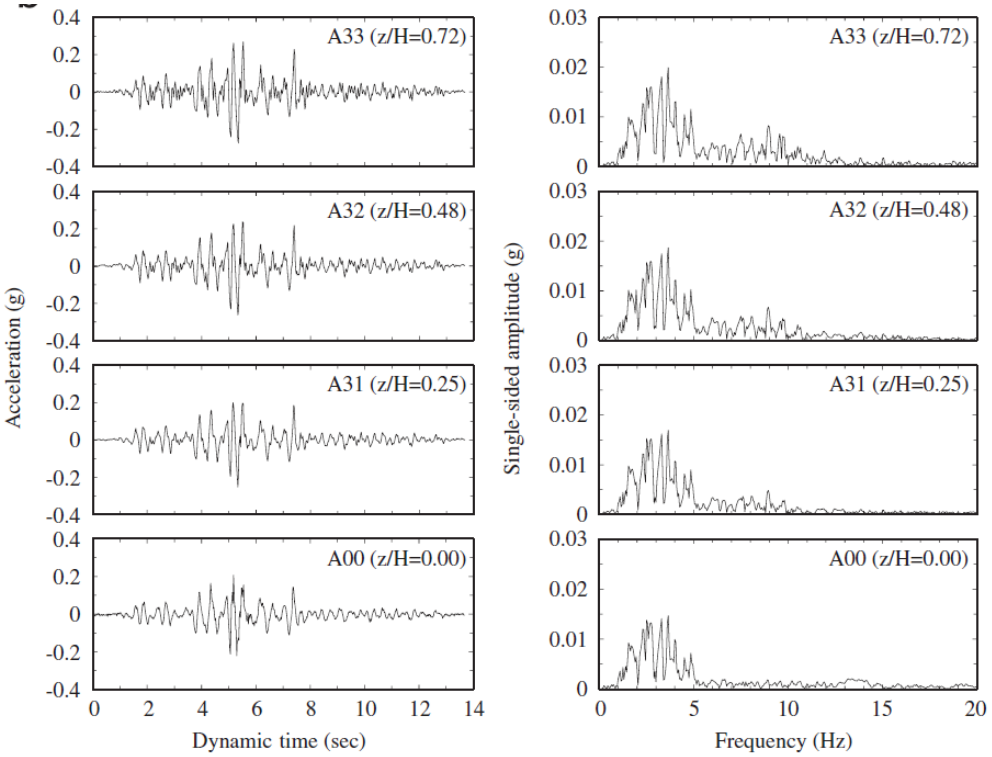

Figure 4.9 Acceleration records and Fourier spectrums at different depths of the ECRD model (maximum bedrock acceleration=0.221g). Accelerometer A00, A31, A32, A33 at downstream slope (Kim M.K. et Al., 2011).

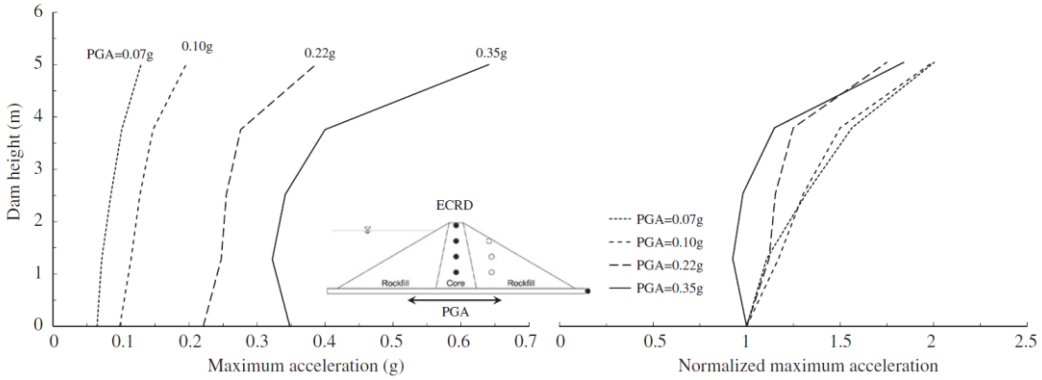

Figure 4.10 Maximum acceleration and normalized acceleration distributions at the center for the centrifuge tests (in the prototype scale) (Kim M.K. et Al., 2011).

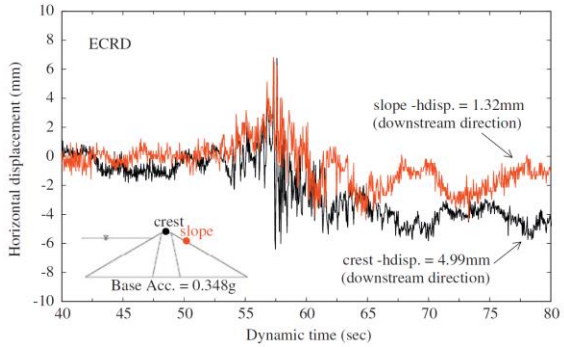

Figure 4.11 Horizontal displacement obtained by the image-processing technique for a PGA=0,35g (Kim M.K. et Al., 2011).

Kim et al. (2011) performed the numerical analysis of the ECRD prototype, using the two-dimensional commercial explicit finite difference code FLAC 2D.

The experimental and computed results (Kim et al., 2011) will be compared with the numerical response obtained by the present study (see the following Par. 4.3).

4.3. Numerical modelling of centrifuge TEST 1

The previously dynamic centrifuge *test 1* of an ECRD has been numerically simulated in order to calibrate and reproduce the numerical response of an earth dam under seismic motion, using the Finite Element Modeling (FEM) software.

Four of eight tests reported in Table 4.5 (the starred bold tests) were selected and numerically performed. The experimental and numerical results will be expressed and compared in term of acceleration, Fourier Spectrum and displacements at crest and the downstream shell.

4.3.1. Description of the Numerical Model

The Quake/W FEM software was used to simulate and reproduce the experimental results of TEST 1. The software consists of a 2D dynamic finite element analysis that uses both the equivalent linear strain dependent modulus and damping properties and the cyclic non-linear approach. It uses a time-step analysis with Rayleigh damping and allows for variable damping for different elements. The model and the relative mesh are shown in Figure 4.12 and refer to the centrifuge model of Figure 4.3. The embankment is composed by the core and the shells, rested on the rigid foundation.

Local boundaries were placed far enough to minimize wave reflections from the confines. Several attempts have been carried out to reduce local boundary effects and together minimize computational efforts.

The size of the mesh was determined by the criterion considering the maximum frequency and the minimum shear wave velocity to avoid numerical distortion of the propagating ground motion and to obtain an accurate computation of the model response (see Chapter 3.2.3.4).

The seismic input applied at the base of the numerical model was the Ofunato Earthquake motion, scaled from 0,065g up to 0,35g. It was the same located at the base of the centrifuge model, increased by the scale factor of N=40.

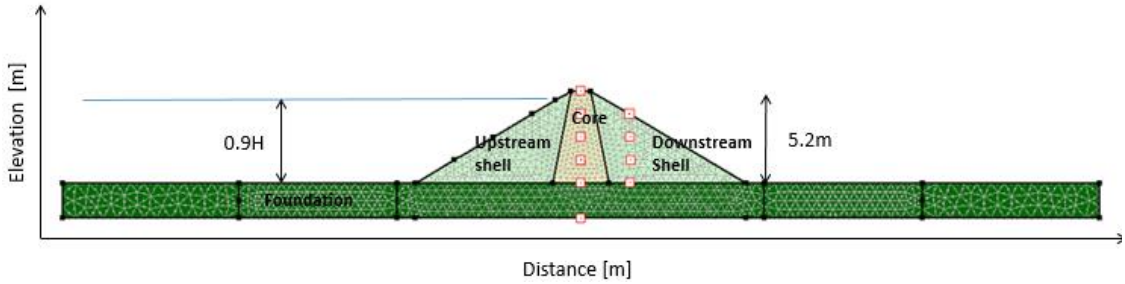

Figure 4.12 Two dimensional finite element mesh of the ECRD

4.3.2.1. Calibration of the constitutive model

Prior to the dynamic analysis, the static analysis should be carried out to establish the existing in-situ stresses. Indeed, the static stress distribution affects the seismic response and stability of the dam (i.e. the dynamic shear modulus of the dam structure and foundation materials depends on the static confining pressure).

In the first phase of the numerical studies, a sub-stage was modeled using the QUAKE/W "in-situ stress" module and this is used to simulate the development of geostatic stresses in a dam with an empty reservoir condition (hence, just after construction).

In the second phase of the static analysis, hydrostatic pressure was applied to the upstream face of the dam using the "Load-deformation analysis" unit of the SIGMA/W module.

Based on the full reservoir level ($H_{Reservoir}$=0,9H), the hydrostatic pressure was calculated for a triangular variation towards the base of the reservoir, with a zero value at the reservoir water level. Hydrostatic pressure was calculated using $P=hx\gamma$; where γ is the unit weight of water and "h" is the depth from the reservoir water level. Continuous hydrostatic pressure is applied as pressure on the foundation on the upstream. According to the statement of Par. 3.2.3.6, hydrodynamic reservoir effects have been neglected in the first analyses. In a second moment, the numerical analyses were repeated considering the relative hydrodynamic pressures on the upstream slope, using the Zangar (1952) solution (Par. 3.2.3.6).

The seepage flow inside the dam body was not considered to reproduce the centrifuge experiment carried out by Kim et Al. (2011).

Since the dam centrifuge model rested on the rigid container, the foundation was assumed to be as a linear elastic material.

The foundation parameters are presented in the following Table 4.6.

Foundation Parameters					
γ **[kN/m³]**	φ **[°]**	**c [kPa]**	**V_s [m/sec]**	ν	**D_{max} [%]**
27	45	0	3'103.7	0.2	1

Table 4.6 Parameters adopted in the numerical analysis of the dam for the foundation.

The geotechnical parameters used in the numerical analysis for the rockfill shell and the impervious zone are presented in Table 4.4.

Dynamic shear modulus values at low strain (G_{max}) for both core and shell materials were obtained from the shear waves velocity V_s. The shear wave velocity V_s of the materials was obtained by the resonant column test results (Kim M.K. et Al., 2011), Figure 4.6. The equations were implemented in the internal code in Quake/W to provide confining-pressure-dependent shear modulus values for all elements.

Quake/W FEM software was used to evaluate the seismic dam-foundation response. In this study, two different approaches were adopted for the constitutive model of the dam body materials: the *equivalent linear strain dependent properties* and the *cyclic non-linear analysis* associated with the Mohr-Coulomb failure criterion, able to account of plastic yielding.

The *equivalent linear method* is based on an iterative process to estimate nonlinear strain dependent properties (see Par. 3.2.3.5).

The strain dependency curves of the shear modulus G/G_{max} and damping ratio D used in this analysis for rockfill and impervious zone were calibrated against laboratory results of resonant column test.

The strain dependent behavior of the soil has been fitted with the modified hyperbolic model proposed by Yokota et Al. (1981). The degradation of the shear modulus G (Eq. 4.4) and the damping ratio D (Eq.4.5) functions are expressed as:

$$\frac{G}{G_{max}} = \frac{1}{1+\alpha \cdot \gamma^{\beta}} \qquad (4.4)$$

$$D = D_{max} \cdot e^{\lambda \cdot \frac{G}{G_0}} \qquad (4.5)$$

Where γ is the shear strain expressed in (%), D is expressed in (%) and α,β,λ are fitting parameters. D_{max} is another fitting parameter and corresponds to the maximum damping value. A trial and error procedure has been implemented in order to calibrate parameters with experimental data.

Results are reported in Figure 4.13 and 4.14 for the rockfill and at Figure 4.15 and 4.16 for the core.

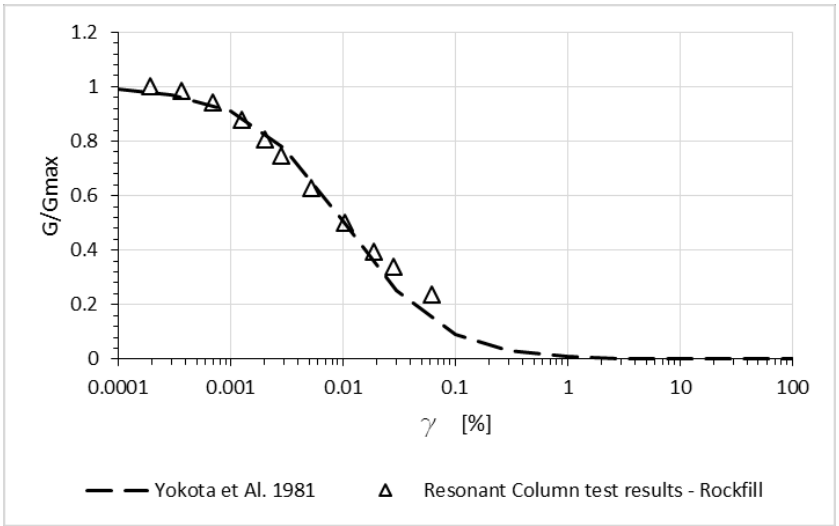

Figure 4.13 Calibration of stiffness degradation with shear strain for the rockfill

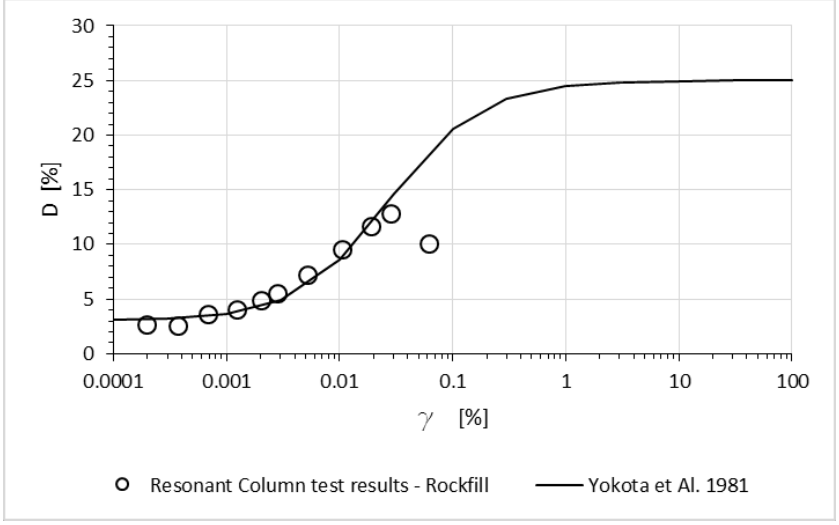

Figure 4.14 Calibration of damping ratio increase with shear strain for the rockfill

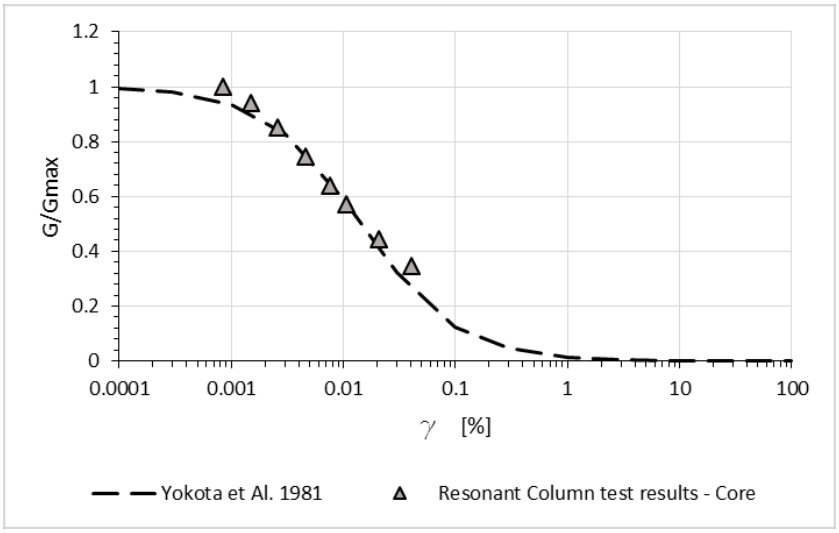

Figure 4.15 Calibration of stiffness degradation with shear strain for the core

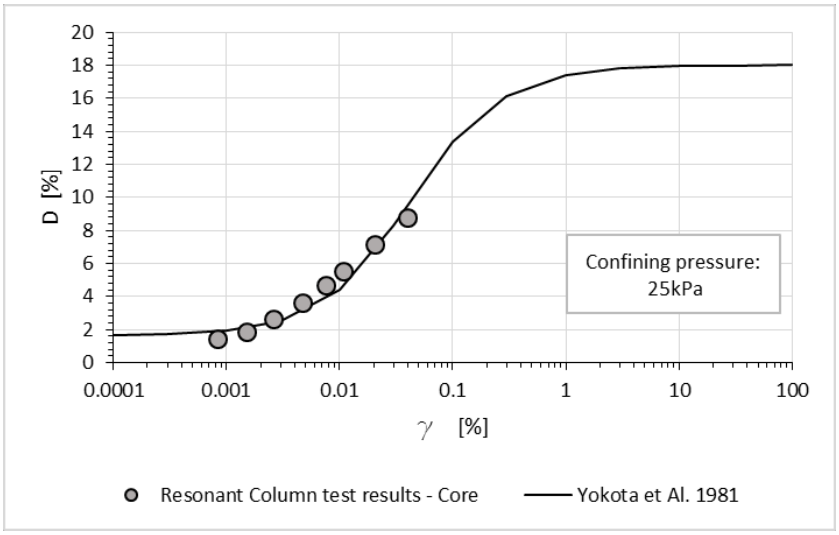

Figure 4.16 Calibration of damping ratio increase with shear strain for the core

The calibrated parameters are reported in Table 4.7 respectively for the shell and the core materials.

Dam Materials	**Parameters**			
	α	β	λ	**D_{max} (%)**
Rockfill	98	1	-2.1	25
Core	70	1	-2.4	18

Table 4.7 Parameters adopted in the numerical analysis of the dam

The *cyclic non-linear analysis* associated with the Mohr-Coulomb failure criterion may accurately represent the non-linear stress-strain of soils following the actual stress-strain path during cyclic loading.

The cyclic non-linear model was defined by the so-called backbone curve. The associated Masing criteria were used to define unload and reload loops. The stress-strain relationship of various materials was expressed by means of the hyperbolic model, according to Hardin and Drnevich (1972):

$$F(\gamma) = \frac{G_{max}\,\gamma}{\left(1+\frac{G_{max}}{\tau_{max}}\right)|\gamma|} \quad (4.6)$$

The curve was defined by two parameters which are the slope at zero strain and the asymptotes at large strains. In terms of soil properties the initial slope is represented by the small strain shear modulus G_{max} as defined before in the present paragraph, and the asymptote is the shear strength (Table 4.4).

In the Non-Linear model the hysteretic damping is related to the shear Modulus G by the Equation (4.7), (Harding & Drnevic, 1972):

$$D = D_{max}\left(1 - \frac{G}{G_{max}}\right) \quad (4.7)$$

Mass and stiffness-dependent Rayleigh damping is used at low strain. At higher strains, damping occurs primarily through hysteretic looping.

All parameters were defined according to the available data obtained from laboratory tests carried out by the KOCED staff of KAIST and the work produced by Kim M.K. et Al. (2011).

4.3.2.2. Results

The comparison between the experimental and the numerical results was expressed in terms of maximum acceleration distribution in the core and in the downstream shell. Moreover, Fourier Spectrum in term of acceleration results were evaluated at dam crest (point A), for all tests (PGA=0.065g; 0.11g; 0.22g and 0.35g).

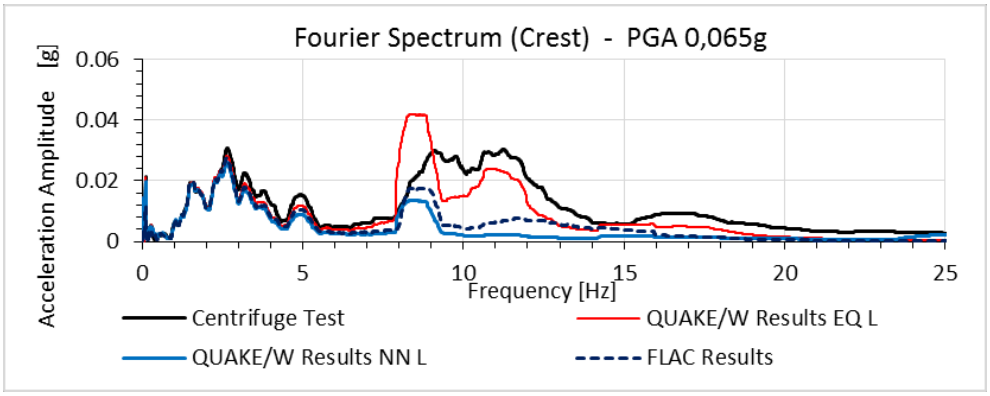

Figure 4.17 Fourier amplitude spectrum for the acceleration at crest for the ECRD, for 0.065g

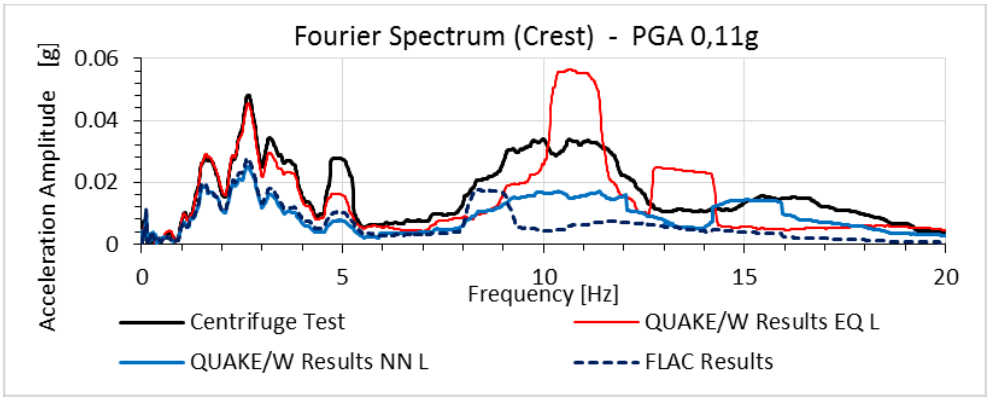

Figure 4.18 Fourier amplitude spectrum for the acceleration at crest for the ECRD, for 0.11g

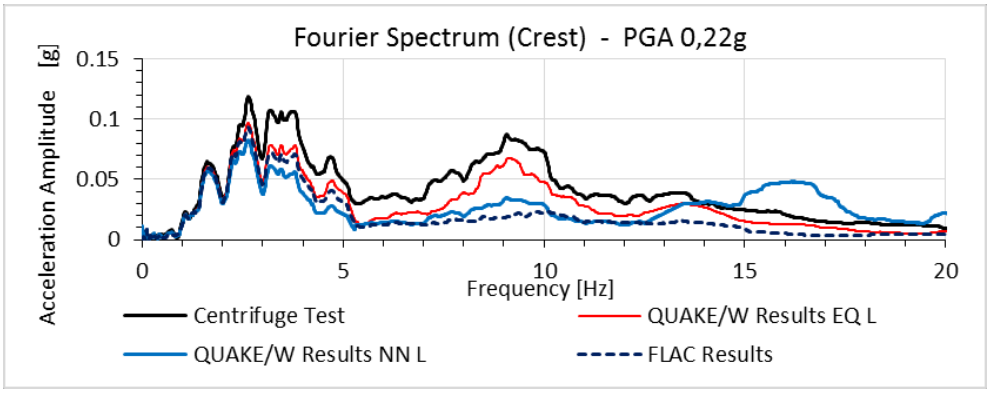

Figure 4.19 Fourier amplitude spectrum for the acceleration at crest for the ECRD, for 0.22g

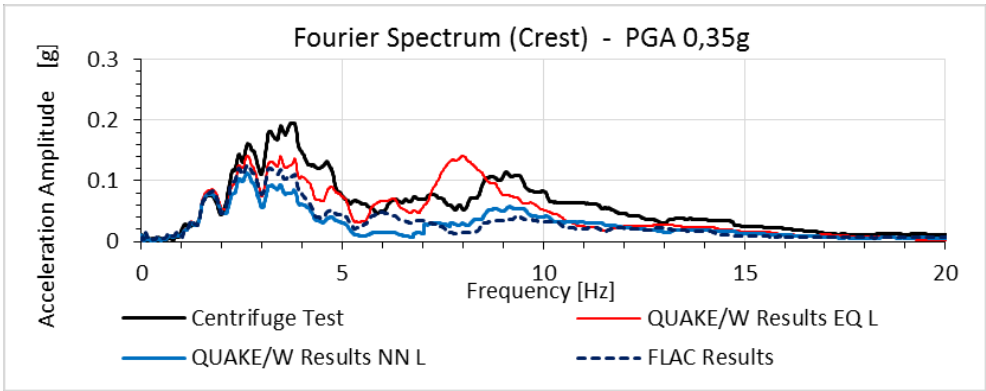

Figure 4.20 Fourier amplitude spectrum for the acceleration at crest for the ECRD, for 0.35g

Results show the comparison between the centrifuge test, the relative numerical analyses carried out by Kim M.K. et Al. (2011) and the numerical response obtained by the present work. This latter result was performed using the FEM software Quake/W, with both the equivalent linear model and the cyclic non-linear model.

Observing the Fourier amplitude contents for all the stage tests (Figures 4.17, 4.18, 4.19 and 4.20), it can be noted that the computed analyses match quite well the experimental results in the range from 0 to 5 Hz, which represents the dominant frequency of the input motion.

As expected, the best fitting is for moderate earthquakes, whereas the higher discrepancy is observable for higher seismic motions. Experimental results tend to exaggerate the amplification in the frequency range from 6 to 13 Hz. Generally, it can be noted a smaller amplification in the numerical outcomes, even if maximum amplification was observed for the analyses with the equivalent linear model.

However, the numerical results don't exhibit a relevant difference with the recorded ones and the model seems to reproduce the stiffness of the centrifuge model, because of the correspondence of peak spectral period.

Moreover, computed acceleration distributions were compared with the centrifuge test and the previous numerical results (Kim M.K. et Al., 2011).

The computed acceleration distributions along the center line of the core and the rockfill downstream slope were compared with the centrifuge results respectively in Figure 4.22 and 4.23, at four different earthquake levels.

Those figures show that the acceleration distributions obtained with the numerical analyses of the present study are in good agreement with those obtained with the centrifuge test and the previous analyses. Results are observed in the center line of the core (solid point) and into the downstream shell (empty points), as illustrated in Figure 4.21.

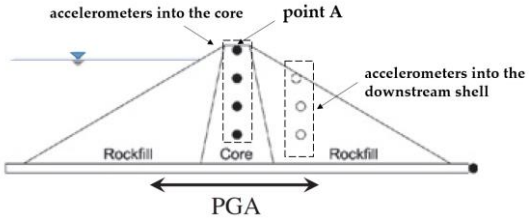

Figure 4.21 Position of the accelerometers into the dam

It can be observed that the distribution of the peak accelerations depends on the magnitude of the earthquake and the zoning condition. Numerical results show that the peak acceleration tends to increase from the bedrock to the dam crest as much as the experimental results, especially for low to moderate earthquake (PGA=0,3g).

The numerical results agree with the experimental results, especially in the numerical analyses with a non-linear approach. It can be observed that the cyclic non-linear model can reproduce the peak acceleration at crest even at higher input motions (Fig. 4.22). The performed numerical analyses seem to show a better agreement than the numerical analyses of the previous study (Kim M.K. et Al., 2011).

Fig. 4.22 shows that the numerical analyses with the cyclic non-linear approach may reproduce the maximum acceleration close to the experimental results on crest, even for the highest earthquake input motion (0,35g).

Moreover, the numerical results with the cyclic non-linear approach and the experimental results broadly show a similar increasing trend, in both the core zone (Fig. 4.22) and the shell zone (Fig. 4.23).

The equivalent linear model tends to exaggerate the results in terms of peak acceleration, especially for the higher level of motion. Thus, as the input acceleration increases, the difference becomes a bit larger especially in the computation with the equivalent linear method. Since this last method is essentially linear during each iteration, there is a tendency to exaggerate the response, especially for higher level of motion.

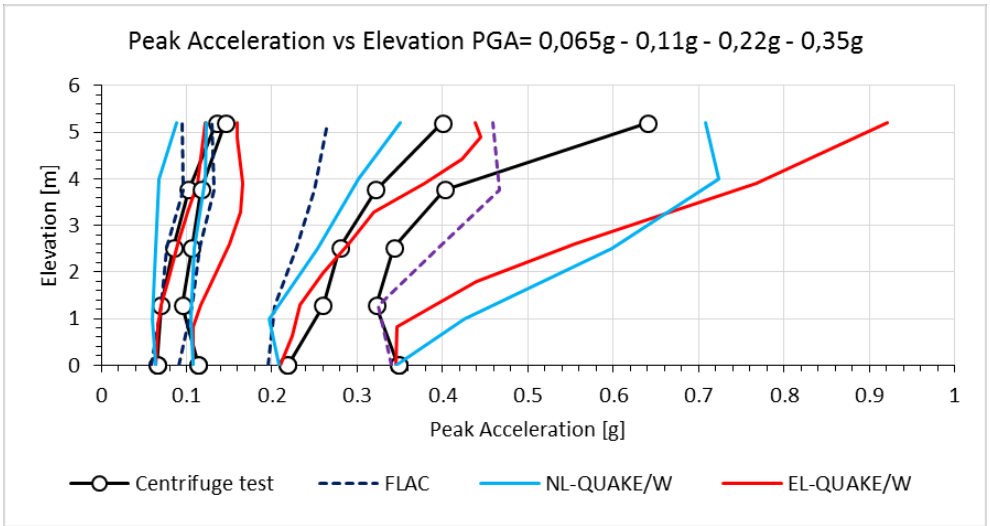

Figure 4.22 Maximum Horizontal Acceleration distribution in the prototype scale for the numerical analyses and the centrifuge test into the core

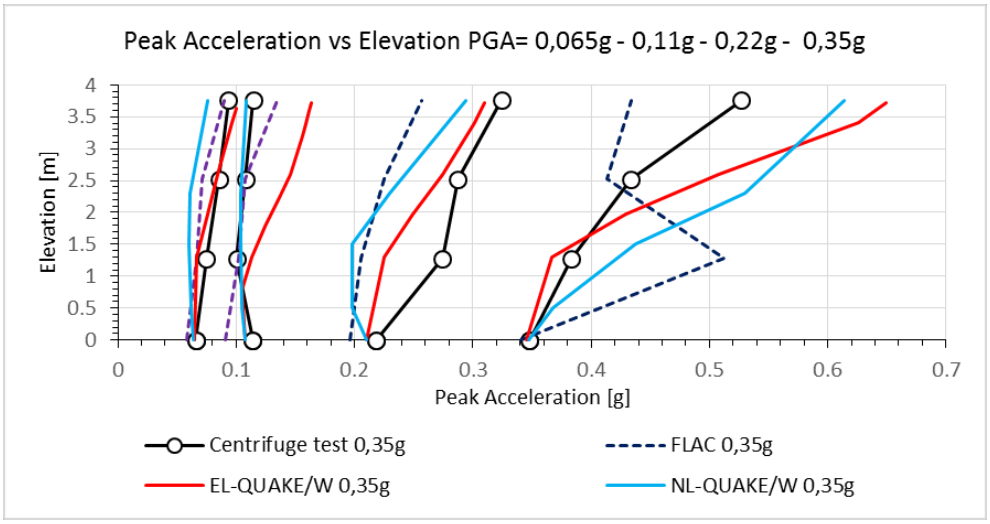

Figure 4.23 Maximum Horizontal Acceleration distribution in the prototype scale for the numerical analyses and the centrifuge test into the shell

The shape of the acceleration distribution into the core could be affected by a different distribution of the shear stiffness of the core.

In the numerical analysis, the shear modulus G_{max} was considered to vary with depth in the embankment, according to the shear wave velocity distribution plotted in the updated Figure 4.6, obtained from resonant column tests on the soil.

During the centrifuge test, the dam model was constructed by a hand compactor which probably was not able to keep a uniform density. This method of construction could have affected the stiffness distribution into the dam core.

The computed permanent displacements and the available experimental results were compared for the earthquake scaled at 0,35g.

In the centrifuge experiment, the maximum horizontal displacement was 4,99 mm at crest (see Figure 4.11). The maximum vertical settlement was 9.72 mm with the scaled seismic motion at PGA of 0.35g (see Figure 4.7) (Kim M.K. et Al., 2011).

Figure 4.24 shows the horizontal displacement histories at the crest of the numerical analyses with the equivalent linear and the cyclic non-linear method during the Ofunato Earthquake, scaled at 0,35g. The calculated horizontal displacements are compared with the available centrifuge results. The previous numerical results (Kim M.K. et Al., 2011) are not available for the horizontal displacement histories.

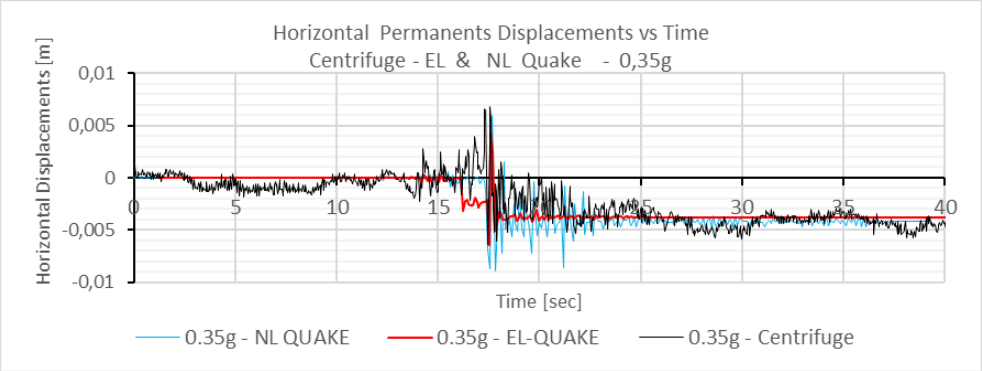

Figure 4.24 Horizontal displacements obtained by centrifuge test and the present numerical analyses

It may be observed that numerical results are in good agreement with those obtained with the centrifuge, where the residual value is of about 5 mm at crest. Figure 4.24 shows that in both cases, the numerical and the experimental results tent to reach the same stable displacement value.

The numerical analyses can reproduce the beginning of the increase of horizontal displacements. The displacement increases after about 17sec from the beginning of the event for both the experimental and numerical results and reaches the maximum value which remains constant until the end of the earthquake.

Vertical displacements histories are plotted in Figure 4.25, where the numerical analyses at crest using both the equivalent linear analysis and the cyclic non-linear method are plotted. The previous numerical analysis with FLAC code and the residual vertical settlement observed at the end of the centrifuge test at 0,35g are compared with the calculated settlements.

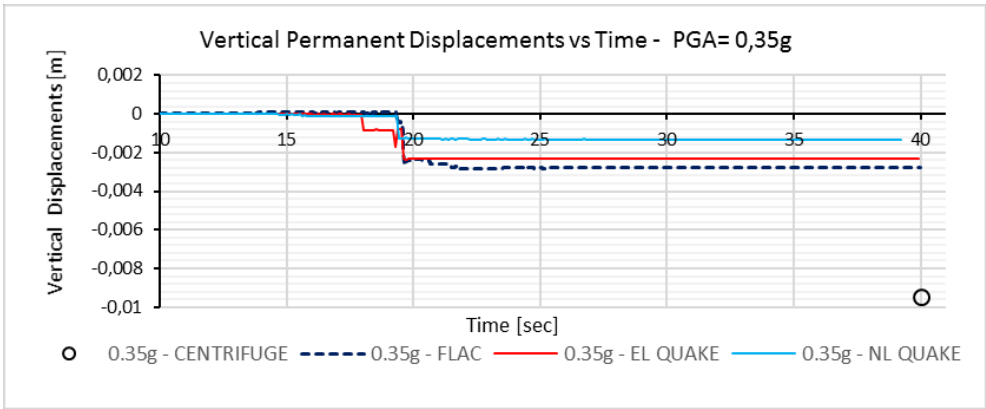

Figure 4.25 Vertical displacements obtained by centrifuge test and the numerical analyses

The QUAKE/W numerical settlement histories at crest show sufficient agreement with the numerical settlement histories obtained by the previous numerical analysis. The residual settlements observed at the end of the earthquake ranges from about 1 to 3 mm. These results show that the crest settlements start to increase after about 20sec from the beginning of the dynamic event. The vertical predicted displacements at crest show a stable trend: the maximum value remains constant up to the end of the motion.

The results in term of vertical settlements was available for the experiment at 0,35g. The centrifuge available result shows a higher residual settlement value. The experimental vertical displacements were obtained by the laser technique whose data capture definition was not too accurate. Experimental results could show higher value due to the accuracy level of its measuring method.

However, comparing the calculated results with the Swaisgood's trend (Swaisgood, 2003, see Par. 3.2.4), it can be noted a good agreement between the numerical crest settlement ratios and the collected data (Fig. 4.26).

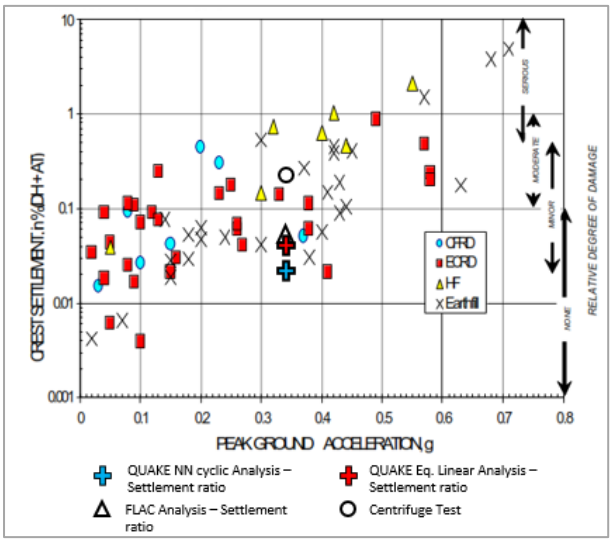

Figure 4.26 Comparison of the crest settlement ratio of the numerical analyses and the centrifuge tests to the case history database

The aforementioned analyses were carried out considering only the hydrostatic pressures on the upstream slope.

In order to evaluate the effect of the hydrodynamic pressure on the dam seismic response, those analyses were repeated. The hydrodynamic pressures were evaluated using the approximate solution proposed by Zangar (1952) for an inclined face (Eq. 3.12).

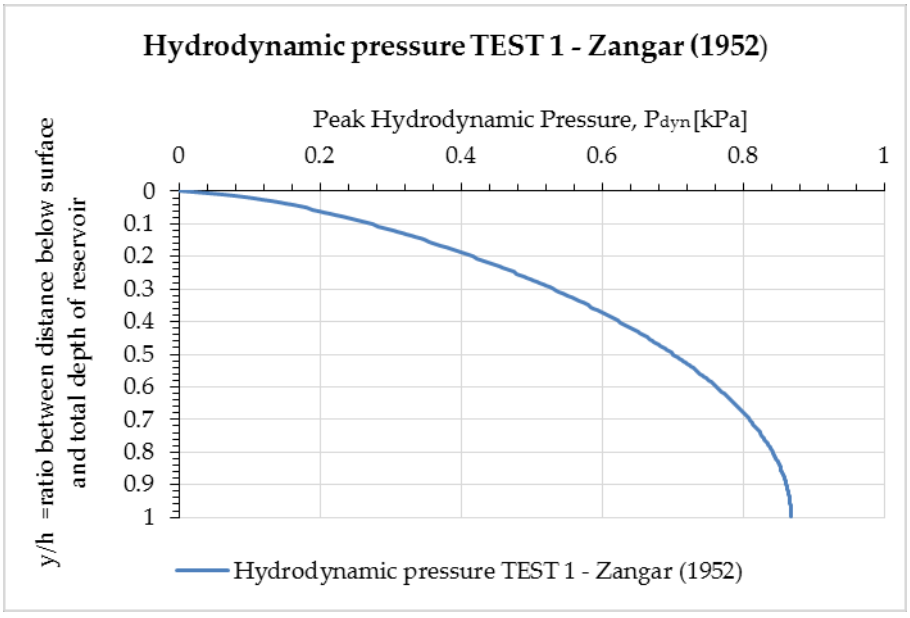

Figure 4.26.a Hydrodynamic pressure distribution on the upstream face of the ECRD prototype

The figure 4.26.a depicts the hydrodynamic pressure distribution on the upstream slope of the earth dam. The pressure distribution is expressed in

function of the ratio "y/h" of the distance below the surface and the total depth of the reservoir.

It can be seen that the hydrodynamic pressure on the inclined face of the ECRD prototype of TEST 1 is very low (lower than 1 kPa) and it doesn't modify the seismic behavior of the dam.

Analyses were carried out for the highest earthquake level (0,35g). Results, expressed in term of acceleration distribution, Fourier Spectrum, horizontal displacements and vertical settlements, show the same behavior as those evaluated without hydrodynamic effects.

In this case, a 5.2m high dam was investigated and the hydrodynamic pressure distribution showed negligible effects. Higher dams are affected by higher pressure values, but, as discussed at Par. 3.2.3.6, also in those cases, the effect can be safely ignored.

4.4. Centrifuge TEST 2

The second centrifuge test (*TEST 2*) aimed to investigate the seismic behavior of deterioration reservoir levee using dynamic centrifugal model test (Park S.Y. et Al., 2016b). Therefore, a test in a centrifugal field of 60 g was investigated.

The experiment examined the earth dam response under seismic motion with a reinforcement of its crest, in order to investigate its storage capacity (Figure 4.27). The result provided its influence on the acceleration response, displacements, vertical settlements and the development of excess pore water pressure in the embankment.

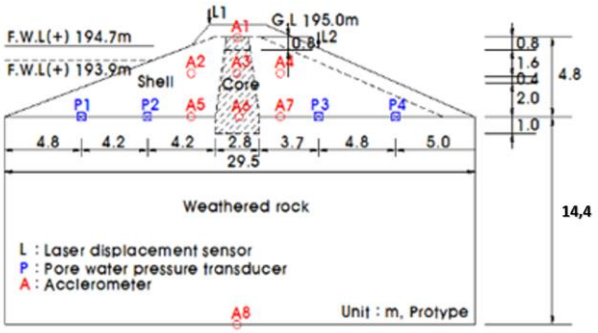

Figure 4.27 Model configuration and points of the measuring instruments (Park S.Y. et Al., 2016b)

In this study, the aforementioned centrifuge test has been evaluated and numerically reproduced using the FEM software Quake/W.

4.4.1. TEST 2 conditions

The model was constructed inside a specific Equivalent Shear Beam (ESB) Container with flexible end walls, able to simulate the shear deformation of a horizontal soil layer subjected to an earthquake in the field (Fig. 4.28).

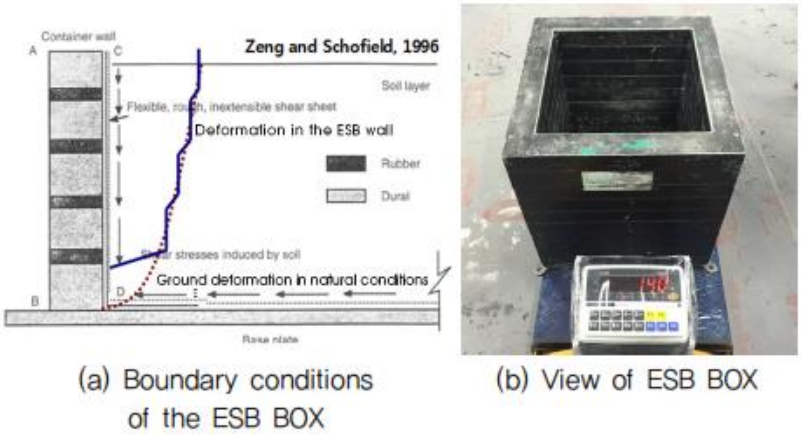

Figure 4.28 Schematic figure of ESB BOX (Park S.Y. et Al., 2016b)

The earth dam model layouts and its instrumentation are plotted in Figure 4.27 (Park S.Y. et Al., 2016b).

The slope of the earth dam model was 1:2,75 (Vertical: Horizontal) for the upstream slope and 1:2,4 (Vertical: Horizontal) for the downstream slope.

A scaling ratio (N) of 60 (referring to the centrifuge acceleration of 60g) was selected.

The model was about 90 mm high, simulating 5,5 m high in a prototype scale on a foundation of 14,4 m.

The dam model was constructed on four soil layers. The layers were manually compacted in order to keep uniform densities and to reproduce construction stages (see Figure 4.29 a). Every layers was modeled using specific wood elements (see Figure 4.29 b). The terraced slopes were shaped in order to obtain the desired shape (Figure 4.29 c and d).

The reservoir was filled up to 4,5 m in the prototype scale which imposed a water load on the upstream slope during the earthquake simulation.

Accelerometers and pore water pressure transducers were embedded in the embankment and at the contact with the foundation. Those devices were placed in the upstream and in the downstream of the embankment. They investigated the amplification of the earthquake acceleration and the development of pore water pressures (see Figure 4.27). Laser sensors were used to measure the displacement in the crest (L1) and in the downstream slope (L2), as illustrate in Figure 4.27.

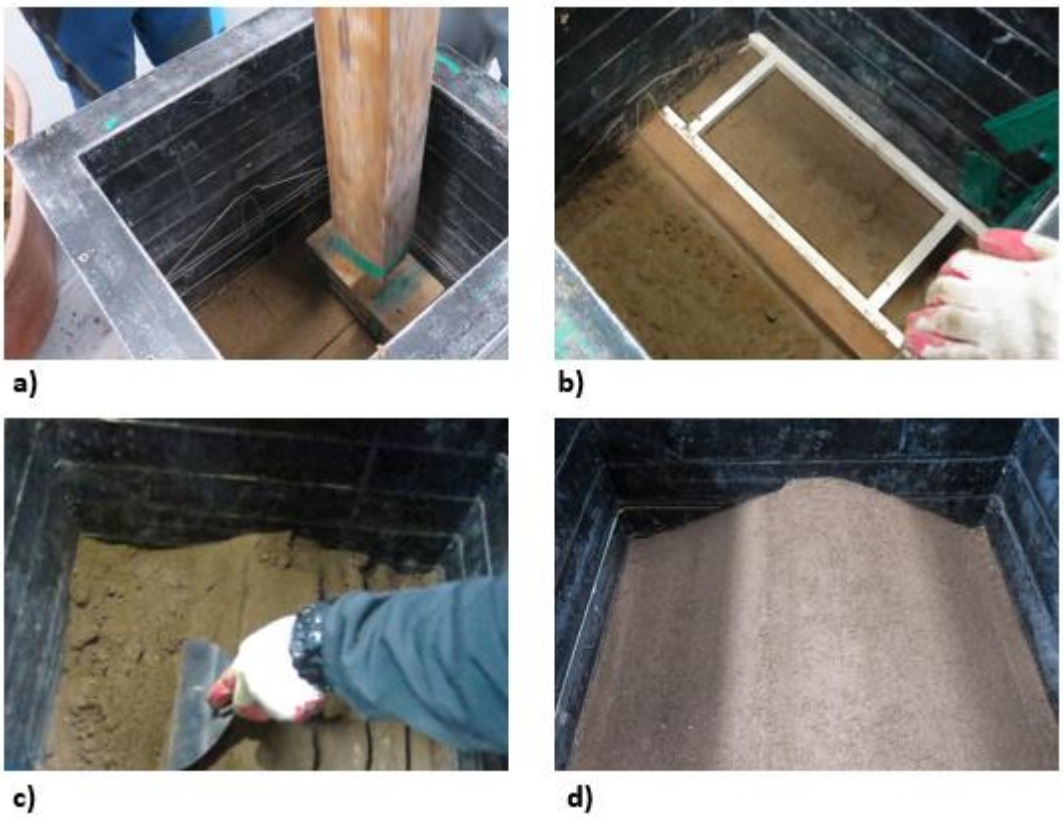

Figure 4.29 Construction of the model

A series of staged tests were performed with real earthquake histories (Hachinohe and Ofunato Earthquake, see Figure 4.30) whose acceleration magnitude was scaled as illustrated in Table 4.8. In order to study the seismic response of the dam under the higher motion, the step number 12 was performed. In Table 4.8, the starred bold writings represent the selected input motion used for the numerical analysis.

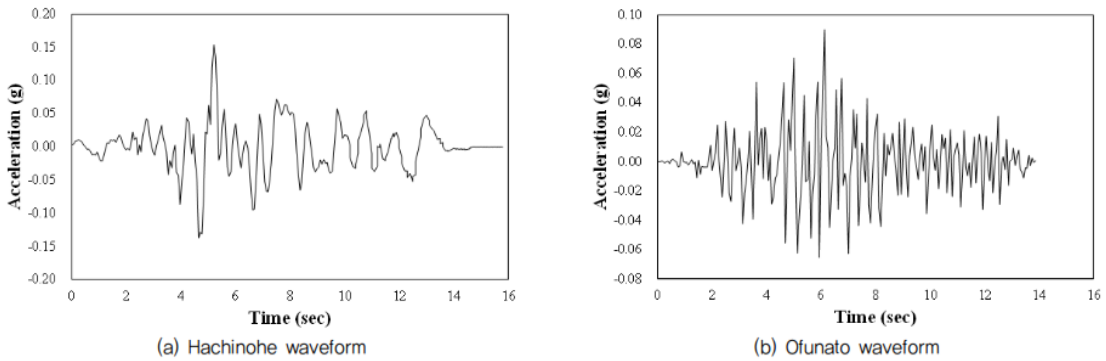

Figure 4.30 Time history of real earthquakes (Park S.Y. et Al., 2016)

STEP	PGA	
	Hachinohe wave [g]	**Ofunato wave [g]**
1	0.018009	0.010137
2	0.031388	0.017804
3	0.043579	0.027523
4	0.053383	0.044641
5	0.077482	0.084125
6	0.12882	0.115446
7	0.173189	0.186817
8	0.192786	0.187866
9	0.250883	0.214229
10	0.291664	0.245689
11	-	0.275239
12(*)	**-**	**0.330392**

Table 4.8 Maximum acceleration response of seismic waveform (Park S.Y. et Al., 2016b). The bold writing are the selected input motion for the numerical analysis.

Based on the experimental results, the amplification of the acceleration, the horizontal and vertical deformations of the embankment were analyzed.

4.4.2. Materials

The material properties of the core and the shell are summarized in Table 4.9 and Figure 4.31, whose data were found from the works of Park S.Y. et Al. (2016*a)* and Park S.Y. et Al. (2016*b*).

Materials	**Core**	**Shell**	**Bedrock**
Specific Gravity [Gs]	2.672	2.223	2.650
Water content [%]	20.00	16.14	-
Density ρt [g/cm3]	1.936	1.964	2.100
Poisson's ratio ν	0.30	0.35	0.23
Cohesion, c [kN/m^2]	10.0	0.0	0.0
Shear resistance angle, φ [°]	27.4	35.0	45.0
Permeability, k [cm/sec]	$2.96*10^{-7}$	$1.35*10^{-3}$	$1.00*10^{-10}$
Van Genuchten's parameter, *a* [1/m]	1.28	9.81	1.00
Van Genuchten's parameter, *n*	1.65	5.00	4.00

Table 4.9 Material properties of the earth dam model (Park S.Y. et Al., 2016a).

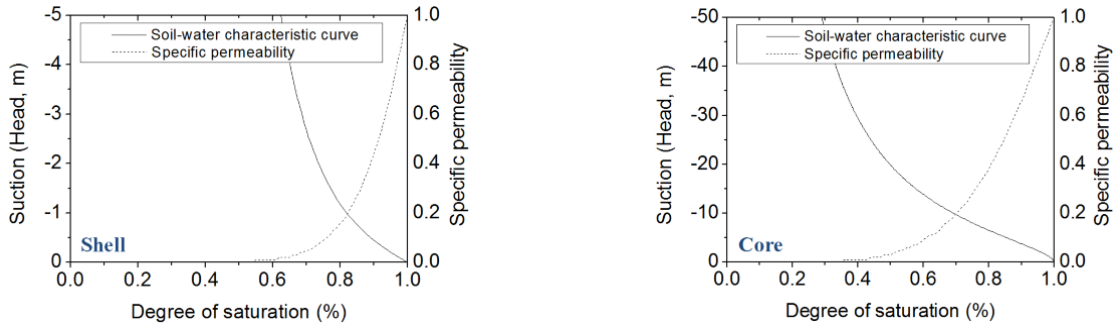

Figure 4.31 Permeability of materials and water characteristic curve (Park S.Y. et Al., 2016a).

4.4.3. Results of the Centrifuge Test 2

Results were expressed in term of maximum acceleration distribution along the center line of the core and the response spectrum at the crest and in the downstream slope.

During the centrifuge test, the vertical displacement histories at the two points were obtained. The two points are the *L1* in the crest and *L2* in the downstream slope as illustrated in Figure 4.27. All the measuring instruments are clearly depicted in Figure 4.27.

Figure 4.32 shows the evolution of the measured excess pore water pressures generated in four nodes of the dam (P1, P2, P3, P4 of Figure 3.27) by the Ofunato Earthquake, at step n.12 with a PGA of 0,33g.

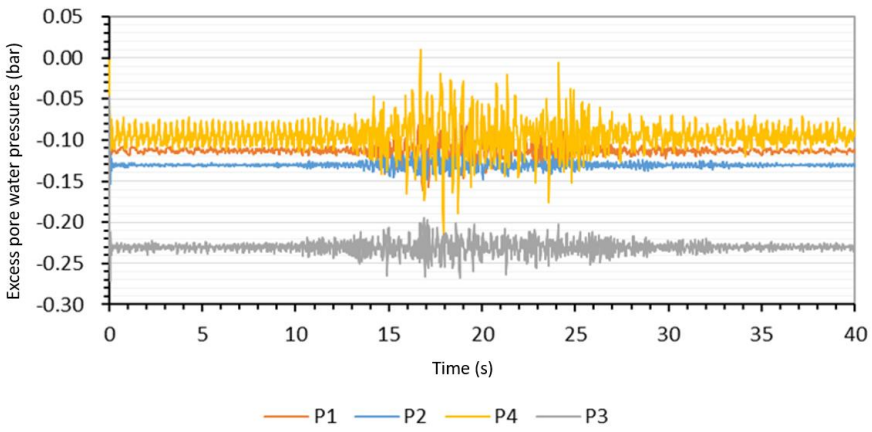

Figure 4.32 Time history graph of excess pore water pressure during the dynamic process of Ofunato Earthquake of PGA=0.33g (Park S.Y. et Al., 2016b)

The four nodes are located at different positions at the contact between the embankment and the foundation and it could be observed that nodes tends to dilate. The maximum value was obtained in the transducer P4, located at the downstream toe of the dam. Although the dam has been subjected under the

highest seismic motion (PGA=0,33g), the effect on the excess pore water pressures developed into the dam body seems to be very low and may be negligible in the reproduction of the numerical analysis.

All the centrifuge results will be compared with the numerical analysis response and they will be discussed in the following Paragraph 4.4.4.

4.4.4. Description of the Numerical Model

The software used for the purpose is the Quake/W FEM software package. This software consists of a bi-dimensional dynamic finite element analysis that uses both the equivalent linear strain dependent modulus and damping properties and the cyclic non-linear approach. It uses a time-step analysis with Rayleigh damping and allows for variable damping for different elements. The geometry of the model and the mesh is showed in Figure 4.33. The model refers to the centrifuge model of Figure 4.27. This model is represented by the embankments composed by the core and the upstream and downstream shell, rested on the foundation of 14.4m.

As in the previous numerical analyses related to the *test 1* (see Par. 4.3.1), several attempts were considered in order to reduce local boundaries effects and together minimize computational efforts.

The size of the mesh was determined by a criterion considering the maximum frequency and the minimum shear wave velocity in order to avoid numerical distortion of the propagating ground motion and accurate computation of the model response (Lysmer & Kuhlemeyer, 1969). The seismic input applied at the base of the numerical model was the Ofunato Earthquake scaled at 0,33g, in order to reproduce 12th stage, see Table 4.8.

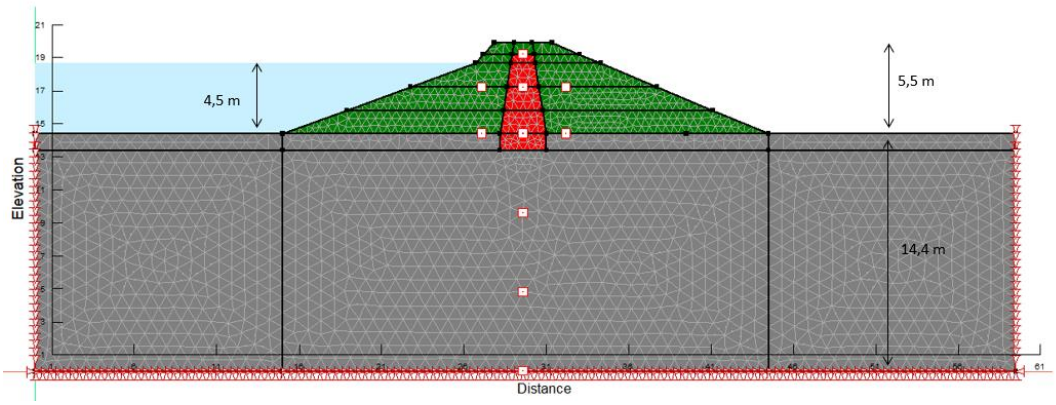

Figure 4.33 Two-dimensional finite element mesh of the earth dam

4.4.4.1. Calibration of the constitutive model

Prior to the dynamic analysis, the static analysis should be carried out to establish the existing in-situ stresses. In the first phase of the numerical studies: a sub-stage was modeled using the SIGMA "in-situ stress" module and this is used to simulate the development of geostatic stresses in the foundation. Then the SIGMA "Load-Deformation" module has been applied in order to reproduce the construction stages of the dam, considering four overlapping layers. In the second phase of the static analysis, hydrostatic pressure was applied to the upstream face of the dam. According to the statement of Par. 3.2.3.6, hydrodynamic effects of the reservoir can be neglected in the analysis.

The following step was to establish the long-term steady-state seepage conditions and pore-pressures, using the SEEP/W module. On the downstream side, the water-table is taken to be at the surface of the foundation, whereas on the upstream side, the water-table is taken considering the full reservoir level.

The model used the finite element method for two dimensional Darcy's flow in both saturated- unsaturated soils.

Using the Van Genuchten (1980) closed form solutions, the Conductivity function (Eq. 4.8) and the Volumetric Water Content function (Eq. 4.9) were estimated for the unsaturated soils (shells and core). The foundation was considered to be saturated.

The *conductivity water content function* is expressed as following (Eq. 4.8):

$$k_w = k_{sat} \frac{\left[1-(a\Psi^{(n-1)})(1+((a\Psi^n)^{-m}))\right]^2}{\left((1+a\Psi)^n\right)^{\frac{m}{2}}} \quad (4.8)$$

Where k_{sat} is the saturated hydraulic conductivity and Ψ is the required suction range. The parameters *a*, *n* and *m* are curve fitting parameters, where $n = \frac{1}{(1-m)}$

The closed form solution for predicting the *volumetric water content function* is governed by the following equation (4.9):

$$\Theta_w = \Theta_r + \frac{\Theta_s - \Theta_r}{\left[1+\left(\frac{\Psi}{a}\right)^n\right]^m} \quad (4.9)$$

Where Θ_w is the volumetric water content, Θ_s and Θ_r, the saturated and residual volumetric water content, Ψ is the negative pore-water pressure and the parameters *a*, *n*, and *m* are the fitting parameters.

The adopted parameters were defined from available experimental data for the different soil types (Park S.Y. et Al. 2016,*b*).

Material	Core	Shell	Bedrock
k_{sat} [cm/sec]	$2.96*10^{-7}$	$1.35*10^{-3}$	$1.00*10^{-10}$
a [1/m]	1.28	9.81	1
N	1.95	5	4
Θ_s [mc/mc]	0.39	0.22	0.22
Θ_r [mc/mc]	0.11	0.01	-

Table 4.10 Material properties used during seepage process (Park S.Y. et Al. 2016,b).

Figure 4.34 shows the resulting piezometric line (water-table) and total head contours (equipotential lines).

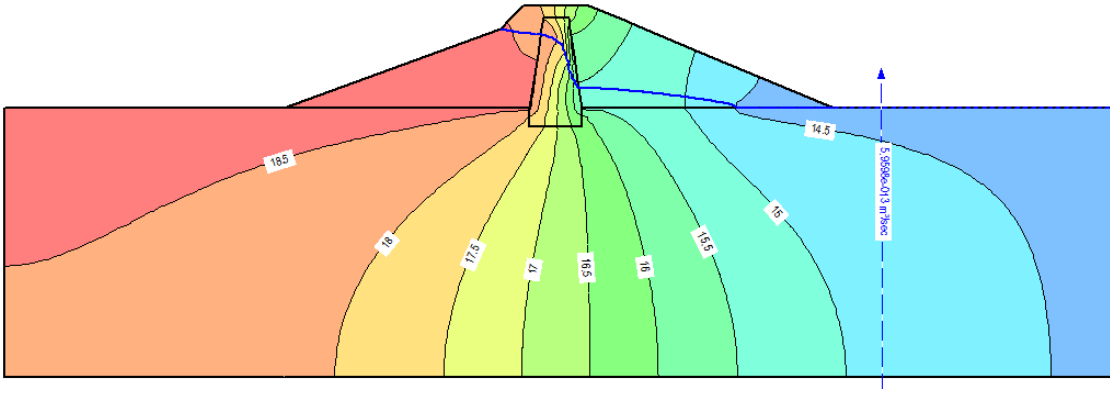

Figure 4.34 Seepage Analysis – equipotential lines

In order to complete the stress state in the static condition, continuous hydrostatic pressure was applied as pressure on the upstream face of the dam.

The geotechnical parameters used in the numerical analysis for the earthfill, impervious zone and foundation are listed in Tables 4.9.

Due to the lack of available records, a series of hypothesis have been carried out for the definition of the material properties.

For the rocky foundation, the constant value of 1000 m/s for the shear waves Velocity Vs was considered.

The following equation (Seed & Idriss, 1970) for the shear modulus at small strain G_{max} of the shell soil was used (Eq. 4.10).

$$G_{max} = 22K\sqrt{P_a\sigma'_m} \qquad (4.10)$$

Where K is a constant, P_a is the atmospheric pressure (kPa) and σ'_m is the mean effective stress (kPa).

The value of 180 was selected for the K constant, according to the recommendation made by Seed & Idriss (1970).

The maximum shear modulus G_{max} per the impervious core has been defined using the following equation proposed by Harding (1978), Eq. (4.11):

$$G_{max} = 625\left(\frac{1}{(0.3+0.7e^2)}\right)(OCR)^k\sqrt{P_a\sigma'_m} \qquad (4.11)$$

$$k = \frac{PI^{0.72}}{50} \qquad (4.12)$$

Where *e* is the void ratio, *OCR* the over-consolidation ratio and *k* an exponent related to the soil plasticity index *PI* and the σ'_m is the mean effective stress. According to the literature (Park S.Y. et Al. 2016,b; Lee C.W. et Al., 2014), the following parameters were used (Tab. 4.11).

Material	**OCR**	**IP**	**e**
Core	1	12	0.6

Table 4.11 Parameters for the definition of the Gmax for the core

The Dynamic analysis was performed using the Quake/W FEM software, using the cyclic non-linear method, associated with the Mohr-Coulomb failure criterion, able to account of plastic yielding.

The cyclic non-linear model is characterized by a backbone curve which follows the "Masing rules" for governing the unloading-reloading path, the stiffness degradation and other effects. The slope at zero strain (G_{max}) and the asymptotes at large strains (shear strength of the soils) define the hyperbolic curve (Eq. 4.6).

The small strain shear modulus G_{max} was previously defined for the dam soils, whereas the soil shear strength parameters are listed in Table 4.9. Damping ratio is related to the shear Modulus G by the Equation (4.7) (Harding & Drnevic, 1972).

Unfortunately, damping ratio vs strain data were not available from laboratory tests on employed materials. For the shell soil, the D_{max} parameter was defined in order to reproduce the average trend among those proposed by Rollins et Al. (1998) for gravel (Fig 4.35).

For the core, the D_{max} parameter was defined according to the trend proposed by Ishibashi and Zhang (1993), as depicted in Figure 4.36.

At small strain, D is set to its specified minimum value D_{min} (Table 4.12). The calibrated parameters are listed in Table 4.12.

Material	D min [%]	D max [%]
Shell soil	1	17
Core soil	1	25

Table 4.12 Parameters adopted regarding the damping ratio calibration

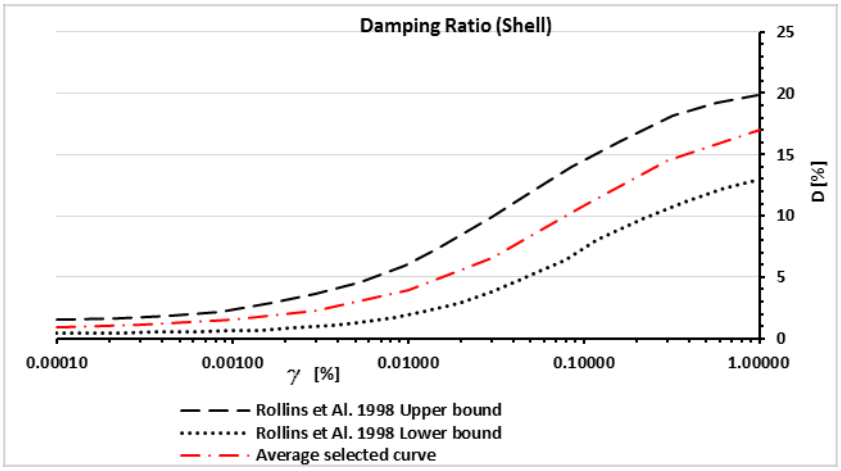

Figure 4.35 Calibration of damping ratio increase with shear strain for shell soil

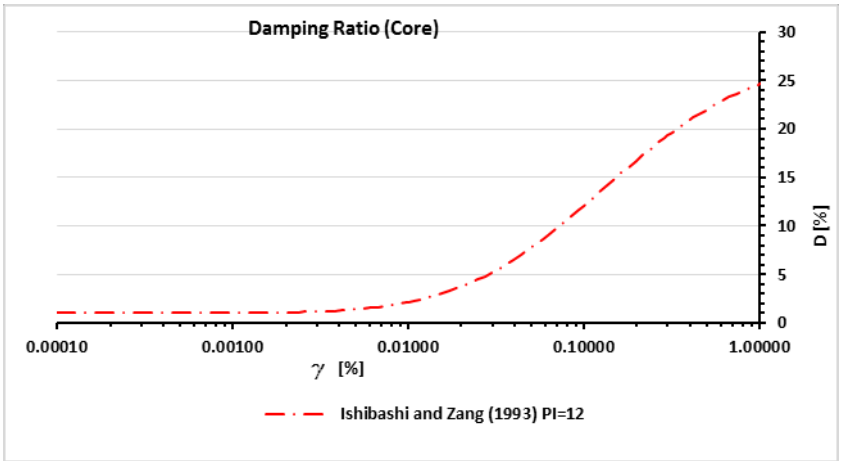

Figure 4.36 Calibration of damping increase with shear strain for core soil

4.4.4.2. Results

The centrifuge test results (*Stage 12*, see Table 4.8, Park S.Y. et Al., 2016b) have been compared with the numerical results obtained for the present work, performing dynamic analyses using the FEM software Quake/W, with the cyclic non-linear model.

The comparison of predicted and centrifuge experimental results, expressed in terms of the maximum acceleration distribution, are depicted in Figure 4.37, 4.38, 4.39.

The comparison is shown respectively for the core, the upstream and downstream shells, for the 12th tests with PGA of 0.33g (see Table 4.8).

Moreover, results about the Acceleration Spectra have been evaluated at points A1, A2, A4 and A7 and depicted in Figure 4.40, 4.41, 4.42 and 4.43.

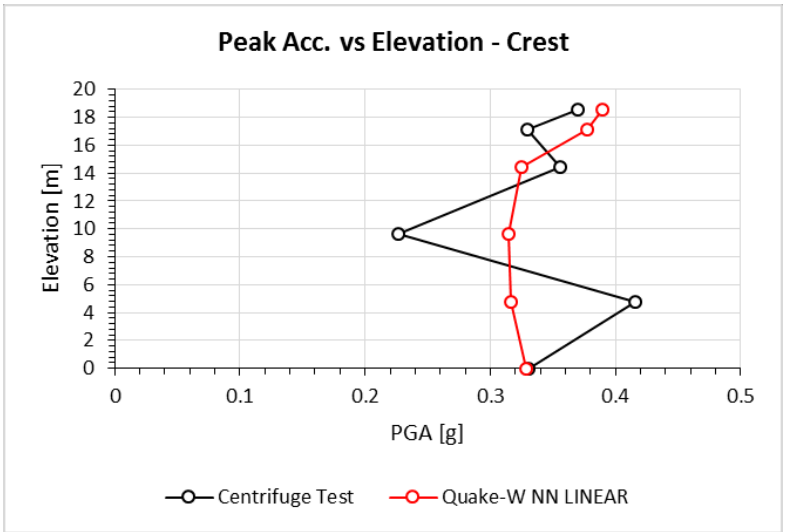

Figure 4.37 Comparison of maximum acceleration distribution along the core

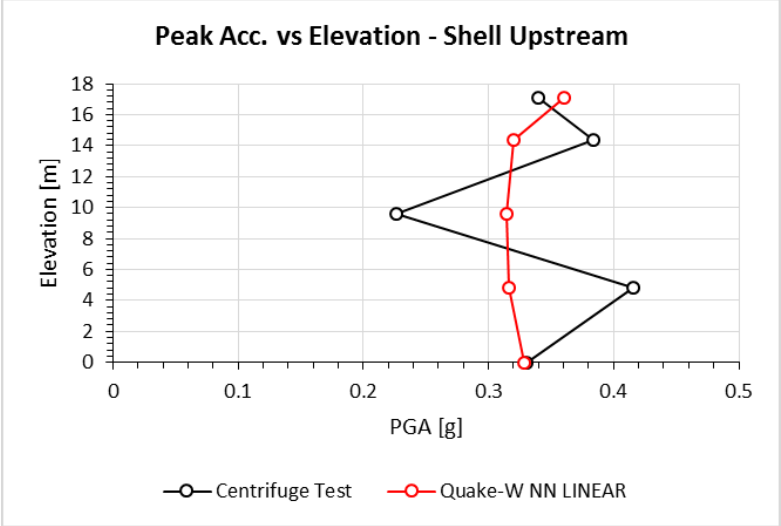

Figure 4.38 Comparison of maximum acceleration distribution along the upstream shell

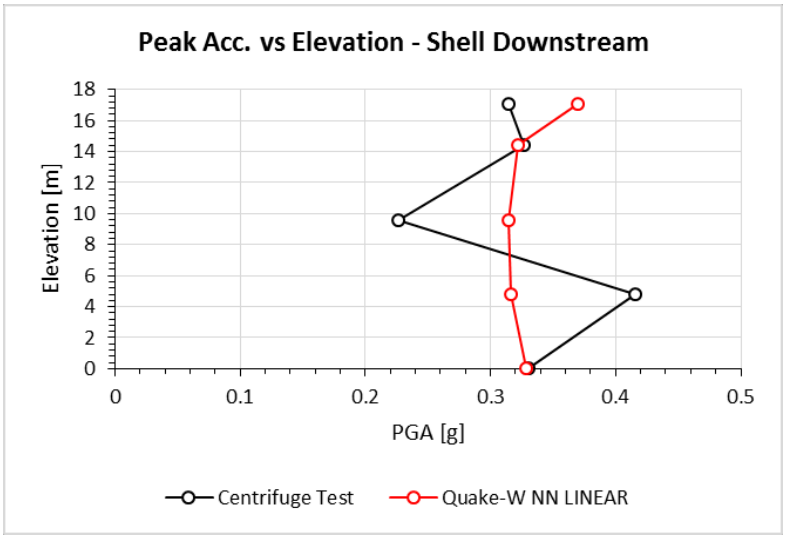

Figure 4.39 Comparison of maximum acceleration distribution along the downstream shell

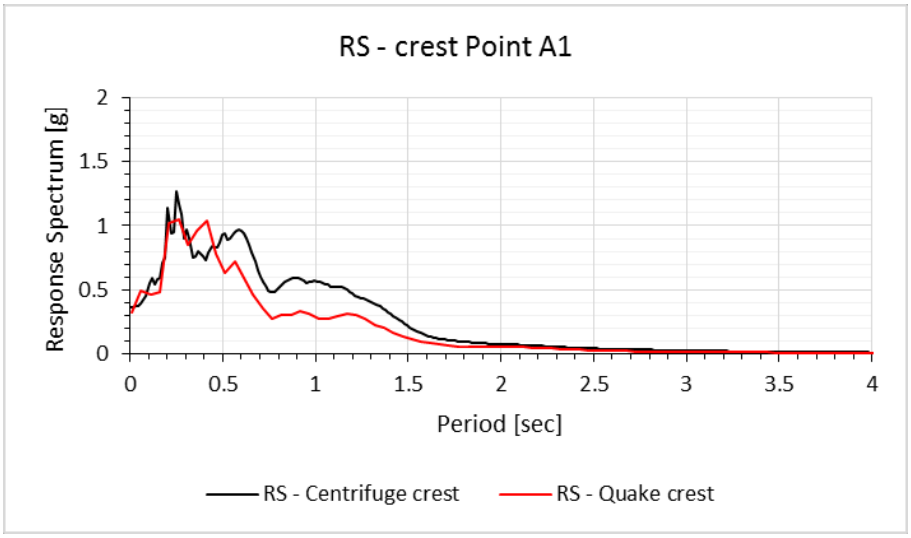

Figure 4.40 Comparison of acceleration spectra at point A1

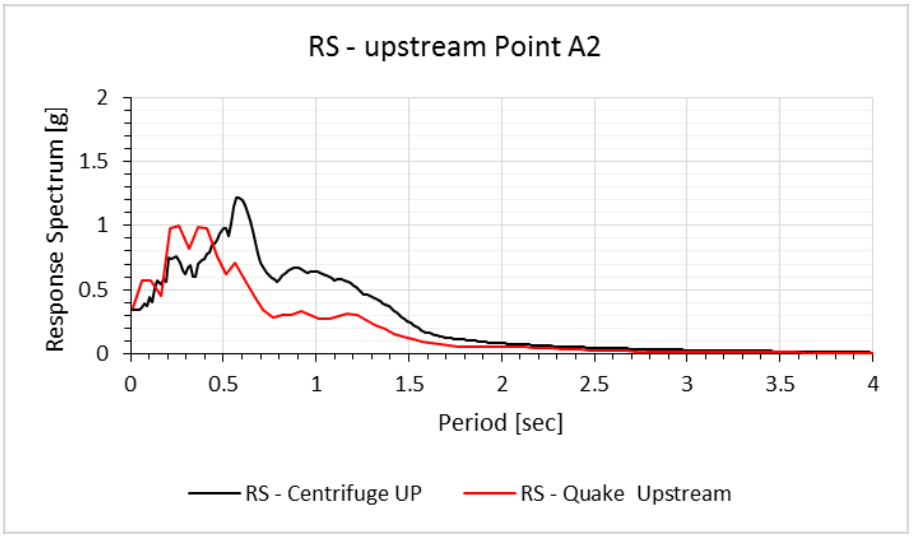

Figure 4.41 Comparison of acceleration spectra at point A2

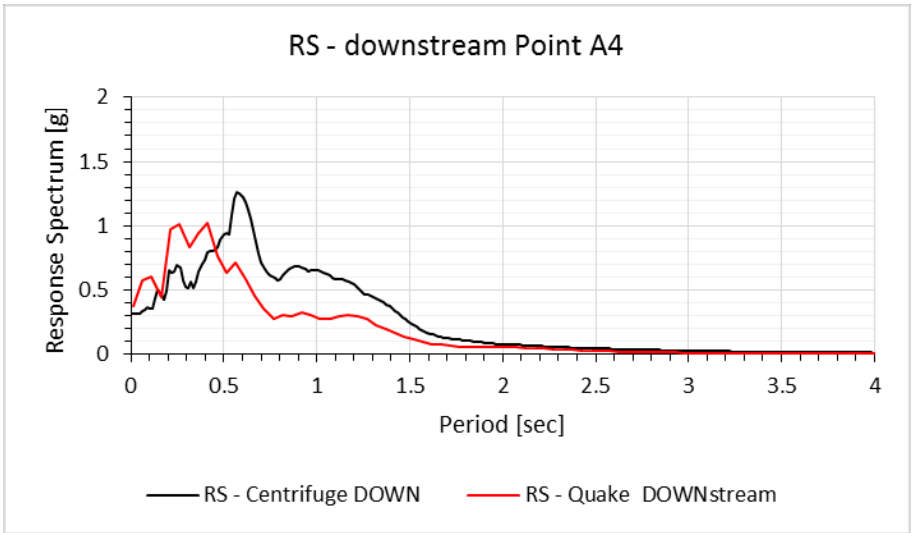

Figure 4.42 Comparison of acceleration spectra at point A4

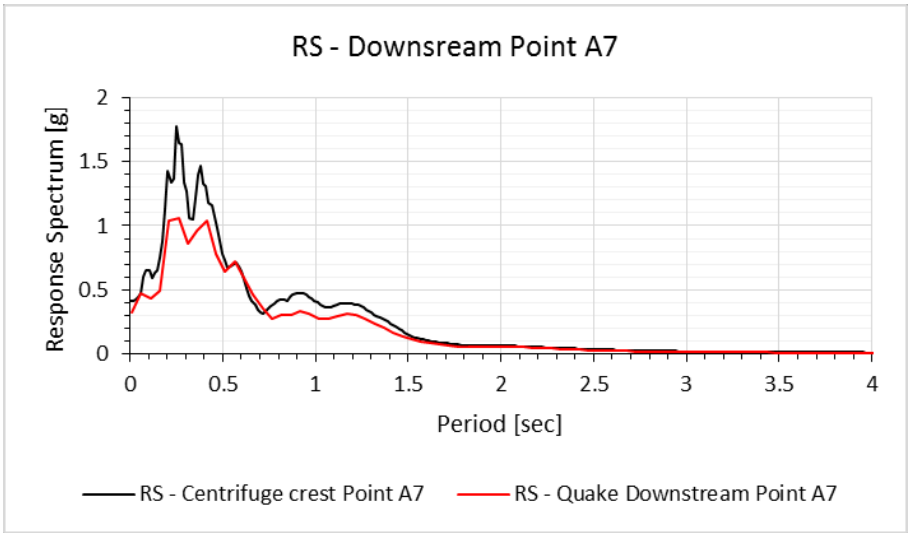

Figure 4.43 Comparison of acceleration spectra at point A7

The comparison of the acceleration distribution shows a similar trend of the numerical analysis with the centrifuge results. During the centrifuge test the detected amplification at crest was not so high and generally the maximum acceleration distribution doesn't show the typical increasing trend. In detail, this is observable in the upstream (Fig. 4.37) and downstream distribution (Fig. 4.37 and 4.39). The numerical analysis results tend to reproduce the average distribution of the maximum acceleration, and especially in the core, the predicted results seem to be quite in agreement with the experimental ones. Similar results are obtained for the maximum acceleration at crest and in the shells on the points at higher elevation.

The maximum acceleration at crest is 0,39g for the numerical analysis and 0.37g in the centrifuge test (Fig. 4.37). In the upstream slope, the maximum predicted value is 0,36g whereas the detected value is 0,34g (Fig. 4.38). In the downstream slope, the maximum predicted value is 0,37g whereas the detected value in the centrifuge test is 0,31g (Fig. 4.38).

The comparison between the computed and the experimental acceleration spectra shows similar results, especially for the point A1 (Fig. 4.40). Computed response spectra are almost identical to the experimental spectra for point A7 (Fig. 4.43) but with a slight underestimation of peak spectral accelerations. It is important to note that at point A7, detected experimental results are not in agreement with the typical increasing trend of the amplification, generally observed from the bottom to the top of the dam.

Computed acceleration spectra for point A2 and A4 show some differences in shape between measured and predicted response spectra, probably due to some low frequency wave affecting the measured data (Fig. 4.41 and Fig. 4.42).

However, in general the stiffness of the numerical model seems to reproduce the stiffness of the centrifuge model because of the correspondence of peak spectral period. The overall underestimation of the peak acceleration spectra is probably associated to higher energy dissipation, probably due to a possible overestimation on the calibration of the damping.

Available displacement results of the centrifuge test with PGA of 0,35g were compared with the numerical results.

Vertical settlement experimental results for the two points L1 and L2 (see Figure 4.27) were detected.

Figure 4.44 shows the vertical displacements histories observable at crest (point L1) after the numerical analyses. These settlements are compared with the available centrifuge test results.

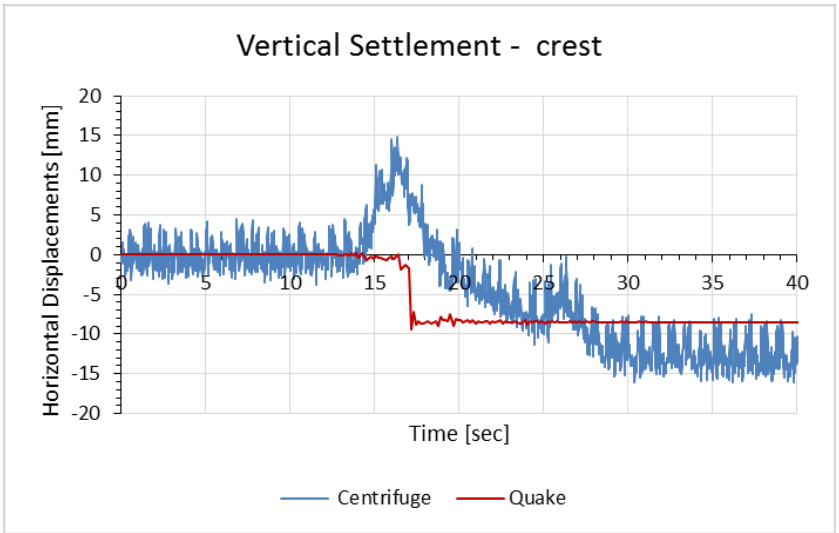

Figure 4.44 Vertical displacements obtained by centrifuge test and the present numerical analyses at point L1

The residual settlements observed at the end of the centrifuge test are quite variable. The measured time history is irregular and characterized by a sharp peak on the positive side. The observed vertical displacement tends to a stable value, after about 30 seconds from the beginning of the event.

The measured vertical settlement reaches a stable average value of 12.1mm.

The vertical predicted displacements at crest shows a more stable trend. The maximum value is of 8.6mm and remains constant until the end of the earthquake. Figure 4.45 shows that the stable value obtained from the numerical analysis seems to be quite in agreement with the stable vertical value observed at the end of the centrifuge test. Moreover, in both cases the vertical displacement begins to increase after the beginning of the strong motion, after about 15sec from the start of the event.

However, in both cases results agree with the trend observed by Swaisgood (2003) where a series of earth dams that experienced an earthquake were studied (Par. 3.2.4).

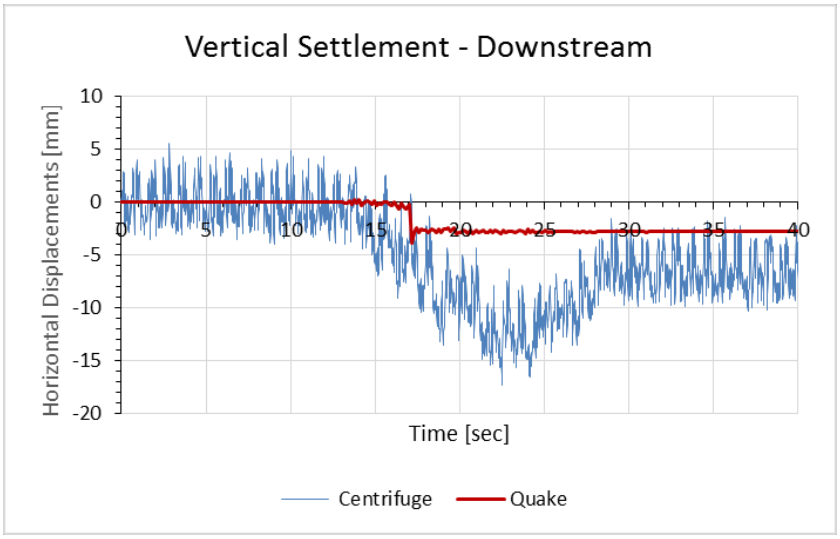

Figure 4.45 Vertical displacements obtained by centrifuge test and the present numerical analyses at point L2

A similar result is observable for the vertical settlement on the vertical slope (point L2). The residual settlements observed at the end of the centrifuge test are quite variable. The measured time history is irregular and characterized by a sharp peak on the negative side. Also in this case, the observed vertical displacements tend to a stable value, about 30 seconds after the beginning of the event.

The measured vertical settlement reaches a stable average value of 6.2 mm.

The vertical predicted displacement at crest shows a more stable trend.

The maximum value is of 3mm and remains constant until the end of the earthquake.

Also in this case, the vertical displacements begin to increase after the beginning of the strong motion, after about 15 sec from the start of the event for both the experimental and numerical results.

The numerical results show slightly lower values than the experimental results but it is important to note that the crest settlements in the centrifuge test were obtained by a laser technique whose data capture definition was not be too accurate.

Chapter 5

PARAMETRIC SEISMIC ANALYSIS OF EARTH DAMS IN ITALY

In this Chapter, the analysis aimed at studying the seismic response of existing strategic dams in Italy, according to the methodology explained at Chapter 3. This section contains several parametric studies performed to assess the effects of different factors on the predicted seismic response of earth dam models. The earth core rockfill dam models are used as the basis for the investigation. Their geometry has been defined according to the prescription by the Italian Code and the literature suggestions on the Italian existing earth structures (Chapter 2).

First, the location of the dam model has been determined and thus the adequate seismic inputs have been assigned.

The calibration of the models is performed respectively for the rock foundation, the core and the shells of the embankment.

5.1. The case study

This paragraph is devoted to the presentation of the case studies. As mentioned before, the analysis is applied to the study of the seismic response of strategic dam models whose geometry is defined according to the literature on existing earth dams in Italy and the standards suggested by the Italian Code (see Chapter 2). Following, the description of the dam's location, the selection of the input motions and the geometrical and geotechnical characteristics of the embankments and the rock foundation are presented.

5.1.1. The location

The location of the case study has been defined considering a site with the higher seismic risk in Italy.

Figure 5.1 The location at Roccaforte del Greco (RG) in Calabria Region, South of Italy

The hypothesis is based on studying the seismic behavior of earth dam models placed on a site with a high seismic risk in Italy. The site is considered the bedrock at Roccaforte del Greco in Reggio Calabria, in the Southern Italy, at about 1400 m above the see.

Before defining of the seismic actions on the site of interest, it is necessary to understand the actual tectonics configuration of the Region.

The actual configuration of the Calabria region is due to the rapid southeast advance of the Calabria Arc. The movement is believed to be driven by the rollback and the retreat of the subduction zone due to the sinking of the old Mesozoic seafloor of the Ionian Sea.

Figure 5.2 (Gvritzman and Nur, 2001) shows the Calabria was connected to Sardinia about 15 million years ago, and an old deep ocean existed instead of the actual Tyrrhenian Sea.

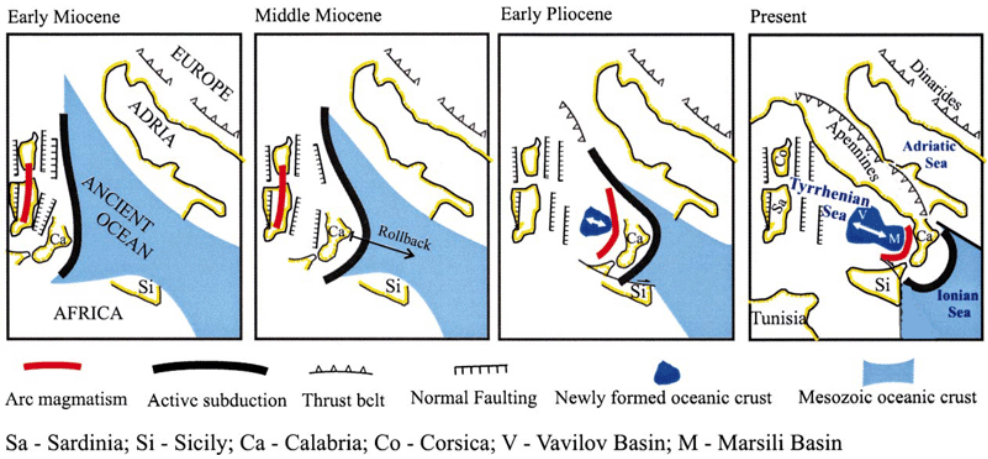

Figure 5.2 Tectonic assessment of Calabrian arc (Gvirtzman & Nur, 2001).

This separation resulted in the creation of a new oceanic crust and the northern part of the subduction zone collided with Italy creating the Apennine Mountains.

The remaining piece of the subduction zone is wedged between Sicily and Peninsular Italy. This collision has broken the advance of Calabria but probably the Region, or piece of it, will continue its advance to the Ionian Sea.

The Italian tectonic setting is described in Figure 5.3, according to the Seismic Zonation, ZS9 project (Meletti and Valensise, 2004). As shown by the Figure 5.3, the Calabria arc is comprised between two different seismic zones, named 929 (the Tyrrhenian zone) and 930 (The Ionian zone) which reflect two different seismicity levels.

The higher intensity earthquake has been noticed in the basins of Crati, Savuto and Messina's channel (929 zone). In this zone, earthquakes (1783s sequence, the beginning 1900s events) with magnitude higher than 7 were recorded. On the contrary, only four events have been exceeded the magnitude 6 on the Ionian coast of Calabria (zone 930) (Meletti and Valensise, 2004).

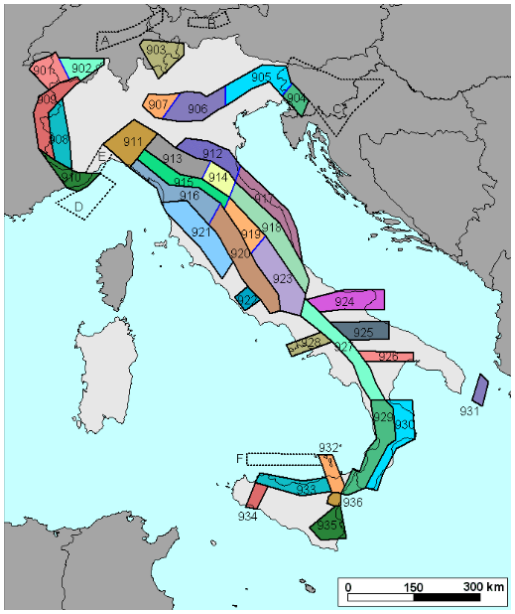

Figure 5.3 Italian Seismic sources, according to ZS) project (Meletti and Valensise, 2004)

5.1.2. Definition of the model

5.1.2.1. Definition of the geometry

A considerable number of earth dams in Italy are built on areas of significant seismic activity. Especially in case of strategic structures, the seismic retrofit is recommended by the actual Italian Codes (M.LL.PP., 2008, M.LL.PP, 2014).

Strategic dams are structure whose functions are strategic for the community and they are usually used for hydroelectric power generation or potable use. Their collapse or damage could cause catastrophic effects. The main aim of this study is to investigate the seismic dam response of hypothetical existing strategic cases to establish and further improve the current knowledge about their seismic response.

Two types of large earth core rockfill dams have been investigated, with a height respectively of 30m and 60m. Moreover, the study performs a series of numerical analyses for the 60m high dam model with an inclined core (ICD). The inclined core was assumed to have the same volume as the vertical one.

The geometry of the hypothetical models is defined according to the literature (see Chapter 2) and the standards suggested from the Italian Codes (M.LL.PP, 2014).

Figures 5.4a and 5.4b show the hypothetical simplified sections for the vertical (VCD) and inclined core dam (ICD). The sections geometrically respect the

standard characteristics of typical cross sections of earth core rockfill dam in Italy (ECRD).

The dam's slope inclination is 1:2 (Vertical: Horizontal) to achieved an adequate factor of slope safety under static conditions. The core-shell interfaces range between 5:1 (Vertical: Horizontal) in the VCD model and 0,5:1 (Vertical: Horizontal) for the downstream interface of the ICD model (see Paragraph 2.1.2).

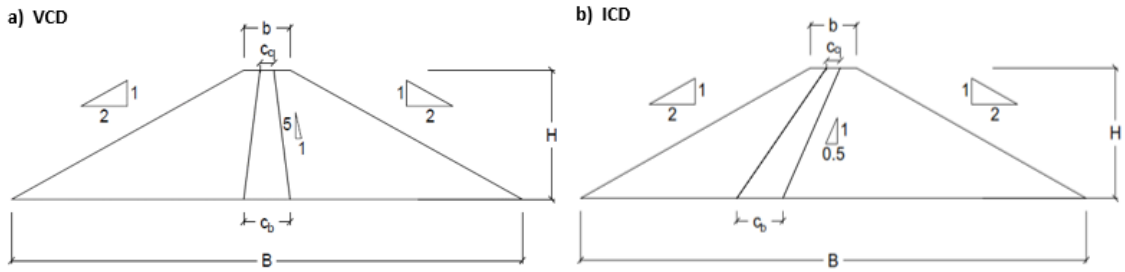

Figure 5.4 Simplified sections for vertical (VCD) and inclined core dam (ICD)

Tables 5.1 and 5.2 show the geometrical characteristics for the VCD and the ICD models, according to the recommendations suggested by the literature (Paragraph 2.1.2.) and the Italian Codes (M.LL.PP, 2014).

	Vertical CORE (VCD)		H [m]	Crest width b [m]	Dam width at base B [m]	Core width at crest Cc [m]	Core width at base C_b [m]	Slope V:H shell	Slope V:H core
ECRD	Case	Type		b=0.2H, b_{min}=4m	B=b+4H	Cc=0.11H	C_b=0.53H		
	1	Strategic	30	6,00	126	4.00	16	1:2	5:1
	2	Strategic	60	12,00	252	8.00	32	1:2	5:1

Table 5.1 Geometrical characteristics of the VCD model

ECRD	Inclined CORE (ICD)		H [m]	Crest width b [m]	Dam width at base B [m]	Core width at crest Cc [m]	Core width at base C_b [m]	Slope V:H shell	Slope V:H core
	Case	Type		b=0.2H b_{min}=4m	B=b+4H	Cc=0.11H	C_b=0.53H		
	1	Strategic	30	6,00	126	4.00	16	1:2	1:0.5
	2	Strategic	60	12,00	252	8.00	32	1:2	1:0.5

Table 5.2 Geometrical characteristics of the ICD model

5.1.2.2. Definition of the water level

According to the Italian Codes (M.LL.PP., 2008, M.LL.PP.,2014), the freeboard height should observe the minimum value for protecting the water tightness in case of waves generated from wind and earthquake.

Since it is supposed the construction is located at 1400m above the see level, the freeboards for the 60m high and 30m high dam have been defined respectively of 5m and 3m.

Thus, the reservoir water level is 55m for the 60m high dam and 27m for the 30m high dam, according to the suggestions of Italian Codes (M.LL.PP., 2008, M.LL.PP.,2014).

5.1.3. Selection of the input motion

According to the selecting procedures defined by the Italian Building Code (M.LL.PP., 2008) and the Italian Dam Code (M.LL.PP, 2014), a series of natural accelerograms were selected and applied at the base of the dam models, in order to study the response under different seismic conditions.

In Chapter 4.2, the limit states of dams have been defined. In order to study the dam response under operability and ultimate conditions, the *Damage Limit State* (DLS) and *Collapse Limit State* (CLS) have been selected. The selected earthquakes for the DLS and CLS represent respectively moderate and strong input motions.

According to the description at Chapter 4.2, the selection procedure of the input motions for the specific site has been performed as follow:

1. Definition of the T_R as function of the nominal life of the existing structure V_N and its relevant class C_U;

2. Estimation of the *PGA* and the relative Target Response Spectra;
3. Definition of the couple Magnitude *M* and Distance *R* which mostly contributes to the characterization of the seismic hazard of the site;
4. Selection of a series of accelerograms which respect the spectrum compatibility criterion.

According to geometry of the dam models and the assumption of considering strategic structures, a return period of T_R=100 years and of T_R=1946 years were selected respectively for the DLS and the CLS limit states (Table 5.3). As defined by the Italian Dam Code (M.LL.PP, 2014), the nominal life V_N for existing Italian dams is 50 years at least (Table 3.2, Chapter 3.2.1). Since Italian existing earth dams have been constructed at least 50 years ago in most cases, a V_N of 50 years was selected. A coefficient of usage C_U was 2 (Table 3.1, Chapter 3.2.1) for strategic structures with a relevant civil function.

Strategic Dam	**V_N**	**C_U**	**V_R**	**T_R [years]**	
				DLS	CLS
	Years		years	P_{VR}=63%	P_{VR}=5%
	≥ 50	2	100	100	1946

Table 5.3 Return period TR for existing and strategic dam models

According to the ESSE1 project of the National Institute of Geophysics and Volcanology (Meletti and Montaldo, 2007) and to the selected return periods T_R, the PGA values of 0,125g and 0,445g for the DLS and the CLS seismic events were defined. Figure 5.5 and Figure 5.6 show the relative target response spectra for the rigid (Vs>800 m/s) and horizontal ground.

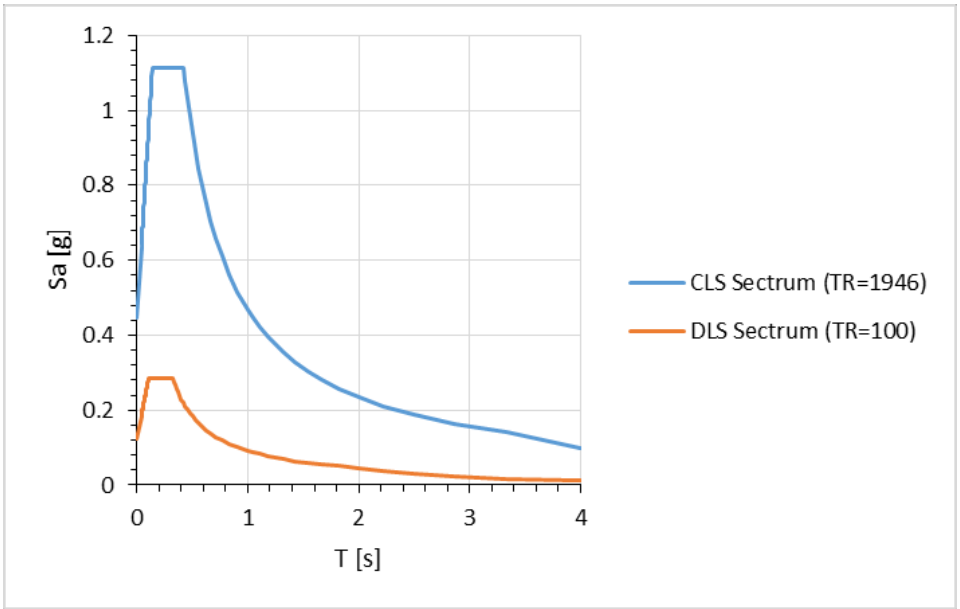

Figure 5.5 Target response spectra for horizontal component of motion for DLS and CLS events

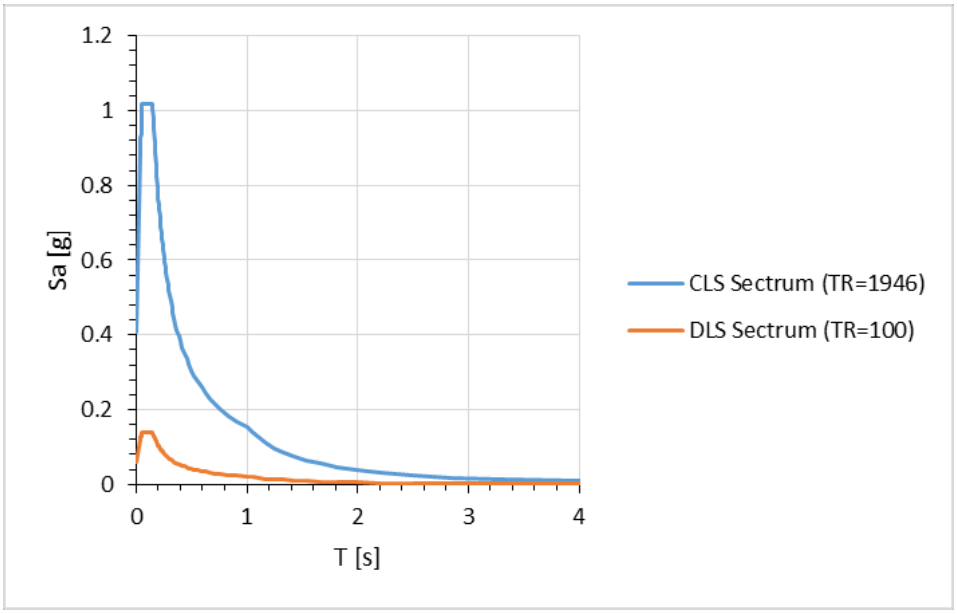

Figure 5.6 Target response spectra for vertical component of motion for DLS and CLS events

The coupled Magnitude- Distance (M-R) have been selected with the disaggregation method, according to the ESSE1 project (http://esse1-gis.mi.ingv.it/).

The disaggregation plots are represented in Figure 5.7*a* and 5.7*b* for respectively the DLS and the CLS.

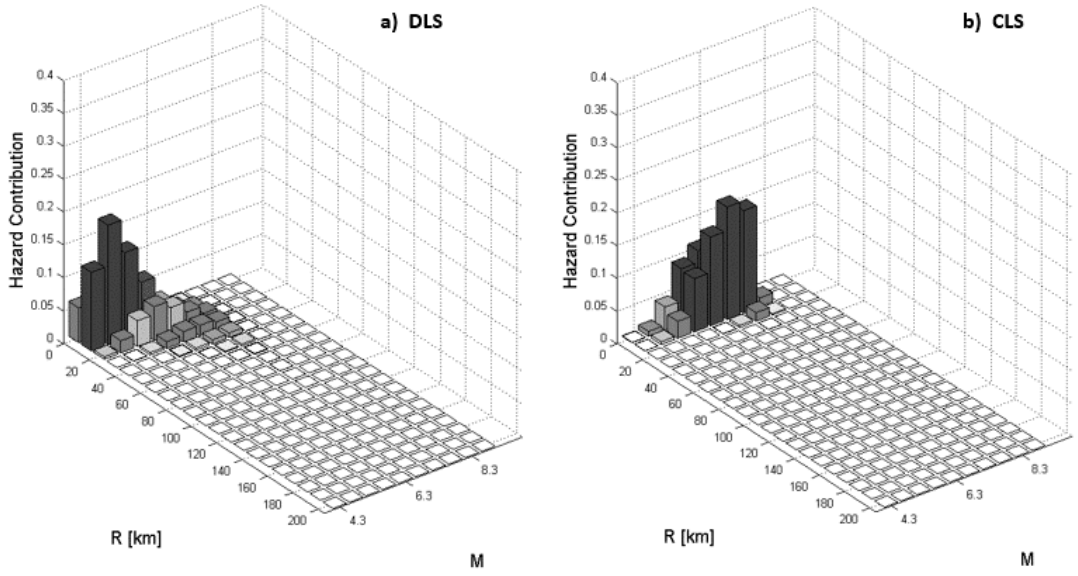

Figure 5.7 Disaggregation of seismic risk for Roccaforte del Greco site, for DLS (a) and CLS (b).

In the Figure 5.7, different greyscale colours represent different level of hazard contribution.

For the specific limite states, the intervals of magnitude and distance have been selected of :

- 4,5-5,5 for Magnitude and 0-20 km for distance in case of DLS events;
- 5-7,5 for Mgnitude and 0-10 km for distance in case of CLS events.

A series of accelerograms have been initially extracted in function of the Magnitude-distance pairs from the European Strong Motion Database (ESM), including the two horizontal and vertical components.

ESM also includes: European Strong-Motion Database (http://www.isesd.cv.ic.ac.uk, FP5 1998-2002), the ITalian ACcelerometric Archive (ITACA, http://itaca.mi.ingv.it), the Strong Ground Motion Database of Turkiye (http://kyhdata.deprem.gov.tr/) and the HEllenic Accelerogram Database (HEAD, http://www.itsak.gr/en/page/data/strong_motion/).

The selection has been performed by means the use of the REXEL software (Iervolino, Galasso and Cosenza, 2010).

All candidate records were first scaled to the target PGA applying a constant scaling F_S.

According to the literature, limit values for FS of 0,25 and 4 are selected (Krinitszky and Chang, 1979; Vanmarke, 1979).

With the respect of the spectrum compatibility criterion (see Chapter 4.2.2.3.), the selection of the earthquake records has been performed.

Five different accelerograms have been selected for the DLS and the CLS events. Figures 5.8 and 5.9 show the compatibility between the response spectrum of the horizontal and vertical records and the relative target spectra. According to the Italian Dam Code (M.LL.PP., 2014), five accelerograms for both the DLS and CLS events have been selected.

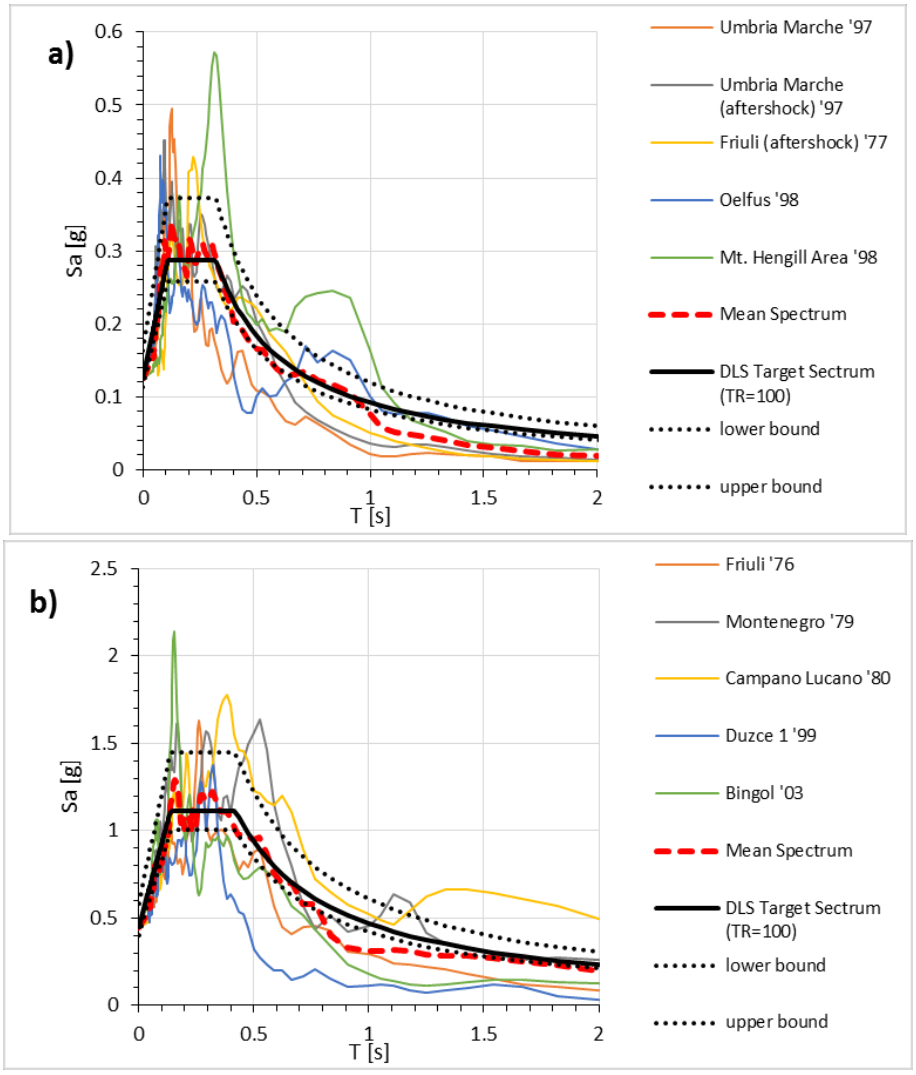

Figure 5.8 Comparison between the Spectral Response of the selected accelerograms and the Spectral Response Code for the DLS (a) and CLS (b) for the horizontal component.

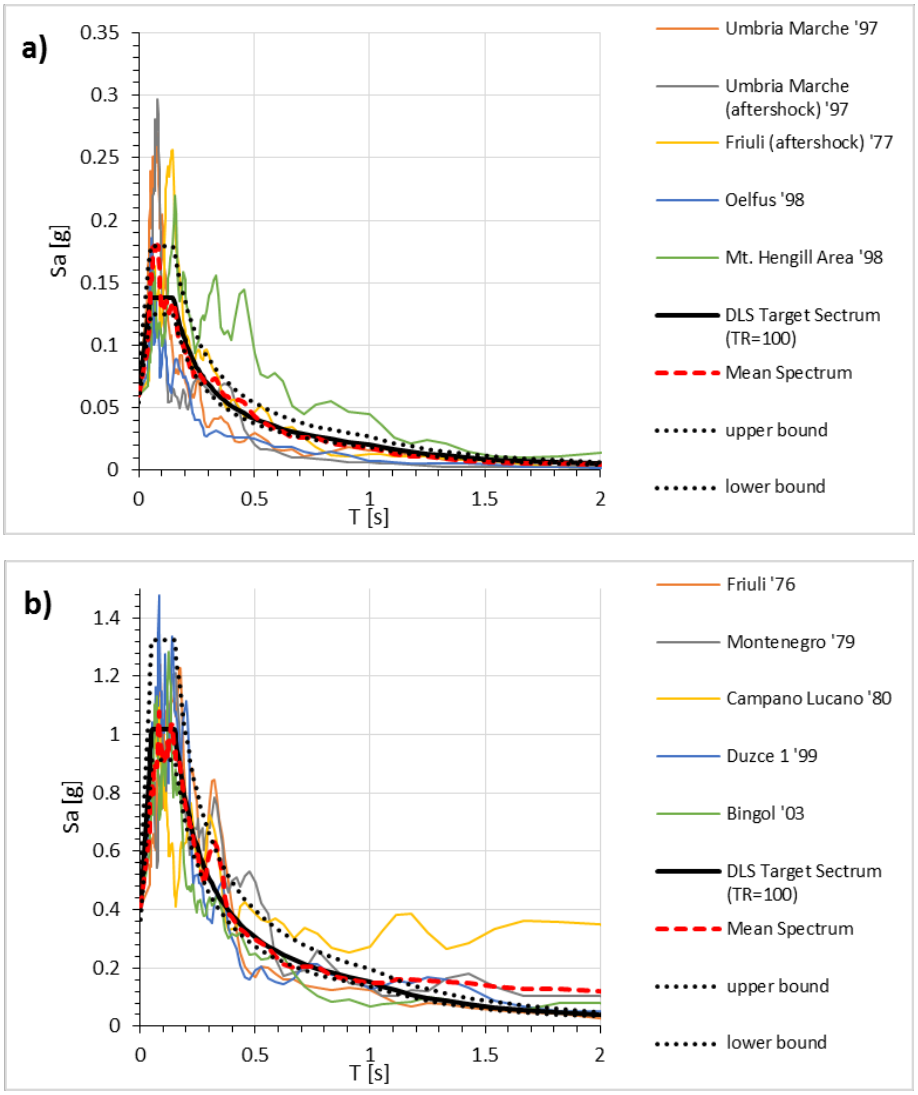

Figure 5.9 Comparison between the Spectral Response of the selected accelerograms and the Spectral Response Code for the DLS (a) and CLS (b) for the vertical component.

The observance of the spectrum compatibility criterion aims to obtain a close match between the spectral shape of each records and the target spectrum in the period range of 0,15 sec-0,7 sec. The selected interval is large enough to contain the fundamental period of the studied dam models. They are about 0,38s and 0,25s, respectively for the 60m and the 30m high dams.

The basic characteristics of the selected accelerograms together with the unscaled PGA and the scaled I_{ax}, for the horizontal and vertical components of motion, are listed in Table 5.4 and Table 5.5 for the DLS and CLS events.

DLS											
Waveform ID	**Earth. ID**	**Station ID**	**Earth. name**	**Date**	**Mw**	**Ep. Dist. [Km]**	**PGA x [g]**	**PGA z [g]**	**FSx**	**FSz**	**Iax [cm/sec]**
000652	292	ST236	Umbria Marche	14/10/1997	5.6	12	0.07	0.05	1.76	1.33	11
000822	350	ST236	Umbria Marche (aftershock)	03/10/1997	5.3	5	0.16	0.21	0.80	0.28	9
000982	72	ST309	Friuli	16/09/1977	5.4	9	0.19	0.06	0.66	1.00	3
005038	1509	ST2495	Oelfus	13/11/1998	5.1	11	0.04	0.07	3.26	0.85	8
005090	1464	ST2495	Mt. Hengill Area	04/06/1998	5.4	18	0.03	0.02	3.99	3.02	13

Table 5.4 Main characteristics of natural records selected for the DLS events

CLS											
Waveform ID	**Earth. ID**	**Station ID**	**Earth. name**	**Date**	**Mw**	**Ep. Dist. [Km]**	**PGA x [g]**	**PGA z [g]**	**FSx**	**FSz**	**Iax [cm/sec]**
000055	34	ST20	Friuli	06/05/1976	6.5	23	0.36	0.27	1.25	1.53	125
000198	93	ST64	Montenegro	15/04/1979	6.9	21	0.18	0.21	2.47	1.93	385
000290	146	ST96	Campano Lucano	23/11/1980	6.9	32	0.22	0.23	2.07	1.73	558
006500	497	ST3136	Ducze 1	12/11/1999	7.2	23	0.50	0.18	0.90	2.24	162
007142	2309	ST539	Bingol	01/05/2003	6.3	14	0.51	0.45	0.87	0.90	151

Table 5.5 Main characteristics of natural records selected for the CLS events

5.1.4. Numerical Model of the dam

5.1.4.1. Discretisation and boundary condition

According to the statements described in section 5.1.2, the numerical models of the dam were constructed considering the 2D sections shown in Figures 5.4a and b. Their geometry was defined as specified in Table 5.1 and Table 5.2.

The size of the mesh was determined considering the maximum frequency f_{max} and the average shear wave velocity V_s (Kuhelemeyer and Lysmer, 1973) to avoid numerical distortion of the propagating ground motion and to obtain an accurate computation of the response.

The 2D geometry, the mesh used for the 60m and 30m high vertical core dam (VCD) and the 60m high inclined core (ICD) sections are shown in Figures 5.10, 5.11, and 5.12.

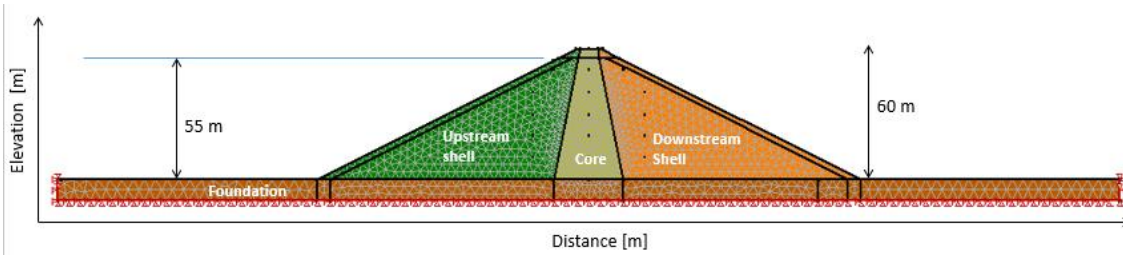

Figure 5.10 2D numerical model of 60m VCD section

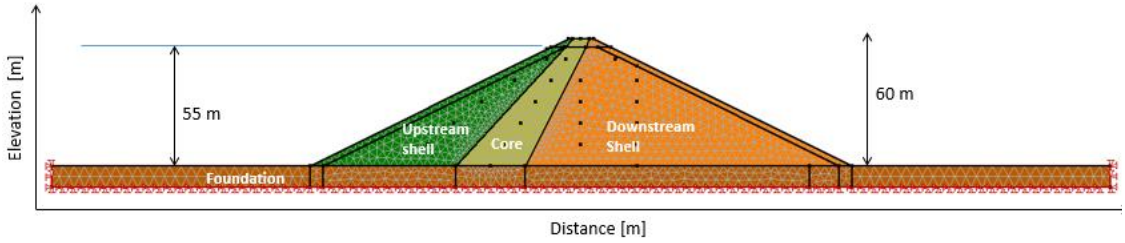

Figure 5.11 2D numerical model of 60m ICD section

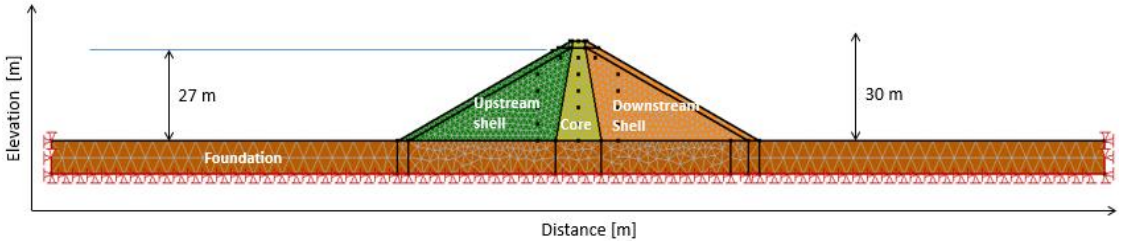

Figure 5.12 2D numerical model of 30m VCD section

The models were constructed directly on the rocky foundation which was extended for about 10m below the earth dam base. This dimension has been selected after a series of numerical analysis with different foundation extensions. The results obtained with a larger rocky foundation extension (30 m depth) gave the same numerical results, thus a foundation extension of 10 m has been fixed to reduce computational efforts.

The far-off foundation lateral boundaries have been extended over 120 m sideways to minimize wave reflection from the boundaries during the dynamic analysis.

In order to define the lateral dimensions as a balance between computational efforts and the reduction of local effects, several attempts have been carried out.

Different boundary conditions have been applied for static and dynamic analysis.

For the static analysis, boundaries with horizontal fixities sideways of the rock foundation were assumed, whereas vertical fixities sideways for the dynamic analysis.

In both cases elementary boundaries have been assumed (see Par. 3.2.3.2) which were extended over 120 m, as explained before.

Both for the static and the dynamic analysis, the bottom of the foundation rock has been restrained from both horizontal and vertical movements.

5.1.4.2. Input motion application

The use of a free surface record is not appropriated as the input motion of the numerical analyses. The national and international databases usually refer to outcrop motions (Figure 5.13).

The outcrop motion is the motion which occurs at the free surface, hence the outcrop motion is twice the upward-propagating train motion.

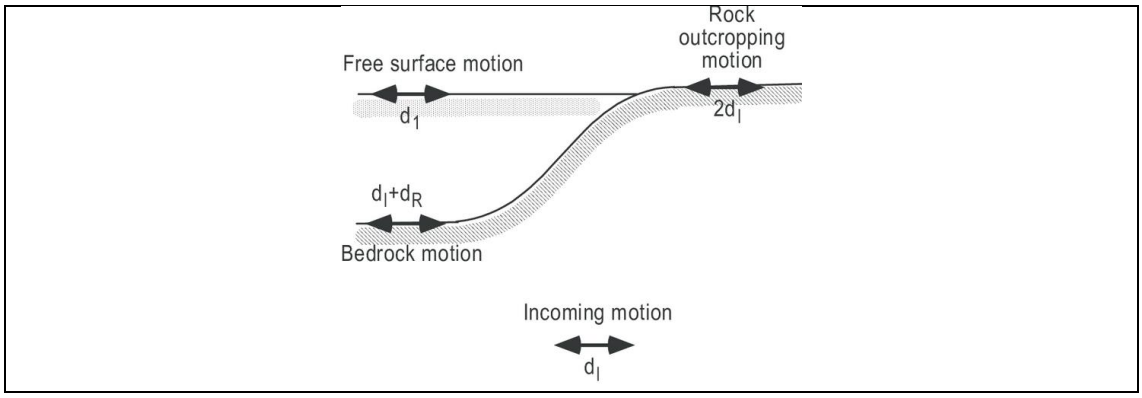

Figure 5.13 Terminology used in site response analysis, and shear wave amplitude at various locations (J. P. Bardet and T. Tobita,2001)

When motion waves travel upwards from deep in the ground they are refracted and reflected at the soil-rock interface. This alters the motion at the soil-rock interface and consequently the motion is different from that at rock outcrop.

The input motion at deeper location can be computed through a "deconvolution" analysis using a 1D wave propagating code such as the equivalent-linear software STRATA (Kottke and Rathje, 2011).

The motion applied at the base of the model is thus a "within" motion where the upward and downward propagating wave pass through.

In the present case, the motion applied at the base have been modified through the STRATA software. It was verified that the computed results at the free surface were similar to the outcrop measurements.

Moreover, earthquake records can often have some drift in the data as illustrated Table 5.2. This aspect does not have a great effect on the dynamic response

analysis of a structure, but it can lead to an unrealistic picture of computed displacement from double integration of the acceleration record. The "baseline correction" process is based on a simple linear regression which ensure that the area under the curve is the same above and below the zero acceleration axes (that is, the slope of the modified linear regression line is zero).

The "baseline correction" process has been performed for all analysis and every seismic input motion has been corrected using the procedure implemented in the software QUAKE/W.

5.1.4.3. Hydrodynamic effects and seepage flow

According to the affirmation of Chapter 3.2.3.6, the hydrodynamic effects of the reservoir have been neglected in the analysis.

In the phase of the static analysis, hydrostatic pressure has been applied to the upstream face of the dam. Based on the full reservoir level (see Par. 5.1.2.2), the hydrostatic pressure is calculated for a triangular variation towards the base of the reservoir. Hydrostatic pressure, is calculated using ($P=h\times\gamma_\omega$), where γ_ω is the water unit weight and h is the depth from the reservoir water level, with a zero value at the reservoir water level. Continuous hydrostatic pressure is applied as pressure on the upstream face of the dam.

The dynamic numerical analysis has been performed in terms of total stresses.

In this study, according to the statement of Chapter 3.2.3.7, the increase of pore water pressure during the seismic motion has been neglected.

Moreover, the experimental centrifuge tests (Park S.Y. et Al., 2016b) on earth core dam demonstrated that water pressure reaches low values of pressure subjected under a high level of motion (PGA of 0.33g).

The numerical analysis with the adopted constitutive model showed a good agreement with the experimental results (Test 2, case 2, Paragraph 4.4) in term of peak acceleration, the relative response spectrum and permanent displacements at crest (see Paragraph 4.4).

5.1.5. Constitutive modelling of dam materials

5.1.5.1. The foundation

Generally, dams are mostly constructed on the top of the bedrock, thus the dam models have been performed considering the foundation as the rigid bedrock. The rocky foundation has been modelled with a linear elastic model.

Since the dam modes is supposed to be located on a site at Roccaforte del Greco, in the South of Italy, the foundation properties refer to the bedrock characteristics of the aforementioned site. Foundation properties were obtained from the work of Albano et Al. (2012) and Albano (2013).

In this study, it has been supposed the rocky foundation was a metamorphic rock with a constant value of the Young Modulus E_r.

The parameters adopted for the constitutive model of the foundation are summarized in Table 5.6.

Foundation		
γ [kN/m^3]	E_r [MPa]	ν
27	70'821	0.25

Table 5.6 Parameters used for the constitutive model of the intact metamorphic foundation

5.1.5.2. The shell

The analysis was performed and repeated adopting two constitutive models: the equivalent linear model and the cyclic nonlinear approach which is associated with a Mohr Coulomb failure criterion.

In the case of the equivalent linear approach, the following parameters for the calibration of the model have been used:

- The unit weight of the soil;
- The small strain shear modulus G;
- The Poisson's ratio;
- The function describing the degradation of the shear modulus G with shear strain;
- The function describing the increment of the damping ratio D with the shear strain;
- Friction angle;
- Cohesion;
- Dilatancy angle.

In the case of the cyclic non-linear approach, the following parameters for the calibration of the model have been used:

- The unit weight of the soil;
- The small strain shear modulus G_{max};
- The Poisson's ratio;
- The minimum damping ratio D;
- The maximum damping ratio D_{max};
- Friction angle;
- Cohesion;
- Dilatancy angle.

With the Non-Linear soil model, G_{max} is obtained from the slope of the hyperbolic stress-strain curve. As the strain increases, the slope of the hyperbolic curve decreases which means that the soil stiffness modulus decreases. The G-reduction is indirectly inherent in the shape of the hyperbolic stress-strain curve

All the parameters of the models have been calibrated according to data recovered by the literature from rockfill shells or rockfill embankments.

Regarding the literature (Aghaei Araei et al., 2012, Albano et Al. 2014, Lanzo et Al., 2015, Mu-Kwang Kim et Al., 2011, Selcuk and Terzi, 2015, Woodward and Griffiths, 1996, Yu et Al. 2005), the geotechnical parameters used in the numerical analysis for the rockfill soil are presented in Table 5.7. Those values have been defined as the median values collected for this material.

Soil Properties - SHELL				
ν	γ	c	φ	ψ
-	[kN/m3]	[kPa]	[°]	[°]
0.3	22	10	40	0

Table 5.7 Shell properties

The shear stiffness at small strain was determined as a function of confining pressures. The shown functions were collected from the literature for typical rockfill materials (Albano et Al., 2014; Andrianopolis et Al., 2014; Ata Araei et Al., 2011; Mu-Kwang et Al., 2011; Seed et Al., 1985), see Figure 5.14.

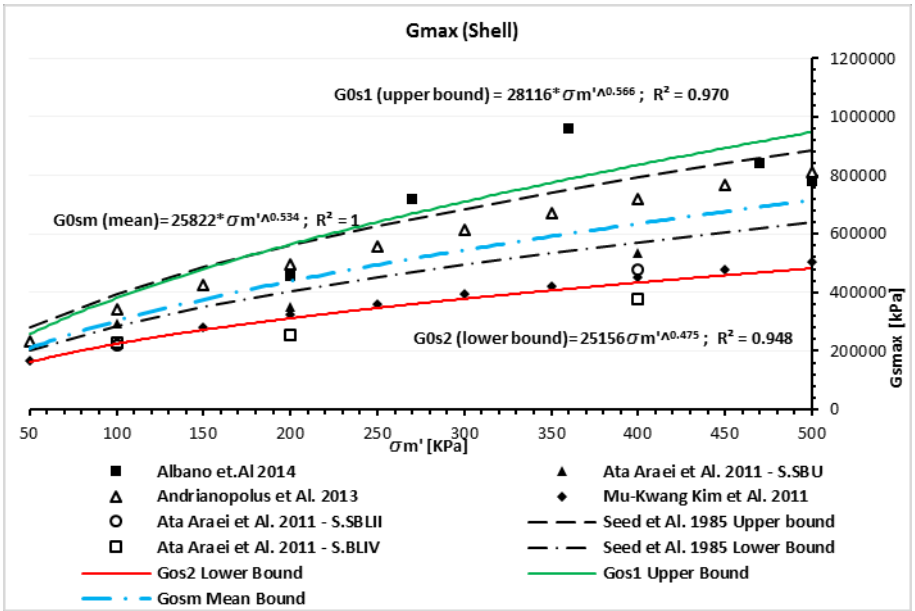

Figure 5.14 Dependency of small-strain shear modulus G_{max} on confining pressure σ_m'

To define the data range for the dependency relation of the shear modulus G on confining pressure, the upper and lower bounds have been defined, as shown on Figure 5.14.

The aforementioned curves have been defined by the following relations:

$$G_{0,s} = K \cdot {\sigma_m}^n \quad (5.1)$$

Where the *K* and *n* are the parameters to be calibrated with collected results for the lower and upper bounds (see Table 5.8).

$G_{0,shell}$	Parameters	
	K	*n*
$G_{0,s1}$=*Upper bound*	28'116	0.566
$G_{0,s2}$=*Lower bound*	25'156	0.475
$G_{0,sm}$=*mean*	25'822	0.534

Table 5.8 Parameters adopted in the numerical model of the shells

In case of the *equivalent linear method*, the strain dependent behaviour of the soil was fitted with relations proposed by Yokota et Al. (1981): Equation (4.4) for the degradation of the shear modulus G, and Equation (4.5) for the damping ratio D.

The fitting parameters were performed with available data collected from the literature for compacted gravel soil and rockfill shell materials (Albano et Al., 2012; Ata Araei et Al., 2012; Mu-Kwang Kim et Al., 2011; Gazetas & Dakulas, 1992; Vucetic & Dobry, 1991; Seed et Al., 1986; Rollins et Al., 1998).

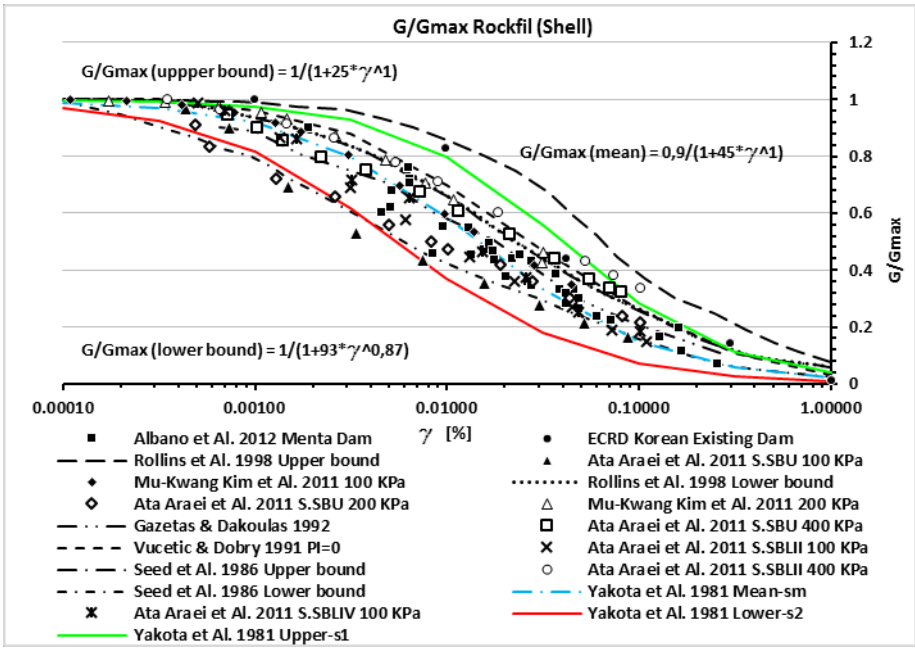

Figure 5.15 Stiffness degradation with shear strain for rockfill

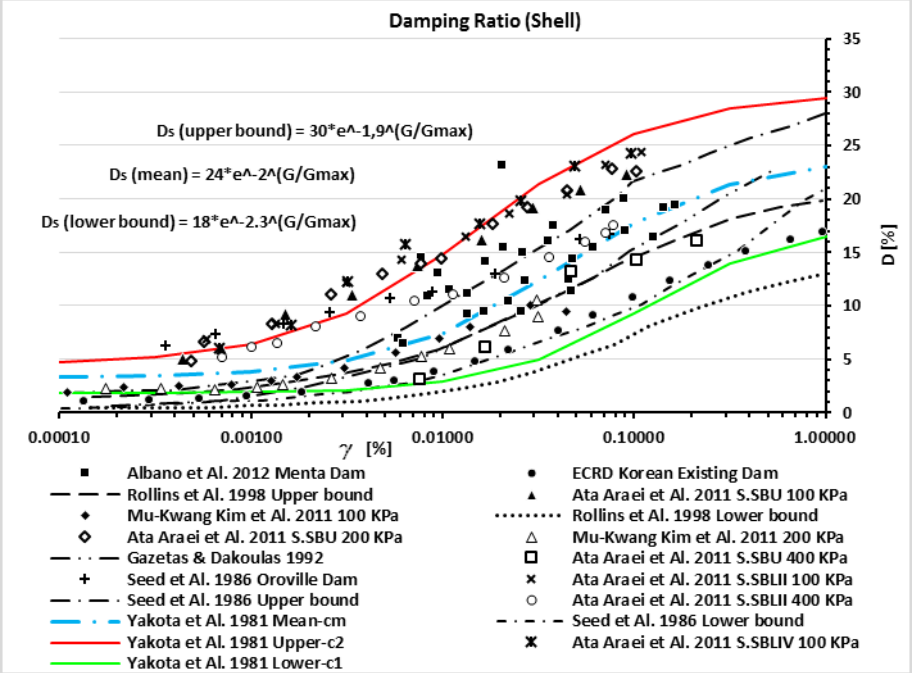

Figure 5.16 Damping ratio increase with shear strain for rockfill

In order to define the data range observed for the strain dependency curves of the shear modulus G/G0 and damping ratio D, the upper and lower bound, and the mean curve have been defined as shown on Figure 5.15 and Figure 5.16.

The calibrated parameters for the aforementioned curves are reported in Table 5.9 and Table 5.10.

$G/G_{0,shell}$			Parameters	
Curves	γref [%]	G/G0 (γ_{ref})	α	β
G/G_{01}=Upper bound	0.04	0.5	25	1
G/G_{02}=Lower bound	0.0054	0.5	93	0.87
G/G_{0m}=Mean curve	0.015	0.5	45	1

Table 5.9 Parameters of the model adopted in the numerical analysis for the stiffness degradation curves

D shell			Parameters		
Curves	γref [%]	D (γ_{ref}) [%]	D_{min} [%]	D_{max} [%]	λ
D_2=Upper bound	0.0054	11.54	4.75	30	1.9
D_1=Lower bound	0.04	5.60	1.80	18	2.3
D_m=Mean curve	0.015	8.94	3.30	24	2

Table 5.10 Parameters of the model adopted in the numerical analysis for the Damping increase

In order to identify the different dynamic soil property curves, the decay G/G0 and increasing D functions are defined in function of the "*reference shear strain*", γ_{ref}. The reference shear strain is defined as the shear value at G/G0=0,5 for the hyperbolic stress-strain behaviour (Hardin e Drnevich, 1972).

The *cyclic non-linear method,* associated with the Mohr Coulomb criterion is characterized by the hyperbolic backbone curve (Eq. 4.6).

The backbone curve is defined by the slope at zero strain and the asymptote at large strains. The slope is represented by the small strain shear modulus G_{max}, defined in Figure 5.14 and Table 5.8. The asymptote is the shear strength defined at Table 5.7.

The damping is related to the Shear Modulus G by the Eq. (4.7), where the G_{max} is the aforementioned parameter and the parameter D_{max} is defined in Table 5.10. When the shear modulus G is equal to G_{max}, at the beginning of the analysis, D is set to the specified minimum value D_{min} (Table 5.10).

5.1.5.3. The core

According to the statements of the previous paragraph, the parametric analysis was performed and repeated adopting the two constitutive models: the equivalent linear approach and the cyclic non-linear model, associated with the Mohr Coulomb failure criterion.

All the parameters of the models have been calibrated according to the collected data of compacted impervious material or dam core soils.

Data were collected from the literature (Bilotta et Al., 2010; Cascone & Rampello, 2003; Lanzo et Al., 2015; Lizarraga & Lai, 2014; Mu-Kwang Kim et Al., 2011; Selçuk &Terzi, 2015; Woodward & Griffiths, 1996; Wu et Al., 2009; Yu et Al., 2005), and from the resonant column tests carried out on the core soil of the "Farneto del Principe" Dam, located, at Roggiano di Gravina, in the Southern Italy. The experimental test was performed at the Geotechnical Laboratory of the University of Pisa.

The geotechnical parameters used in the numerical analysis for the core soil are listed in Table 5.11. Those values have been defined as the median values found for the material.

Soil Properties - CORE				
ν	γ	c	φ	ψ
-	[kN/m3]	[kPa]	[°]	[°]
0.4	20	30	25	0

Table 5.11 Core properties

The shear stiffness at small strain G_{max} was determined as a function of confining pressures and the following relations were collected from the literature (Andrianopolis et Al., 2014; Amorosi & Elia, 2008; Lanzo et Al., 2015; Hardin, 1978; Rampello et Al., 2009; Alberti et Al., 2015; Mu-Kwang et Al., 2011), Figure 5.17.

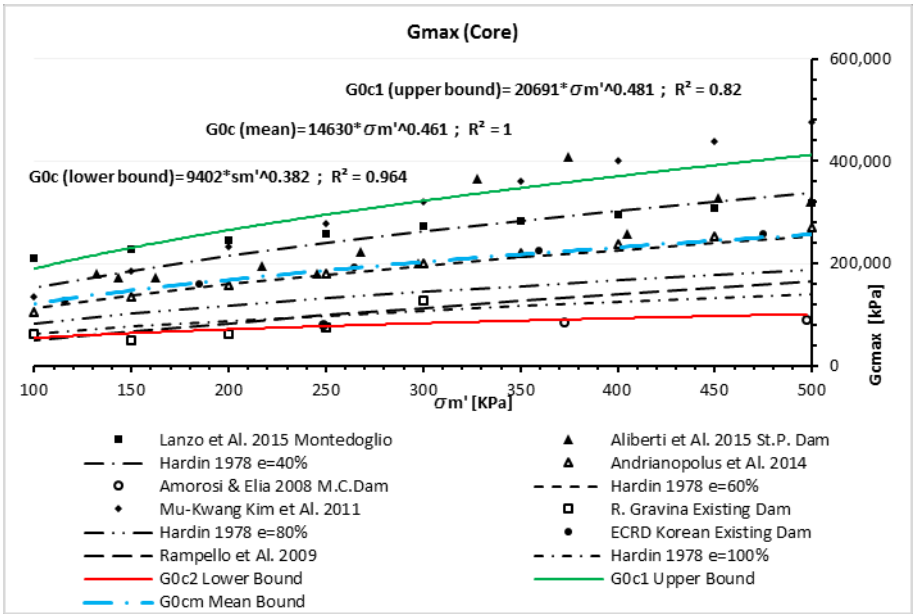

Figure 5.17 Dependency of small-strain shear modulus G_{max} on confining pressure $\sigma m'$

In order to define the data range for the dependency relation of the shear modulus G and confining pressure, the upper and lower bound have been defined, as shown on Figure 5.17.

The aforementioned upper and lower bounds have been defined by the following relation:

$$G_{0,c} = K \cdot {\sigma_m}^n \quad (5.2)$$

Where the *K* and *n* are parameters to be calibrated with the collected results for the lower and upper bounds (see Table 5.12).

$G_{0,core}$	**Parameters**	
	K	*n*
$G_{0,c1}$=*Upper bound*	20'691	0.481
$G_{0,c2}$=*Lower bound*	9'402	0.382
$G_{0,cm}$=*Mean*	14'630	0.461

Table 5.12 Parameters adopted in the numerical model of the core

In the case of the equivalent linear method, the strain dependent behaviour of the soil has been fitted with relations proposed by Yokota et Al. (1981): Equation (4.4) for the degradation of the shear modulus G and Equation (4.5) for the damping ratio D.

The fitting parameters were performed with available data collected from the literature for compacted impervious material and dam core soils (Mu-Kwang Kim et Al., 2011; Gazetas & Dakulas, 1992; Vucetic & Dobry, 1991).

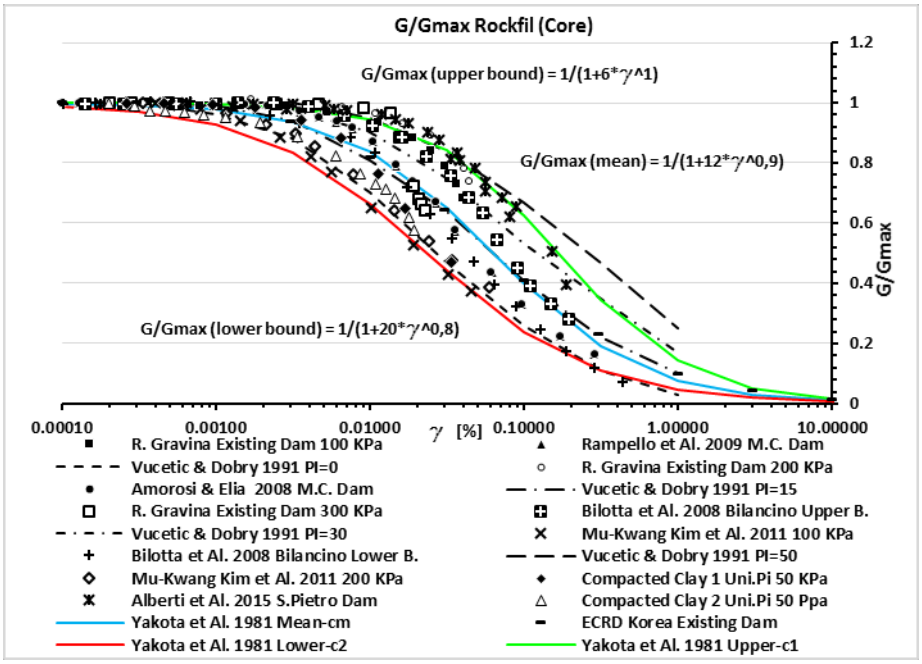

Figure 5.18 Stiffness degradation with shear strain for impervious core

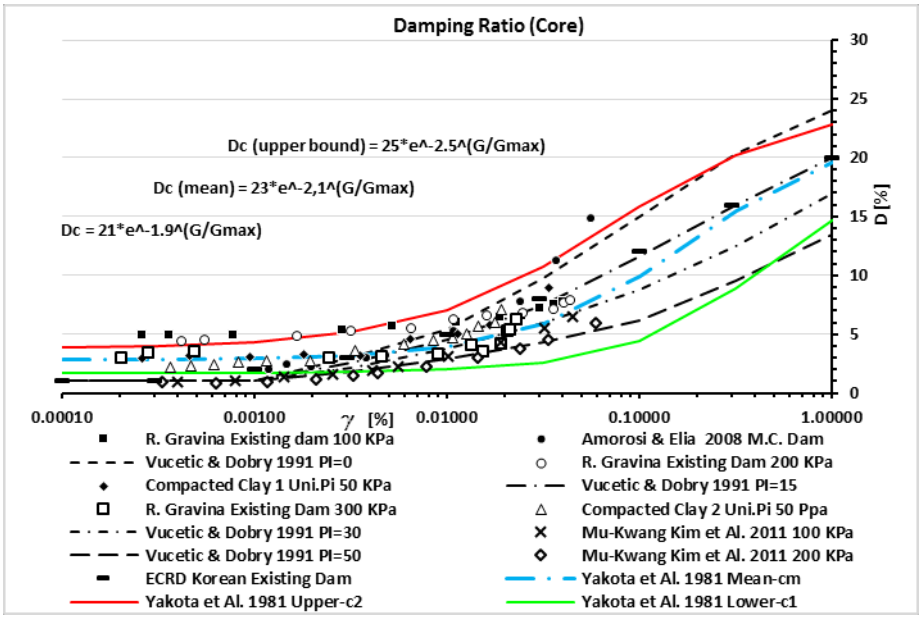

Figure 5.19 Damping ratio increase with shear strain for impervious core

In order to define the data range observed for the strain dependency curves of the shear modulus G/G0 and damping ratio D, the upper and lower bound, and the mean curve have been defined, as shown on Figure 5.18 and Figure 5.19.

The calibrated parameters for the aforementioned curves are reported in Table 5.13 and Table 5.14.

To identify the different dynamic soil properties curves, the decay G/G_0 and increasing D functions are defined in function of the "*reference shear strain*", γ_{ref}. The reference shear strain is defined as the shear value at G/G0=0,5 for the hyperbolic stress-strain (Hardin e Drnevich, 1972).

$G/G_{0,core}$			**Parameters**	
Curves	**γ_{ref} [%]**	**G/G_0 (γ_{ref})**	α	β
G/G_{01}=Upper bound	0.17	0.5	6	1
G/G_{02}=Lower bound	0.024	0.5	20	0.8
G/G_{0m}=Mean curve	0.064	0.5	12	0.9

Table 5.13Parameters of the model adopted in the numerical analysis for the stiffness degradation curves

D_{core}			**Parameters**		
Curves	**γref [%]**	**D (γ_{ref}) [%]**	**D_{min} [%]**	**D_{max} [%]**	λ
D_2=Upper bound	0.024	9.72	3.80	25	-2.5
D_1=Lower bound	0.17	6.10	1.70	21	-1.9
D_m=Mean curve	0.064	8.09	2.80	23	-2.1

Table 5.14Parameters of the model adopted in the numerical analysis for the Damping increase

The *cyclic non-linear method*, associated with the Mohr Coulomb criterion is characterized by the hyperbolic backbone curve (Eq. 4.6).

The backbone curve is defined by the slope at zero strain and the asymptote at large strains. The slope is represented by the small strain shear modulus G_{max} defined in Figure 5.17 and Table 5.12. The asymptote is the shear strength defined at Table 5.11.

The damping is related to the Shear Modulus G by the Eq. (4.7), where the G_{max} is the aforementioned parameter and the parameter D_{max} is defined at Table 5.14. When the G is equal to G_{max}, at the beginning of the analysis, D is set to the specified minimum value D_{min} (Table 5.14).

5.1.6. Static analysis

Before any dynamic analysis, the static analysis should be performed to establish the existing in-situ stresses.

The first step was to establish the long-term steady-state seepage conditions and pore-pressures. On the downstream side, the water-table is taken to be at the surface of the foundation, whereas on the upstream side, the water-table is taken as defined at Par. 5.1.2.2.

The model uses the finite element method for two dimensional Darcy's flow in both saturated- unsaturated soils.

Using the Van Genuchten (1980) closed form solutions, the Volumetric Water Content function (Eq. 4.9) and the Conductivity function (Eq. 4.8) were estimated for the unsaturated soils (shells and core). The foundation was considered to be saturated. The parameters adopted for the aforementioned functions are defined from available experimental data for similar soil types (Park S.Y. et Al. 2016), see Table 4.10).

Figure 5.20, 5.21 and 5.22 show the results about the seepage analyses for the 30m high dam and the 60m high dam with vertical and inclined core.

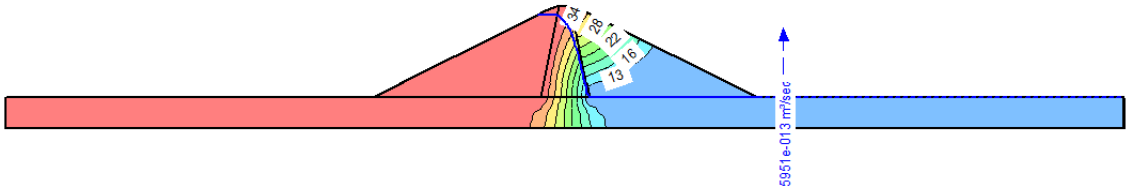

Figure 5.20 Seepage Analysis for 30 high dam model

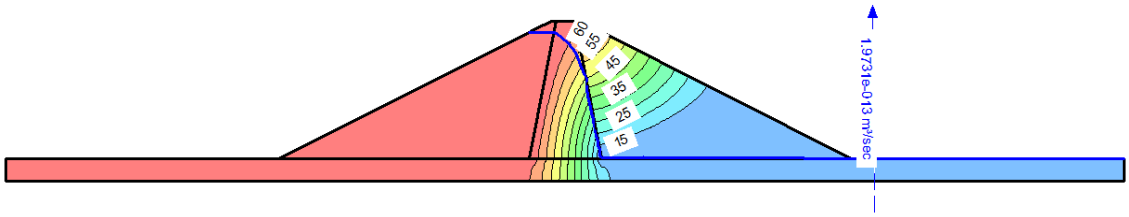

Figure 5.21 Seepage Analysis for 60 high vertical core dam model (VCD)

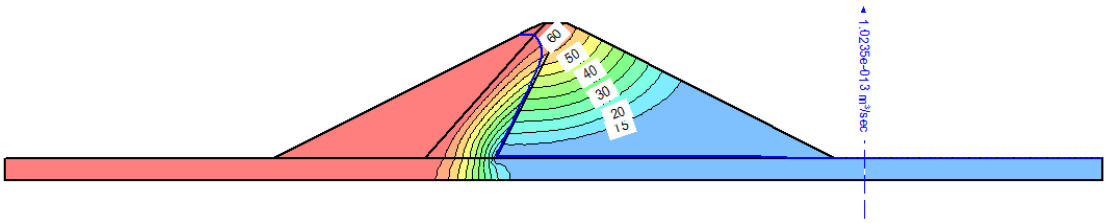

Figure 5.22 Seepage Analysis for 60 high inclined core dam model (ICD)

To simulate the development of effective and total geostatic stresses in the dam model, the QUAKE/W "in-situ stress" module was used. The previously computed pore-pressures was used in the static stress analysis. According to the Paragraph 5.1.4.3, the hydrostatic pressure is applied to the upstream face of the dam for a full reservoir condition.

The geotechnical parameters for the definition of the constitutive model for the rockfill, the impervious core and foundation are presented respectively in Table 5.7, Table 5.11 and Table 5.6. The dependency of the rockfill and core stiffness on the confining effective stress were defined at Par. 5.1.5.2 and Par. 5.1.5.3.

Figures 5.23, 5.24 and 5.25 show the horizontal and vertical stress distribution for the 2D models, at the end of the static analysis. The figures show the results about the stress distribution when the dependency of stiffness on the confining pressures refers to the mean curves (see Figures 5.14 and 5.17; Tables 5.8 and 5.12).

The maximum stress distributions occur in the middle of the dam body and stresses appeared to be concentrated in the basement of dam body. The calculated vertical stresses are consistent with the weight of the dam materials.

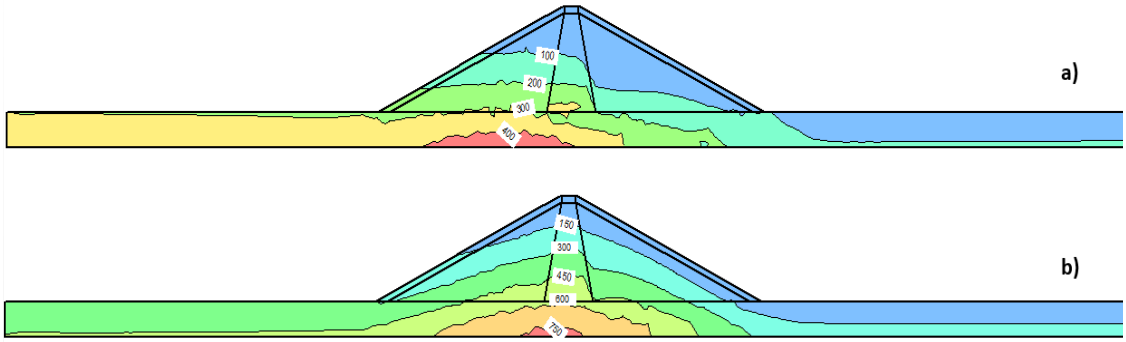

Figure 5.23 Contours of horizontal (a) and (b) vertical total stresses (kPa) at the end of static analysis for 30 high dam model

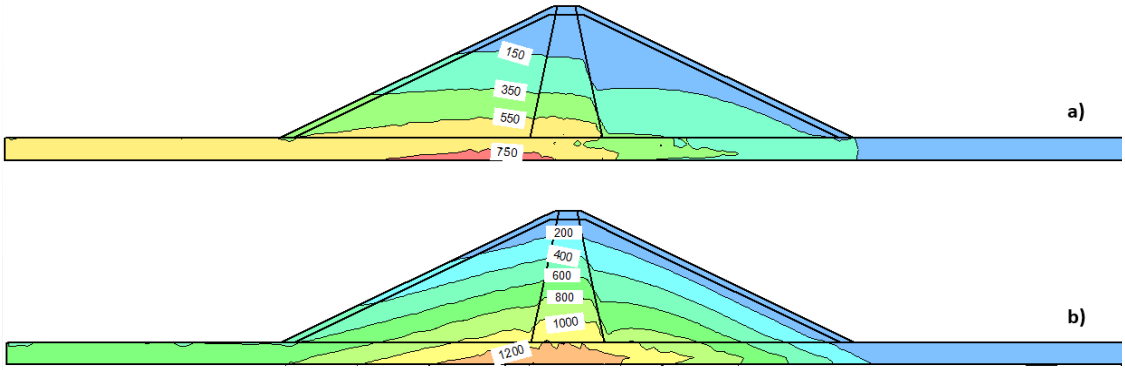

Figure 5.24 Contours of horizontal (a) and (b) vertical total stresses (kPa) at the end of static analysis for 60 high vertical core dam model (VCD)

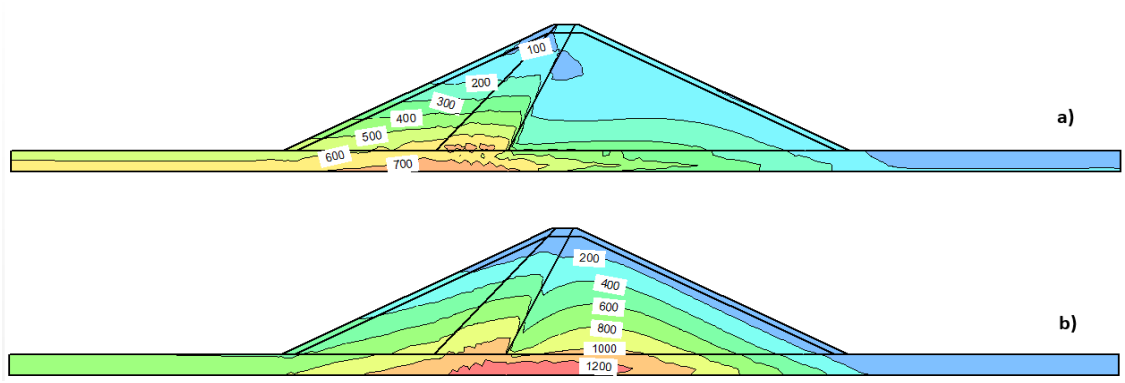

Figure 5.25 Contours of horizontal (a) and (b) vertical total stresses (kPa) at the end of static analysis for 60 high inclined core dam model (ICD)

5.1.7. Dynamic analysis

In this study, Quake/W FEM software was used to evaluate the seismic dam-foundation response. The two-dimensional dynamic finite element analysis uses both the *equivalent linear strain dependent modulus and damping properties*, and the *cyclic non-linear model* which is associated with a *Mohr Coulomb failure criterion*.

In the *Equivalent linear analysis*, the dependency of the stiffness on the strain level has been applied by means of the collected data interpolation using the Yokota's function (Yokota et Al.,1981; (Eq. 4.4)).

Figures 5.15 and 5.18 showed for stiffness degradation with the shear strain for the rockfill and the core respectively.

Three different curves have been selected to defined the data range, as shown in Tables 5.9 and 5.13.

Moreover, the hysteretic strain dependent damping was introduced in the model. Experimental data range for the damping ratio curve was defined using the correspondent Yokota's function (Yokota et Al.,1981; (Eq. 4.5)). Three different curves have been selected to defined the data range, as shown in Tables 5.10 and 5.14.

In the *Cyclic non-linear analysis*, the stress strain behaviour is characterised by the hyperbolic backbone curve, associated to the G_{max} function, and the soil strength. The G_{max} function has been applied by means of the collected data interpolation, using the Yokota's function (Yokota et Al.,1981; (Eq. 4.4)). Three different curves have been selected in order to defined the data range for the rockfill and core soil, as shown in Tables 5.8 and 5.12. The damping is related to the Shear Modulus G adopting the Equation 4.7 (Hardin and Drnevich, 1972), whose parameters are defined in Table 5.10 and 5.14.

Refer to Paragraph 5.1.5.2 and 5.1.5.3 for more details on the used strain dependency of the shear modulus and damping ratios for rockfill and the impervious soils.

The selected time history records were defined at Paragraph. 5.1.3. and applied at the model's base as described at Parahraph 5.1.4.2.

In the dynamic deformation analysis, incremental stresses were considered as a driving force for permanent deformation based on stress redistribution. As

mentioned in Rampello et al. (2009), permanent displacements are resulted from plastic strains that accumulate during the earthquake because of progressive plastic loading which are influenced by the duration of the strong motion.

The following paragraphs will discuss the seismic response of the hypothetical existing Italian earth dam models and the parametric analysis results for the evaluation of influential factors on dam performance.

5.2. The parametric seismic analysis

This paragraph contains parametric studies performed to assess the effects of different factors and modelling approach on the predicted seismic response of earth core rockfill dams.

A series of different scenarios were investigated to understand the influence of the following factors:

- The effect of the impedance ratio *I*;
- Effect of different earthquake input intensity;
- Effect of soil dynamic parameters;
- Effect of dam geometry;
- Combined effect of vertical and horizontal component of seismic input.

A total number of *150 simulations* has been performed, considering the 2D ECRD prototype, whose models have been defined in the previous Paragraph 6.1.

Results have been evaluated considering the dam response in term of the amplification ratio between the maximum acceleration at crest and the value at the basement (PGA,c/PGA,b) and in term of the ratio between the Response Spectrum integral at crest and at the basement.

Moreover, the permanent displacements at crest and the relative displacements between the core and the shell have been evaluated. Those parameters can define the performance of the dam under different input motions, with different geometry configurations and considering the combined effect of vertical and horizontal components of the motion. Figure 5.26 shows the crest and the basement points.

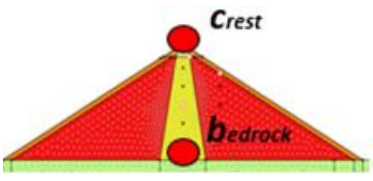

Figure 5.26 Position of measured points

The prediction of the permanent settlement at the dam crest may be adopted for checking the freeboard loss. It can represent an effective indicator of dam performance with respect to other damage mechanisms that are very difficult to simulate. Permanent settlement at the dam crest is a suitable indicator of

structure performance to characterized dam mechanical response under different seismic scenarios (Sica et Al. 2008). Moreover, the relative displacements between the shell and the core have been discussed. Relative displacements can show the interaction between the two zones and possible fractures due to differential settlements among the contact between the core and the shells.

5.2.1. Effect of the impedance ratio

This section examines the influence of the impedance ratio between the bedrock and the dam body, considering different scenarios where different dam impedance values have been evaluated.

The *impedance ratio* is evaluated by Eq. (5.3) as the ratio between the bedrock impedance ($\rho_r V_{s,r}$) and the dam body impedance ($\rho_s V_{s,s}$). The impedance of the soil is the product of the density ρ and the shear wave velocity V_s.

$$I = \frac{\rho_r V_{s,r}}{\rho_s V_{s,s}} \quad (5.3)$$

Since the embankment is composed by two different materials, the dam body impedance ($\rho_s V_{s,s}$) is evaluated as the weighted average $\bar{I}$ with the shell's area and the core one. The $\bar{I}$ is calculated as:

$$\bar{I} = \frac{I_c A_c + I_s A_s}{A_c + A_s} \quad (5.3.a)$$

Where the I_c is the impedance ratio for the core, the I_s the impedance ratio for the shell and A_c and A_s are the areas of the core and the shell respectively.

The static analysis was the same for all the aforementioned analyses and they were performed on the 60m high vertical care dam model. The dynamic analyses were performed using the equivalent linear strain dependent modulus and damping properties.

As shown in Table 5.15, the dynamic analyses are repeated for 4 different values of impedance ratio. They were calculated for different stiffness functions of the shell and the core (see Par. 5.1.5.2 and 5.1.5.3). Then, the stiffness functions were combined with different dynamic soil properties for the shell and the core, as expressed in Table 5.14.

To identify the different dynamic soil properties, the curves G/G_0 and D were defined in function of the relative *"reference shear strain"* value (γ_{ref}).

The reference shear strain is defined for the hyperbolic stress-strain as the shear value when $G/G_0=0,5$ (Hardin e Drnevich, 1972).

Several seismic scenarios were considered for the 60m high model dam with the vertical core. The analyses were indeed performed and repeated considering the selected seismic motions for both the CLS and the DLS events, defined at Paragraph 5.1.3.

Case studies - CLS and DLS					
Type	**SHELL**		**CORE**		**I=ρrVr/ρsVs**
M1	*G0_s upper*	*D shell(γ_{ref})=5.6%*	*G0_c upper*	*D core(γ_{ref})=6.10%*	*6.52*
M2	*G0_s upper*	*D shell(γ_{ref})=5.6%*	*G0_c lower*	*D core(γ_{ref})=6.10%*	*6.91*
M3	*G0_s lower*	*D shell(γ_{ref})=5.6%*	*G0_c upper*	*D core(γ_{ref})=6.10%*	*8.66*
M4	*G0_s lower*	*D shell(γ_{ref})=5.6%*	*G0_c lower*	*D core(γ_{ref})=6.10%*	*9.37*
M5	G0_s upper	*D shell(γ_{ref})=5.6%*	G0_c upper	*D core(γ_{ref})=9.72%*	*6.52*
M6	*G0_s upper*	*D shell(γ_{ref})=5.6%*	*G0_c lower*	*D core(γ_{ref})=9.72%*	*6.91*
M7	G0_s lower	*D shell(γ_{ref})=5.6%*	G0_c upper	*D core(γ_{ref})=9.72%*	*8.66*
M8	*G0_s lower*	*D shell(γ_{ref})=5.6%*	*G0_c lower*	*D core(γ_{ref})=9.72%*	*9.37*
M9	*G0_s upper*	*D shell(γ_{ref})=11.54%*	*G0_c upper*	*D core(γ_{ref})=6.10%*	*6.52*
M10	*G0_s upper*	*D shell(γ_{ref})=11.54%*	*G0_c lower*	*D core(γ_{ref})=6.10%*	*6.91*
M11	*G0_s lower*	*D shell(γ_{ref})=11.54%*	*G0_c upper*	*D core(γ_{ref})=6.10%*	*8.66*
M12	*G0_s lower*	*D shell(γ_{ref})=11.54%*	*G0_c lower*	*D core(γ_{ref})=6.10%*	*9.37*
M13	G0_s upper	*D shell(γ_{ref})=11.54%*	G0_c upper	*D core(γ_{ref})=9.72%*	*6.52*
M14	*G0_s upper*	*D shell(γ_{ref})=11.54%*	*G0_c lower*	*D core(γ_{ref})=9.72%*	*6.91*
M15	G0_s lower	*D shell(γ_{ref})=11.54%*	G0_c upper	*D core(γ_{ref})=9.72%*	*8.66*
M16	*G0_s lower*	*D shell(γ_{ref})=11.54%*	*G0_c lower*	*D core(γ_{ref})=9.72%*	*9.37*

Table 5.15 The different scenarios for the 4 impedance ratio values

The seismic response of the dam was expressed in function of the amplification of the spectral response between the basement and the core.

The amplification ratio is expressed as the ratio between the integral of the response spectrum at crest and the integral of the response spectrum at the bedrock. As previously mentioned, the analysis was repeated for both the CLS and DLS scenarios.

Figures 5.27, 5.28, 5.29 and 5.30 show the results for the CLS seismic events.

Figures 5.31, 5.32, 5.33 and 5.34 show the results for the DLS seismic events.

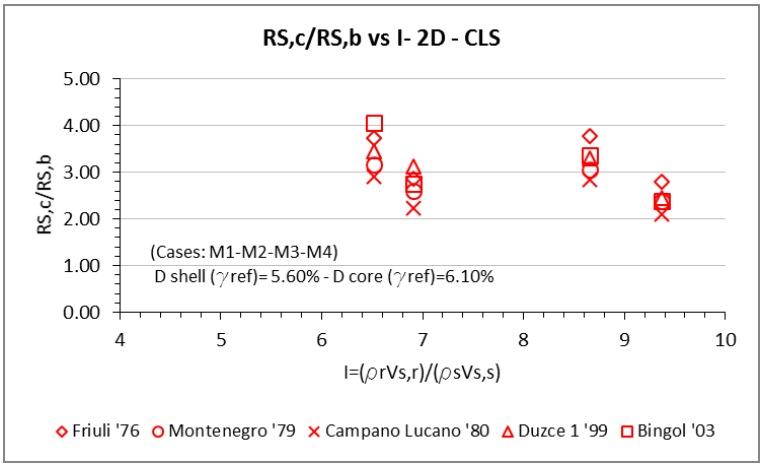

Figure 5.27 The amplification of the spectral response between the basement and the core for the cases: M1, M2, M3, M4, for CLS seismic events.

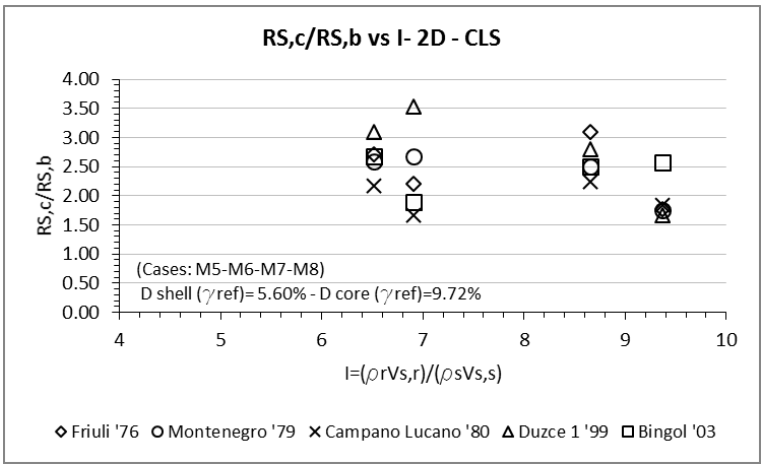

Figure 5.28 The amplification of the spectral response between the basement and the core for the cases: M5, M6, M7, M8, for CLS seismic events.

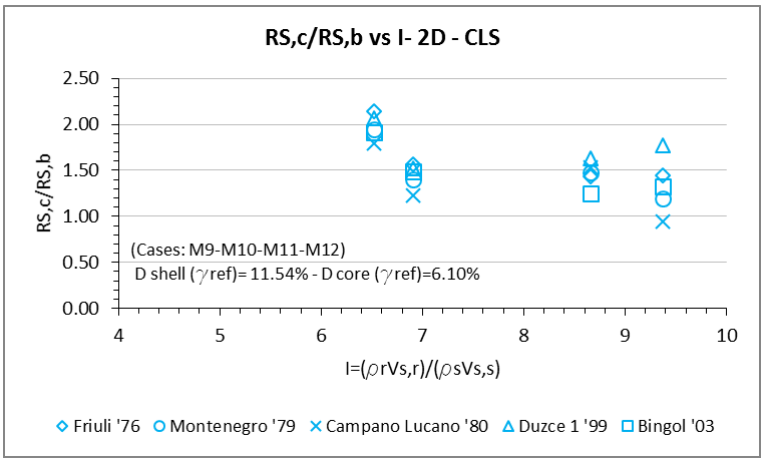

Figure 5.29 The amplification of the spectral response between the basement and the core for the cases: M9, M10, M11, M12, for CLS seismic events.

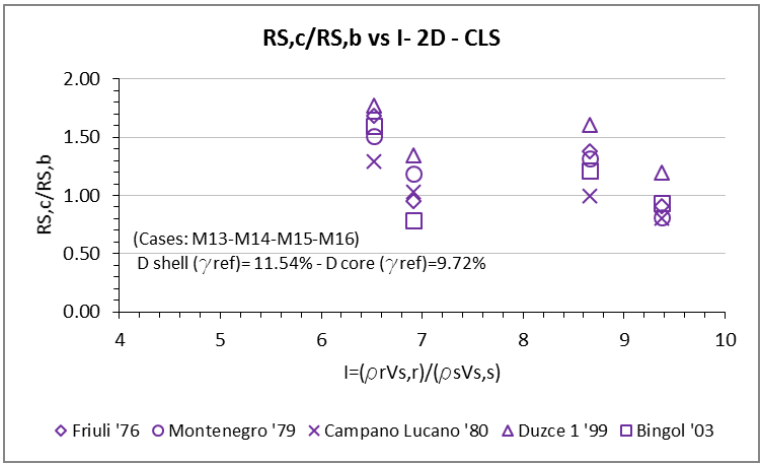

Figure 5.30 The amplification of the spectral response between the basement and the core for the cases: M13, M14, M15, M16, for CLS seismic events.

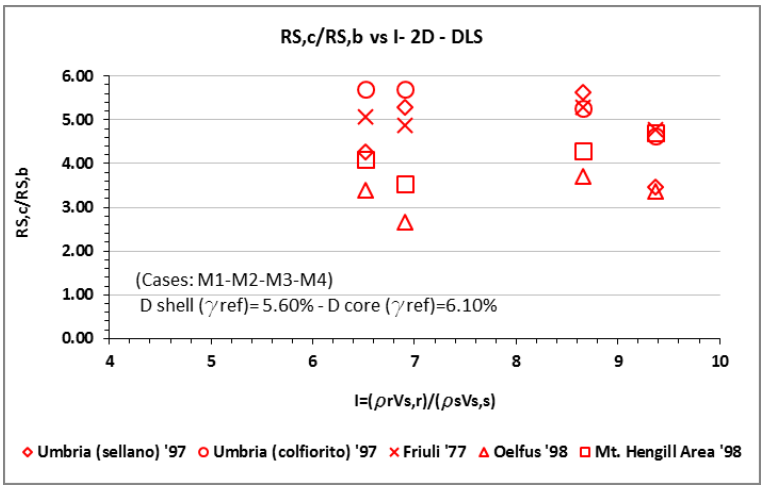

Figure 5.31 The amplification of the spectral response between the basement and the core for the cases: M1, M2, M3, M4, for DLS seismic events.

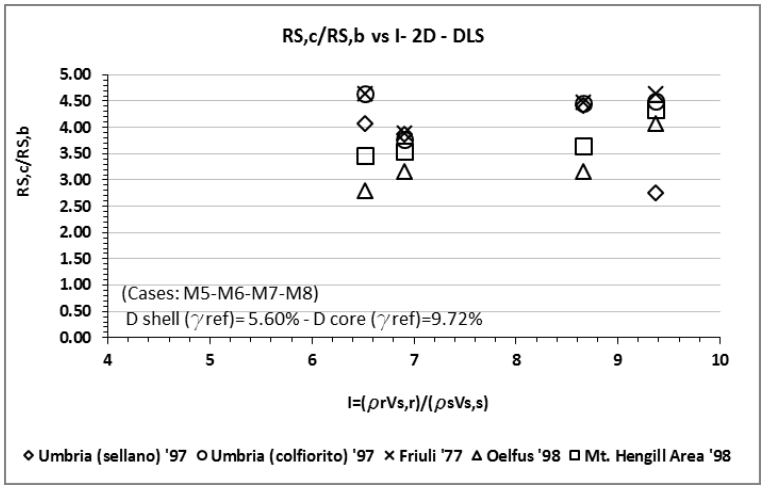

Figure 5.32 The amplification of the spectral response between the basement and the core for the cases: M5, M6, M7, M8, for DLS seismic events.

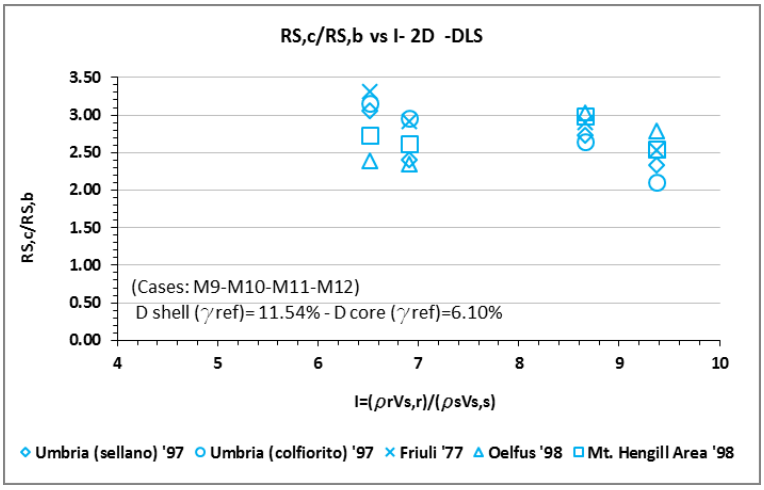

Figure 5.33 The amplification of the spectral response between the basement and the core for the cases: M9, M10, M11, M12, for DLS seismic events.

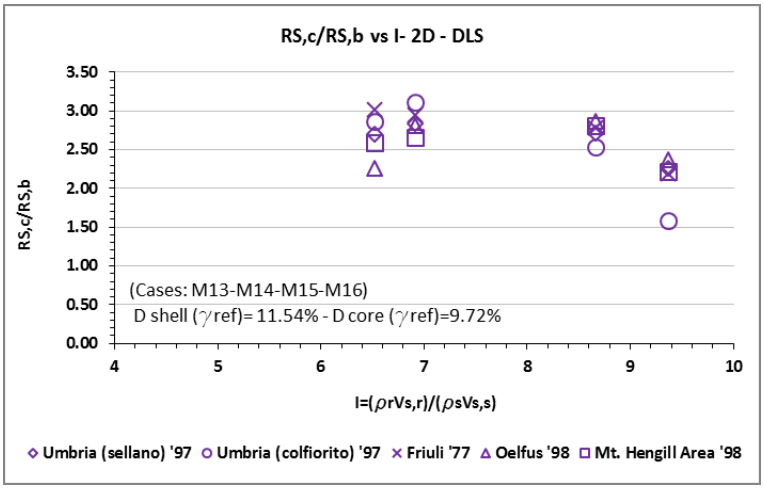

Figure 5.34 The amplification of the spectral response between the basement and the core for the cases: M13, M14, M15, M16, for DLS seismic events.

The results show an influence on the amplification of the seismic response of the dam.

Altogether for the CLS and DLS events, results seem apparently to show a decrease of the amplification of the motion with the increase of the impedance ratio. However, looking at every single earthquake, the overall trend doesn't seem to be confirmed.

In this case it is not possible to confirm a general trend. The amplification in term spectral acceleration doesn't seem to reflect a correlation with the impedance ratio. However, it is worth noting here that dam response was observed within a specific impedance range (I). The observed range was between 6,5 and 10. This restricted range does not seem to represent a reasonable field of values which can demonstrate some clear tendency

5.2.2. Effect of soil dynamic properties G/G_0 and D

The section aims to investigate the effects of using an accurate description of the decay of the shear modulus G or the increasing of the damping ratio function on the seismic response of earth dams.

The analysis studied the effect of using different combination of the dynamic soil properties for the rockfill shell and the impervious core.

Different G/G_0 curves were combined with the same damping ratio incremental relation for both the rockfill and the impervious soil, and vice versa (different damping ratio functions with the same G/G_0 relation).

The curves have been described at Paragraph 5.1.5.2 and 5.1.5.3 for the rockfill and the impervious soil respectively. Three curves define the collected data range for both the G/G_0 and D functions versus the shear stain level.

For the sake of simplicity, the decay relation of the shear modulus G has been identified according to the relative *"reference shear strain"* value (γ_{ref}) when G/G_0=0,5. The relative increase function of the damping ratio was identified in function of its minimum value D_{min} (Table 5.10 and 6.14).

The investigation was concerned with both the CLS and DLS seismic events. Therefore, ten separate analyses were carried out: five for the CLS motions and five for the DLS events.

The seismic events were identified and characterized by their synthetic parameter of *Arias Intensity*, *Ia* (Arias, 1970).

The Arias Intensity reflects the energy developed by a seismic motion and its expression is defined in Equation 5.4.

$$I_a = \frac{\pi}{2g}\int_0^{\infty}[a(t)]^2 dt \qquad (5.4)$$

The Arias Intensity has the measurement unit of velocity and is usually expressed in meters per second or centimeter per second. It is obtained by the integration of the square acceleration over the entire duration of the motion. The Arias Intensity of the horizontal motion for every selected seismic event is shown at Tables 5.4 and 5.5.

The static analysis was the same for all the analyses and they were performed on the 60m high vertical core dam model. The dynamic analyses were performed

using the equivalent linear strain dependent modulus and damping properties. In the dynamic deformation analysis, incremental stresses were considered as a driving force for permanent deformation based on stress redistribution. The shear stiffness at small strain was determined as a function of the confining pressure and it is related to the mean curves, expressed for the core and the shell at Par. 5.1.5.2 and 5.1.5.3.

Results are expressed in function of the amplification of the response between the basement and the core. The amplification is defined in term of the spectral acceleration and horizontal peak acceleration. The amplification response in term of the spectral acceleration is obtained as the ratio between the integral of the response spectrum at crest and at the bedrock. The amplification response in term of the peak horizontal acceleration is the ratio between the peak ground acceleration at the crest and the correspondent value at the basement.

Analyses with the same damping ratio curve associated with different G-γ decay functions were performed for CLS and DLS events. (Figures 5.35 and 5.36). The response is expressed in term of the spectral acceleration amplification.

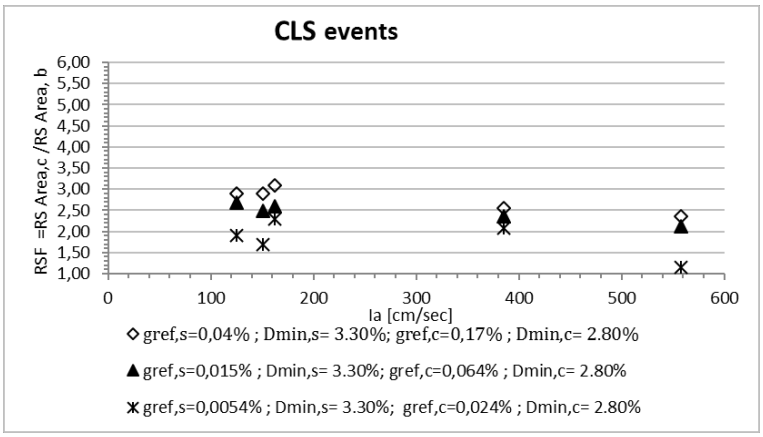

Figure 5.35 Amplification response in term of the spectral acceleration for the CLS events: analysis with the mean function for D and different G/G0 curves.

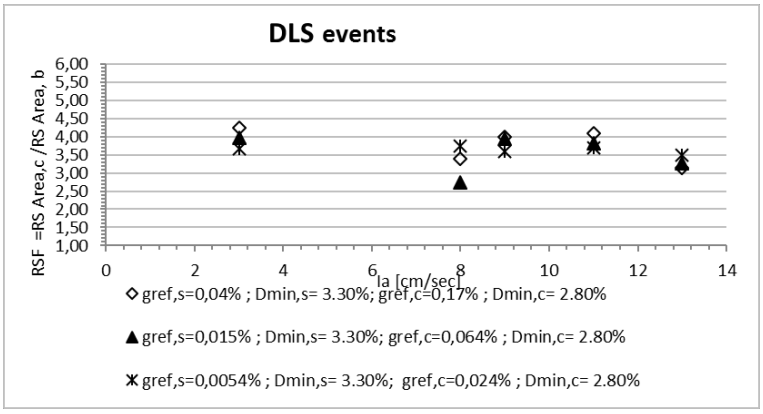

Figure 5.36 Amplification response in term of the spectral acceleration for the DLS events: analysis with the mean function for D and different G/G0 curves

Analyses with the same G-γ decay curve associated with different damping increase functions were performed for CLS and DLS events. (Figures 5.37 and 5.38). The response is expressed in term of the spectral acceleration amplification.

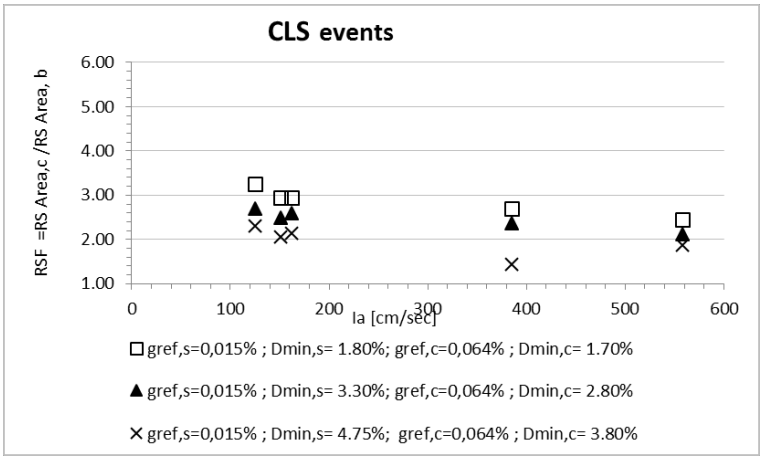

Figure 5.37 Amplification response in term of the spectral acceleration for the CLS events: analysis with the mean G/G0 curve and different functions for D.

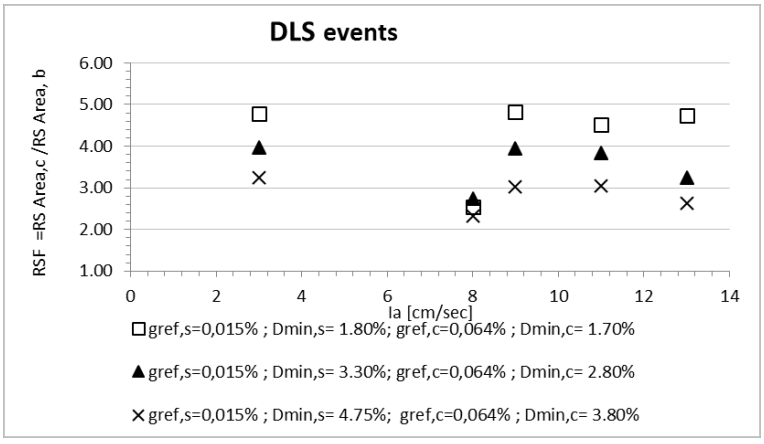

Figure 5.38 Amplification response in term of the spectral acceleration for the DLS events: analysis with the mean G/G0 curve and different functions for D.

The following figures plot the results about the amplification of the peak horizontal acceleration, for the CLS and DLS events. Figures 5.39 and 5.40 show the results for the analyses performed using the same damping ratio function associated with different G-γ decay curves.

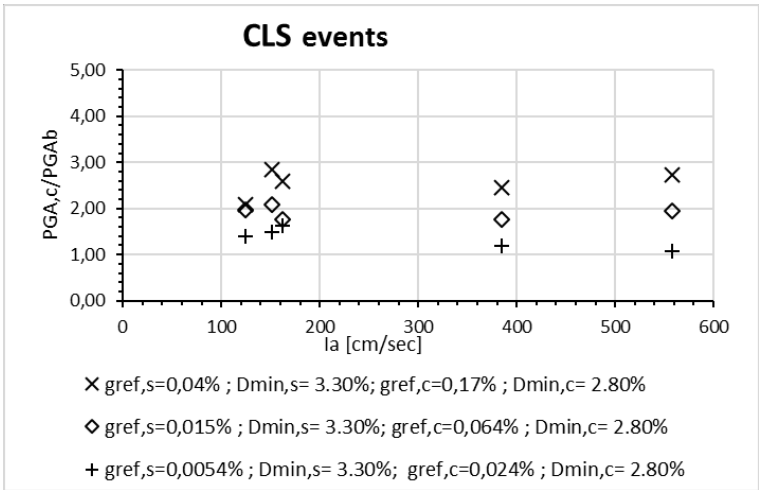

Figure 5.39 Amplification response in term of the peak horizontal acceleration for the CLS events: analysis with the mean function for D and different G/G0 curves.

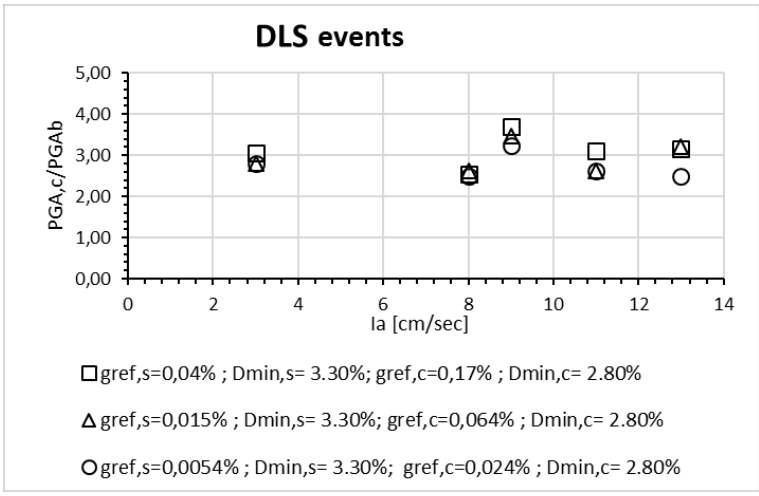

Figure 5.40 Amplification response in term of the peak horizontal acceleration for the DLS events: analysis with the mean function for D and different G/G0 curves.

Figures 5.41 and 5.42 show the results for the analyses performed using the same G-γ decay curves associated with different damping ratio functions.

6

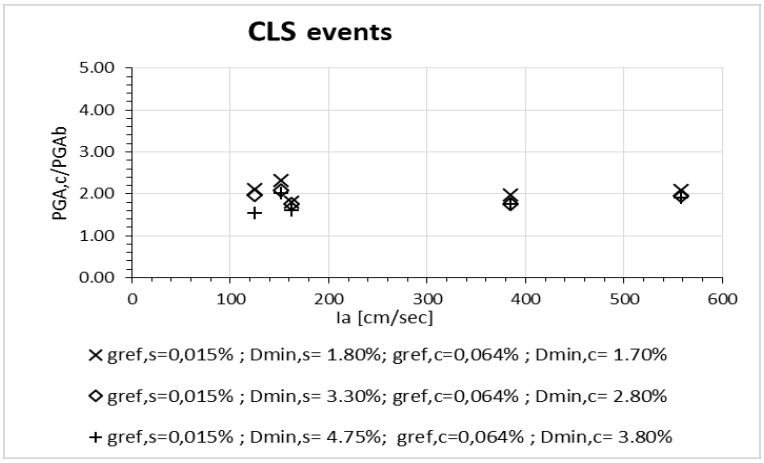

Figure 5.41 Amplification response in term of the peak horizontal acceleration for the CLS events: analysis with the mean G/G0 curve and different functions for D.

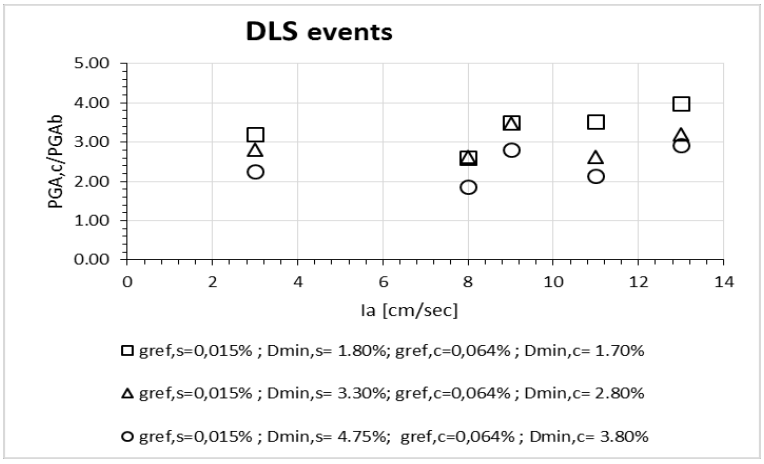

Figure 5.42 Amplification response in term of the peak horizontal acceleration for the DLS events: analysis with the mean G/G0 curve and different functions for D.

Observing the previous pictures, it may be observed that the damping ratio function plays a strong influence on the amplification response for weaker seismic events (DLS events). It should be especially noted when the results are in term of spectral acceleration (Figure 5.38). According to the variation of the damping ratio curve, the seismic response shows an amplification which varies from 2.5 up to 5 times in almost all the seismic events. Similar results are obtained in term of the amplification of the peak horizontal acceleration. In this case the influence is weaker with respect to the results for the spectral amplification.

In case of stronger events, it should be noted that the results are slightly affected by the variation of the damping ratio function (Figure 5.37). Moreover, when the seismic response is expressed in term of the peak acceleration amplification, the influence seems to be even negligible. In the latter case, the mean damping ratio function seems to be representative of the damping soil behavior.

The variability of the G/G_0 curve seems to be a slighter influencer than the damping in both weaker and stronger events.

Observing in the case of DLS events, it should be noted that the sensitivity of the response to the variation of G-γ decay curves appears very slight or negligible (Figure 5.36 and 5.40). For CLS events, the response seems to be slightly more sensitive to the variation of the G/G_0 curve but even in this case the mean function should be representative of the stiffness degradation related to the shear strain of the soils. The results are shown in term of spectral amplification (Figure 5.35) and peak horizontal acceleration amplification (Figure 5.39).

5.2.3. Effect of earthquake input intensity

It is well known that the dynamic behaviour of an earth construction is influenced by the characteristic of the input motion intensity due to its peak horizontal acceleration, its frequency content and the duration of the event.

In order to consider the effect of different input on the seismic response of earth dam, the amplification ratio between the crest and the basement in term of spectral response and peak accelerations have been compared with the Arias Intensity (Eq. 5.4) of each earthquake.

From previous analysis, results are thus summarised to study the effect of different ground motion intensities.

Figures 5.43, 5.44, 5.45 and 5.46 plot the seismic response for both CLS and DLS events, whose intensity is expressed in function of Arias Intensity, I_a. The solid dots represent the stronger events (CLS), whereas the empty dots the weaker earthquakes (DLS).

In Figures 5.43 and 5.44 the response is expressed as the ratio between the integral of the spectral response at the crest and the basement. In the first picture, the analyses with the mean damping ratio curve associated with different G/G_0 functions are shown. In Figure 5.44, the analyses with the mean G/G_0 function associated with different damping ratio functions are shown.

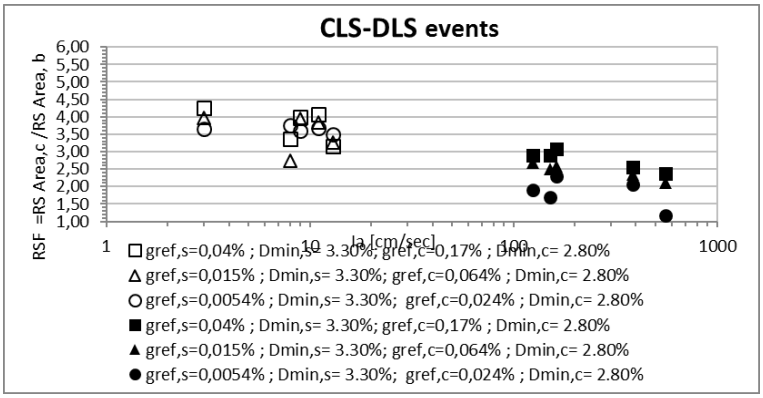

Figure 5.43 Amplification response in term of the spectral acceleration for the DLS and CLS events: analysis with the mean D curve and different functions for G/G0.

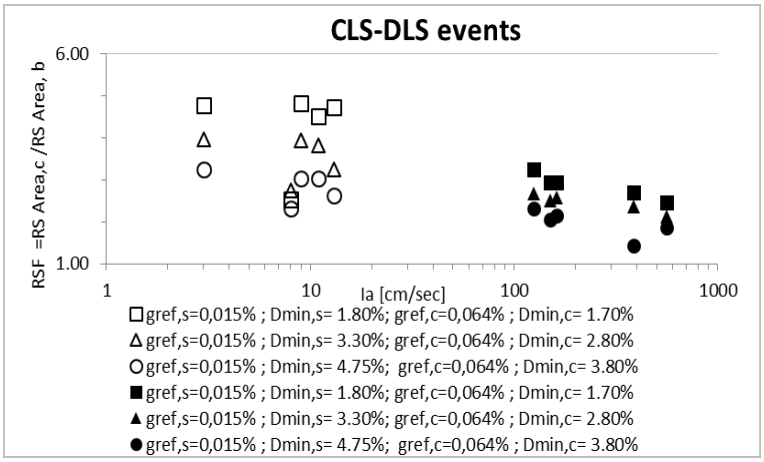

Figure 5.44 Amplification response in term of the spectral acceleration for the DLS and CLS events: analysis with the mean G/G0 curve and different functions for D.

In Figures 5.45 and 5.46 the response is expressed as the amplification of the peak horizontal acceleration. In the first picture, the analyses with the mean damping ratio function associated with different G/G_0 curves are shown. In Figure 5.46, the analyses with the mean G/G_0 function associated with different damping ratio curves are shown.

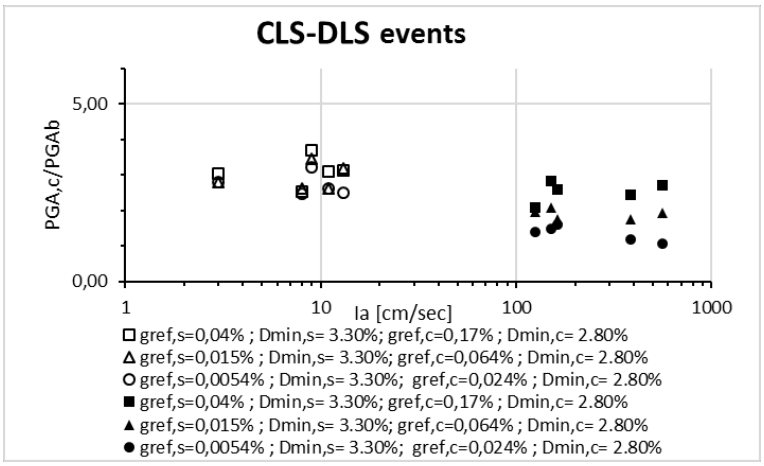

Figure 5.45 Amplification response in term of the peak horizontal acceleration for the DLS and CLS events: analysis with the mean D curve and different functions for G/G0.

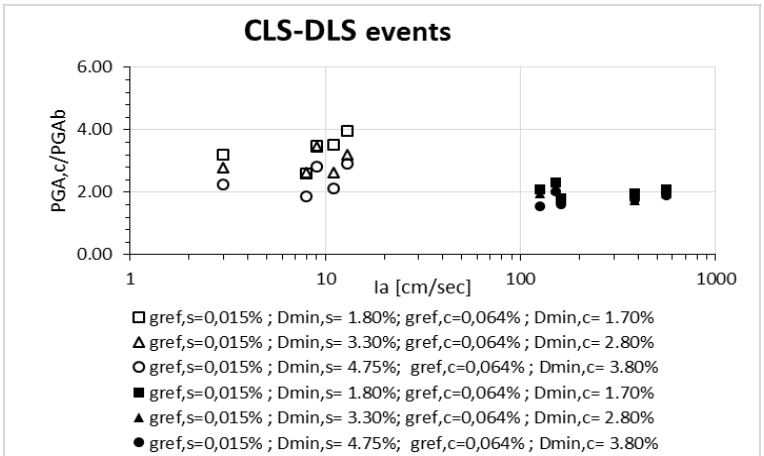

Figure 5.46 Amplification response in term of the peak horizontal acceleration for the DLS and CLS events: analysis with the mean G/G0 curve and different functions for D.

All the results show higher amplification for weaker than stronger events.

The Spectral Acceleration amplification show a range from 2.74 to 4.25, and from 2.31 to 4.82 for the DLS events (Fig. 5.43 and 5.44). For the CLS events, the amplification range varies from 1.16 to 3.09 (Fig. 5.43) and from 1.44 to 3.25 (Fig. 5.44).

Similar results are obtained for the response in term of peak acceleration amplification. Even in this case, DLS results show higher amplification than the CLS. Figures 5.45 and 5.46 show amplification range respectively from 1,86 to 3,97, and from 2.48 to 3,69 for the DLS events. For the CLS, the amplification range varies from 1,55 to 2.31 (Fig. 5.45) and from 1.07 to 1.83 (Fig. 5.46).

For the DLS accelerograms, the seismic signal undergoes a strong amplification trend. For CLS accelerograms, the dynamic signal undergoes very slight amplification of the spectral acceleration or peak acceleration amplitude, propagating from the basement to the top of the dam. This observation agrees with the remark on the peak accelerations on soft soil sites (Idriss, 1990). From low to moderate acceleration levels (less than about 0,4g), peak accelerations at soft sites are likely to be greater than on rock sites. At higher acceleration level, the low stiffness and nonlinearity of soft soils induce an attenuation on the amplification of the motion.

Such difference can be attributed to the higher shear strains induces by the stronger earthquakes, which produce higher energy dissipation. Figures 5.47 and

5.48 show the permanent settlements observed for the different earthquakes. The permanent vertical displacements are plotted in function of the Arias Intensity I_a of each record.

As expected, larger displacements are obtained for earthquake with higher intensity. Moreover, observing the latter figures, it should be noted that the permanent vertical displacements can be neglected for events with an I_a less than 100 cm/sec.

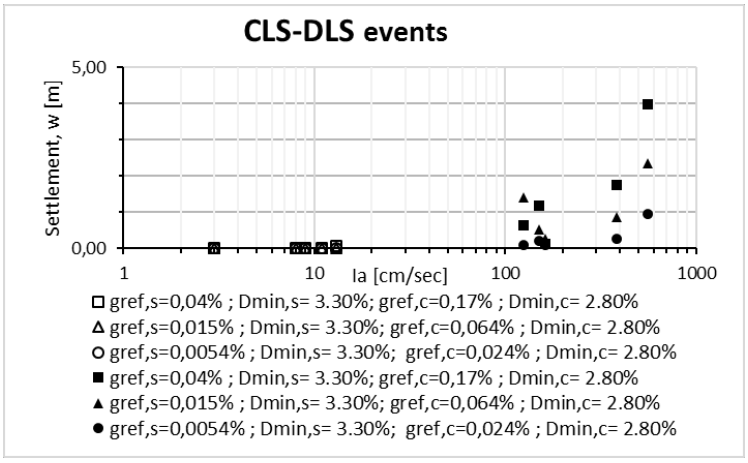

Figure 5.47 Vertical displacement at crest for DLS and CLS events: analysis with the mean D curve and different functions for G/G0

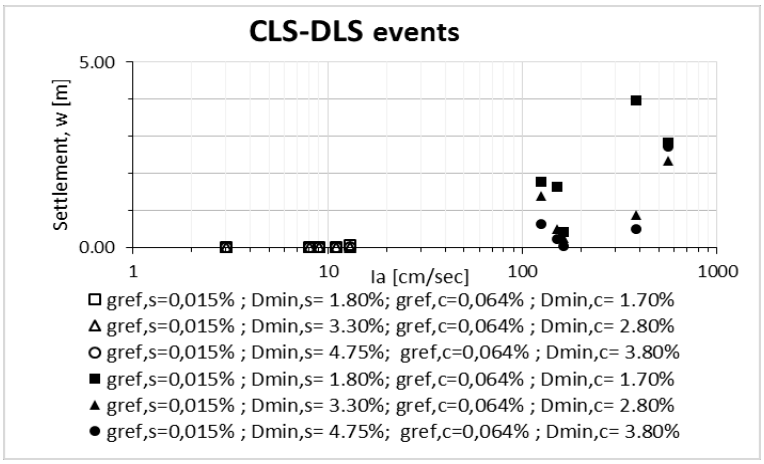

Figure 5.48 Vertical displacement at crest for DLS and CLS events: analysis with the mean G/G0 curve and different functions for D.

According to the study by Lanzo et Al. (1015), the Arias Intensity I_a may be considered an important parameter to guide the selection of the input motions, due to its strong influence on the seismic response of the earth dam.

5.2.4. Effect of dam geometry

Two different dam cross sections were studied to evaluate the effect of the core configuration on the seismic response of earth dams. Two 60m high models with vertical (VCD) and inclined (ICD) clay core with the same volume were performed.

The study evaluates the influence of two layouts, maintaining the same slope of the shells, the basement size and crest width (See Par 5.1.2.1).

In order to evaluate the behavior of both dams during earthquake, nonlinear dynamic analyses with the same mesh are carried out. For the model configuration see Paragraph 5.1.4.1.

The static analysis was performed for the 60m high vertical core dam model and the inclined dam model. The dynamic analyses were performed using the cyclic nonlinear approach where the hyperbolic backbone curve (Eq. 4.6) is defined by the shear modulus G_{max} and the shear strength properties (see Tab. 5.7 for the shell and Tab. 5.11 for the core). In this case, the mean function of the shear modulus G_{max} was performed. The dependency of the mean function of shear modulus G_{max} on confining pressure is defined at Table 5.8 for the shell and Table 5.12 for the core.

The analysis was performed considering the stronger earthquakes selected for the CLS (See 5.1.3).

The seismic response was performed in term of vertical settlements on crest and differential settlements between the core and the shell.

The behavior of the two dams (ICD and VCD) were compared (Figure 5.49).

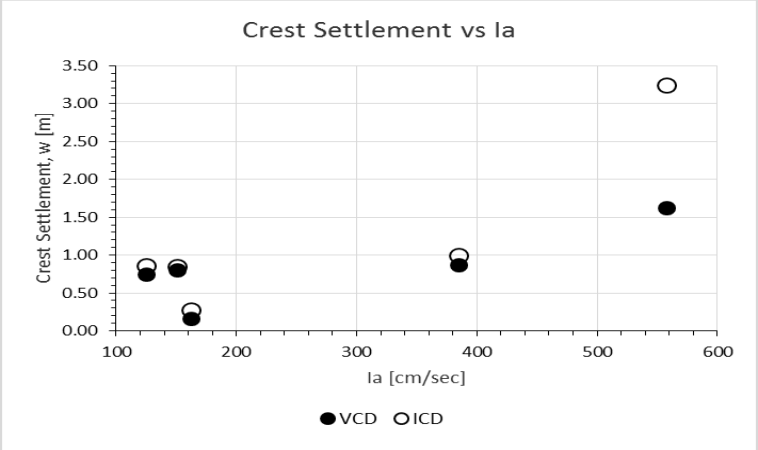

Figure 5.49 Vertical displacements after CLS earthquakes for the VCD and ICD

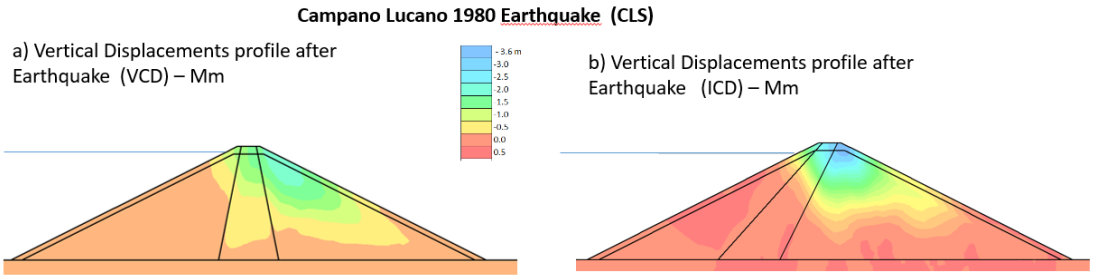

Figure 5.50 Contour of permanent vertical displacements at crest for the VCD (a) and ICD (b) for the strong Campano-Lucano 1980 earthquake

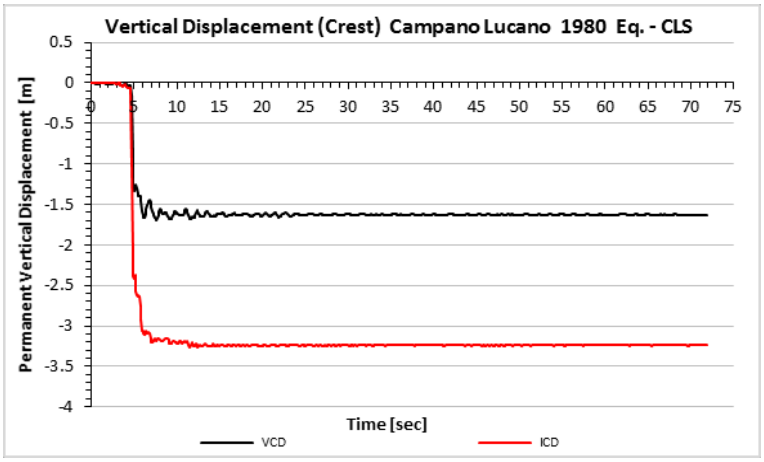

Figure 5.51 Vertical crest displacement histories for the ICD and VCD for the strongest earthquake (Campano-Lucano 1980)

It should be noted that the performance of the dam doesn't seem to be affected by the core configuration, except for the stronger seismic event.

Table 5.16 makes a summary of the crest settlements observed in the two layouts.

Dam Height= 60m		**VCD**	**ICD**
Earthquake	I_{max} [cm/sec]	Crest Settlement, w [m]	Crest Settlement, w [m]
Friuli '76	125	0.75	0.86
Montenegro '79	385	0.87	0.99
Campano Lucano '80	558	1.63	3.24
Duzce 1 '99	162	0.16	0.27
Bingol '03	151	0.80	0.85

Table 5.16 Table with the summary of the crest settlements for the VCD and ICD for CLS earthquakes

For brevity, a sample of results calculated for the strongest Campano-Lucano earthquake is reported in Figure 5.50, where are plotted vertical displacement shaded areas.

Figure 5.51 shows the calculated vertical displacements at the crest for both the ICD and VCD models during the Campano Lucano motion. It may be observed that the magnitude of the calculated settlement for the ICD is double to the value for the VCD.

Figures 5.50a and 5.50b show that the maximum settlement occurs in the downstream side of the crest in the inclined core dam; whereas in the vertical core dam, the maximum settlement is in the downstream shell.

It may be observed that vertical displacement on the crest is affected by the core configuration the very strong event with the highest Arias Intensity I*a* value (about 550 cm/sec) and higher significant duration $D_{5\text{-}95}$.

It should be noted that the higher crest settlement is obtained for the earthquake which has a fundamental period of about 0.4 sec. The first fundamental frequency of the embankment has been calculated with the Gazetas and Dakulas (1992) formulation (5.4a):

$$T_1 = 2.57 \frac{H}{\overline{Vs}} \qquad (5.4a)$$

Where H is the height and $\overline{Vs}$ is the mean shear wave velocity into the dam embankment. The calculated first fundamental period of the model is equal to 0.38sec. This is very close to the fundamental period of the Campano Lucano earthquake, and hence the higher amplification is due to the resonance effect.

According to the diagram which correlate the crest settlement ratio with the relative degree of damage (Swaisgood, 2003), the performance level of the dam seems to vary from moderate to serious.

The Campano Lucano earthquake produce a serious damage with a crest settlement ratio of 2.7% for the VCD model and about 5% for the ICD.

Differential settlements between the core and the shell may induce cracks and damages inside the embankment.

In order to observe the interaction between the core and the shell and evaluate the correlation with the level of damage, the results about differential settlements

are shown on Figure 5.53. Differential settlement represents the relative displacement between the crest and a specific point in the downstream rockfill (Figure 5.52)

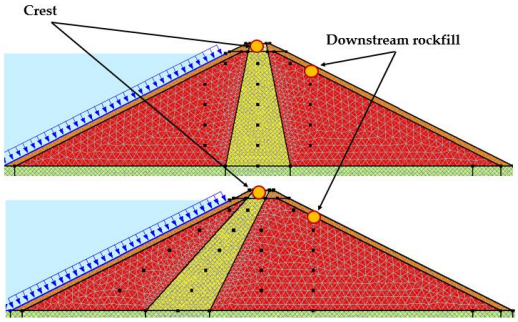

Figure 5.52: Sketch of the dam showing the locations of the monitoring points for the ICD and the VCD

Figure 5.53 plots the relative displacements between the core and the shell with the crest settlement ratio, which represent the ratio between the crest settlement and dam height. The crest settlement ratio may be the representative parameter of the seismic performance of the dam. According to Swaisgood (2003) and Sica and Pagano (2009), the permanent settlement of 1% at dam crest can be adopted as a plausible limit threshold to assess dam performance.

The Figure 5.53 shows the correlation between the differential settlement and the relative degree of damage. It may be noted that a relative displacement higher than 25 cm can be the cause of a serious degree of damage for the 60m high embankments. As expected, the maximum level of damage occurs for the strongest earthquake.

During the Campano Lucano event the differential settlement between the core and the shell achieves the highest value of 1,4 m. In this case a collapse mechanism may occur. For the confining action of water on the upstream face, displacements are all oriented in downstream direction. The contour of the permanent vertical displacements shows that significant settlements are confined in the downstream shell, but they may also affect part of the core compromising the water tightness of the embankment (Figure 5.50a and b).

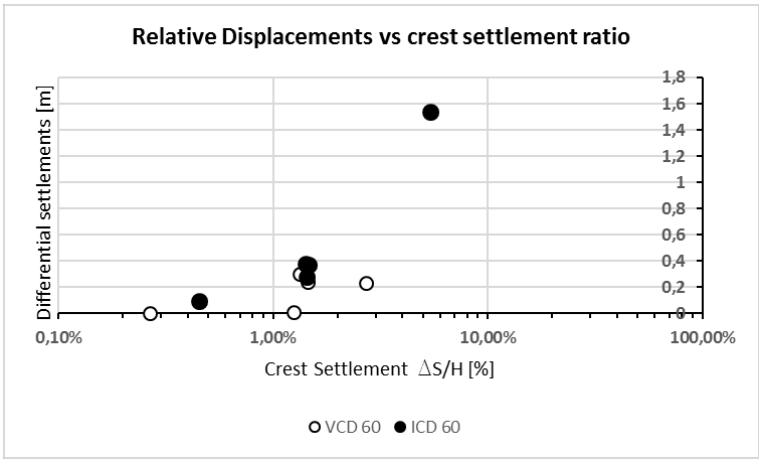

Figure 5.53: Differential settlements vs crest settlements ratio for ICD and VCD under CLS events

Figure 5.54 compared the calculated settlements at the crest of the dam with the shell. Figure shows a correlation between those results. It may be assessed that the vertical displacement at shell tends to increase with the vertical displacements at crest.

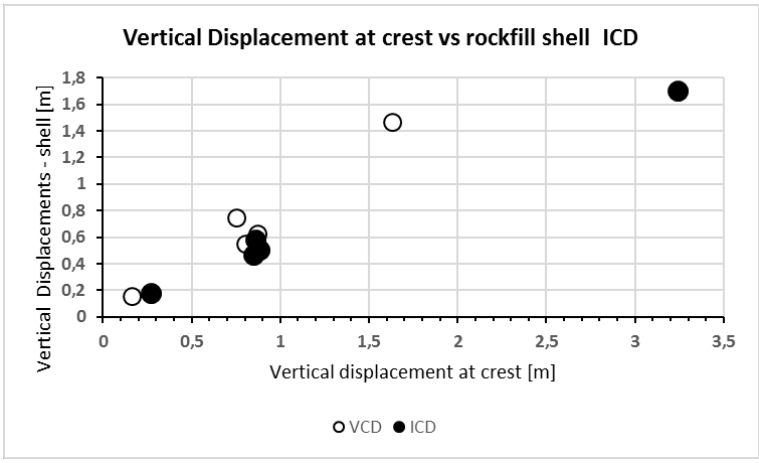

Figure 5.54 Comparison between the vertical settlements on the downstream shell and the crest for ICD and VCD models under CLS events

In order to evaluate the influence of earthquake polarity on asymmetric configuration, the analyses were repeated under the reversed acceleration time histories. Each positive acceleration peaks were reversed to the negative and vice-versa.

Figure 5.55 shows vertical settlements at crest against the Arias Intensity for each reversed record. The calculated displacements are summarised in Table 5.17 for the VCD and ICD models.

I may be observed a change on the seismic response of the dams. The seismic response of a dam may be affected by the polarity of an earthquake. The direction

of the motion may probably influence the response in term of displacements due to an asymmetrical configuration of the embankment and its stress distribution. Similar result can be observed even in the central vertical core configuration due to its asymmetric boundary conditions.

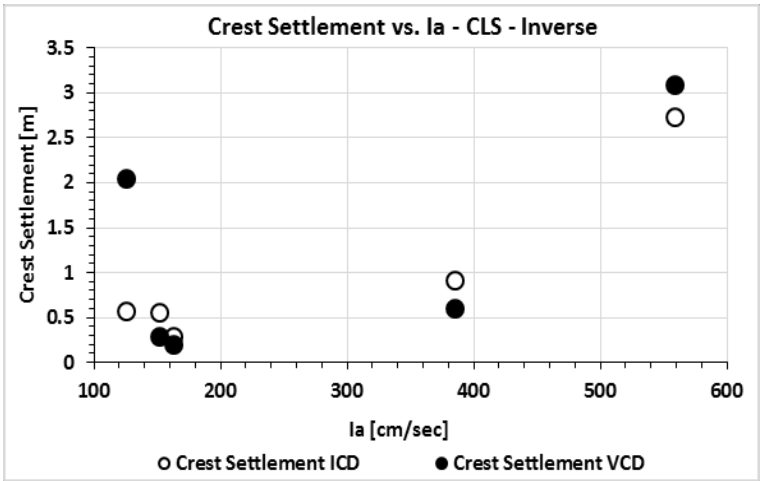

Figure 5.55 Vertical displacements after CLS reversed earthquakes for the VCD and ICD

Dam Height= 60m		**VCD**	**ICD**
Reversed Earthquake	Ia_x [cm/sec]	Crest Settlement, w [m]	Crest Settlement, w [m]
Friuli '76	125	2.05	0.58
Montenegro '79	385	0.60	0.92
Campano Lucano '80	558	3.09	2.74
Duzce 1 '99	162	0.21	0.30
Bingol '03	151	0.29	0.56

Table 5.17 Table with the summary of the crest settlements for the VCD and ICD for inverse CLS earthquakes

The analysis shows that the core layout doesn't affect the performance of a dam in term of vertical settlement on crest during an earthquake.

It may be observed that vertical displacement on the crest is effectively higher in the ICD than in the VCD for a very strong event with an Arias Intensity I_a of more than 550 cm/sec. Moreover, running the analysis with reversed events, the results demonstrate a certain dependency of the seismic response of a dam to the polarity of the input motion.

5.2.5. Combined effect of vertical and horizontal components of the seismic input

In this section, the combined effect of the vertical and horizontal components of motion were studied (see Par. 5.1.3).

The analyses were performed with horizontal and vertical components of motion for CLS events. The dynamic analyses for the 30m high and 60m high vertical core dam sections were performed. The rocky foundation underlies the embankment.

The dynamic analyses were performed using the cyclic non-linear approach where the hyperbolic backbone curve (Eq. 4.6) was defined by the shear modulus G_{max} and the shear strength properties (see Tab. 5.7 for the shell and Tab. 5.11 for the core). In this case, the mean function of the shear modulus G_{max} was performed. The small-strain shear modulus G_0 was assumed to vary with confining stresses, according to the collected data for the rockfill and the impervious soil (see Par. 5.1.5.2 and 5.1.5.3). In this case, the "mean" function was used (see Figures 5.14 and 5.17, and Table 5.8 and 5.12).

As previously discussed, two set of analyses were carried out. In the first set of analyses, only the horizontal components of motion were performed. In the second set, the same suite of records with the appropriate vertical components of motion was applied.

The vertical settlement of the dam crest w and the peak acceleration amplification (PGA,c/PGA,b) were considered as indicative parameters of the general response of the dam under different seismic motions. The response has been compared with the Arias Intensity of each earthquake, for the 30m and 60m high dam sections.

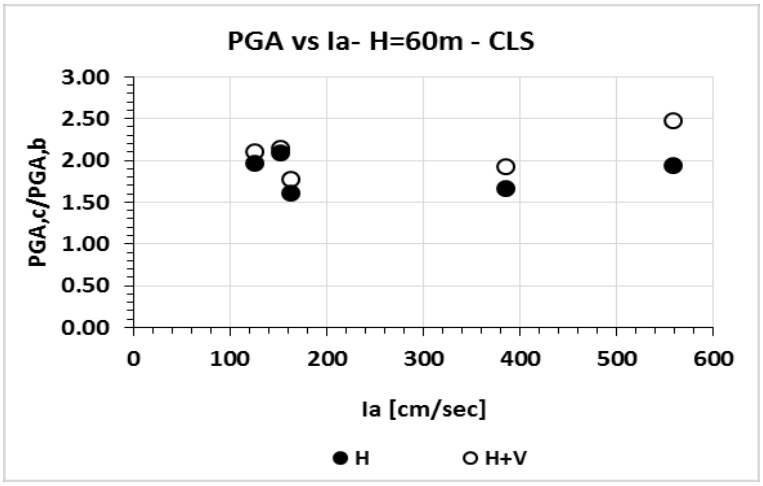

Figure 5.56 Peak acceleration amplification crest/basement vs Ia for CLS on 60m high dam.

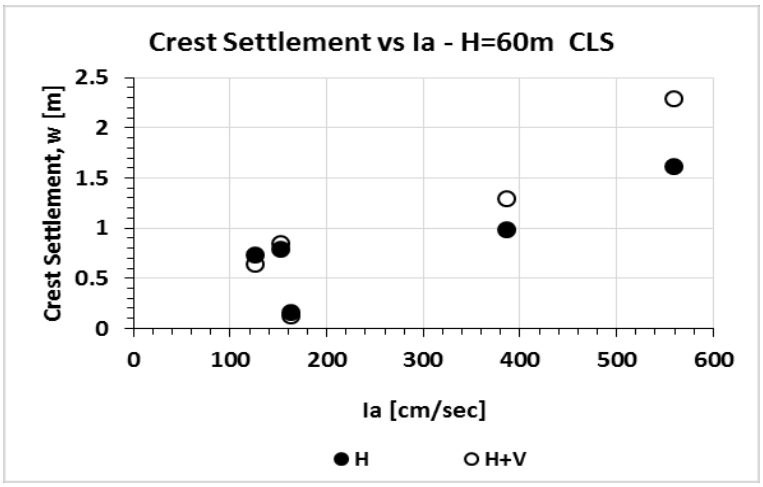

Figure 5.57 Vertical displacement at crest vs Ia for CLS on 60m high dam.

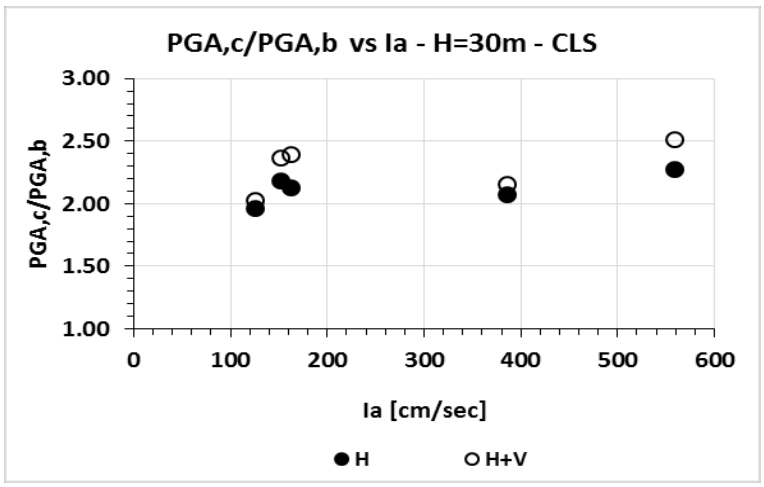

Figure 5.58 Peak acceleration amplification crest/basement vs Ia for CLS on 30m high dam.

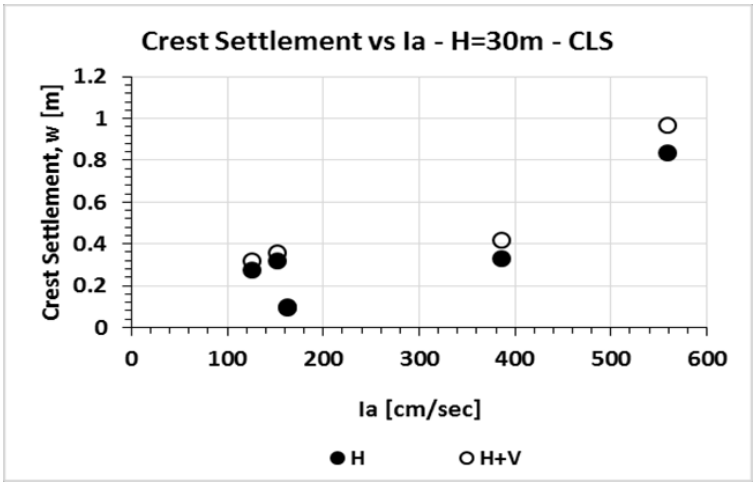

Figure 5.59 Vertical displacement at crest vs Ia for CLS on 30m high dam.

Observing the results about the amplification of the peak acceleration between the crest and the basement, no significant effects were observed. In Figures 5.56 and 5.58 are plotted the results for the 60m and 30m high dam sections. The response in term of amplification does not seem to be sensitive to the vertical component of the input motion even at higher earthquakes.

Observing the results in term of vertical settlement at dam crest, it may be noted a slight difference in the dam performance. The seismic response appears sensitive to the vertical component of motions, especially for stronger earthquakes.

The maximum influence can be observed for the stronger input motion, with an Arias Intensity of I_a=558 cm/sec. Especially for the 60m high earth dam (Figure 5.57), it can be observed an increase of the vertical crest settlement of a 50%. Such effects are less pronounced for the 30m high dam model (Figure 5.59).

However, the seismic performance of the dam for the CLS doesn't seem to be influenced by the vertical component of motion.

It is worth to note that the relative degree of damage, expressed as the "settlement ratio" (S/H= vertical settlement/dam height), does not seem to be influenced by the vertical component of motion.

Figure 5.60 shows that the relative degree of damage is not sensitive to the computation of the vertical component of motion. In particular, the 30m high dam reflects this behavior even for the stronger earthquakes.

The 60m high dam subjected to the strongest event with an I_a of 558cm/sec shows the maximum settlement ratio. The analysis with the vertical component of motion exhibits a value of about 3,8%, whereas the value of 2.7% is obtained for the computation with only the horizontal component. According to the Figure 3.22, a "serious" damage for the dam is expected in both cases.

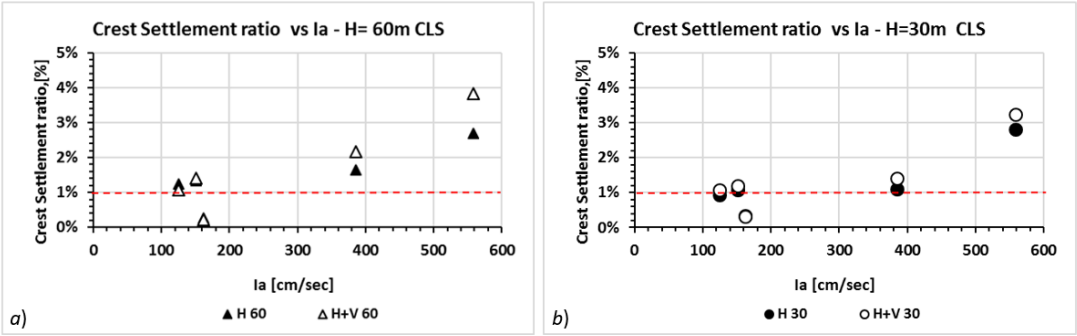

Figure 5.60: Crest settlement ratio vs Ia for 60m (a) and 30m (b) high dams, under CLS events

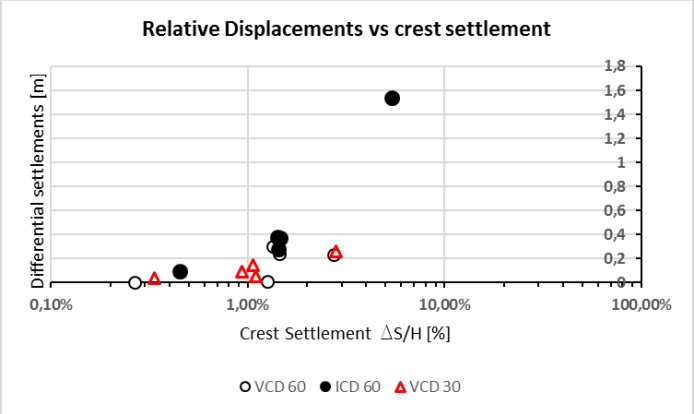

Figure 5.61: Differential settlement vs Crest settlement ratio for 60m and 30m high dams, under CLS events

Figure 5.60 outlines that the degree of damage is not influenced by the computation of the vertical component of motion which doesn't affect the seismic performance of the dam. Moreover, it can be assessed that its computation could be ignored for seismic events with Arias Intensity lower than 200 cm/sec.

Figure 5.61 plots the differential settlements of 30m high dams with the response of higher embankments observed in the previous paragraph. The results are obtained considering the only horizontal component of motion, since the vertical component is not influent on the performance of the dam. As expected, a serious degree of damage can be achieved when lower value of differential settlements for 30m high dams occur, comparing to those obtained for 60m high dams under CLS events. Lanzo et Al. (2015) studied the seismic response of Montedoglio zoned dam, a 64m high embankment located in the center of Italy.

A suite composed of eighteen records was selected as seismic input. Two sets of analyses were carried out. One set was computed with the horizontal component of ground motion. In the second set, the horizontal motion was computed with the corresponding vertical component. The seismic response of the dam was analyzed in terms of permanent settlements at crest. The authors commented that the inclusion of the vertical components led to a general increase of about 75% of the computed crest settlement. It should be noted that results were performed for a limited range of earthquake intensity (see Figure 5.62).

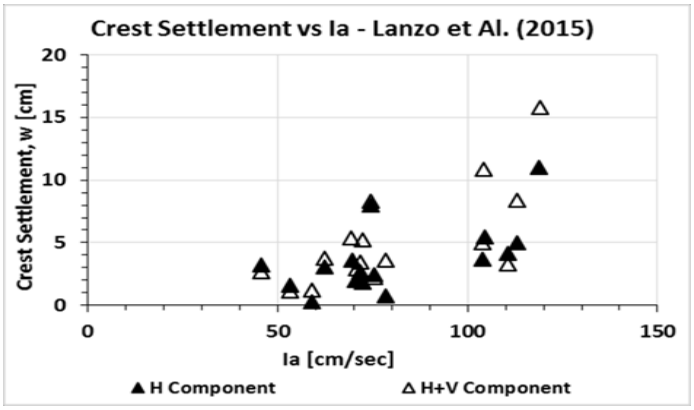

Figure 5.62 Crest permanent settlement vs Ia (Lanzo et Al., 2015)

Observing Figure 5.62, it can be assessed that not all results show an increase of the crest settlement with the application of the vertical components. Moreover, the study doesn't compute the response for higher levels of seismic excitation. The analyses were computed under seismic events with I_a lower than 130 cm/sec. However, it can be noted that their results seem to agree with the observation of the present study. The crest settlement doesn't seem to be sensitive to the vertical component of motion when the seismic excitation have an Arias Intensity lower than 200 cm/sec. It should be noted that the vertical component of motion can be negligible for weak/moderate earthquakes.

Generally, it can be assessed that the usual practice of ignoring the vertical component of motion may be considered reliable of the seismic behavior of earth dam, even for the case of higher embankments. However, in case of higher intensity earthquakes, it can be assessed that the vertical component of motion when analyzing the seismic performance of dams should be reconsidered; also bearing in mind that analysis could be conducted with more sophisticated analyses.

Chapter 6

CONCLUSION

6.1. Final remarks

As described at the beginning of the thesis, the main aim of this research was the definition of a methodology for the evaluation of seismic safety degree of the Italian existing earth zoned dams.

According to the definition of the methodology for assessing the behavior of existing earth dams, the following sequence of steps has been adopted:

- Evaluation of performance objectives;
- Definition of the seismic input, according to the recent Italian regulations (M.LL.PP., 2008, M.LL.PP., 2014);
- Definition of the geometrical model of the dam and foundation, and the specific constitutive model of the soil;
- Evaluation of the seismic response by means of the interpretation of the numerical results.

The aforementioned steps were applied for the evaluation of the seismic response of hypothetical strategic earth core rockfill dams, located in the south of Italy, where the seismicity of the territory is high. The dam response was studied considering the amplification of the acceleration and the spectra acceleration between the basement and the crest, observing the permanent settlements at crest and the differential settlement between the core and the shell.

According to the limit states by recent regulations (M.LL.PP., 2008, M.LL.PP., 2014) and literature criteria, dam performance was assessed. The permanent vertical settlement at crest can be considered as a representative and effective indicator of dam performance. Moreover, in order to measure the effect of differential settlement which can produce fractures between the core and the

shell, the correlation between the relative displacement and the settlement ratio was observed.

Thus, permanent settlements at crest and differential settlements can be correlated to the structure performance and can represent suitable indicators of dam mechanical response under different seismic scenarios.

In order to quantify the safety degree of existing dam, threshold values provided by the literature and based on the seismic behavior of existing earth structure were proposed.

The seismic inputs have been selected according to the standardized procedure assessed by current regulations (M.LL.PP. 2008 and M.LL.PP.2014).

Although advanced constitutive models allow considerable flexibility and generality in modeling the response of soils under cyclic loading, their description usually requires many more parameters than the equivalent linear model or the cyclic nonlinear model, adopted in this study. The constitutive model for the materials was defined considering the right balance between the accuracy of the response and the reliability of parameters. However, the comparison of the results between predicted and experimental analyses demonstrates that the compromise can be accepted.

In order to improve the current knowledges on the dam seismic behavior, this study has also investigated the role of different factors and scenarios affecting the dynamic response.

Hydrodynamic effects were studied comparing the numerical results obtained by two sets of analyses. One set was performed considering the dynamic pressures induced by the reservoir on the upstream face of the dam. The results were compared with the outcomes obtained without considering hydrodynamic loads.

Those analyses were performed to reproduce the seismic behavior of an ECRD model under dynamic motion in a centrifuge test. The model simulated a 5,2m high prototype and the test was carried out preventing the seepage into the embankment by means of placing a glue membrane on the upstream slope. Results demonstrated that the hydrodynamic effect can be safety ignored, according to the statements observed in the literature for earth dams.

Material and geometric influential factors with the effects of different seismic scenarios were separately considered, performing a series of two dimensional numerical analyses.

Therefore, comments were made regarding the influence of such parameters and their application on the evaluation of the seismic response of earth dams.

The parametric analysis showed the following results:

- Various scenarios with different impedance of the embankment were evaluated for studying the effect of stiffening characteristic of dam materials. The response was expressed as amplification of the spectral response between the basement and the core and as amplification of the maximum acceleration. Analyses were repeated for different input motions and combined effects of soil properties. Results demonstrate an apparent influence on the impedance ratio from the embankment and the foundation. Altogether, for the CLS and DLS events, the amplification of the motion seems to decrease with the increase of the impedance ratio. However, looking at every single earthquake, it should note that the overall trend doesn't seem to be confirmed. In this case, it could not be confirmed a general trend; thus, the dam behavior in term of amplification of the acceleration and spectral acceleration doesn't seem to reflect a correlation with the impedance ratio. However, this conclusion may be weakened by the limited range of the impedance ratio defined for the specific case studies. The observed range varies between 6,5 and 10 of impedance values (I) and this restriction doesn't seem to represent a reasonable field of values which can demonstrate some clear tendency.
- Different configurations of dynamic soil properties were studied to evaluate the effects of using an accurate description of the shear modulus G decay and the increasing of the damping ratio functions, in equivalent linear analyses. Results were showed in term of spectral amplification and peak horizontal acceleration. It may be assessed that the damping function plays a strong influence on the amplification response during weaker events (DLS). The influence can be observed when results are expressed in term of amplification of spectral acceleration and peak acceleration between the basement and the crest of the dam. During stronger events (CLS), the results are not sensitive to the use of different increasing

damping ratio functions. In the latter cases, the use of the mean damping ratio as representative of the average behavior of soil seems to be reliable.

Moreover, the variability of the G/G_0 curve seems to have a slighter influence than the damping ratio in both weak and strong events.

Especially for the case of DLS events, the sensitivity of the response to the decay curve of shear modulus G appears very slight or negligible. For stronger events, the response seems to be slightly more sensitive to the G/G_0 but also in this case a mean function could be representative of the stiffness variation with shear strain of the soils.

- The effect of the earthquake magnitude on the seismic response of Italian earth dams was studied comparing the numerical results from different seismic motion intensities. For the DLS accelerograms, it can be assessed that the seismic signal undergoes a strong amplification trend. For CLS accelerograms, the dynamic signal, propagating from the basement to the top of the dam, undergoes very slight amplification of the spectral acceleration or peak acceleration amplitude. Such difference can be attributed to the higher shear strains induced by the stronger earthquakes which produce higher energy dissipation. As expected, larger displacements are obtained for earthquake with higher intensity. In particular, results seem to show that the permanent vertical displacements measured at crest and obtained for events with an I_a lower than 100 cm/sec are rather small.

  According to the observation from the study by Lanzo et Al. (1015), the Arias Intensity I_a may be considered as an important parameter to guide the selection of the input motions, due to the strong influence of the parameter on the seismic response of the earth dam.

- The analyses of two different configurations were studied to understand the effects of the geometry on the seismic response of earth dam. The seismic behavior of a vertical core dam (VCD) and inclined core dam (ICD) with the same volume were compared. During CLS events, the numerical analysis shows that the inclined core configuration doesn't have a strong influence on the vertical settlement at crest.

The analysis demonstrates that the ICD represents a very disadvantageous configuration for only the Campano Lucano earthquake. The Campano Lucano earthquake is a very strong motion with an Arias Intensity I_a of more than 550 cm/sec. During this event, the observed vertical displacement on crest is effectively higher in the ICD than in the VCD. It may be observed that the magnitude of the calculated settlement for the ICD is double to the value for the VCD. It may be observed that vertical displacement on the crest is affected by the core configuration for the very strong event. It should be noted that the higher crest settlement is detected for the earthquake with the similar fundamental period as the 60m high earth dam. Observing the interaction between the core and the shell, differential settlements with the settlement ratio (S/H) were studied and the correlation with the level of damage was evaluated. Results demonstrate that relative displacements higher than 25cm may produce a serious degree of damage in both embankment configurations. Moreover, repeating the numerical analysis for reversed strong motion, it may be demonstrated a certain dependence of the response from the polarity of the input motion.

- The effect of adding the vertical component of motion doesn't seem to have a strong influence on the numerical response of earth dams. Results show that the vertical component of motion doesn't seem to affect the dam behavior and the application of this component together with the horizontal one could be ignored for input motion with Ia<200cm/sec. Generally, it can be assessed that the usual practice of ignoring the vertical component of motion may be considered reliable of the seismic behavior of earth dam, even in case of high embankments. Results show that the relative degree of damage is about the same expected from analyses computed with or without the vertical component of motion. However, in case of high intensity earthquakes, it can be assessed that the vertical component of motion should be reconsidered when analyzing the seismic performance of dams, also bearing in mind that numerical investigation could be conducted with more sophisticated analyses.

6.2. Recommendations for further researches

The previous section summarizes the fundamental findings of this research. During this study, some limitations have been identified. These observations represent the suggestions for further investigations and analyses, in order to extend and perhaps complement the current study. One issue which needs further developments is represented by the adopted constitutive model for the stress-strain response of the rockfill and the impervious soil of the core.

The approach adopted in the analysis was not able to reproduce a faithful response of soils under cyclic loading of variable amplitudes. For instance, the adopted model was not able to treat the soil as a two-phase material with fully coupled soil skeleton response and excess pore water pressure development. Inelastic soil behavior under cyclic loading can be properly described through elastic–plastic constitutive models developed within the framework of bounding surface plasticity, kinematic hardening plasticity or generalized plasticity.

The evaluation of the development of excess pore water pressure is fundamental when liquefaction phenomenon may occur in presence of layers of loose saturated sand into the embankment. However, it should be underlined that advanced constitutive models required many parameters. Their calibration requires to define ad-hoc laboratory test for the estimation of a large number of suitable and available parameters. Moreover, the increase of their complexity requires an increase of computational efforts which need longer time of analyses.

A more complete definition of the dynamic reservoir-dam interaction (RDI) is another key factor which should be considered in the analysis, since the RDI can change the fundamental period of the dam and the amplification of the acceleration within the structure. Moreover, further investigations should be performed to study the presence of an impermeable barrier under the core on the seismic response of earth dam. In Italy, most times rockfill dams are placed on an alluvial soil along the bed river. In those cases, earth zoned dam can have an impermeable barrier in the foundation soil to the bedrock which can have an influence on the overall dam performance.

In this study, the hypothesis of a flat canyon shape was considered. It is evident that in case of a narrow shape canyon, some full three-dimensional analyses should be performed, to take into account of stiffening effect of dam-canyon interaction on the dam response.

References

Abrahamson, N. (1992). Non-stationary spectral matching. 63(1), 30.

Aghaei Araei, A., Razeghi, H. R., Tabatabaei, S.H., and Ghalandarzadeh, A. (2012), "Loading frequency effect on stiffness, damping and cyclic strength of modeled rockfill materials". *Soil Dynamics and Earthquake Engineering*, Elsevier, 33(1), 1-18.

Aghaei Araei, A., Razeghi, H.R., Ghalandarzadeh, A. and Hashemi Tabatabaei, S. (2012), "Effects of loading rate and initial stress state on stress-strain behavior of rock-fill materials under monotonic and cyclic loading conditions". *Scientia Iranica*, 19(5), 1220-1235.

Albano M, Numerical modeling of the seismic performance of bituminous faced rockfill dams, P.h.D. Thesis in Civil Engineering, Università Degli Studi Di Cassino E Del Lazio Meridionale, Cassino, (2013)

Albano M., Modoni G., Russo G., Croce P., (2012), Performance based seismic analysis of an existing rockfill dam, *in* "Proceeding of Second International Conference on Performance-Based Design in Earthquake Geotechnical Engineering", Taormina (Italy).

Aliberti D., Biondi G., Cascone E. (2015), Verifica allo stato limite di collasso di una diga in terra zonata, *in* Incontro Annuale dei Ricercatori di Geotecnica 2015-IARG", Cagliari [in Italian].

Ambraseys, N. N. (1960), The seismic stability of earth dams, in "Proceeding 2nd World Conf. on Earthquake Engineering", Tokyo, III, 1345-1363.

Ambraseys, N., Smit, P., Sigbjornsson, R., Suhadolc, P. and Margaris, B. (2002), Internet-Site for European Strong-Motion Data, European Commission, Research-Directorate General, Environment and Climate Programme.

Amorosi, A., Elia, G. (2008), "Analisi dinamica accoppiata della diga Marana Capacciotti". *Rivista Italiana di Geotecnica*, Patron editore, Bologna, 52 (4): 78-95 [in Italian].

Andrianopoulos K. I., Papadimitriou A. G., Bouckovalas G. D., Karamitros D. K. (2014), "Insight into the seismic response of earth dams with an emphasis on seismic coefficient estimation", *Computers and Geotechnics*, 55, 195 -210.

Arias A. (1970), "A measure of earthquake intensity", in R.J. Hansen, ed . Seismic Design for Nuclear Power Plants, MIT Press, Cambridge, Massachusettes, pp.438-483.

Aubry D., Hujeux J. C., Lassoudiere F. and Meimon Y. (1982): "A double memoty model with multiple mechanism for cyclic soil behavior", *Iternational Symposium on Numerical Models in Geomechanics*, Zurigh, 3-13

Aubry D. and Moderessi A., (1996): GEFDYN, "Manual Scientifique, Ecole Centrale Paris", http://mssmat.ecp.fr/sols/logiciels/gefdyn/notice_line/index.htm

Bardet, J.P., Ichii, k., Lin, C.H. (2000), "Equivalent linear earthquake site response analysis of layered soil deposits". Department of Civil and Environmental Engineering. University of Southern California.

Bardet J.P., Tobita T. (2001): "NERA, a Computer Program for Nonlinear Earthquake site Response Analyses of Layered Soil Deposits", University of Southern California, Department of Civil Engineering

Bazzurro P. and Cornell C. A. (1999), "Disaggregation of seismic hazard", *Bull. Seis. Soc. Am*. 89, 501-520.

Bharat S., Varshney R.S. (1995), *Engineering for embankment dams*, A.A. Balkema Publisher.

Bilotta E. and Siervo L. (2012), "Effects of asynchronous ground motion on the equivalent seismic coefficient of a slope". *Electronic Journal of Geotechnical Engineering*. Vol. 17 Bund. S., 2531-2541.

Bilotta E., and Taylor N. (2005): *Modellazione geotecnica in centrifuga*. Benevento: Hevelius Edizioni srl.

Bilotta, E., Pagano, L., & Sica, S. (2010), "Effect of ground-motion asynchronism on the equivalent acceleration of earth dams". *Soil Dynamics and Earthquake Engineering*, 30, 561-579.

Bolt, B.A. (1993). Earthquakes, W.H. Freeman, New York, 331 pp.

Bommer , J., & Acevedo, A. (2004), "The use of real earthquake accelerograms as input to dynamic analysis". *Journal of Earthquake Engineering*, 8(Special Issue 1), 43-91.

Bommer, J.J. Stafford, P.J. & Alarcon, J.E. (2009), "Empirical Equations for the Prediction of the Significant, Bracketed, and Uniform Duration of Earthquake Ground Motion". BSSA, 99,3217-3233.

Bray, J. D. and Travasarou, T. (2007), "Simplified procedure for estimating earthquake-induced deviatoric slope displacements", *Journal of Geotechnical and Geoenvironmental Engineering*, ASCE 133(4), 381-392.

Brigante, A., Sica, S. (2012), "Seismic response of a Zoned Earth Dam (Case Study)", *Electronic journal of geotechnical engineering*, Vol. 17, Bund. S., 2495-2508.

Bureau, G., Volpe, R., Roth, W., & Udaka, T. (1985), "Seismic analysis of concrete face rockfill dams. In Concrete Face Rockfill Dams", *Design, Construction and Performance, ASCE*, 479-508.

Butterfield, R. (2000). "Scale-modelling of fluid flow in geotechnical centrifuges". *Soils and Foundations* 40 (6), 39-45.

Cascone E. and Rampello S. (2003), "Decoupled seismic analysis of an earth dam", *Soil Dynamics and Earthquake Engineering* 23: 349–365.

Castro, G., R.B. Seed, T.O. Keller, and H.B. Seed (1992), "Steady-state strength analysis of Lower San Fernando Dam slide". *J. of Geot. Eng. ASCE*, 1 I8(3). 406-427.

Chopra, A. K. (1967b), "Reservoir-dam interaction during earthquakes", *Bulletin of the Seismological Society of America* 57(4), 675-687.

Chopra, A. K. (1968), "Earthquake Behavior of Reservoir-Dam Systems", *Journal of the Engineering Mechanics Division, ASCE* 94(6), 1475-1500.

Chwang, A. T. (1978), "Hydrodynamic pressures on sloping dams during earthquakes. Part 2. Exact theory", *Journal of Fluid Mechanics,* 87(2), 343-348.

Chwang, A. T. and Housner, G. W. (1978), "Hydrodynamic pressures on sloping dams during earthquakes. Part 1. Momentum method", *Journal of Fluid Mechanics*, 87(2), 335-341.

Cornell, C. A. (1968), "Engineering seismic risk analysis", *Bull. Seismol. Soc. Am.* 58, 1583–1606.

Croce, P., Pane, V., Znidarcic, D., Ko, H.Y., Olsen, H.W., Schiffmann, R.L. (1984). "Evaluation of consolidation theories by centrifuge modelling". Proc. Symp. Application of Centrifuge Modelling to Geotechnical Design, University of Manchester, Balkema, Rotterdam.

Dakoulas, P. & Hashmi, H. (1991), Response of earth dams in canyons subject to asynchronous base excitation, in "Proceeding Second International Conf. of Geotech. Earthq. Engrg. & Soil Dyn.", St. Louis, Vol. II, 1105-1112.

Dakoulas, P. and Gazetas, G. (1986). "Seismic lateral vibration of embankment dams in semi-cylindrical valleys", *Earthq. Engr. and Struct. Dyn*. No. 14, 19-40.

Dakoulas, P. and Gazetas, G. (1987), "Vibration characteristics of dams in narrow canyons", *Journal of Geotechnical Engineering* 113(8), 899-904.

Darbre, G. R. (2000), "State of practice in earthquake analysis of dams", Federal Office for Water and Geology, Safety of Dams, P.O.Box 957, CH-2501 Bienne, Switzerland.

Darendeli, B. M. (2001), Development of a new family of normalized modulus reduction and material damping curves. PhD dissertation, University of Texas at Austin, TX, USA.

Ebrahimian, B. (2011), Front. Archit. Civ. Eng. China 5: 24. doi:10.1007/s11709-010-0082-6.

Elia, G., Amorosi, A., Chan, C. and Kavvadas, M. J. (2011), "Fully coupled dynamic analysis of an earth dam", *Geotechnique* 61(7), 549-563.

Finn, W., Lee, K., Maartman, C., & Lo, R. (1978), Cyclic pore pressures under un-isotropic conditions, in "Proceedings of the ASCE Speciality Conference on Earthquake Engineering and Soil Dynamics", 1, p. 457-491. New York.

Gazetas, G. (1987), "Seismic response of earth dams: some recent developments", *Soil Dynamics and Earthquake Engineering*, 6(1), 3-47.

Gazetas, G., & Dakoulas, P. (1992), "Seismic analysis and design of rockfill dams: state-of-the-art". *Soil Dynamics and Earthquake Engineering*, 11, 27-61.

Gruppo di lavoro MPS: 2004, Redazione della mappa di pericolosità sismica prevista dall'Ordinanza PCM 3274 del 20 marzo 2003. Rapporto conclusivo per il dipartimento di Protezione Civile, INGV, Milano - Roma, aprile 2004, 65pp. and 5 appendici,(http://zonesismiche.mi.ingv.it/elaborazioni/).

Gvirtzman, Z., & Nur, A. (2001), Residual topography, lithospheric structure and sunken slabs in the central Mediterranean. Earth and Planetary Science Letters, 187, 117-130.

H. B. Seed (1979), "Considerations in the earthquake-resistant design of earth and rockfill dams," *Geotechnique*, vol. 29, no. 3, pp. 215–263.

Hall, J. F. and Chopra, A. K. (1980), Dynamic response of embankment, concrete-gravity and arch dams including hydrodynamic interaction, Technical Report EERC-80/39, Earthquake Engineering Research Centre, University of California, Berkeley.

Hall, J. F. and Chopra, A. K. (1982a), "Hydrodynamic effects in earthquake response of embankment dams", J*ournal of the Geotechnical Engineering Division, ASCE* 108(GT4), 591-597.

Hall, J. F. and Chopra, A. K. (1982c), "Two-dimensional dynamic analysis of concrete gravity and embankment dams including hydrodynamic effects", *Earthquake Engineering & Structural Dynamics*, 10(2), 305-302.

Harder L. F., Kelso K. I., Kishida T., Kayen R. (2011), "Preliminary Observations of the Fujinuma Dam Failure Following the March 11, 2011 Tohoku Offshore Earthquake, Japan"; Geotechnical Extreme Events Reconnaissance (GEER), Association Report No. 25e.

Hardin, B., & Drnevich, V. (1972), "Shear modulus and damping in soils: design equations and curves". *Journal of Soil Mechanics and Foundations Division, ASCE*, 98(SM7), 667-692.

Hardin, B.O. (1978), "The Nature of Stress Stain Behavior of Soils", Earthquake Engineering and Soil Dynamics. ASCE. 1, 3–90.

Hatanaka, M. (1955), "Fundamental consideration on the earthquake resistant properties of the earth dam". Bull. No. It, Disaster Prevention Research Inst., Kyoto Univ.

Idriss, I. M. and Sun, J. I. (1992), SHAKE91: A computer program for conducting equivalent-linear seismic response analyses of horizontally layered soil deposits, Technical report, University of California, Davis.

Idriss, I. M., J., L., Hwang, R. and Seed, H. B. (1973), QUAD-4: A computer program for evaluating the seismic response of soil structures by variable damping finite element procedures, Technical Report Report EERC 73-16, Earthquake Engineering Research Center, University of California, Berkeley.

Idriss, I. M., Seed H.B. (1968), "Seismic response of horizontal soil layers". *Journal of Soil Mech. and Found Engrg., Proc. of ASCE*, Vol. 94, No. 4, 1003-103.

Idriss, I.M. and Sun, J.I. (1992), User's Manual for SHAKE91. Center for Geotechnical Modeling. Department of Civil Engineering, University of California, Davis.

Iervolino I., Galasso C., Cosenza E., (2010), "REXEL: computer aided record selection for code-based seismic structural analysis", *Bull Earthquake Engineering*, 8:339–362.

Inglod, T.S. (1979), "The effects of compaction on retaining walls". *Geotechnique* 29, No. 3, 265-283.

Ishihara, .K.G. (1996), Soil behavior in earthquake engineering. Clarendon Press, Oxford.

Ishihara, K. (2010). "Performances of rockfill dams during recent large earthquakes". Fift Interantional Conference on Recent Advances in Geotechnical Earthquake Engineering and Soil Dynamics, (p. 1-11).

San Diego, California.

Ishihara, K., Tatsuoka, F., & Yasuda, S. (1975), "Undrained deformation and liquefaction of sand under cyclic stresses". *Soils and foundations*, 15(4), 85-100.

ITACA, W. G. (2010), Data Base of the Italian strong motion records – (http://itaca.mi.ingv.it).

Itasca Consulting Group, Inc. Fast Lagrangian analysis of continua. 2005.

Kallioglou, P., Tika, TH., and Pitilakis, K. (2008), "Shear modulus and damping ratio of cohesive soils". *Journal of Earthquake Engineering*, 12, 879-913.

Kazama, M., Toyota, H., and Inutomi, T. (1995), Stress strain relationships in soils directly obtained from centrifuge shaking table tests, in "Proceeding 2nd Engineering for offshore and coastal facilities. International workshop on Wind and Earthquake engineering for offshore and coastal facilities".

Khan, Z. H., Cascante, G., El Naggar, M. H., and Lai, C. G. (2008), "Measurement of frequency- dependent dynamic properties of soils using the resonant-column device". *Journal of Geotechnical and Geo-environmental Engineering, ASCE*, 134(9), 1319-1326.

Kim D. S., Kim N.R., Choo Y.W., (2009): "Physical Modelling of Geotechnical Systems using Centrifuge", International Symposium on Urban Geotechnics, Incheon, Korea.

Kim M.K., Lee S.H., Choo Y.K., Kim D.S. (2011), "Seismic behaviors of earth-core and concrete-faced rock-fill dams by dynamic centrifuge tests", *Soil Dynamics and Earthquake Engineering* 31 1579–1593.

Kim D.S., Kim N.R, Choo Y.W. and Cho G.C. (2013), "A newly developed state of the art geotechnical centrifuge in Korea", *KSCE Journal of Civil Engineering,* 17(1):77-84.

Kottke AR, Rathje EM. *Technical Manual for Strata*. PEER Report 2008/10. University of California, Berkeley, California.

Kramer, S. (1996), *Geotechnical Earthquake Engineering*. Upper Saddle River, New Jersey 07458: Prentice-Hall.

Krinitszky, E.L. & Chang, F. K. (1979), Specifying peak motions for design earthquakes. SOA for Assessing Earth. Hazards in the U.S., paper S-73-1, US Army Corps of Eng., Vicksburg, Mississippi.

Kuhleimeyer , R., & Lysmer, J. (1973), "Finite element method accuracy for wave propagation problems". *Journal of the soil mechanics and foundations division*, *ASCE*, 99(SM5), 421-427.

L. 21 ottobre 1994, n. 584. In materia di "Misure urgenti in materia di dighe" [in Italian].

Lai C.G., Foti S., Rota M. (2009), Input sismico e stabilità geotecnica dei siti di costruzione, IUSS Press, Maggioli Editore, Pavia

Lai, C.G., Pallara, O., Lo Presti, D.C.F., Turco, E. (2001), "Low-Strain Stiffness and Material Damping Ratio Coupling in Soils. Advanced Laboratory Stress-Strain Testing of Geomaterials". Outcome of TC29 of ISSMGE From 1994 to 2001. Ed. F.Tatsuoka, S. Shibuya, & R. Kuwano. Balkema, 265-274.

Lanzo G., Pagliaroli A., Scasserra G., Effects of ground motion characteristics on seismic response of earth dams: some remarks on duration parameters and vertical shaking". SECED 2015 Conference: Earthquake Risk and Engineering towards a Resilient World, 10 July 2015, Cambridge UK.

Lanzo G., Pigliaroli A., Scassera G. (2015), Selection of ground motion time histories for the nonlinear analysis of earth dams, *In* "Proceedings of the XVI ECSMGE Geotechnical Engineering for Infrastructure and Development, Ice publishing", 2031-36.

Lee, C.W., Maeng, Y.S., Kim, Y.S. (2014), "Studies on Behavior Characteristics of Raised Reservoir Levee Using Centrifugal Model Test", *Korean Soc. Hazard Mitig*. Vol. 14, No. 3 pp. 151-161.

Lizarraga H. S., Lai C. G. (2014), "Effects of spatial variability of soil properties on the seismic response of an embankment dam", *International Journal of Soil Dynamics and Earthquake Engineering*, (64)113–128.

Lysmer J, Kuhlemeyer RL. (1969), "Finite dynamic model for infinite media", *Journal of the Engineering Mechanics Division* 95(4):859–78.

M.LL.PP. (2008). Norme Tecniche per le Costruzioni (NTC 2008), 14/01/2008. GU 29 (Suppl.Ord. 30) [in Italian].

M.LL.PP. (2014), Norme Tecniche per la progettazione e la costruzione degli sbarramenti di ritenuta (dighe e traverse), 26/06/2014.

Makdisi, F. I. and Seed, H. B. (1978), "Simplified procedure for estimating dam and embankment earthquake-induced deformations", *Journal of Geotechnical Engineering, ASCE* 104(7), 849-867.

Marcuson, W., Hynes, M., & Franklin, A. (2007), Seismic Design and Analysis of Embankment Dams: State of Practice. Burmister Lecture – (www.civil.columbia.edu/ling/burmister).

Martin, G.R., Finn, W.D.L. & Seed, H.B. (1975), "Effects of system compliance on liquefaction test", *Journal of Geotechnical Engineering*, *ASCE*, Vol. 104, No. GT4, 463-479.

Matsumoto N. (2011), "Amended 4 th Quick Report on Dams," Japanese Committee on Large Dams.

McGuire R. K. (1995), "Probabilistic seismic hazard analysis and design earthquakes: closing the loop", *Bull. Seism. Soc. Am*. 85, 1275-1284.

Mejia, L. H. and Seed, H. B. (1983), "Comparison of 2-D and 3-D dynamic analyses of earth dams", *J. Geotech. Engrg., ASCE* 1983, 109, GTll, 1383-1398.

Mejia, L. H., Seed, H. B. and Lysmer J. (1982), "Dynamic analysis of earth dam in three dimensions", *J. Geotech. Engrg*., ASCE, 108, GT12, 1586-1604.

Meletti C., Montaldo V., (2007), Stime di pericolosità sismica per diverse probabilità di superamento in 50 anni: valori di ag. Progetto. DPC-INGV S1, Deliverable D2, (http://esse1.mi.ingv.it/d2.html).

Meletti, C. (2007), Proseguimento della assistenza al DPC per il completamento e la gestione della mappa di pericolosità sismica prevista dall'Ordinanza PCM 3274 e progettazione di ulteriori sviluppi. Tratto da Progetto S1: (http://esse1.mi.ingv.it).

Meletti, C., & Valensise, G. (2004), Zonazione sismogenetica ZS9. App.2 al Rapporto Conclusivo, INGV.

Meng, J. (2007), "Earthquake ground motion simulation with frequency-dependent soil properties", *Soil Dynamics and Earthquake Engineering, Elsevier*, 27, 234-241.

Meza-Fajardo, K.C., and Lai, C.G. (2007), "Explicit causal relations between material damping ratio and phase velocity from exact solutions of the dispersion equations of linear viscoelasticity". *Geophysical Journal International*, 171(3), 1247-1257.

MOCT. Design standard for dam. Korea: Ministry of Construction and Transportation; (2005). [in Korean].

Modoni, G., Gazzellone, A. (2010), Semplified theoretical analysis of seismic response of artificially compacted gravels, *in* "Proceeding Fifth international conference on Recent advances in geotechnical earthquake engineering and soil dynamics", San Diego, Paper No. 1.28a.

Mononobe, N., Takata, A. and Matumura, M. (1936), Seismic stability of the earth dam, *in* Transactions of the 2nd Congress on Large Dams, Washington D. C. 4, 435-444.

Narita, K. (2000), Design and construction of embankment dams. Dept.of Civil Eng., Aichi Institute of Technology, pp. 18.

Newmark, N. M. (1965), "Effects of earthquakes on dams and embankments", *Geotechnique*, 15(2), 139-160.

Ng C.W.W., Li X.S., Van Laak P.A., Hou D.Y.J. (2004), "Centrifuge modeling of loose fill embankment subjected to uni-axial and bi-axial earthquake". *Soil Dynamics and Earthquake Engineering*, 24(4), 305–18.

Ordinanza PCM 3519 del 28 aprile 2006 dalla G.U. n.108 del 11/05/06 "Criteri generali per l'individuazione delle zone sismiche e per la formazione e l'aggiornamento degli elenchi delle medesime zone", [in Italian].

Park S. Y., Chang S.H., Lim H. T., Kim J. M., Kim Y. S. (2016), "Seismic Behavior of Deterioration Reservoir Embankment Using Dynamic Centrifugal Model

Tests", *Journal of the Korean Society of Agricultural Engineer*, Vol. 58, No. 3, pp. 91-100,

Park S.Y., Chang S.H., Lim H.T., Kim J.M., Kim Y.S. (2016a), "Behavior of seepage and seismic for the deterioration reservoir using numerical analysis", *Journal of the Korean Society of Agricultural Engineering*, Vol. 58, No. 3, pp. 81-90.

Peiris L.M.N., Madabhushi S.P.G., Schofield .A.N. (2008), "Centrifuge modeling of rock-fill embankments on deep loose saturated sand deposits subjected to earthquakes", *Journal of Geotechnical and Geoenvironmental Engineering* 134(9), 1364–74.

Pelecanos, L., (2013), Seismic response and analysis of earth dams, PhD thesis, Imperial College London.

Pelecanos, L., Kontoe, S., Zdravkovic, L. (2016), "Dam–reservoir interaction effects on the elastic dynamic response of concrete and earth dams", *Soil Dynamics and Earthquake Engineering* 82:138.

Potts, D. M. and Zdravkovi_c, L. (1999), *Finite element analysis in geotechnical engineering: Theory*, Thomas Telford, London.

Prevost, J. H., Abdel-Ghaffar, A. M. and Lacy, S. J. (1985), "Nonlinear Dynamic Analysis of Earth Dam: A Comparative Study", *J. Geotech. Engr., ASCE,* 111(7), 882-897.

Prevost, J. H., Abdel-Ghaffar, A. M. and Lacy, S. J. (1985), "Nonlinear Dynamic Analysis of Earth Dam: A Comparative Study". *J. Geotech. Engr., ASCE*, 111(7), 882-897.

Rampello S., Cascone E., Grosso N. (2009), "Evaluation of the seismic response of a homogeneous earth dam", *Soil Dynamics and Earthquake Engineering* , 29 (5): 782-798.

Rathje EM, Kottke A. "Strata". (https://nees.org/resources/strata2013).

Razeghi H.R., Aghaei Araei A., Ghalandarzadeh A. and Hashemi Tabatabaei S. (2014), "Rate-dependence of rock ll behavior on propagated near fault ground motions", *Scientia Iranica,* 21(4), 1263-1280.

Rix, G. J., and Meng, J. (2005), "A non-resonance method for measuring dynamic soil properties", *Geotechnical Testing Journal,* ASTM, 28(1), pp.1-8.

Rollins, K.M., Evans, M.D., Diehl, N.B. and Daily, W.D. (1998), "Shear modulus and damping relationships for gravels", *Journal of Geotechnical and Geo-environmental Engineering, ASCE*, 124(5), 398-405.

Saleh, S. and Madabhushi, S. P. G. (2010), "Hydrodynamic pressures behind flexible and rigid dams", *Dams & Reservoirs* 20(2), 73-82.

Schnabel, P., Lysmer, J. and Seed, H. B. (1970), SHAKE: A computer program for the earthquake response for horizontally layered sites, Technical Report EERC 72-2, Earthquake Engineering Research Centre, University of California, Berkeley.

Schofield, A.N. (1980). "Cambridge geotechnical centrifuge operations". Géotechnique 30 (3), 227-268

Seco e Pinto, P., & Simao, P. (2010). "Understanding seismic embankment dam behavior through case histories". Fifth international conference on recent advances in geotechnical earthquake engineering and soil dynamics, SOAP 2. San Diego.

Seed, H. B. (1973), Stability of earth and rockfill dams during earthquakes, in Hirschfeld and H. Poulos, eds, `Embankment - Dam Engineering', John Wiley.

Seed, H. B., Lee, K. L. and Idriss, I. M. (1969), "Analysis of Sheffield dam failure", *Journal of the Soil Mechanics and Foundation Engineering Division, ASCE* 95(SM6), 1453-1490.

Seed, H., Martin, P., & Lysmer, J. (1976), "Pore pressure changes during earthquakes", *Journal of Geotechnical Engineering, ASCE*, GT4, 323346.

Seed, H., Pyke, R., & Martin, G. (1975), "Analysis of the effect of Multi-Directional Shaking on the Liquefaction Characteristics of Sands", Report No. EERC 75-41, University of California, Earthquake Engineering Research Center, Berkeley, CA.

Seed, H., Seed, R., Lai, S., & Khamenehpo-Ur, B. (1985), Seismic design of concrete faced rockfill dams, *In* "Proceedings of the Symposium Concrete Face Rockfill Dams-design, Construction and Performance", 459-478.

Seed, H.B., Wong, R.T., Idriss, I.M. and Tokimatsu, K. (1986), "Moduli and damping factors for dynamic analyses of cohesionless soils", *Journal Geotech. Engineering,* 112(11), 1016-1032.

Selkuk M. E. and Terzi N. U. (2015), "Seismic Response of Ambar Dam to Recorded Earthquake", *International Journal of Advanced Research* 3(11), 979- 994.

Sharp MK, Adalier K. (2006). "Seismic response of earth dam with varying depth of liquefiable foundation layer", *Soil Dynamics and Earthquake Engineering* 26(11), 1028–37.

Shibuya, S., Mitachi, T., Fukuda, F., and Degoshi, T. (1995), "Strain-rate effects on shear modulus and damping of normally consolidated clay", Geotechnical Testing Journal, 18(3), 365-375.

Sica, S., Pagano, L. and Modaressi, A. (2008), "Influence of past loading history on the seismic response of earth dams", *Computers & Geotechnics* 35, 61-85.

Sica S., Pagano L. (2009), "Performance-based analysis of earth dams: procedure and application to sample case", *Soils and Foundations* Vol. 49, No. 6, 921–939, Japanese Geotechnical Society.

Smerzini C., Paolucci R., Galasso C., Iervolino I. (2012), Engineering ground motion selection based on displacement-spectrum compatibility, *in* "Proc of. 15WCEE", Lisboa, PT. Paper No. 2354.

Spallarossa, D., & Barani, S. (2007), Disaggregazione della pericolosità sismica in termini di M-R-ε. Progetto DPC-INGV S1, Deliverable D14.

Stephens T. (2010), "Manual on small earth dams: A guide to siting, design and construction", FAO.

Sugito, M. (1995), "Frequency-dependent equivalent strain for equi-linearized technique", *in* "Proceedings of the First International Conference on Earthquake Geotechnical Engineering", 1, A.A. Balkena, Rotterdam, the Netherlands, 655-660.

Tan, C.S. e Scott, R.F. (1985). "Centrifuge scaling considerations for fluid-particle systems", *Géotechnique* 35 (4), 461-470.

Terzaghi K. (1950), *Mechanisms of Landslides*. Engineering Geology (Berkley) Volume, Geological Society of America, New York, NY, USA.

Towhata I.; Goto, H.; Kazama, M.; Kiyota, T.; Nakamura, S.; Wakamatsu, K.; Wakai, A.; Yasuda, S.; Yoshida, N. (2011), "On Gigantic Tohoku Pacific Earthquake in Japan," Earthquake News, Bulletin of the International Society for Soil Mechanics and Geotechnical Engineering, Volume 5, Issue 2.

Travasarou, T. Bray, J. D. & Abrahamson, N. A. (2003), "Empirical attenuation relationship for Arias intensity". *Earthq. Eng. Sturct.Dynam*. 32, 1133–1155.

Vanmarke, E. H. (1979), SOA for assessing earthquake hazards in the United States: representation of earthquake ground motion: scaled accelerograms and equivalent response spectra. Miscellaneous paper S-73-1, Report 14, U. S. Army Corps of Engineers Waterways Experiment Station, Vicksburg, Mississippi.

Vrymoed, J. (1981), "Dynamic FEM model of Oroville dam", *Journal of the Geotechnical Engineering Division, ASCE* 107(GT8), 1057-1077.

W. F. Marcuson (1981), Moderator's report for session on 'Earth dams and stability of slopes under dynamic loads *in* "Proceedings of the International Conference on Recent Advances in Geotechnical Earthquake Engineering and Soil Dynamics", vol. 3, p. 1175, St. Louis, Mo, USA.

Westergaard, H. M. (1933), "Water pressures on dams during earthquakes", *Transactions, ASCE* 98(1), 418-433.

Wieland M. (2012), Seismic Design and Performance Criteria for Large Storage Dams, *in* "Proceeding 15 WCEE", Lisboa,

Wieland M., "ICOLD's revised seismic design and performance criteria for large storage dam", Zurich.

Wolf, J. P. (1985), *Dynamic soil-structure interaction*, Prentice Hall, New Jersey.

Woodward; D.V. (1996), "Griffiths, Influence of viscous damping in the dynamic analysis of an earth dam using simple constitutive models", *Computers and Geotechnics*. Vol. 19. No. 3. pp. 245-263.

Wu, C., Ni, C., and Ko, H., (2009), "Seismic Response of an Earth Dam: Finite Element Coupling Analysis and Validation from Centrifuge Tests", *Journal of Rock Mechanics and Geotechnical Engineering*, Vol. 1, No. 1, pp. 56–70.

Yamada, S., Hyodo, M., Orense, R. P., Dinesh, S. V., and Hyodo, T. (2008), "Strain-dependent dynamic properties of remolded sand-clay mixtures", *Journal of Geotechnical and Geo-environmental Engineering, ASCE,* 134(7), 972-981.

Yokota K., Imai T., Konno M. (1981), "Dynamic de-formation characteristics of soils determined by laboratory tests". *OYO Tec*. Rep. 3, pp. 13-37.

Yu Y., Xie L., Zhang B. (2005), "Stability of earth-rockfill dams: Influence of geometry on the three-dimensional effect", *Computers and Geotechnics* 32(5): 326-339 CrossRef, ISI.

Yule, D.E. Matheu, E.E. & Beaty, M.H. (2004), Duration parameters for the selection of ground motion time histories for nonlinear analysis of embankment dams. Technical Report 36th Joint Meeting U.S.-Japan Panel on Wind and Seismic effects, Nat. Inst. of Standard and Technologies, Gaithersburg, Maryland, 17-22.

Zangar, C. N. (1953), Hydrodynamic pressures on dams due to horizontal earthquakes, *in* "Proceedings of the Society of Experimental Stress Analysis 10", 93-102.

Zangar, C. N. and Haefeli, R. J. (1952), "Electric analog indicates effect of horizontal earthquake shock on dams", *Civil Engineering* 22, 278-279.